# Molten Salt Reactor Chemistry

## Fission products and simulants

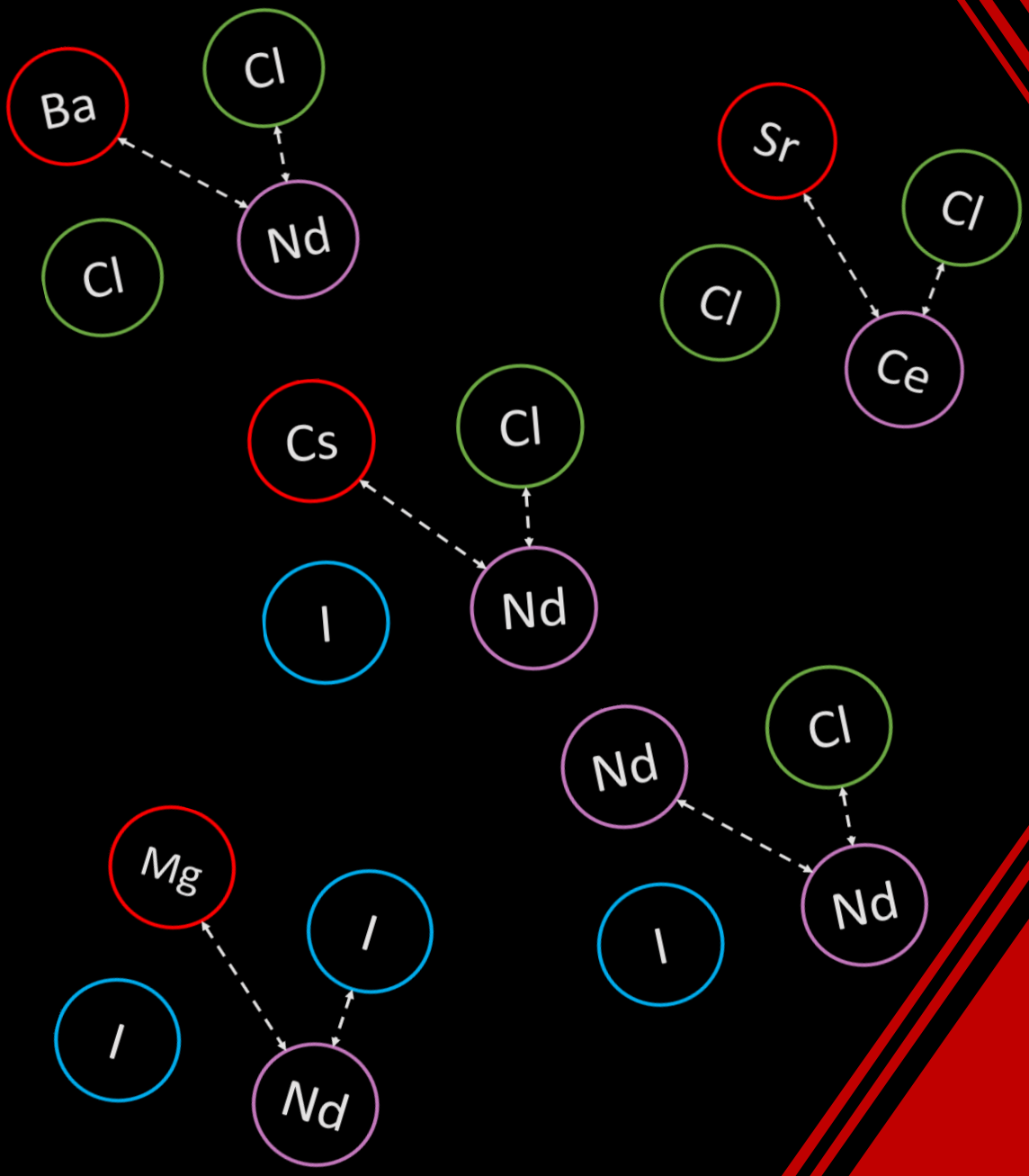


by Dennis Charley Alders

# MOLTEN SALT REACTOR CHEMISTRY

## FISSION PRODUCTS AND SIMULANTS

# MOLTEN SALT REACTOR CHEMISTRY

FISSION PRODUCTS AND SIMULANTS

**Proefschrift**

ter verkrijging van de graad van doctor
aan de Technische Universiteit Delft,
op gezag van de Rector Magnificus Prof.dr.ir. H. Bijl,
voorzitter van het College voor Promoties,
in het openbaar te verdedigen op dinsdag 3 maart 2026 om 15:00 uur

door

**Dennis Charley ALDERS**

Dit proefschrift is goedgekeurd door de promotoren.

Samenstelling promotiecommissie:

| | |
|---|---|
| Rector Magnificus, | voorzitter |
| Dr. A.L. Smith, | Technische Universiteit Delft, promotor |
| Prof.dr. R.J.M. Konings, | Technische Universiteit Delft, promotor |
| | |
| *Onafhankelijke leden:* | |
| Prof.dr.ir. T.J.H. Vlugt, | Technische Universiteit Delft |
| Prof.dr.ir. A.G. Denkova, | Technische Universiteit Delft |
| Dr. P. Benigni, | Centre National de la Recherche Scientifique / Aix-Marseille University, France |
| Dr. S. Delpech, | Centre National de la Recherche Scientifique, France |
| Dr.ir. M. Rohde, | Technische Universiteit Delft, reservelid |
| | |
| *Overige leden* | |
| Dr. E. Capelli, | ORANO group, France |

*Keywords:* Molten Salt Reactor, molten chlorides, fission products, CALPHAD, thermodynamics

*Printed by:* ProefschriftMaken

*Cover by:* Me.

*Funding:* This work has received its funding from the ORANO group.

This research was performed in the Reactor Physics and Nuclear Materials group of the department Radiation Science and Technology, faculty of Applied Science at the Delft University of Technology.



ISBN 978-94-6534-214-6

An electronic version of this dissertation is available at
http://repository.tudelft.nl/.

# CONTENTS

# 1

# INTRODUCTION

*Writing an introduction can be a bit of a mixed bag. On the one hand you want to give sufficient information on societal context and background of your work, but how far do you go? Most authors in the nuclear field take it back to the energy crisis and lowering $CO_2$ emissions, but plenty has been written on that already. The fact that there is an energy crisis should be apparent to anyone reading this. The (current) entry point to this story is one step closer to the subject matter: we want to build nuclear reactors, like the Molten Salt Reactor, that offer advantages over traditional reactors. What are the current knowledge gaps that have to be addressed before we can move forward with this undertaking?*

1

The Molten Salt Reactor (MSR) is a type of nuclear reactor selected by the Generation IV International Forum [1], which could prove a great aid in attaining the climate goals set in the Paris agreement [2]. Before large-scale adoption of MSR technology can be realised, however, some key knowledge gaps need to be addressed. The reason for this is the highly complex chemistry of the molten fuel salt that arises following the dissolution of fission products in the salt under irradiation. In particular, what this work is interested in exploring is the thermochemical behaviour of fission products in molten chloride reactors, and their effect on the melting and vaporization behaviour of molten chloride fuels.

## 1.1. A BRIEF HISTORY OF NUCLEAR ENERGY

In a nuclear (fission) reaction, energy is generated through the fission reaction of a fissile element like uranium ($^{235}$U) or plutonium ($^{239}$Pu). A graphical depiction of this reaction is given in Figure 1.1. The fissioning of the heavy nucleus (U or Pu) releases energy, neutrons and fission products. Generating this energy is the goal of a nuclear reactor, and the released neutrons are vital for sustaining the chain reactions, as these neutrons can in turn fission other heavy nuclei. The fission products that are produced by splitting the heavy atom are waste products, which will be discussed in more detail in Section 1.3.1.

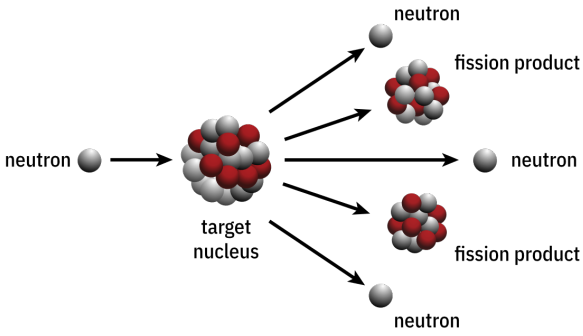


Figure 1.1: Schematic representation of the fission reaction [3]. The target nucleus, ($^{235}$U or $^{239}$Pu), captures a neutron and fissions, creating energy, more neutrons and fission products.

### 1.1.1. FROM THE MANHATTAN PROJECT TO THE FIRST REACTOR

After the discovery of nuclear fission between 1938 and 1939 [4], the first potential chain reaction using nuclear fission was hypothesized shortly after [5, 6]. This discovery directly led to the infamous Manhattan Project [7, 8], renowned for the creation of nuclear weapons. At the same time, Chicago Pile-1 (CP-1), the first artificial nuclear reactor labelled as "a crude pile of black bricks and wooden timbers" [9] reached criticality [10]. After the experiments with the Chicago Pile reactors, the Experimental Breeder Reactor I (EBR-I) - a liquid metal cooled reactor that used metallic uranium as a fuel - became the

first electricity-generating nuclear power plant in 1951 [11], marking the start of a new era in energy technology.

### 1.1.2. EARLY MOLTEN SALT REACTORS IN THE USA

The first commercial use of nuclear reactors for power generation was in the form of Shippingport reactors, which were water-cooled solid-fueled reactors [12]. Following the introduction of nuclear reactors as power generators, a new design for a reactor with a liquid fuel that could operate at high temperatures and deliver a high power density was investigated in the Aircraft Reactor Experiment (ARE) [13] at Oak Ridge National Laboratory in 1954. In this experiment, a fuel consisting of three end-members was used: NaF, $ZrF_4$ and $UF_4$. The aim of this project was to investigate whether a nuclear-powered aircraft would be feasible. After the conclusion of this project in 1954, the idea of using a MSR for aircraft propulsion was shelved, but the interest in molten salt reactors remained. A follow-up project was designed to study the neutron economy in a molten salt reactor, with the aim of investigating the possibility of using thorium as fertile material in a breeder reactor [14]. This experiment, descriptively called the Molten Salt Reactor Experiment (MSRE), proved the viability of a molten salt fueled reactor concept, operating for four years (1965-1969) and producing over 90 GWh of energy using a fuel with four end-members: $LiF-BeF_2-ZrF_4-UF_4$. The subsequent actualization of a thorium-based molten salt breeder reactor did not come to fruition [15], however, as the liquid-metal fast breeder reactor concept was favoured instead [16].

### 1.1.3. RECENT HISTORY

Historically, the overwhelming majority of operated nuclear reactors worldwide are Pressurized Water Reactors (PWR) or Boiling Water Reactors (BWR) [17]. These reactors generally use fuel assemblies consisting of solid pellets of uranium oxide ($UO_2$) or mixed oxide $(U,Pu)O_2$ fuel, and water as coolant. Research into molten salt reactors had stagnated after the MSRE in favour of solid-fueled reactor types. This changed in the early 2000s, when six reactor designs were selected by the Generation IV International Forum for the future of nuclear energy, based on the criteria of safety, sustainability, economics and proliferation resistance [1]. One of these six reactor types was the Molten Salt Reactor. Since then, many new insights into fuel characteristics, neutron economy, thermal hydraulics and other important aspects have been obtained. Along with the renewed interest in MSRs came an increase in research in Europe [18, 19], China [20], Canada [21] and the United States [22]. Furthermore, start-up companies emerged, such as Terrapower, Thorizon, Stellaria, NAREA, Saltfoss and more, wanting to fill this niche in the nuclear energy market. The molten salt reactor, among other concepts such as the small modular reactor, became the face of the nuclear renaissance.

## 1.2. MSR OVERVIEW

The Molten Salt Reactor (MSR) is a type of nuclear reactor that, as the name implies, uses liquid salts as a fuel and coolant. Section 1.2.1 will briefly discuss some of the key

characteristics that make the European MSFR (Molten Salt Fast Reactor) an attractive option for use as nuclear energy system. Additionally, the choice of salt matrix, be it fluorides or chlorides, is discussed in Section 1.2.2. A scheme of the MSR is presented in Figure 1.2. This figure shows the MSR, along with a heat exchanger and power generation loop. The molten fuel is pumped through the core and heat exchanger by either forced convection, or natural convection, through design optimization.

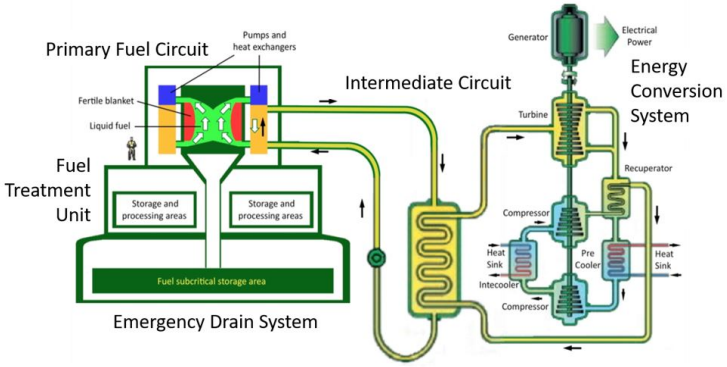


Figure 1.2: Schematic overview of a Molten Salt Fast Reactor [23], based on the European design by Merle et al. [24].

### 1.2.1. CHARACTERISTICS

Given the amount of experience with Light Water Reactors (LWR) [25–27], one might wonder why there is a need for new types of nuclear reactors in the first place, and what advantages the MSR has to offer that justify the interest in it despite the low technology readiness level (TRL) [28]. The advantages of a Molten Salt Reactor can be classified in terms of **Safety**, **Sustainability Economics** and **Environmental Impact**.

Some of the characteristics that make these salts an interesting option for molten salt reactors are a low vapor pressure and high thermal stability under operating conditions, operation at atmospheric pressure, a negative temperature feedback coefficient, high actinide solubility and potential for fission product retention [29, 30]. The combination of these properties leads to increased inherent safety characteristics.

For the fission reaction to occur and for the core to maintain criticality, a minimum density of fissile elements needs to be present in the reactor core, otherwise there are not enough neutrons to sustain the chain reaction. When the temperature of the fuel rises, its volume increases due to thermal expansion. This leads to fewer fissile isotopes in the core, which in turn leads to a lower reaction rate. This means that the density of the liquid fuel and concentration of fissile elements is of critical importance to the criticality and safe operation of the reactor. In an MSR, two processes occur during the chain reaction that influence the (bulk) density of the molten salt: thermal expansion and cavity formation. Due to thermal expansion, if the fuel heats up too much, the reactivity (*i.e.* the concentration of fissile elements) is lowered because fewer fissile isotopes will be in

the critical geometry of the core. Furthermore, cavities that follow from the formation of bubbles in the molten salt, (*e.g.* through gaseous fission products) cause the fuel to have a negative void coefficient, meaning that the reactivity will decrease upon fission product formation. These processes cause an MSR to self-regulate when the temperature increases significantly.

Another passive safety is installed in the MSR in the form of a freeze plug. This solid, actively cooled, block of salt is located below the reactor core, and will melt if the temperature of the fuel becomes too high. If this happens, the reactor will be drained by gravity, placing the fuel in a subcritical geometry and stopping the chain reaction. Adding to these characteristics, the fact that the MSR operates at atmospheric pressure means that if there is a crack or other minor breach of containment, there is no driving force to expel the radioactive material to the coolant or the environment. Furthermore, because of the high melting point of the fuel, if there is a leak, the fuel will solidify upon exposure to the temperatures outside the reactor [31]. Moreover, molten salts, as long as they are molten, are immune to the effects of radiolysis brought on by the production of radioactive fission products [28, 32].

In addition to the safety characteristics the MSR offers, as listed above, there are also several economic and environmental factors that make the MSR an attractive option. As mentioned in the paragraph above, the ability of the MSR to operate at atmospheric pressures offers a safety advantage, but it also means that there is a greater degree of freedom when it comes to reactor design. In fact, the lower pressure requirement reduces the necessary structural section thickness [28], leading to a lower material cost for the nuclear power plant itself. Furthermore, due to the high operating temperature of the MSR, it can not only be used for electricity production, but also as a source of heat for energy-intensive industrial processes such as hydrogen production.

Finally, the burn-up that can be achieved using a Molten Salt Reactor is higher than that of a LWR, meaning that less of the fissile material in the fuel goes to waste. In fact, the spent nuclear fuel (SNF) from Light Water Reactors and other solid-fueled reactors could be used as a fuel source for Molten Salt Reactors because of the flexibility it offers in terms of fuel composition and fuel cycle. The MSR can be used to burn plutonium (from Pu stockpiles) and minor actinides (Np, Am, Cm, Cf). This feature is particularly interesting, as minor actinides are responsible for the bulk of the radiotoxicity in SNF, and burning these will lower the duration of the radiotoxicity from 20,000 years to several hundreds of years [33]. Furthermore, since there is currently no other use for spent nuclear fuel, there is no competition for this feedstock, offering another economic advantage. Finally, through processes such as helium bubbling and selective precipitation, it may be possible to split the waste stream of an MSR by taking out the noble metals (valorising the process) and produced radionuclides (further lowering SNF radiotoxicity).

1

### 1.2.2. INFLUENCE OF THE SALT MATRIX

In the ARE and MSRE, the nuclear fuels that were used were fluoride based fuels consisting of $NaF-ZrF_4-UF_4$ and $LiF-BeF_2-ZrF_4-UF_4$, respectively [14, 29]. Fluorides offer great thermal stability and low vapor pressure [29, 30], are slighlty less corrosive to the reactor structural materials than chlorides [34], and have a low neutron absorption cross section for both thermal and fast neutrons [35]. Additionally, despite the high melting points of the end-members, low melting points of the fuel can be achieved by forming eutectic mixtures.

Molten chlorides have not been used as nuclear fuels to date, but they offer similarly advantageous characteristics. The melting points of pure chlorides are generally lower than those of fluorides, and also offer great thermal stability and a low vapor pressure [36, 37]. Compared to fluorides, chlorides offer a generally higher solubility limit for actinides, but their corrosion behaviour could be more severe [36]. Chloride salts are also more compatible with the current reprocessing schemes used for oxide fuels, and the reprocessing and fuel fabrication of chloride fuels is therefore easier to integrate in the current infrastructure. Furthermore, the thermal neutron capture cross section of $^{35}Cl$, one of two stable chlorine isotopes and responsible for 75% of chlorine found in nature, is drastically higher than that of fluorine [35]. Because of this, to use chlorides in an MSR with thermal neutrons (E = 0.025 eV), enrichment to $^{37}Cl$ may be necessary depending on the concentration of fissile elements [36]. This difference is much smaller for fast neutrons (E = 500 keV), and there is no enrichment necessary. For this reason, chloride fuels are mainly attractive for molten salt fast reactors, explaining the general shift in interest towards chloride salts in the MSR community

## 1.3. THERMOCHEMISTRY IN MSR

For the development of a MSR, the thermochemical behaviour of the fuel, usually comprised of three or four end-members, must be understood. Aside from the thermochemical behaviour of the base fuel salt, there are two processes important for the thermochemistry inside an MSR during reactor operation: corrosion and fission. Molten halide salts are generally highly corrosive and hygroscopic [34, 38] and containing these salts for longer durations at elevated temperatures can be a challenge. While corrosion is a very important and very interesting aspect of MSR thermochemistry to study, it is not the focus of this work. This work is focused on the changes in thermochemistry of a molten salt fuel that are brought on by fission products.

### 1.3.1. FISSION PRODUCTS

Fission products, as shown in Figure 1.1, are side products from the fission reaction. During the chain reaction many different elements are produced as fission products, as shown in Figure 1.3.

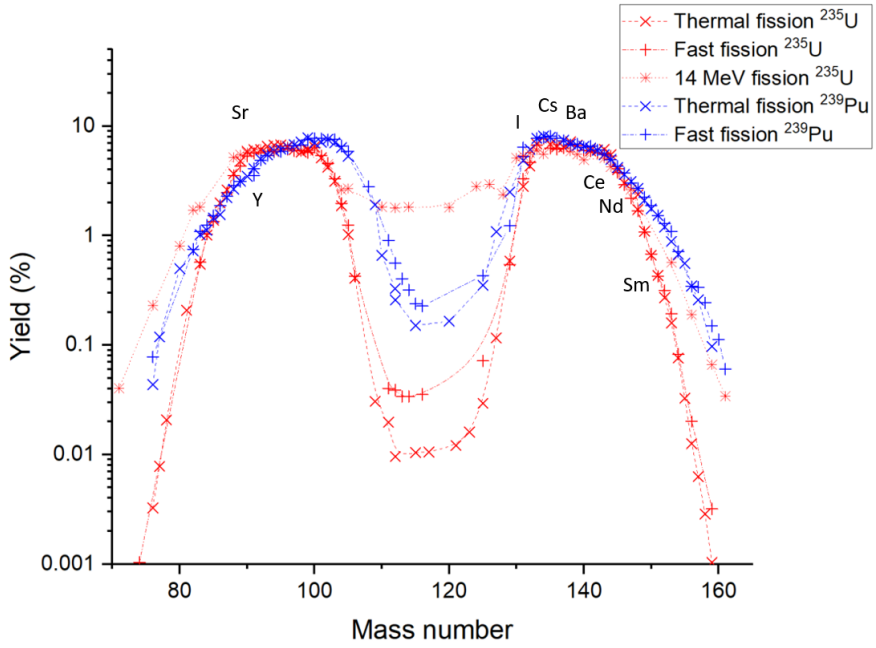


Figure 1.3: Fission yield mass distributions for thermal (0.0253 eV) and fast (500 keV) neutrons for $^{235}$U and $^{239}$Pu, and high energy (14 MeV) neutrons for $^{235}$U. Data from Crouch et al. [39]. Indicated on the figure are the mass numbers of the fission products of interest in this work.

Not all of the elements produced during the fission reaction will interact with the base fuel salt. Gaseous fission products such as $^{135}$Xe will form gas bubbles and leave the melt, while elements in the platinoid group such as $^{106}$Ru form a separate metallic phase. The elements that are expected to dissolve into the melt can be categorised as one of two subspecies: elements that pose a solidification or precipitation risk, and elements that pose a risk of volatilization.

### PRECIPITATING ELEMENTS

Precipitation inside the fuel of an MSR is undesirable. Precipitates can cause clogging in the reactor or the heat exchangers, and precipitation of the fissile element creates hotspots of activity. Therefore, precipitation of any elements in a molten salt reactor must be investigated thoroughly to assess the risks it poses to reactor operation.

Elements that can interact with the melt and pose a precipitation risk are the rare earth elements (Ce, Nd, Sm, Y) due to their chemical similarity to fissile elements U and Pu and relatively high melting points. Additionally, alkaline-earth elements strontium and barium can be classified as elements that pose a solidification risk due to the high melting point of the elemental chlorides by themselves. For this reason, the interactions of these elements with the base fuel salt must be investigated. For this purpose, the thermochemistry of molten salt systems with precipitating elements must be modelled.

### VOLATILE ELEMENTS

Due to the high radiotoxicity of $^{135}$Cs, $^{137}$Cs, $^{129}$I and $^{131}$I it is imperative to know what happens to these potentially volatile species. In solid fueled reactors, cesium and iodine are often classified as volatile fission products, in addition to gaseous products like xenon and krypton. In a molten salt reactor, Xe and Kr do not interact with chlorides and form bubbles, but Cs and I could dissolve in the fuel salt. Seeing as Cs has a higher fission yield than I [40], both CsI and CsCl are expected to form in a reactor. However, as shown for fluoride-based systems, CsI can be present as a volatile species and can easily leave the melt [41]. Whether similar behaviour is observed in chloride systems must be investigated.

## 1.4. THESIS OVERVIEW

This thesis work addresses the knowledge gaps in our current understanding of molten chloride fuel thermodynamics by investigating the effect of fission products on molten salt thermochemistry. The complexity of the systems investigated in this dissertation incrementally increases as more species are added: for a binary system, only the interactions between the two end-members have to be modelled. For a ternary system, *i.e.* a system with three end-members, the amount of interactions that have to be modelled already increases to four (three binary interactions, and one ternary interaction). For a quaternary system, that number increases further to nine interactions (six binary interactions, two ternary interactions and a quaternary interaction), and so on. This complexity is what motivates the need for CALPHAD models, as these thermodynamic descriptions of molten salt systems are very adept at extrapolation to higher order systems, possibly reducing the need for higher-order optimizations.

Compared to molten fluoride salts, the knowledge on chloride salt thermodynamics is much less advanced, necessitating the studies presented in this dissertation. The understanding of fission product behaviour can be used in safety calculations (as is done in Chapter 9), to determine any possible threats to the margin to solidification of the molten fuel salt, or the retention of otherwise volatile fission products. For example, volatility of CsI [41] and behaviour of fission products and corrosion products [42] have been studied for molten fluoride salts, but not for molten chlorides. A graphical overview of this thesis structure is given in Figure 1.4. An overview of the salt systems modelled in this work is given in Figure 1.5.

The first chapter, this one, is dedicated to a brief introduction of the Molten Salt Reactor and fission product chemistry. After this general introduction on the context of this research, Chapter 2 introduces the various experimental techniques used throughout this work, as well as estimation methods for the so-called mixing enthalpies, which are not always experimentally measured. Chapter 2 also describes in detail the estimation methods, which allowed us to obtain accurate predictions of the mixing enthalpies of unknown systems. It finally introduces the mathematical description of the thermodynamic models themselves for the liquid, solid and gas phases in the systems of interest.

As mentioned before, the aim of this work is to characterise the thermochemical behaviour of fission products in molten salts. However, for this we need enough information on the thermodynamics of $PuCl_3$-based systems, the availablility of which is scarce. To remedy this, we must find a way to investigate $PuCl_3$ without using $PuCl_3$. This is covered in Chapter 3 with the introduction and analysis of simulant chemistry, to act as a surrogate for $PuCl_3$. Additionally, Chapter 3 treats the thermodynamic description of the base fuel $NaCl-MgCl_2-PuCl_3$. From there, Chapters 4 and 5 present an investigation of the thermochemical behaviour of fission products Ba and Sr in simulant systems and actinide systems, respectively. The addition of iodine as a fission product to the thermodynamic database is presented in Chapters 6 and 7. In Chapter 8, the addition of cesium to the thermodynamic model is presented. The culmination of this work is given in Chapter 9 through the application calculations, which allow us to answer the main question of this work: how does the addition of fission products to a molten salt system affect their precipitation and volatilization behaviour? Finally, in the same chapter, the conclusions and recommendations of this dissertation are presented.

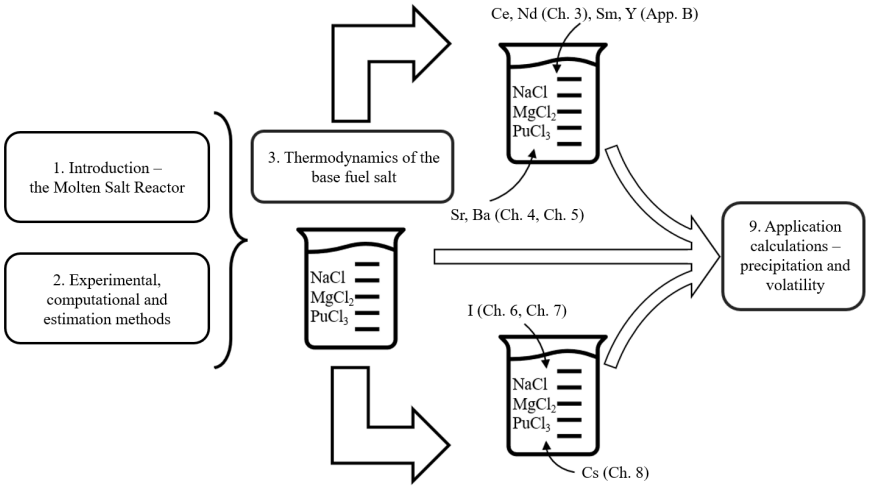


Figure 1.4: Graphical overview of this thesis.

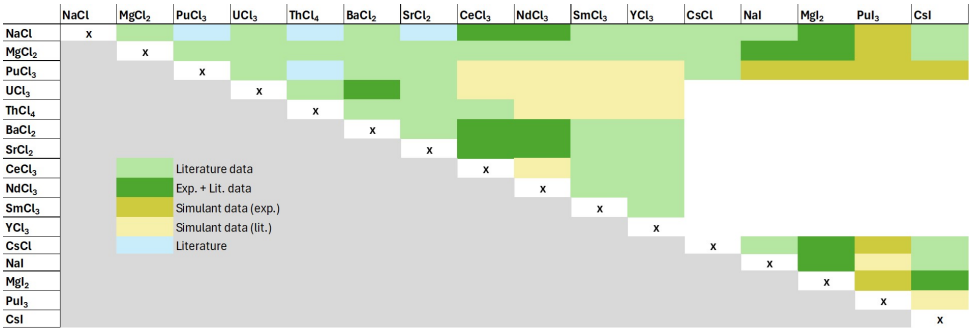


Figure 1.5: Overview of the modelled systems containing fission products (Sr, Ba, Ce, Nd, Sm, Y, Cs, I) in this work. The color-coding corresponds to the origin of the thermodynamic model: based on data from the literature (light green), based on own experimental data and/or data from the literature (green), based on own simulant data (olive), based on simulant data from the literature (yellow) or taken entirely from the literature without further optimization (blue).

# BIBLIOGRAPHY


(1) Abram, T.; Ion, S. *Energy Policy* **2008**, *36*, 4323–4330.

(2) Agreement, P. In *report of the conference of the parties to the United Nations framework convention on climate change (21st session, 2015: Paris). Retrived December*, 2015; Vol. 4, p 2.

(3) Atomic Archive - AJ Software and Multimedia Nuclear Fission.

(4) Hahn, O.; Strassmann, F. *Naturwissenschaften* **1939**, *27*, 89–95.

(5) Szilard, L., *Improvements in or relating to the transmutation of chemical elements*; Patent Office: 1962.

(6) Halban, H. v.; Joliot, F.; Kowarski, L.; Perrin, F. *Journal de Physique et le Radium* **1939**, *10*, 428–429.

(7) Smyth, H. D. *Reviews of Modern Physics* **1945**, *17*, 351.

(8) Goldwhite, H. *Journal of Fluorine Chemistry* **1986**, *33*, 109–132.

(9) Commission, U. A. E., *The first reactor. [Oak Ridge, Tennessee]*; U.S. Atomic Energy Commission, Division of Techn ical Information: 1967.

(10) Gandini, A. In *Enrico Fermi: His Work and Legacy*; Springer: 2004, pp 204–221.

(11) Cochran, T. B.; Feiveson, H. A.; Patterson, W.; Pshakin, G.; Ramana, M.; Schneider, M.; Suzuki, T.; von Hippel, F., *Fast breeder reactor programs: history and status*; International Panel on Fissile Materials Princeton, NJ: 2010.

(12) Cummins, W. E.; Matzie, R. *Progress in Nuclear Energy* **2018**, *102*, 9–37.

(13) Cottrell, W.; Hungerford, H.; Leslie, J.; Meem, J. *Operation of the aircraft reactor experiment*; tech. rep.; Oak Ridge National Lab.(ORNL), Oak Ridge, TN (United States), 1955.

(14) Haubenreich, P. N.; Engel, J. *Nuclear Applications and technology* **1970**, *8*, 118–136.

(15) Robertson, R. C. *Conceptual Design Study of a Single-Fluid Molten Salt Breeder Reactor*. Tech. rep.; comp.; Oak Ridge National Lab.(ORNL), Oak Ridge, TN (United States), 1971.

(16) MacPherson, H. *Nuclear Science and engineering* **1985**, *90*, 374–380.

(17) Kok, K. D. In *Nuclear engineering handbook*; CRC Press: 2016, pp 3–10.

(18) Origins, I. *IO+* **2025**.

(19) Energynews *Energynews* **2024**.

(20) International, N. E. *Nuclear Engineering International* **2025**.

(21) News, W. N. *World Nuclear News* **2024**.

(22) Bhardwaj, A. *Interesting Engineering* **2025**.

(23) SAMOSAFER Consortium Schematic of the MSFR.

(24) Merle-Lucotte, E.; Allibert, M.; Brovchenko, M.; Heuer, D.; Ghetta, V.; Laureau, A.; Rubiolo, P. In *Thorium Energy for the World: Proceedings of the ThEC13 Conference, CERN, Globe of Science and Innovation, Geneva, Switzerland, October 27-31, 2013*, 2016, pp 223–231.

(25) Pershagen, B.; Bowen, M., *Light water reactor safety*; Elsevier: 2013.

(26) Shah, V. N.; Ware, A. G.; Atwood, C. L.; Sattison, M. B.; Hartley, R. S.; Hsu, C. *Assessment of field experience related to pressurized water reactor primary system leaks*; tech. rep.; Idaho National Lab.(INL), Idaho Falls, ID (United States), 1999.

(27) Theriault, K. In *Nuclear Engineering Handbook*; CRC Press: 2016, pp 85–140.

(28) Roper, R.; Harkema, M.; Sabharwall, P.; Riddle, C.; Chisholm, B.; Day, B.; Marotta, P. *Annals of Nuclear Energy* **2022**, *169*, 108924.

(29) Bettis, E.; Schroeder, R.; Cristy, G.; Savage, H.; Affel, R.; Hemphill, L. *Nuclear Science and Engineering* **1957**, *2*, 804–825.

(30) Le Brun, C. *Journal of Nuclear Materials* **2007**, *360*, 1–5.

(31) Beneš, O.; Konings, R. J. M. Comprehensive Nuclear Materials, Vol. 3, ch. 3.13, 2012.

(32) Luzzi, L.; Di Marcello, V.; Cammi, A., et al., *Multi-Physics Approach to the modeling and analysis of Molten Salt Reactors*; Nova Science Publishers, Inc.: 2012.

(33) Stacey, W. M., *Nuclear reactor physics*; John Wiley & Sons: 2018.

(34) Raiman, S. S.; Lee, S. *Journal of Nuclear Materials* **2018**, *511*, 523–535.

(35) Kopecky, J. Atlas of Neutron Capture Cross Sections (NGATLAS), 1999.

(36) Faure, B.; Kooyman, T. *Progress in Nuclear Energy* **2022**, *144*, 104082.

(37) Clark, P. *Physical Properties of Fused Salt Mixtures: Eutectic Compositions and Melting Points. Data from Open Literature, 1963–June 30, 1965.* Tech. rep.; Sandia National Lab.(SNL-NM), Albuquerque, NM (United States), 1966.

(38) Sridharan, K.; Allen, T. In *Molten salts chemistry*; Elsevier: 2013, pp 241–267.

(39) Crouch, E. *Atomic data and nuclear data tables* **1977**, *19*, 417–532.

(40) Taube, M. *Fast reactors using molten chloride salts as fuel*; tech. rep.; INFCE (Switzerland), 1978.

(41) Beneš, O.; Capelli, E.; Morelová, N.; Colle, J.-Y.; Tosolin, A.; Wiss, T.; Cremer, B.; Konings, R. *Physical Chemistry Chemical Physics* **2021**, *23*, 9512–9523.

(42) Dumaire, T. Advances in the chemistry of Molten Salt fuels with emphasis on Fission Products and Corrosion Products, Ph.D. Thesis, Delft University of Technology, 2024.

# 2

# METHODS

*At the core of this work are the methods we used to assess phase equilibria in molten salt systems. These methods include experimental methods, such as X-Ray diffraction (XRD), Neutron Diffraction (ND), solution calorimetry and Differential Scanning Calorimetry (DSC), as well as computational methods such as the CALculation of PHAse Diagrams (CALPHAD) method and all of its models, which are described hereafter.*

2

This chapter on methods will be divided into two main sections. The first part of the chapter, Section 4.2 will be focused on the experimental methods used in this work. The experimental methods are subdivided further by measurement technique, with a brief introduction and practical application example for each technique. The second part of the chapter focuses on the estimation method for the mixing enthalpy. Subsequently, computational methods, with a brief introduction of the CALPHAD method and the models selected for the liquid and solid solutions, are presented. Finally, an overview of the thermodynamic database obtained and used in this work is presented.

## 2.1. EXPERIMENTAL METHODS

The purpose of the experimental methods outlined in this section is to better understand the thermochemistry of molten salt systems. To illustrate the importance of the experimental techniques described hereafter, an example of a phase diagram is presented in Figure 2.1. This system, the $BaCl_2$−$CeCl_3$ system investigated in this work, includes an intermediate ($Ba_3Ce_2Cl_{12}$) and a high-temperature solid solution ($Ba_{1-x}Ce_xCl_{2+x}$).

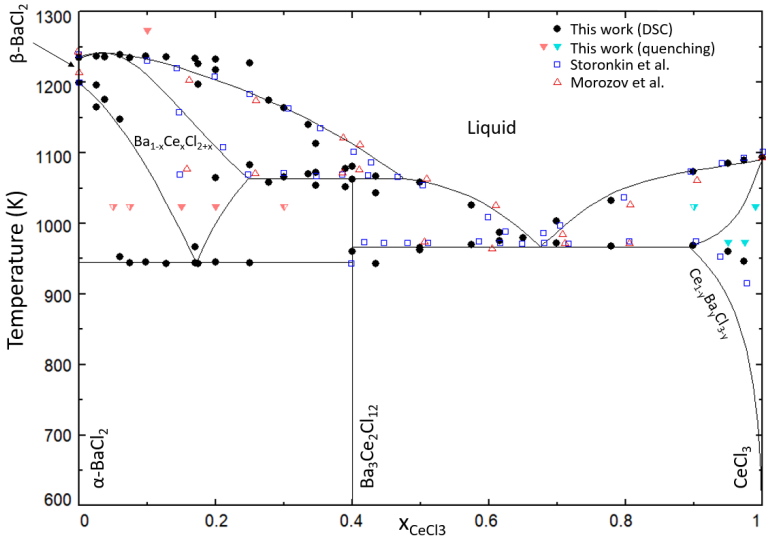


Figure 2.1: Phase diagram of the $BaCl_2$−$CeCl_3$ salt system [1], used to illustrate the purpose of the different experimental techniques as used in this thesis work, which are outlined in this chapter.

The intermediate $Ba_3Ce_2Cl_{12}$ can be synthesised using the sample preparation method described in Section 2.1.1. To characterise the solid solution $Ba_{1-x}Ce_xCl_{2+x}$, which is not thermodynamically stable at room temperature, the quenching procedure that is also outlined in Section 2.1.1 needs to be performed. In both aforementioned cases, the structure and purity of the product can be analyzed with X-Ray Diffraction (XRD, Section 2.1.2) or Neutron Diffraction (ND, Section 2.1.3) to identify phase composition and purity. The standard enthalpy of formation of the intermediate $Ba_3Ce_2Cl_{12}$ can be measured using solution calorimetry (Section 2.1.5). The invariant equilibria in this system,

displayed on the phase diagram as data points, can be measured by performing Differential Scanning Calorimetry (DSC, Section 2.1.4) measurements at various compositions. Finally, the data obtained from all of the aforementioned experiments can be used as input for the thermodynamic modelling outlined in Section 2.3.



### 2.1.1. SAMPLE PREPARATION

Due to the fact that the compounds used in this work are sensitive towards oxygen and atmospheric water, all sample preparation is carried out in a Jacomex GP Concept glove box under dry argon atmosphere ($H_2O, O_2 < 5$ ppm). Weighing is carried out using a Mettler-Toledo XPE105DR balance that has a 0.01 mg uncertainty. The targeted compounds are synthesised by mixing and grinding the end members in a stoichiometric ratio in an agate mortar, and subsequent subjection to thermal treatment in a Borel TU 1600-38-250 tubular furnace. When in the furnace, the atmosphere is continuously flushed with argon to minimize the possibility of oxygen contaminating the sample. All sample containers are composed of a stainless steel outer container and a nickel liner inside to prevent the chlorides from interacting with the stainless steel. A schematic representation of this crucible-and-liner combination is presented in Figure 2.2.

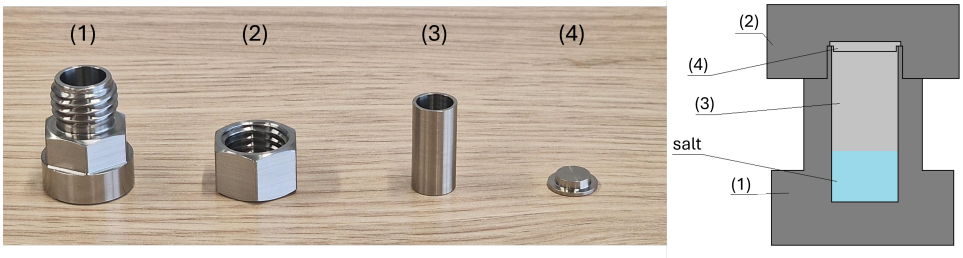


Figure 2.2: Synthesis crucible used in this work, consisting of a stainless steel outer container (1) and screw-cap (2), inside which a nickel liner (3) is placed and covered with a nickel cap (4). The schematic drawing shows the assembled synthesis crucible.

The sample preparation as described in this section is used for the synthesis of intermediate compounds in a fused-salt system that are stable at room temperature.

In some phase diagrams relevant to molten salt systems, phases that are only stable at elevated temperatures exist. To investigate these phases crystallographically and see which phase mixtures are stable at high temperature, a quenching experiment is conducted. In this experiment, a stoichiometric mixture of salts is heated to an appropriate, sample-dependent temperature, and quenched by dropping the sample in a bath of water. For the quenching experiments, it is of utmost importance that no water is able to penetrate into the sample holder in the quenching process, as the investigated compounds are very sensitive towards water. A crucible as shown in Figure 2.3 is used to keep the sample dry and under argon atmosphere.

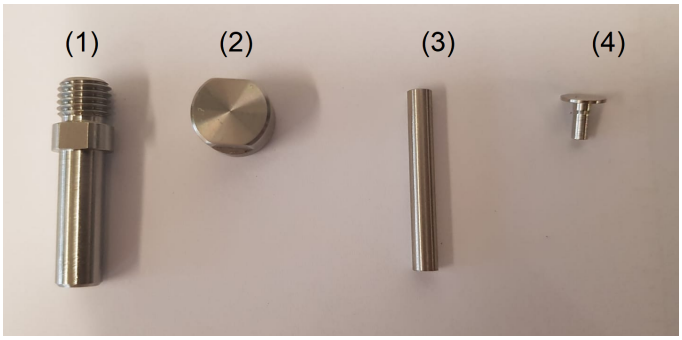


Figure 2.3: Stainless steel crucible (1) with screw-cap from the same material (2), along with a nickel liner (3) and nickel cap (4) to prevent crucible corrosion and ensure optimal airtightness. This type of container is used in quenching experiments and DSC measurements.

The furnace used for quenching is an MTI split vertical quenching tube furnace (OTF-1500X-80-VTQ), which contains an electromagnet that holds the sample in the heated part of the furnace. When the sample is at the desired temperature and has been left to equilibrate for at least two hours, the electromagnet is shut off and the sample is quenched in a bath of water. After drying the container, it can be re-introduced in the glovebox and the sample can be recovered for further analysis.

### 2.1.2. X-RAY DIFFRACTION (XRD)

#### LAB XRD

XRD measurements were carried out using a PANalytical X'pert pro diffractometer with a Cu-anode (0.4 mm x 12 mm line focus, 45 kV, 40 mA). Scattered X-ray intensities were measured with a real-time multi-step detector (X'Celerator). The angle $2\theta$ was set to cover a range from $10^o$ to $120^o$. Measurements were typically performed for 7-8 hours, with a step size of $0.0036^o$/s. Refinement of the measured XRD data was performed by applying the method of Rietveld, Loopstra and van Laar [2, 3], using the FullProf software, Version 5.10 [4].

Because the compounds used in this work are air- and water sensitive, an airthight XRD sample holder is necessary. A schematic of this piece of equipment is shown in Figure 2.4.

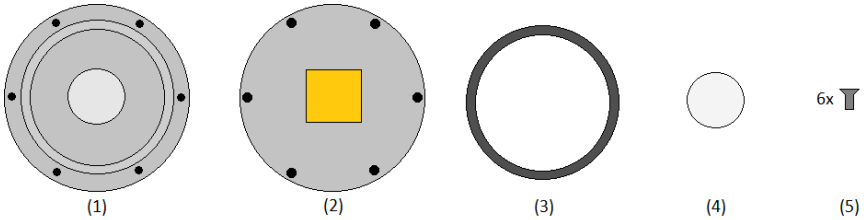


Figure 2.4: The rubber ring (3) facilitates an airtight seal between the top half (2) and bottom half (1) of the sample holder. These two components can be screwed together with the appropriate screws (5) to ensure no air goes inside the sample chamber when taken out of the glove box. The top half contains a kapton window that is transparent to the X-Rays.

In the schematic shown in the above figure, the powdered sample is deposited on the plastic disc (4) and flattened. The result is a cylinder of powder between 3-10 mm in diameter, and approximately 1 mm in height. After loading the sample, the entire sample holder is assembled inside the dry atmosphere of the glovebox and XRD can be performed.

#### SYNCHROTRON XRD

In addition to XRD measurements obtained in our lab, high resolution synchrotron XRD (sXRD) measurements were performed. The resolution of these synchrotron data is much higher than that of the lab XRD, and was used to investigate small impurities that would otherwise be invisible on XRD. The sXRD measurements were performed at the ID22 beamline at ESRF, which has a 9-channel Si 111 multianalyser detector. The wavelength of the synchrotron radiation was $\lambda$ = 0.76533 Å, and the sample was enclosed in a 300 $\mu$m diameter glass capillary sealed with epoxy glue. Data were collected from $0 \leq 2\theta \leq 66^o$.

### 2.1.3. NEUTRON DIFFRACTION (ND)

Neutron diffraction data were recorded on the beamline PEARL at the Hoger Onderwijs Reactor at TU Delft [5]. The data were collected at room temperature, at a fixed wavelength ($\lambda$=1.667 Å) for 12 h over a range of $2\theta$ between 10 and 160 °. Structural analysis was performed by the method of Rietveld, Loopstra and van Laar [2, 3] with the Fullprof suite [6]. For the ND experiment carried out in this work, a specific sample can consisting of a 100 mm x 10 mm cylinder made of vanadium is used. Vanadium was used for this purpose because of its chemical stability and relative transparence to neutrons. A schematic of this sample can is shown in Figure 2.5.

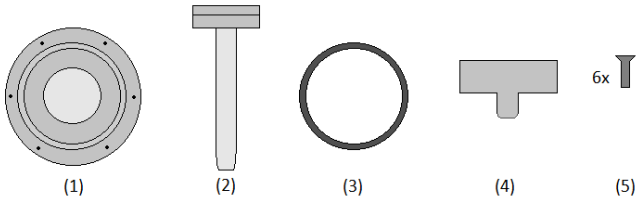


Figure 2.5: Schematic of the ND sample container with a top-down view (1) and side view (2) of the container. The teflon ring (3) facilitates an airtight seal between the lid (4) and vanadium holder (1) of the sample can. These two components can be screwed together with the appropriate screws (5) to ensure the desired airtight seal.

In the figure above, the sample to be measured is deposited in the vanadium holder (1) which is topped off with a Viton O-ring (3). The lid (4) is then placed on top and tightened with screws (5), ensuring an airtight seal.

### 2.1.4. DIFFERENTIAL SCANNING CALORIMETRY (DSC)

The temperatures of invariant equilibria in the investigated systems were measured using a Setaram multi-detector high-temperature calorimeter (MHTC-96 type) equipped with a 3D heat flux DSC module, capable of measuring up to 1673 K. Sample preparation was done by mixing end-members in the desired stoichiometric ratios. The samples were contained in a nickel liner, which in turn was inserted in a tightly closed stainless steel crucible [7], shown in Figure 2.3. Equilibration of the sample was done in the calorimeter itself during the first heating cycle by heating the mixtures to a temperature above the melting points of both end-members. Invariant equilibrium temperatures were collected on the subsequent cycles.

The temperature was monitored throughout the experiments by a series of interconnected S-type thermocouples. The temperature on the heating ramp (10 K·min$^{-1}$) was calibrated and corrected for the effect of the heating rate by measuring the melting points of standard high purity metals (In, Sn, Pb, Al, Ag, Au) at 2-4-6-8-10-12 K·min$^{-1}$. The calibration procedure was performed as recommended by Höne et al. [8] and Gatta et al. [9]. The transition temperatures in the investigated phase diagrams were derived on the heating ramp as the onset temperature using tangential analysis of the recorded heat flow. The liquidus temperature of mixtures was derived from the peak maximum (indicated with "Peak" in Figure 2.6) of the last thermal event. An example of a DSC curve is shown in Figure 2.6. The uncertainty on the measured temperatures is estimated to be ± 5 K for pure compounds and ±10 K for mixtures.

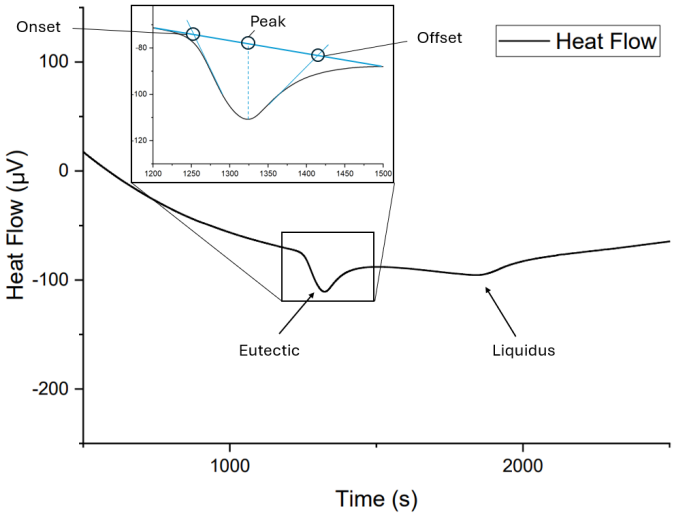


Figure 2.6: Example of a typical DSC curve, showing the heat flow through the sample over time, with peaks corresponding to a eutectic and a liquidus equilibrium. Additionally, the onset, offset and peak temperatures are shown for the eutectic peak.

### 2.1.5. SOLUTION CALORIMETRY

The dissolution enthalpy of intermediate compounds, used to derive their standard enthaply of formation at 298 K, was measured using a TA Instruments Precision Solution Calorimeter (semiadiabatic or isoperibolic calorimeter) and a TAM IV thermostat. The experimental setup consists of a 25 mL Pyrex glass reaction vessel and a motorized gold stirrer, shown in Figure 2.8. The temperature change during dissolution was monitored with a thermistor, while a heater was used for calibration during the measurement and equilibration of the initial baseline in the optimal operating range of the calorimeter (25 ± 0.3 K) before starting the experiment. The sample container was a 1 mL glass ampoule sealed airtight using beewax, also shown in Figure 2.7. Sample preparation was performed inside the dry argon atmosphere of the glovebox, with the airtight sealing being performed in air. The salt was dissolved in 25 mL deionized $H_2O$ by breaking the bottom of the glass ampoule on the sapphire breaking tip mounted on the bottom of the reaction vessel. The heat of breaking of the glass is exothermic with an energy below 10 mJ, and can thus be neglected. The temperature during measurements was maintained in an oil bath with a temperature of 25 ± $10^{-4}$ K. Electrical calibrations were performed before and after each dissolution measurement, so as to determine the energy equivalent of the system.

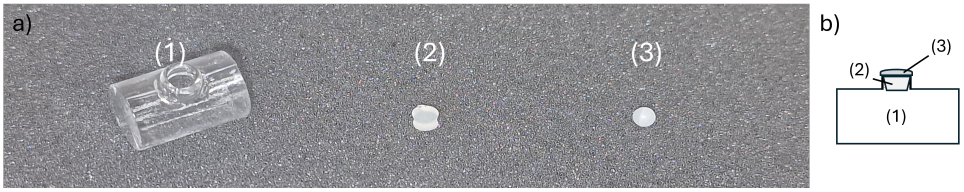


Figure 2.7: Picture (a) and schematic drawing (b) of the container used in solution calorimetry experiments. The thin-walled glass container (1) is filled with the sample, after which the opening on the top is blocked with the stopper (2) and the atmosphere is sealed inside the container by melting the wax (3) over the top.

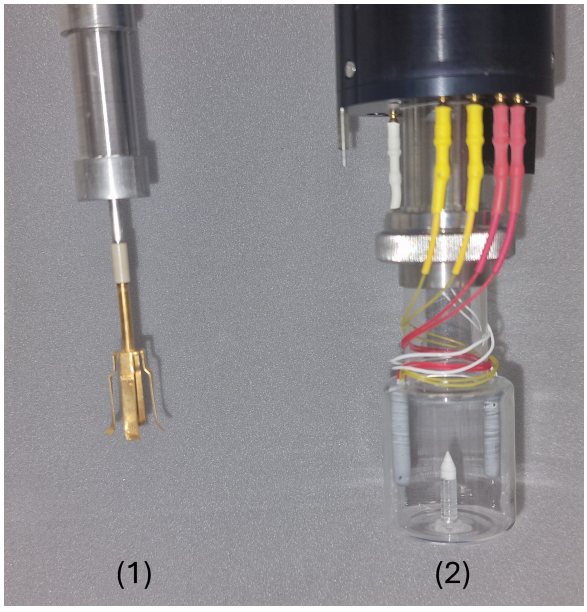


Figure 2.8: TA Instruments Precision Solution Calorimeter experimental setup, showing the gold stirrer (1) where the sample container shown in Figure 2.7 is placed during an experiment and the 25 mL Pyrex reaction vessel (2).

The enthalpy of dissolution of KCl (Sigma Aldrich, 99.7%) in 1000$H_2O$ (distilled water) (molality $m$ = 0.05551 mol·kg$^{-1}$) was first measured to check the instrument accuracy, which yielded $\Delta_{diss}H^o_m$ (1000$H_2O$, 298.15 K) = 17.510 ± 0.024 kJ·mol$^{-1}$. This corresponds to a dissolution enthalpy in 500$H_2O$ equal to $\Delta_{diss}H^o_m$ (500$H_2O$, 298.15 K) = 17.560 ± 0.024 kJ·mol$^{-1}$ after correction, recommended by the National Bureau of Standards (NBS) [10] to $m$ = 0.111 mol·kg$^{-1}$, which is in very good agreement with the value recommended by the NBS [10, 11]: $\Delta_{diss}H^o_m$ (1000$H_2O$, 298.15 K) = 17.584 ± 0.017 kJ·mol$^{-1}$. The measured value corresponds to an enthalpy at infinite dilution of $\Delta_{diss}H^o_m$ ($\infty H_2O$, 298.15 K) = 17.217 ± 0.024 kJ·mol$^{-1}$, in good agreement with the NBS data in refs [10] and [11], $\Delta_{diss}H^o_m$ ($\infty H_2O$, 298.15 K) = 17.241 ± 0.018 kJ·mol$^{-1}$, and that in ref [12], i.e. $\Delta_{diss}H^o_m$ ($\infty H_2O$, 298.15 K) = 17.22 kJ·mol$^{-1}$.

### 2.1.6. PURE COMPOUNDS

All pure compounds used in the experimental part of this work were bought from the supplier, listed in Table 2.1, with the exception of $NdI_3$ and $UCl_3$. The purity of these compounds was verified with XRD and DSC. The $NdI_3$ used in the experiments in this work was synthesised from the elements in a silica ampoule, followed by purification through sublimation [13], by Karl Krämer at Bern University. $UCl_3$ was synthesised through the reduction reaction of elemental silicon with $UCl_4$ from an in-house prepared stock [14]. The purity was confirmed in our lab with XRD and DSC, as shown in Table 2.1.



| Compound | Supplier | CAS No | Reported purity | Melting point (DSC, K)[a] | Melting point (lit., K)[b] |
|---|---|---|---|---|---|
| NaCl | Merck | 7647-14-5 | 99.998% | 1074 | 1074 ± 1 [15] |
| $MgCl_2$ | Thermo-Fischer | 7786-30-3 | 99.99% | 988 | 987 [15] |
| $NdCl_3$ | Thermo-Fischer | 10024-93-8 | 99.99% | 1031 | 1030 ± 2 [16] |
| $CeCl_3$ | Alfa Aesar | 7790-86-5 | 99.9% | 1087 | 1090 ± 2 [16] |
| $UCl_3$ | Nick ter Veer | 10025-93-1 | - | 1112 | 1115 ± 2 [17] |
| $SrCl_2$ | Thermo-Fischer | 10476-85-4 | 99.999% | 1144 | 1147 ± 1 K [15] |
| $BaCl_2$ | Merck | 10361-37-2 | 99.999% | 1235 | 1235 ± 2 [18] |
| CsCl | Alfa Aesar | 7647-17-8 | 99.998% | 925 | 918 [15] |
| NaI | Thermo-Fischer | 7681-82-5 | 99.999% | 934 | 934 [19] |
| $MgI_2$ | Thermo-Fischer | 10377-58-9 | 99.999% | 911 | 912 ± 15 [20] |
| $NdI_3$ | Karl Krämer | 13813-24-6 | 99.9% | 1057 | 1059 ± 2 [16] |
| CsI | Merck | 7789-17-5 | 99.999% | 904 | 905 [19] |

Table 2.1: Pure compounds used in the experiments in this work.
[a] Uncertainty on all values of ± 5 K.
[b] If no uncertainty is listed, it is not reported in the literature

## 2.2. ESTIMATION METHODS

The mathematical definition of the mixing enthalpy ($\Delta H_{mix}$) is given in Eq. 2.1, and is a function of the enthalpy of a mixture ($H_{mixture}$), the enthalpies of the consituent end-members ($H_i$) and their molar fractions ($x_i$). The mixing enthalpy of a molten salt system is an important quantity because it is used as one of the fitting parameters for the CALPHAD models in this work. It allows us to bootstrap the excess Gibbs energy in the thermodynamic models to a physically meaningful value. Without this property, there is a number of possible of combinations of parameters which yield the same modelled phase diagram. However important this property is, there is not always experimental data available to fit to. To remedy this, estimation methods are used, and this section serves to illustrate and motivate which estimation method is most appropriate for the systems of interest.

$$\Delta H_{mix} = H_{mixture} - \Sigma_i x_i H_i \tag{2.1}$$

### 2.2.1. MIXING ENTHALPY ESTIMATION

Unfortunately, the mixing enthalpy is not known for every molten salt system. This is particularly true for systems involving higher actinides, such as plutonium. The absence of experimental mixing enthalpy data is not new, however. Several theories have emerged over hte years trying to predict the mixing enthalpy of binary systems, such as those of Reiss, Katz and Kleppa [21], Blander et al. [22], Davis and Rice [23] and most

recently Schorne-Pinto et al. [24]. The latter two approaches are very similar, as they both rely on the relative sizes of the ions in the molten salt solution through the distance parameter $\delta_{12}$ (in $Å^{-1}$). This distance parameter is defined as in Equation 2.2, where $r$ stands for the ionic radius of the cation or anion. The ionic radii used for this are Shannon radii in sixfold coordination [25].

$$\delta_{12} = \frac{r^{\text{cation}_1} - r^{\text{cation}_2}}{\left(r^{\text{cation}_1} + r^{\text{anion}}\right)\left(r^{\text{cation}_2} + r^{\text{anion}}\right)} \tag{2.2}$$

Davis suggested that for simple binaries, the mixing enthalpy related linearly to the distance parameter $\delta_{12}$. More recent work has shown that, while this is indeed true for simple binaries with relatively small cations, a second-order polynomial expression is often the more accurate choice [24, 26–28] for larger ions. An example of this is given in Figures 2.9-2.11 in which the mixing enthalpy, measured by various authors in the literature [29–33], for the ACl-$MCl_3$ systems (A = Na, K, Cs; M = Ln, Ac) is shown at different compositions. These figures show that there is a quadratic relation between $\delta_{12}$ and the enthalpy of mixing. The error bars in the figure have been taken from the literature when reported, and an error of ± 5% was assumed in case there was no reported error, based on the average reported errors in the literature.

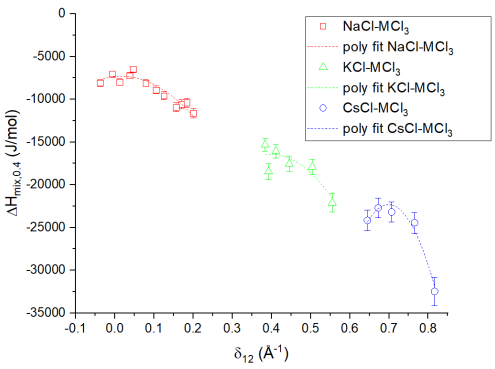


Figure 2.9: Mixing enthalpy of the systems NaCl−$MCl_3$ (M = La, Ce, Nd, Pr, Sm, Gd, Tm, Er, Tb, Yb, Y, U; open red squares) [28, 29, 31–38], KCl−$MCl_3$ (M = La, Ce, Nd, Gd, Y, U; open green triangles) [28–30, 32, 34, 35, 39] and CsCl−$MCl_3$ (M = La, Ce, Nd, Gd, Y; open blue circles) [28–30, 34, 35, 37] at x($MCl_3$) = 0.4 as reported in the literature. Polynomial fits of the mixing enthalpy are shown for the NaCl−$MCl_3$ systems (dashed red line), KCl−$MCl_3$ system (dashed green line) and CsCl−$MCl_3$ systems (dashed blue line).

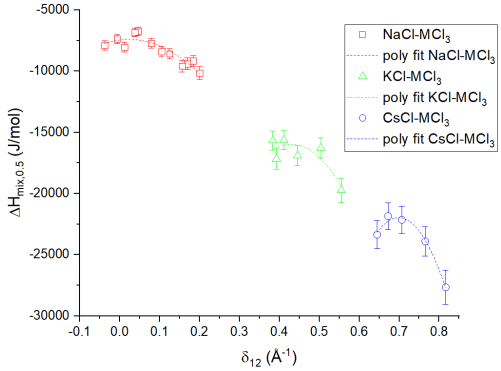


Figure 2.10: Mixing enthalpy of the systems NaCl−$MCl_3$ (M = La, Ce, Nd, Pr, Sm, Gd, Tm, Er, Tb, Yb, Y, U; open red squares) [28, 29, 31–38], KCl−$MCl_3$ (M = La, Ce, Nd, Gd, Y, U; open green triangles) [28–30, 32, 34, 35, 39] and CsCl−$MCl_3$ (M = La, Ce, Nd, Gd, Y; open blue circles) [28–30, 34, 35, 37] at x($MCl_3$) = 0.5 as reported in the literature. Polynomial fits of the mixing enthalpy are shown for the NaCl−$MCl_3$ systems (dashed red line), KCl−$MCl_3$ system (dashed green line) and CsCl−$MCl_3$ systems (dashed blue line).

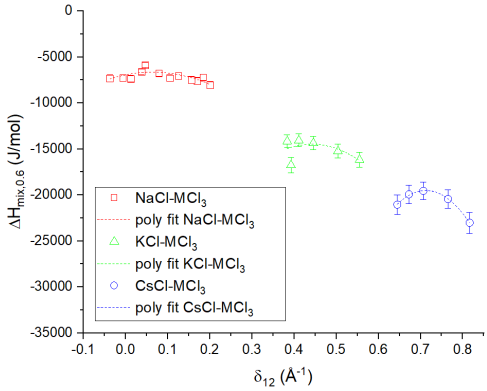


Figure 2.11: Mixing enthalpy of the systems NaCl−$MCl_3$ (M = La, Ce, Nd, Pr, Sm, Gd, Tm, Er, Tb, Yb, Y, U; open red squares) [28, 29, 31–38], KCl−$MCl_3$ (M = La, Ce, Nd, Gd, Y, U; open green triangles) [28–30, 32, 34, 35, 39] and CsCl−$MCl_3$ (M = La, Ce, Nd, Gd, Y; open blue circles) [28–30, 34, 35, 37] at x($MCl_3$) = 0.6 as reported in the literature. Polynomial fits of the mixing enthalpy are shown for the NaCl−$MCl_3$ systems (dashed red line), KCl−$MCl_3$ system (dashed green line) and CsCl−$MCl_3$ systems (dashed blue line).

The figures above show that the relation Davis used to estimate the mixing enthalpy at equimolar composition seems to hold for different compositions too. Schorne-Pinto et al. [24] made this observation as well, while noting that this method is time-consuming.

In addition to the trend observed in Figures 2.9-2.11, *i.e.* corresponding to the change in $M^{3+}$ cation, another trend can be observed in the mixing enthalpy. This is shown in Figures 2.12-2.14, where the same data are viewed with changing alkali cation, rather than the rare earth cation. In these figures, a selection of the data is made to include only the systems in which experimental data have been reported in the literature for all systems ACl−$MCl_3$ (A = Na-Cs; M = Ln, Ac). In general, the mixing enthalpy of a system becomes more negative when the size of the alkali cation increases.

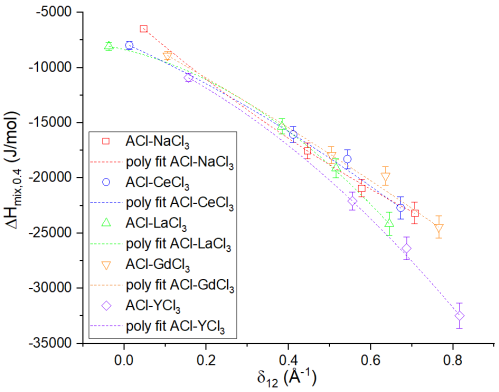


Figure 2.12: Mixing enthalpy of the systems ACl−$LaCl_3$ (A = Na, K, Rb, Cs; open green downward triangles) [29], ACl−$CeCl_3$ (A = Na, K, Rb, Cs; open blue circles) [28], ACl−$NdCl_3$ (A = Na, K, Rb, Cs; open red squares) [30], ACl−$GdCl_3$ (A = Na, K, Rb, Cs; open upward orange triangles) [34] and ACl−$YCl_3$ (A = Na, K, Rb, Cs; open purple diamonds) [35] at x($MCl_3$) = 0.4 as reported in the literature. Polynomial fits of the mixing enthalpy are shown for the ACl−$LaCl_3$ (dashed green line), ACl−$CeCl_3$ (dashed blue line) ACl−$NdCl_3$ (dashed red line), ACl−$GdCl_3$ (dashed orange line) and ACl−$YCl_3$ (dashed purple line) systems.

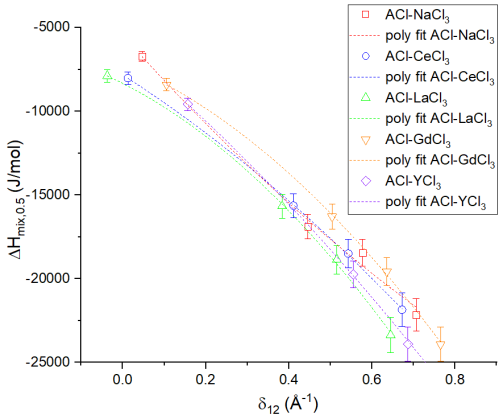


Figure 2.13: Mixing enthalpy of the systems ACl−$LaCl_3$ (A = Na, K, Rb, Cs; open green downward triangles) [29], ACl−$CeCl_3$ (A = Na, K, Rb, Cs; open blue circles) [28], ACl−$NdCl_3$ (A = Na, K, Rb, Cs; open red squares) [30], ACl−$GdCl_3$ (A = Na, K, Rb, Cs; open upward orange triangles) [34] and ACl−$YCl_3$ (A = Na, K, Rb, Cs; open purple diamonds) [35] at x($MCl_3$) = 0.5 as reported in the literature. Polynomial fits of the mixing enthalpy are shown for the ACl−$LaCl_3$ (dashed green line), ACl−$CeCl_3$ (dashed blue line) ACl−$NdCl_3$ (dashed red line), ACl−$GdCl_3$ (dashed orange line) and ACl−$YCl_3$ (dashed purple line) systems.

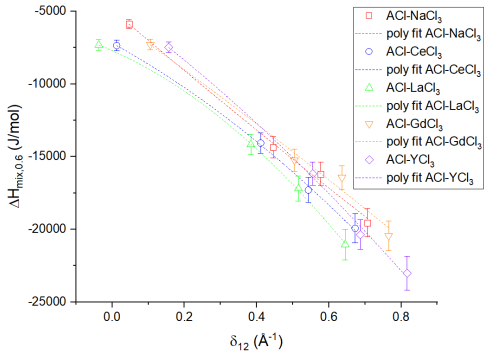


Figure 2.14: Mixing enthalpy of the systems ACl−$LaCl_3$ (A = Na, K, Rb, Cs; open green downward triangles) [29], ACl−$CeCl_3$ (A = Na, K, Rb, Cs; open blue circles) [28], ACl−$NdCl_3$ (A = Na, K, Rb, Cs; open red squares) [30], ACl−$GdCl_3$ (A = Na, K, Rb, Cs; open upward orange triangles) [34] and ACl−$YCl_3$ (A = Na, K, Rb, Cs; open purple diamonds) [35] at x($MCl_3$) = 0.6 as reported in the literature. Polynomial fits of the mixing enthalpy are shown for the ACl−$LaCl_3$ (dashed green line), ACl−$CeCl_3$ (dashed blue line) ACl−$NdCl_3$ (dashed red line), ACl−$GdCl_3$ (dashed orange line) and ACl−$YCl_3$ (dashed purple line) systems.

The trends observed in Figures 2.9-2.14 can be used to estimate the mixing enthalpies of unknown molten salt systems. The only parameter that is necessary for this is the

ionic radius (in sixfold coordination), which has been reported in the literature by Shannon [25] for the elements of interest, given enough available experimental data on similar systems. In this context, similar systems are systems that have one end member in common, while the second end-member is in the same group for both systems (*e.g.* $MgCl_2$–$CeCl_3$ is similar to $BaCl_2$–$CeCl_3$, because Ba and Mg are alkaline-earth metals, but not $FeCl_2$–$CeCl_3$).

The estimation method as described above is used throughout most of this work, with a notable exception. Due to the lack of available data in the literature, the mixing enthalpy of the systems $BaCl_2$–$RECl_3$ (RE = Ce, Nd, Pu, U) could not be estimated based on experimental data. However, the mixing enthalpy of the systems $BaCl_2$–$MCl_3$ (M = Yb, Gd, La) could be estimated based on the reported data for the systems $MgCl_2$–$RECl_3$ [40], $CaCl_2$–$RECl_3$ [40] and $SrCl_2$–$RECl_3$ [41] (RE = Yb, Gd, La). Using the estimated mixing enthalpy of the $BaCl_2$–$MCl_3$ (M = Yb, Gd, La) systems, further extrapolation to the systems $BaCl_2$–$RECl_3$ (RE = Ce, Nd, Pu, U) could be performed to obtain an estimate of their mixing enthalpies.

Schorne-Pinto et al. present a slightly modified version of Davis' method based on the generally asymmetrical shape of the mixing enthalpy curves of charge-asymmetrical systems. While Schorne-Pinto et al. do link the mixing enthalpy to the distance parameter $\delta_{12}$, they also utilise an apparent trend in minima of the mixing enthalpy curves. These minima correspond to the compositions of maximum short-range ordering ($x_{SRO}$) in the melt. By investigating the evolution of $x_{SRO}$ with respect to $\delta_{12}$, they derive a relation between the two that can be used to predict the composition of maximum short-range ordering, and minimum of the mixing enthalpy curve, in systems for which there is no experimental data available. The mixing enthalpy curve can be described using the Surrounded Ion Model (SIM) [42, 43], shown in equations 2.3 and 2.4. In these equations the parameters *p, q, r* and *s* are the charges of the species A, B and X (A,B = different cations; X = common anion) in the system $A_pX_q$–$B_rX_s$. In this work, the anions are always monovalent halides, hence $q$=$s$ = 1. The charge of the cation can vary per system, so $p$ = 1-2 and $q$ = 2-3.

$$\Delta_{mix}H = \left[(1-x)pq + xrs\right]x'(1-x')\left(f_1 + f_2x' + f_3x'^2\right) \tag{2.3}$$

$$x' = \frac{xrs}{\left[(1-x)pq + xrs\right]} \tag{2.4}$$

A comparison between Schorne-Pinto's approach and the approach used in this work, Davis' method, can be drawn to assess their respective performance. To do so, the mixing enthalpy of the molten salt system NaCl-$UCl_3$, for which experimental data are available, is estimated for comparison with the result of the two different estimation methods. Schorne-Pinto's approach uses the minima of the mixing enthalpy curves to determine the composition of maximum short range ordering for each system, which is given in Figure 2.15.

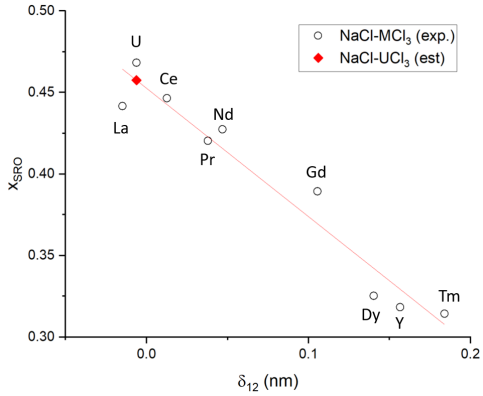


Figure 2.15: Estimation of the composition of maximum short-range ordering ($x_{SRO}$) of the NaCl-$UCl_3$ molten salt system (red diamond) using the approach of Schorne-Pinto et al. [24]

The composition of maximum short-range ordering as shown in Figure 2.15 is assumed to be the minimum of the mixing enthalpy curve as per Schorne-Pinto's approach. The mixing enthalpy at this composition is then estimated by interpolating from the mixing enthalpies of known systems NaCl-$MCl_3$ (M = La, Ce, Nd, Pr, Dy, Gd, Tm, Y) evaluated at their respective compositions of maximum short-range ordering. Doing this yields the estimated minimum value of the mixing enthalpy of the NaCl-$UCl_3$ system. Figure 2.16 shows the estimated value that was obtained using Schorne-Pinto's approach, as well as that obtained using Davis' Method and the experimental data from Matsuura et al. [33].

As seen in Figure 2.16 the estimation method of Schorne-Pinto agrees very well with Davis' Method. There is a slight overestimation compared to the experimental data of Matsuura et al. [33], although the agreement is rather good considering the uncertainties (*i.e.* 6%).

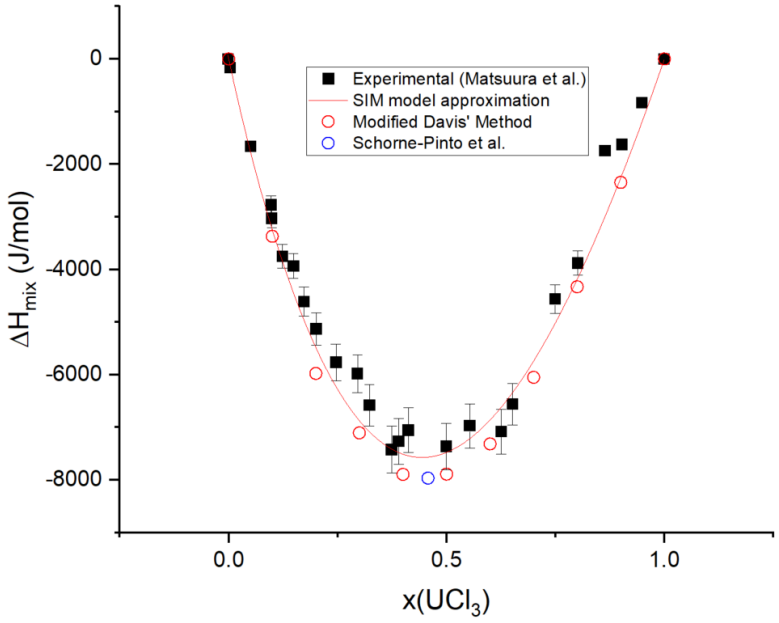


Figure 2.16: Mixing enthalpy of the NaCl-$UCl_3$ system as calculated with Schorne-Pinto's approach (blue circle), Davis' Method (red circles) and experimental data (black squares) [33]. The SIM model based on the experimental data is also shown.

### 2.2.2. METHOD OF CHOICE

As shown in the previous sections, both the estimation method of Davis et al. [23] and that of Schorne-Pinto et al. [24] give good results when predicting the mixing enthalpy of the $NaCl-UCl_3$ salt system. Based on these results alone, the method of Schorne-Pinto et al. might seem the more obvious choice due to its accurate prediction of two properties, those being the composition of maximum SRO and the absolute value of the mixing enthalpy at this composition. The method of Davis, however, also takes this into account to an extent, and gives a more detailed picture of the evolution over the whole composition range. Doing this means that the shape of the mixing enthalpy curve is taken into account as well, which is indirectly tied to the composition of maximum short range ordering. Furthermore, since the method of Schorne-Pinto et al. relies on the composition of maximum short-range ordering, it only works for systems where the mixing enthalpy curve has a single sign, *i.e.* systems where the mixing enthalpy shows either a completely positive, or a completely negative deviation from ideality. In systems such as $CaCl_2-NdCl_3$ or $SrCl_2-YbCl_3$ systems, which are necessary to estimate the mixing enthalpy in $AECl_2-RECl_3$ (AE = alkaline earth; RE = rare earth) systems, the mixing enthalpy curve takes an S-shape. This makes it impossible to take the composition of maximum short range ordering into account, whilst also accounting for the S-shape of the curve.

## 2.3. THERMODYNAMIC MODELLING

The thermodynamic modelling assessment of the molten salt systems was performed with the CALPHAD method [44] using the FactSage software, Version 8.2 [45]. Both experimental data from the literature and obtained in this work were used to adjust the excess parameters of the Gibbs energy functions of the phases present in the systems. The CALPHAD method is based on the minimization of the total Gibbs energy of a system to determine in that way the thermodynamic equilibria for different conditions (*e.g.* composition, temperature, pressure). A schematic of the optimization process using the CALPHAD method is shown in Figure 2.17.

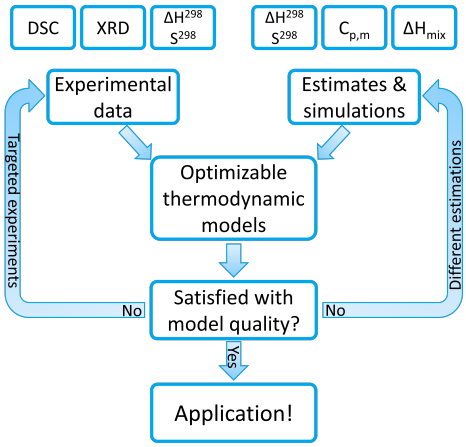


Figure 2.17: Schematic of the CALPHAD method

The goal of thermodynamic modelling in this work is to obtain thermodynamic description that can be used to accurately predict the behaviour of different species of fission products in a molten salt. The models are fit to the available invariant equilibria in the binary and higher order systems, as well as the mixing enthalpy of these systems. In case the enthalpy of fusion ($\Delta H_{melt}$ in kJ·mol$^{-1}$), heat capacity ($c_{p,m}$(T) in J·mol$^{-1}$·K$^{-1}$), standard enthalpy of formation at 298 K ($\Delta_f H^o_m(298)$ in kJ·mol$^{-1}$) or standard entropy at 298 K ($S^o_m(298)$, in J·mol$^{-1}$K$^{-1}$) are known, they are also used as an input for the thermodynamic model, as shown in Figure 2.17.

### 2.3.1. STOICHIOMETRIC COMPOUNDS

The Gibbs energy function for stoichiometric compounds is dependent on the standard enthalpy of formation ($\Delta_f H^o_m(298)$), the standard entropy ($S^o_m(298)$) at the reference temperature of 298.15 K and the heat capacity ($C^o_{p,m}$(T)) as shown in Eq. 2.5 (with T in K).

$$G^o(T) = \Delta_f H^o_m(298) - S^o_m(298)\,T + \int_{298}^{T} C_{p,m}(T)\,dT - T\int_{298}^{T}\frac{C_{p,m}(T)}{T}\,dT \qquad (2.5)$$

The isobaric heat capacity $C_{p,m}$ is expressed as a polynomial that takes the form of Eq. 2.6. The Neumann-Kopp rule was used to determine the heat capacity of intermediate compounds, and the standard enthalpy of formation ($\Delta_f H^o_m(298)$) and standard entropy ($S^o_m(298)$) were optimized to fit the available data.

$$C^o_{p,m}(T) = a + bT + cT^{-2} + dT^2 + eT^{\frac{1}{2}} \tag{2.6}$$

### 2.3.2. LIQUID SOLUTION

The general Gibbs Energy function of a solution is given in Eq. 2.7, and this function applies to liquid and solid solutions.

$$G^o(T) = X_A \cdot G^0_A + X_B \cdot G^0_B + X_A RT ln X_A + X_B RT ln X_B + \Delta G^{excess}_m \tag{2.7}$$

In the above equation, $G^0_i$ are the end-member molar Gibbs energies, and $X_i$ are the molar fractions of the end-members A and B, respectively. The third and fourth terms in Eq. 2.7 represent the configurational entropy. The excess Gibbs energy, $\Delta G^{excess}_m$ in Eq. 2.7, is a measure of how much the mixture of two compounds deviates from the stoichiometric sum of its end-members, *i.e.* the deviation from ideal behaviour. This term also governs the enthalpy of mixing ($\Delta H_{mix}$) and mixing entropy ($S_{mix}$), the former of which is taken from experimental data in the literature, or estimated with the methods outlined in Section 2.2.1.

The excess Gibbs energy terms of the liquid solution are modelled using the quasi-chemical formalism in the quadruplet approximation as proposed by Pelton et al. [46] which has proven to be well-adapted to molten chloride and fluoride systems. This description assumes the existence of cation-anion quadruplets in the liquid, allowing for the modelling of short-range ordering. A schematic representation of a quadruplet is given in Figure 2.18. This formalism allows for the selection of the composition of maximum short-range ordering through its coordination numbers, corresponding to the minimum of the Gibbs energy that is often found near the composition of the lowest eutectic. By fixing either the cation-cation or anion-anion coordination number, the opposite coordination number is also obtained through Eq. 2.8 to respect electroneutrality, where $q_i$ are the charges of the respective ions. The coordination numbers used in the thermodynamic model presented in this work are given in Table **??**.

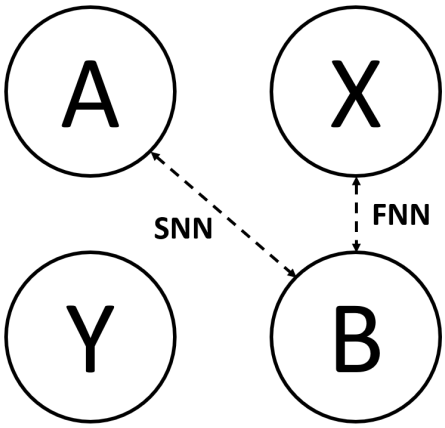


Figure 2.18: Example of a quadruplet AB//XY, where A and B are cations and X and Y are anions. Also indicated are the first-nearest neighbor (FNN) and second-nearest neighbor (SNN) of the chlorine ion.

.

$$\frac{q_A}{Z^A_{AB/XY}} + \frac{q_B}{Z^B_{AB/XY}} = \frac{q_X}{Z^X_{AB/XY}} + \frac{q_Y}{Z^Y_{AB/XY}} \tag{2.8}$$

The excess parameters that are optimized are those related to the second-nearest neighbour exchange reactions as given in Eqs. 2.9-2.11. The associated change in Gibbs energy of Eqs. 2.9-2.11 is expressed in Eqs. 2.12-2.14.

$$(A_2X_2)_{quad} + (B_2X_2)_{quad} \longrightarrow 2(ABX_2)_{quad} \qquad \Delta g_{AB/XX} \tag{2.9}$$

$$(A_2X_2)_{quad} + (A_2Y_2)_{quad} \longrightarrow 2(A_2XY)_{quad} \qquad \Delta g_{AA/XY} \tag{2.10}$$

$$(ABX_2) + (ABY_2) + (A_2XY) + (B_2XY) \longrightarrow 4(ABXY) \qquad \Delta g_{AB/XY} \tag{2.11}$$

$$\Delta g_{AB/XX} = \Delta g^0_{AB/XX} + \Sigma_{i\geq 1} g^{i0}_{AB/XX} \chi^i_{AB/XX} + \Sigma_{j\geq 1} g^{0j}_{AB/XX} \chi^j_{BA/XX} \tag{2.12}$$

$$\Delta g_{AA/XY} = \Delta g^0_{AA/XY} + \Sigma_{i\geq 1} g^{i0}_{AA/XY} \chi^i_{AA/XY} + \Sigma_{j\geq 1} g^{0j}_{AA/XY} \chi^j_{AA/YX} \tag{2.13}$$

$$\begin{aligned} \Delta g_{AB/XY} = \Delta g^0_{AB/XY} + \Sigma_{i\geq 1} ( & g^i_{AB/XY(AX)} \chi^i_{AA/XX} + g^i_{AB/XY(BX)} \chi^j_{BB/XX} \\ & + g^i_{AB/XY(AY)} \chi^j_{AA/YY} + g^i_{AB/XY(BY)} \chi^j_{BB/YY} ) \end{aligned} \tag{2.14}$$

In Eq. 2.12-2.14 the g-terms (*e.g.* $\Delta g^{0}_{AB/XX}$, $g^{i0}_{AA/XY}$, $g^{i}_{AB/XY(AY)}$) are composition-independent coefficients that may depend on temperature. The composition dependence of the Gibbs energy is apparent through $\chi_{AB/XX}$ as these are defined as per Eq. 2.15. In this equation $X_{AA/XX}$ is the cation-cation pair fraction, or the molar fraction of the quadruplet containing two cations A. The fractions of the other quadruplets $\chi_{AB/YY}$, $\chi_{AA/XY}$ and $\chi_{BB/XY}$ are defined in the same way as $\chi_{AB/XX}$ in Eq. 2.16, where $\Sigma n_{ij/kl}$ (i,j = A,B; k,l = X,Y) is the tital amount of moles of quadruplets. For a binary system, $\{X_{AA} + X_{AB} + X_{BB}\}$ is equal to one.

$$\chi_{AB/XX} = \frac{X_{AA/XX}}{X_{AA/XX} + X_{AB/XX} + X_{BB/XX}} \tag{2.15}$$

$$\chi_{AB/XY} = \frac{n_{AB/XY}}{\Sigma n_{ij/kl}} \tag{2.16}$$

When the extrapolation to higher order systems (ternary, quaternary, etc.) is made, Eq. 2.15 becomes more complicated depending on whether there is asymmetry in the system. The pure end-member liquid salts investigated in this work can be classified in one of two categories: ionic liquids (such as NaCl, CsI, etc.) and liquids that form molecular complexes (such as $NdCl_3$, $MgCl_2$). If the components in a system belong to the same group, that system is considered symmetrical, otherwise it is asymmetrical. Using the data for the binary systems as a basis, extrapolations to the ternary and quaternary fields are made with Kohler/Toop interpolations [47, 48]. The choice of interpolation method depends on whether a system can be considered symmetric (Kohler) or asymmetric (Toop).

To determine the composition dependence of the excess Gibbs energy in higher order systems, the probability of finding a certain quadruplet is used. This probability is calculated using Eq. 2.17 [46].

$$\chi_{AB/XY} = 4X_{A/X}(X_{A/Y}/Y_A)(X_{B/Y}/Y_Y)(X_{B/X}/Y_B Y_X) \tag{2.17}$$

$$X_{A/X} = \frac{n_{A/X}}{\Sigma n_{i/k}} \tag{2.18}$$

In the above equation, $\chi_{AB/XY}$ is the probability of finding the quadruplet AB/XY. $X_{A/X}$ (Eq. **??**, i = A,B; k = X,Y) is the probability that the first pair is an A-X pair, while the terms $X_{A/Y}/Y_A$, $X_{B/Y}/Y_Y$ and $X_{B/X}/Y_B Y_X$ are conditional probabilities that pairs 2, 3 and 4 are A-Y, B-Y and B-X respectively. These pairs are also shown in Figure 2.19. The conditions in these probabilities are expressed through the $Y_i$ terms, meaning that the term $X_{A/Y}/Y_A$ is the probability of finding pair A-Y as second pair ($X_{A/Y}$), given that the first pair contained A ($1/Y_A$).

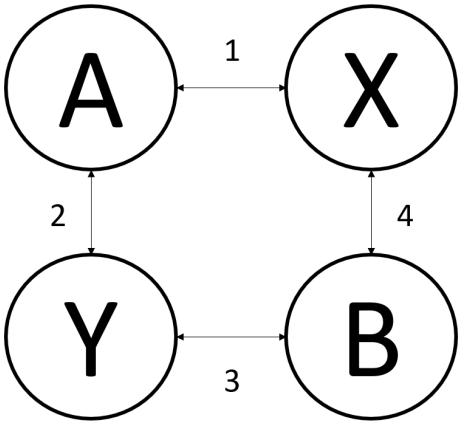


Figure 2.19: AB/XY quadruplet with pairs A-X, A-Y, B-Y and B-X labelled as 1, 2, 3 and 4 respectively. Figure reproduced from Pelton et al. [46].

### 2.3.3. SOLID SOLUTION MODELLING

The thermodynamic description of solid-solutions is done using a two-sublattice polynomial model to be consistent with the description of the JRC Molten Salt Database (JRCMSD) [49]. The excess Gibbs energy of a solid solution, present in Eq. 2.7 as $\Delta G_m^{excess}$, is defined as per Eq. 2.19.

$$\Delta G_m^{excess} = \Sigma_{i,j\geq 1} y_A^i y_B^i L_{AB}^{ij} \tag{2.19}$$

The term $L_{AB}^{ij}$ in Eq. 2.19 is an interaction coefficient that can be a function of temperature if necessary. The equivalent site fractions $y_A$ and $y_B$ are charge equivalent site fractions defined as in Eq. 2.21, where the term $q^i$ is the charge of species *i*.

$$y_A = \frac{q^A X_A}{q^A X_A + q^B X_B} \tag{2.20}$$

$$y_B = \frac{q^B X_B}{q^A X_A + q^B X_B} \tag{2.21}$$

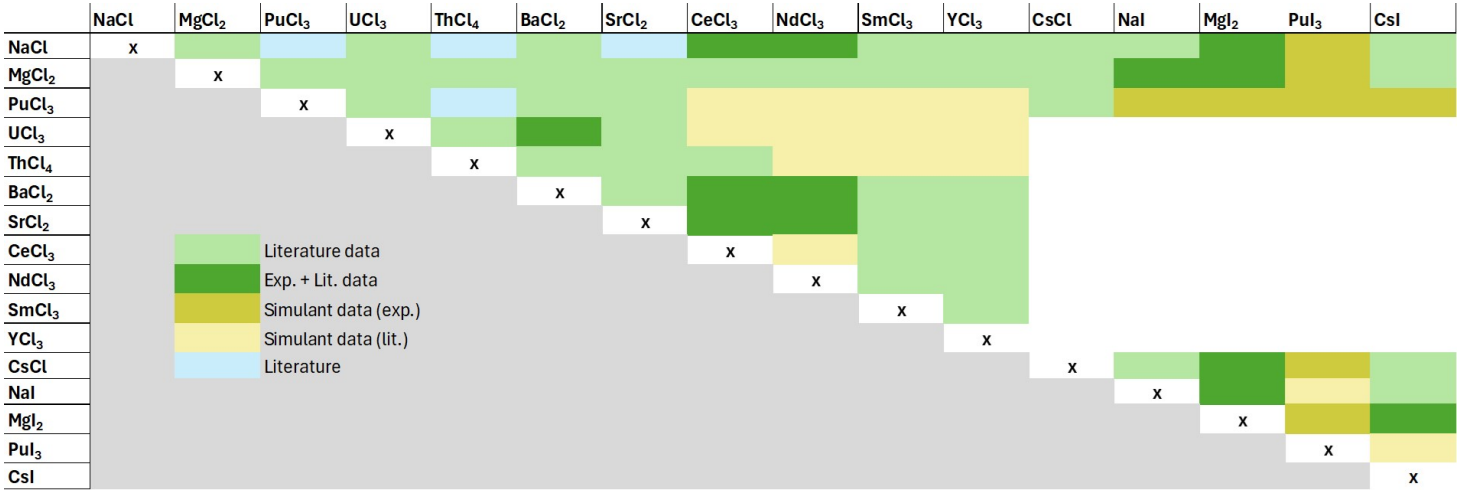


Figure 2.20: Overview of the binary salt systems modelled in this work. The color-coding corresponds to the origin of the thermodynamic model: based on data from the literature (light green), based on own experimental data and/or data from the literature (green), based on own simulant data (olive), based on simulant data from the literature (yellow) or taken entirely from the literature (blue).

## 2.4. THERMODYNAMIC DATABASE

An overview of the assessed binary systems in this dissertation is given in Figure 2.20. The origin of each thermodynamic model is shown in the figure, *e.g.* green for systems where the thermodynamic model is based on own experimental data and/or data from the literature.



### 2.4.1. STOICHIOMETRIC COMPOUNDS

The thermodynamic functions of the stoichiometric compounds included in the thermodynamic database are presented in Table 2.2. They are presented in the following order: first, the thermodynamic functions for the base fuel(s) (NaCl, $MgCl_2$, $PuCl_3$, $UCl_3$, $ThCl_4$), then the soluble fission products ($BaCl_2$, $SrCl_2$, $CeCl_3$, $NdCl_3$, $SmCl_3$, $YCl_3$), and subsequently the volatile fission products (all species with Cs and/or I). Finally, the thermodynamic functions of the intermediate compounds are given, following the same order.

The thermodynamic functions for $NdCl_3$ and $CeCl_3$ were taken from the critical review by Konings and Kovács [16]. The thermodynamic functions for $BaCl_2$ were taken from the IVTAN thermochemical database [18]. The thermodynamic functions for $SrCl_2$ were taken from the JANAF thermochemical tables [15]. A polymorphic transition is reported in the aforementioned tables for $SrCl_2$ with a transition enthalpy of 6 $kJ{\cdot}mol^{-1}$ that was not included in the current thermodynamic modelling assessment. This transition is of second-order, from a cubic structure to a slightly distorted cubic structure, that does not appear in phase equilibria measurements [50]. The thermodynamic functions of NaCl, used in the assessment of the ternary systems, were taken from van Oudenaren et al. [27], who reviewed the available thermodynamic data in their work.

The thermodynamic functions used in this work for $ThCl_4$ were taken from the recommendations by Rand et al. [51] and Capelli et al. [17]. The thermodynamic functions for $UCl_3$(s) and $PuCl_3$(s,l) were also taken from the review by Capelli and Konings [17], and the functions for $UCl_3$(l) were taken from the reassessment by van Oudenaren et al. [27].

Thermodynamic data for NaI, $MgCl_2$ and $MgI_2$ were taken from the JANAF thermochemical database [15]. It should be noted that the heat capacities of NaI and $MgI_2$ as reported in the JANAF thermochemical database are estimated values, rather than experimental data. The thermodynamic functions for $NdI_3$ were taken from the IVTAN thermochemical database [20], and are in good agreement with the review by Konings et al. [16]. The thermodynamic properties of $PuI_3$ were taken from the Barin thermochemical tables [52], which is in good agreement with the functions presented in the OECD-NEA handbook. The thermodynamic functions for CsCl were taken from the JANAF tables [15], and the thermodynamic functions for CsI were taken from the critical review by Roki et al. [53].

Many intermediate compounds also exist in the systems covered in this dissertation. The heat capacity of all intermediate compounds was calculated using the Neumann-Kopp rule, and the standard enthalpy of formation at 298 K and standard entropy at 298 K were optimized. The exceptions to this are the intermediates $NaMgCl_3$ and $Na_2MgCl_4$,

for which Chartrand et al. [54] report heat capacity functions that are used instead of the Neumann-Kopp rule.

Table 2.2: Thermodynamic functions used in the CALPHAD model in this work. The heat capacity is expressed as the following polynomial: $C_{p,m}(T) = a + bT + cT^{-2} + dT^2$. Optimized values are marked in bold.

| **Compound** | $\Delta_f H^o_m$ **(298)** ($J \cdot mol^{-1}$) | $S^o_m$ **(298)** ($J \cdot K^{-1} \cdot mol^{-1}$) | $C_{p,m}$ **(T)** ($J \cdot K^{-1} \cdot mol^{-1}$) **= a + bT + cT$^{-2}$ + dT$^2$ + eT$^{-0.5}$** | | | | | Temperature range (K) | Source |
|---|---|---|---|---|---|---|---|---|---|
| | | | a | b | c | d | e | | |
| NaCl(s) | -411,260 | 72.15 | 47.72158 | 0.0057 | -882.996 | $1.21466 \cdot 10^{-5}$ | | [298-1074] | [27] |
| NaCl(l) | -390,853 | 83.302 | 47.72158 | 0.0057 | -882.996 | $1.21466 \cdot 10^{-5}$ | | [1074-2500] | [55] |
| NaCl(l) | | | 68 | | | | | [1074-2500] | [55] |
| $MgCl_2$(s) | -641,616 | 89.629 | 54.5843 | 0.0214213 | -1,112,119 | $-2.3567 \cdot 10^{-6}$ | 399.177 | [298-2000] | [15] |
| $MgCl_2$(l) | -601,680.1 | 129.236 | 193.4089 | -0.3620139 | -3,788,504 | $3.199871 \cdot 10^{-4}$ | | [298-660] | [15] |
| | | | 92.048 | | | | | [660-2500] | [15] |
| $PuCl_3$(s) | -959,600 | 161.4 | 91.412 | 0.03716 | | 27,400 | | [298-1041] | [17] |
| $PuCl_3$(l) | -931,116 | 170.46 | 144 | | | | | [298-1500] | [17] |
| $UCl_3$(s) | -863,700 | 163.9 | 106.967 | -0.0208595 | -129,994 | $3.6389 \cdot 10^{-5}$ | | [298-1100] | [17] |
| $UCl_3$(l) | -846,616 | 152.919 | 151.1 | | | | | [1100-2500] | [27] |
| $ThCl_4$(s) | -1,186,300 | 183.499 | 120 | 0.0232672 | -615,050 | | | [298-1043] | [17], [55] |
| $ThCl_4$(l) | -1,149,716 | 197.71 | 167.4 | | | | | [1043-2500] | [17], [55] |
| $ThCl_4$(g) | -961370.2 | 399.297 | 106.056 | 0.001363984 | | | | [298-2000] | [52] |
| $\alpha$-$BaCl_2$(s) | -855,200 | 123.7 | 69.371 | $1.912548 \cdot 10^{-2}$ | 5882.698 | $2.499235 \cdot 10^{-9}$ | | [298-1198] | [18] |
| $\beta$-$BaCl_2$(s) | -837,800 | 138.22 | 131 | | | | | [1198-1234] | [18] |
| $BaCl_2$(l) | -821,950 | 151.07 | 109 | | | | | [1234-2500] | [18] |
| $SrCl_2$(s) | -828,850.4 | 114.809 | 79.4826 | $-1.7920 \cdot 10^{-3}$ | -440859.7 | $1.798911 \cdot 10^{-5}$ | | [298-600] | [15] |
| | | | 194.5439 | -0.246728 | -8159846 | $1.6616 \cdot 10^{-4}$ | | [600-1000] | [50] |
| | | | 123.0096 | | | | | [1000-1147] | [50] |
| $SrCl_2$(l) | -812,629 | 128.9515 | 104.6 | | | | | [1147-2500] | [15] |
| $CeCl_3$(s) | -1,059,700 | 151 | 90.9772 | 0.03581 | -271,530 | | | [298-1095] | [16] |
| $CeCl_3$(l) | -1,006,100 | 200.17 | 161.05 | | | | | [1095-3000] | [16] |
| $NdCl_3$(s) | -1,041,816 | 153.43 | 109.08 | $1.641 \cdot 10^{-2}$ | -1,309,950 | | | [298-1032] | [16] |
| $NdCl_3$(l) | -993,716 | 200.04 | 150 | | | | | [1095-3000] | [16] |
| $SmCl_3$(s) | -1,025,300 | 150.1 | 95.3748 | 0.0334442 | -561,350 | | | [298-950] | [16] |
| $SmCl_3$(l) | -977,700 | 200.205 | 144.4 | | | | | [950-3000] | [16] |
| $YCl_3$(s) | -999,976 | 136.817 | 104.7124 | $3.224066 \cdot 10^{-3}$ | -1,211,303 | $-2.0521 \cdot 10^{-9}$ | | [298-994] | [16] |
| $YCl_3$(l) | -968,512.3 | 168.471 | 135.712 | | | | | [994-1700] | [16] |
| $\alpha$-CsCl(s) | -442,834.6 | 101.1817 | 45.8566 | 0.0220957 | | | | [298-2000] | [15] |
| $\beta$-CsCl(s) | -441,267.3 | 101.2143 | 59.7308 | 0.0049371 | | | | [298-2000] | [15] |
| CsCl(l) | -434,462 | 77.404 | | | | | | [298-2000] | [15] |
| NaI(s) | -289,630 | 98.56 | 41.97056 | 0.0251811 | 232,099.4 | $4.761618 \cdot 10^{-9}$ | | [298-934] | [15] |
| NaI(l) | -271,470 | 112.518 | 67 | | | | | [934-3400] | [15] |
| $MgI_2$(s) | -370,000 | 134 | 68.94675 | 0.01854692 | -237.9452 | $1.12469 \cdot 10^{-8}$ | | [298-906] | [15] |
| $MgI_2$(l) | -344,000 | 162.698 | 68.94675 | 0.01854692 | -237.9452 | $1.12469 \cdot 10^{-8}$ | | [298-906] | [15] |
| | | | 100 | | | | | [906-2000] | [15] |

Continued on next page

**Table 2.2 – continued from previous page**

| Compound | $\Delta_f H^o_m(298)$ ($J{\cdot}mol^{-1}$) | $S^o_m(298)$ ($J{\cdot}K^{-1}{\cdot}mol^{-1}$) | $C_{p,m}(T)$ ($J{\cdot}K^{-1}{\cdot}mol^{-1}$) = a + bT + $cT^{-2}$ + $dT^{2}$ + $eT^{-0.5}$ | | | | | Temperature range (K) | Source |
|---|---|---|---|---|---|---|---|---|---|
| | | | a | b | c | d | e | | |
| $MgI_2$(g) | -171,706 | 313.814 | 62.24059 | $5.934506{\cdot}10^{-5}$ | -260,628.2 | $-7.109508{\cdot}10^{-9}$ | | [298-6000] | [15] |
| $\alpha$-$NdI_3$(s) | -643,000 | 218 | 133.254 | -0.0763089 | | -1,657,700 | | [298-847] | [20] |
| $\beta$-$NdI_3$(s) | -619,100 | 234.411 | 117 | | | | | [847-1060] | [20] |
| $NdI_3$(l) | -587,600 | 273.562 | 156 | | | | | [1060-3000] | [20] |
| $PuI_3$(s) | -579,902 | 214.221 | 105.683 | 0.0205979 | $-7.91{\cdot}10^{-9}$ | 140 | | [298-1050] | [52] |
| $PuI_3$(l) | -529,694 | 262.038 | 142.256 | | $2{\cdot}10^{-11}$ | -80 | | [1050-1500] | [52] |
| CsI(s) | -348,100 | 122.2 | 43.815 | 0.0218422 | $2.495766{\cdot}10^{-6}$ | 200,247.2 | | [298-905] | [53] |
| CsI(l) | -331,911.611 | 131.8996 | 74.268 | | | | | [298-2000] | [53] |
| CsI(g) | -153,300 | 275.817 | 37.886 | $3.058{\cdot}10^{-5}$ | -0.0004535 | $4.913{\cdot}10^{-7}$ | | [298-3000] | [53] |
| $Cs_2I_2$(g) | -469,200 | 431.181 | 81.14328 | $6.384707{\cdot}10^{-7}$ | -41,474.24 | $8.06363{\cdot}10^{-11}$ | | [298-6000] | [53] |
| **Intermediate compounds** | | | | | | | | | |
| $NaMgCl_3$(s) | **-1,063,200** | **155.5** | 90 | 0.075 | | | | [298-1000] | [54], this work |
| $Na_2MgCl_4$(s) | **-1,486,000** | **211** | 135 | 0.1125 | | | | [298-773] | [54], this work |
| $Na_6MgCl_8$ | **-3,148,000** | **481.5** | 340.9138 | 0.055621 | -1,117,417 | $7.05{\cdot}10^{-5}$ | 399.177 | [298-6000] | This work |
| $Na_2Mg_3Cl_8$ | **-2,766,000** | **410** | 252.3333 | 0.059943 | -2,226,887 | $3.17{\cdot}10^{-5}$ | 798.354 | [298-6000] | This work |
| $NaPu_2Cl_7$ | **-2,331,000** | **404** | 230.5456 | 0.08002 | 53,977.004 | $1.21466{\cdot}10^{-5}$ | | [298-1500] | This work |
| $NaNd_2Cl_7$ | **-2,508,000** | **379.15** | 265.88958 | 0.038512 | 2,620,782.996 | $1.21466{\cdot}10^{-5}$ | | [298-1500] | This work |
| $NaCe_2Cl_7$ | **-2,542,000** | **374.15** | 229.676 | 0.0773246 | 543,882.996 | $1.21466{\cdot}10^{-5}$ | | [298-1500] | This work |
| $NaU_2Cl_7$ | **-2,112,623** | **438** | 261.65558 | 0.036019 | -260,870.996 | $8.49246{\cdot}10^{-5}$ | | [298-1500] | This work |
| $Na_2ThCl_6$ | -2,051,540 | 328 | 215.7362 | 0.034667 | -616,816 | $2.43{\cdot}10^{-5}$ | | [298-1500] | Dumaire et al. [55] |
| $U_3ThCl_{13}$(s) | **-3,771,000** | **695** | 441.194 | -0.03931 | -1,005,032.00 | 0.000109 | | [298-1500] | This work |
| $Ba_3Ce_2Cl_{12}$ | **-4,711,000** | **689.5** | 390.07 | 0.129 | -525,411.69 | $7.4977{\cdot}10^{-9}$ | | [298-2500] | [1], this work |
| $Ba_3Nd_2Cl_{12}$ | **-4,641,500** | **682** | 486.28 | 0.0902 | -2,602,251.9 | $7.2{\cdot}10^{-9}$ | | [298-1500] | [50], this work |
| $Ba_3Pu_2Cl_{12}$ | **-4,473,000** | **737** | 390.937 | 0.13169644 | -72,448.094 | $7.49771{\cdot}10^{-9}$ | | [298-1500] | This work |
| $Ba_3U_2Cl_{12}$(s) | **-4,380,530** | **650** | 422.047 | 0.01565744 | -242,340 | $7.2785497705{\cdot}10^{-5}$ | | [298-1500] | This work |
| $Ba_3ThCl_{10}$(s) | **-3,770,000** | **555** | 328.406 | 0.08064364 | -597,401.91 | $7.49771{\cdot}10^{-9}$ | | [298-1500] | This work |
| $Ba_3Th_2Cl_{14}$(s) | **-4,965,000** | **738** | 448.699 | 0.10391084 | -1,212,452 | $7.49771{\cdot}10^{-9}$ | | [298-1500] | This work |
| $Sr_9Nd_5Cl_{33}$ | **-12,789,000** | **1800** | 846.40 | 0.8009 | -8,132,324.4 | | | [298-1500] | [50], this work |
| $Sr_9Ce_5Cl_{33}$ | **-12,908,000** | **1639** | 1170.229 | 0.162933 | -5,325,387 | $1.62{\cdot}10^{-4}$ | | [298-1500] | This work |
| $Sr_3PuCl_9$ | **-3,449,000** | **506.127** | 329.79783 | 0.018624 | -1,082,579.1 | $5.396733{\cdot}10^{-5}$ | | [298-1500] | This work |
| $SrUCl_5$(s) | **-1,686,819** | **299** | 186.444961 | -0.022652036 | -570,760 | $5.44{\cdot}10^{-5}$ | | [298-1500] | This work |
| $CsMgCl_3$(s) | **-1,133,000** | **182** | 144.46 | | | | | [298-900] | This work |
| $Cs_2MgCl_4$(s) | **-1,600,000** | **257** | 230 | | | | | [298-900] | This work |
| $Cs_3MgCl_5$(s) | **-2,052,000** | **367** | 192.1541 | 0.087708 | $-2.4{\cdot}10^{-6}$ | -1,112,119 | 399.177 | [298-873] | This work |
| $CsMg_3Cl_7$(s) | **-2,415,000** | **370** | 253.6286 | 0.042843 | $-4.7{\cdot}10^{-6}$ | -2,224,238 | 798.354 | [298-1000] | This work |
| $\alpha$-$Cs_3NdCl_6$(s) | **-2,432,000** | **509** | 246.6538 | 0.08269 | | -1,309,950 | | [298-1500] | This work |
| $\beta$-$Cs_3NdCl_6$(s) | **-2,431,000** | **510.4749263** | 246.6538 | 0.08269 | | -1,309,950 | | [298-1500] | This work |

Continued on next page

Table 2.2 – continued from previous page

| Compound | $\Delta_f H^o_m(298)$ ($J{\cdot}mol^{-1}$) | $S^o_m(298)$ ($J{\cdot}K^{-1}{\cdot}mol^{-1}$) | $C_{p,m}(T)$ ($J{\cdot}K^{-1}{\cdot}mol^{-1}$) = a + bT + $cT^{-2}$ + $dT^{2}$ + $eT^{-0.5}$ | | | | | Temperature range (K) | Source |
|---|---|---|---|---|---|---|---|---|---|
| | | | a | b | c | d | e | | |
| $CsNd_2Cl_7$(s) | **-2,549,000** | **444** | 264.0246 | 0.054908 | | -2,619,900 | | [298-1500] | This work |
| $\alpha$-$Cs_3PuCl_6$(s) | **-2,324,000** | **539** | 256.6609 | 0.034496 | $7.13{\cdot}10^{-8}$ | -741,057 | | [298-1500] | This work |
| $\beta$-$Cs_3PuCl_6$(s) | **-2,323,000** | **540.4705882** | 256.6609 | 0.034496 | $7.13{\cdot}10^{-8}$ | -741,057 | | [298-1500] | This work |
| $CsPu_2Cl_7$(s) | **-2,377,000** | **472** | 237.8036 | 0.051499 | $2.38{\cdot}10^{-8}$ | 152,981.10 | | [298-1500] | This work |
| $Na_2SmCl_5$(s) | **-1,846,000** | **310** | 190.81796 | 0.0448442 | 559584.008 | 2.42932E-05 | | [298-1500] | This work |
| $Na_3Sm_5Cl_{18}$(s) | **-6,367,000** | **980** | 620.03874 | 0.184321 | 2804101.012 | 3.64398E-05 | | [298-1500] | This work |
| $Sr_9Sm_5Cl_{33}$(s) | **-12,600,000** | **1802** | 1192.2174 | 0.151093 | -1160987.3 | 0.000161902 | | [298-1500] | This work |
| $Cs_2SmCl_5$(s) | **-1,979,900** | **386** | 3.6616 | -0.0107472 | 561350 | -1.02605E-08 | | [298-1500] | This work |
| $Cs_3SmCl_6$(s) | **-2,455,000** | **495** | 232.9446 | 0.0997313 | 561350 | 0.000121466 | | [298-1500] | This work |
| $CsSm_2Cl_7$(s) | **-2,516,000** | **458** | 236.6062 | 0.0889841 | 1122700 | 0.000182181 | | [298-1500] | This work |
| $BaSmCl_5$(s) | **-1,886,000** | **280** | 164.7458 | 0.05256968 | 567232.698 | 0.001028149 | | [298-1500] | This work |
| $Ba_2SmCl_7$(s) | **-2,744,600** | **411** | 234.1168 | 0.07169516 | 573115.396 | 0.000327907 | | [298-1500] | This work |
| $Ba_3SmCl_9$(s) | **-3,598,600** | **540** | 303.4878 | 0.09082064 | 578998.094 | 0.002064448 | | [298-1500] | This work |
| $NaYCl_4$(s) | **-1,411,950** | **218** | 152.434 | 0 | -1,212,185.996 | 1.21E-05 | | [298-508] | This work |
| | **-1,410,950** | **219.969** | 152.434 | 0.009 | -1,212,185.996 | 0.000 | | [508-544] | This work |
| | **-1,409,950** | **211.807** | 152.434 | 0.009 | -1,212,185.996 | 0.000 | | [544-1500] | This work |
| $Na_3YCl_6$(s) | **-2,228,400** | **390** | 247.87714 | 0.020324066 | -1213951.988 | 3.64377E-05 | | [298-1500] | This work |
| $NaY_9Cl_{28}$(s) | **-9,410,000** | **1333** | 990.13318 | 0.034716594 | -10902610 | 1.21281E-05 | | [298-1500] | This work |
| $Mg_2Y_3Cl_{13}$(s) | **-4,290,400** | **580** | 423.3058 | 0.052514798 | -5,858,147 | -4.72E-06 | 798.354 | [298-1500] | This work |
| $Sr_2YCl_7$(s) | **-2,658,000** | **370** | 263.6776 | -0.000359934 | -2093022.4 | 3.59762E-05 | | [298-1500] | This work |
| $CsY_2Cl_7$(s) | **-2,484,000** | **405** | 255.2814 | 0.028543832 | -2422606 | -4.1042E-09 | | [298-1500] | This work |
| $Cs_2YCl_5$(s) | **-1,981,782** | **353** | 196.4256 | 0.047415466 | -1211303 | -2.0521E-09 | | [298-1500] | This work |
| $Cs_3YCl_6$(s) | **-2,474,903** | **449** | 242.2822 | 0.069511166 | -1211303 | -2.0521E-09 | | [298-1500] | This work |
| $\alpha$-$Na_7NdI_{10}$(cr) | **-2,684,940** | **890** | 427.0479 | 0.0999588 | $8.04172{\cdot}10^{-5}$ | -33,004.2 | | [298-658] | This work |
| $\beta$-$Na_7NdI_{10}$(cr) | **-2,684,440** | **890.76336** | 427.0479 | 0.0999588 | $8.04172{\cdot}10^{-5}$ | -33,004.2 | | [658-1500] | This work |
| $Na_7PuI_{10}$(cr) | **-2,645,000** | **855** | 399.47692 | 0.1968656 | $2.453132{\cdot}10^{-8}$ | -1,624,835.8 | | [298-6000] | This work |
| $CsMgI_3$(s) | **-742,000** | **255** | 112.76196 | 0.04038912 | $2.5070129{\cdot}10^{-6}$ | 200,009.75 | | [298-1500] | This work |
| $Cs_2MgI_4$(s) | **-1,098,000** | **390** | 156.57717 | 0.06223132 | $5.0027789{\cdot}10^{-6}$ | 400,257.45 | | [298-1500] | This work |
| $Cs_3MgI_5$(s) | **-1,449,500** | **510** | 200.39238 | 0.08407352 | $7.4985449{\cdot}10^{-6}$ | 600,505.15 | | [298-1500] | This work |
| $Cs_3Nd_2I_9$(s) | **-2,413,000** | **805** | 397.953 | -0.0870912 | $1.68246{\cdot}10^{-4}$ | -2,714,656.90 | | [298-1500] | This work |
| $\alpha$-$Cs_3NdI_6$(s) | **-1,715,000** | **650** | 264.699 | -0.0107823 | $8.78666{\cdot}10^{-5}$ | -1,056,956.90 | | [298-1500] | This work |
| $\beta$-$Cs_3NdI_6$(s) | **-1,714,500** | **650.669344** | 264.699 | -0.0107823 | $8.78666{\cdot}10^{-5}$ | -1,056,956.90 | | [298-1500] | This work |
| $CsNd_4I_{13}$(s) | **-2,980,000** | **960** | 576.831 | -0.2833934 | $3.24013{\cdot}10^{-4}$ | -6,430,552.30 | | [298-1500] | This work |
| $Cs_3PuI_6$(s) | **-1,682,480** | **656** | 288.97994 | -0.09932416 | $1.64671213{\cdot}10^{-4}$ | -424,784.00 | | [298-1500] | This work |
| $Cs_3Pu_2I_9$(s) | **-2,356,000** | **765** | 394.65694 | -0.0787262 | $1.64663303{\cdot}10^{-4}$ | -424,644.00 | | [298-1500] | This work |
| $CsPu_4I_{13}$(s) | **-2,815,000** | **853** | 484.81898 | 0.04241758 | $5.489877{\cdot}10^{-5}$ | -141,081.40 | | [298-1500] | This work |

### 2.4.2. SOLUTIONS MODELLING

The excess Gibbs energy parameters and optimized coordination numbers in the liquid solution models modelled in this work are presented in [1, 50, 56, 57] for the systems already published in the open literature. When the excess Gibbs energy parameters have not been optimized in this work, but have been taken from the literature, the source of the excess parameters is given in the respective chapter.



| Chlorides | | | | | |
|---|---|---|---|---|---|
| AX | BY | **Chapter** | AX | BY | **Chapter** |
| NaCl | $MgCl_2$ | 3 | $MgCl_2$ | $PuCl_3$ | 3 |
| NaCl | $PuCl_3$ | 3 | $MgCl_2$ | $NdCl_3$ | 3 |
| NaCl | $NdCl_3$ | 3 | $MgCl_2$ | $CeCl_3$ | 3 |
| NaCl | $CeCl_3$ | 3 | $MgCl_2$ | $BaCl_2$ | 9[a] |
| NaCl | $BaCl_2$ | 4 | $MgCl_2$ | $SrCl_2$ | 9[a] |
| NaCl | $SrCl_2$ | 4 | $MgCl_2$ | $UCl_3$ | 3 |
| NaCl | $UCl_3$ | 3 | $MgCl_2$ | $ThCl_4$ | App. A |
| NaCl | $ThCl_4$ | App. A | $MgCl_2$ | CsCl | 8 |
| NaCl | CsCl | 8 | $MgCl_2$ | $SmCl_3$ | App. B |
| NaCl | $SmCl_3$ | App. B | $MgCl_2$ | $YCl_3$ | App. B |
| NaCl | $YCl_3$ | App.B | | | |
| $PuCl_3$ | $NdCl_3$ | 9[a] | $NdCl_3$ | $CeCl_3$ | 9[a] |
| $PuCl_3$ | $CeCl_3$ | 9[a] | $NdCl_3$ | $SrCl_2$ | 4 |
| $PuCl_3$ | $BaCl_2$ | 4 | $NdCl_3$ | $BaCl_2$ | 4 |
| $PuCl_3$ | $SrCl_2$ | 4 | $NdCl_3$ | $UCl_3$ | 9[a] |
| $PuCl_3$ | $UCl_3$ | 9[a] | $NdCl_3$ | $ThCl_4$ | App. A |
| $PuCl_3$ | $ThCl_4$ | App. A | $NdCl_3$ | CsCl | 8 |
| $PuCl_3$ | CsCl | 8 | $NdCl_3$ | $SmCl_3$ | App. B |
| $PuCl_3$ | $SmCl_3$ | App. B | $NdCl_3$ | $YCl_3$ | App. B |
| $PuCl_3$ | $YCl_3$ | App. B | | | |
| $CeCl_3$ | $BaCl_2$ | 4 | $BaCl_2$ | $SrCl_2$ | 9[a] |
| $CeCl_3$ | $SrCl_2$ | 4 | $BaCl_2$ | $UCl_3$ | 5 |
| $CeCl_3$ | $UCl_3$ | 9[a] | $BaCl_2$ | $ThCl_4$ | 5 |
| $CeCl_3$ | $ThCl_4$ | App. A | $BaCl_2$ | CsCl | 9[a] |
| $CeCl_3$ | CsCl | 9 | $BaCl_2$ | $SmCl_3$ | App. B |
| $CeCl_3$ | $SmCl_3$ | App. B | $BaCl_2$ | $YCl_3$ | App. B |
| $CeCl_3$ | $YCl_3$ | App. B | | | |
| $SrCl_2$ | $UCl_3$ | 5 | $UCl_3$ | $ThCl_4$ | 5 |
| $SrCl_2$ | $ThCl_4$ | 5 | $UCl_3$ | CsCl | 9 |
| $SrCl_2$ | CsCl | 9 | $UCl_3$ | $SmCl_3$ | App. B |
| $SrCl_2$ | $SmCl_3$ | App. B | $UCl_3$ | $YCl_3$ | App. B |
| $SrCl_2$ | $YCl_3$ | App. B | | | |
| $ThCl_4$ | $SmCl_3$ | App. B | CsCl | $SmCl_3$ | App. B |
| $ThCl_4$ | $YCl_3$ | App. B | CsCl | $YCl_3$ | App. B |
| $SmCl_3$ | $YCl_3$ | App. B | | | |
| **Iodides** | | | | | |
| AX | BY | **Chapter** | AX | BY | **Chapter** |
| NaI | $MgI_2$ | 6 | $MgI_2$ | $PuI_3$ | 7 |
| NaI | $PuI_3$ | 7 | $MgI_2$ | $NdI_3$ | 7 |
| NaI | $NdI_3$ | 7 | $MgI_2$ | CsI | 8 |
| NaI | CsI | 8 | | | |
| $PuI_3$ | CsI | 8 | $NdI_3$ | CsI | 8 |
| **Mixed halides** | | | | | |
| AX | BY | **Chapter** | AX | BY | **Chapter** |
| NaCl | NaI | 6 | $MgCl_2$ | $MgI_2$ | 6 |
| $PuCl_3$ | $PuI_3$ | 7 | $NdCl_3$ | $NdI_3$ | 7 |
| CsCl | CsI | 8 | | | |

Table 2.3: Overview of the modelled systems in this work, along with the chapter in which the system is used for the first time.
[a] Model not shown in this work, but used in application calculations in Chapter 9

# BIBLIOGRAPHY


(1) Alders, D. C.; Vlieland, J.; Thijs, M.; Konings, R. J. M.; Smith, A. L. *Journal of Molecular Liquids* **2024**, *396*, 123997.

(2) Rietveld, H. M. *Journal of applied Crystallography* **1969**, *2*, 65–71.

(3) Van Laar, B.; Schenk, H. *Acta Crystallographica Section A: Foundations and Advances* **2018**, *74*, 88–92.

(4) Rodríguez-Carvajal, J. *Physica B: Condensed Matter* **1993**, *192*, 55–69.

(5) Van Eijck, L.; Cussen, L.; Sykora, G.; Schooneveld, E.; Rhodes, N.; Van Well, A.; Pappas, C. *Journal of Applied Crystallography* **2016**, *49*, 1398–1401.

(6) Rodríguez-Carvajal, J. et al. *Laboratoire Léon Brillouin (CEA-CNRS): Saclay, France* **2001**.

(7) Beneš, O.; Konings, R. J. M.; Wurzer, S.; Sierig, M.; Dockendorf, A. *Thermochimica Acta* **2010**, *509*, 62–66.

(8) Höhne, G.; Cammenga, H.; Eysel, W.; Gmelin, E.; Hemminger, W. *Thermochimica Acta* **1990**, *160*, 1–12.

(9) Della Gatta, G.; Richardson, M. J.; Sarge, S. M.; Stølen, S. *Pure and Applied Chemistry* **2006**, *78*, 1455–1476.

(10) Uriano, G. National Bureau of Standards Certificate, Standard Reference Matarial 1655, Potassium Chloride KCl(cr) for Solution Calorimetry, 1981.

(11) Wadsö, I.; Goldberg, R. N. *Pure and Applied Chemistry* **2001**, *73*, 1625–1639.

(12) Wagman, D. D.; Evans, W. H.; Parker, V. B.; Schumm, R. H.; Halow, I.; Bailey, S. M.; Churney, K. L.; Nuttall, R. L. *J. Phys. Chem. Ref. Data* **1982**, *11*.

(13) Motalov, V.; Dunaev, A.; Kudin, L.; Butman, M.; Krämer, K. *International Journal of Mass Spectrometry* **2020**, *457*, 116431.

(14) Rudel, S. S.; Deubner, H. L.; Scheibe, B.; Conrad, M.; Kraus, F. *Zeitschrift für anorganische und allgemeine Chemie* **2018**, *644*, 323–329.

(15) Chase Jr, M. W. *Journal of Physical and Chemical Reference Data, Monograph* **1998**, *9*.

(16) Konings, R. J. M.; Kovács, A. *Handbook on the physics and chemistry of rare earths* **2003**, *33*, 147–247.

(17) Capelli, E.; Konings, R. J., *Halides of the actinides and fission products relevant for molten salt reactors*; Elsevier: 2020, pp 56–283.

(18) Glushko, V.; Gurvich, L.; Weitz, V., et al., *Thermodynamic properties of individual substances*; 2; Nauka Publishing House, Moscow: 1978; Vol. 3, p 861.

(19) Glushko, V.; Gurvich, L.; Weitz, V., et al., *Thermodynamic properties of individual substances*; 2; Nauka Publishing House, Moscow: 1978; Vol. 4, p 381.

(20) Glushko, V.; Gurvich, L.; Weitz, V., et al., *Thermodynamic properties of individual substances*; 2; Nauka Publishing House, Moscow: 1978; Vol. 3, p 776.

(21) Reiss, H.; Katz, J.; Kleppa, O. *The Journal of Chemical Physics* **1962**, *36*, 144–148.

(22) Blander, M. *The Journal of Chemical Physics* **1962**, *37*, 172–173.

(23) Davis, H. T.; Rice, S. A. *The Journal of Chemical Physics* **1964**, *41*, 14–24.

(24) Schorne-Pinto, J.; Yingling, J. A.; Christian, M. S.; Mofrad, A. M.; Aslani, M. A.; Besmann, T. M. *ACS omega* **2021**.

(25) Shannon, R. D. *Acta crystallographica section A: crystal physics, diffraction, theoretical and general crystallography* **1976**, *32*, 751–767.

(26) Østvold, T., *A thermodynamic study of some fused salt mixtures containing alkali and alkaline earth chlorides, bromides and iodides*; Institute of Physical Chemistry, University of Trondheim, NTH: 1971; Vol. 91.

(27) Van Oudenaren, G.; Ocadiz-Flores, J. A.; Smith, A. L. *Journal of Molecular Liquids* **2021**, *342*, 117470.

(28) Papatheodorou, G.; Kleppa, O. *The Journal of Physical Chemistry* **1974**, *78*, 178–181.

(29) Papatheodorou, G.; Ostvold, T. *The Journal of Physical Chemistry* **1974**, *78*, 181–185.

(30) Gaune-Escard, M.; Bogacz, A.; Rycerz, L.; Szczepaniak, W. *Thermochimica Acta* **1994**, *236*, 67–80.

(31) Gaune-Escard, M.; Rycerz, L.; Szczepaniak, W.; Bogacz, A. *Thermochimica Acta* **1994**, *236*, 59–66.

(32) Gaune-Escard, M.; Rycerz, L.; Hoch, M. *Journal of Molecular Liquids* **1999**, *83*, 83–94.

(33) Matsuura, H.; Takagi, R.; Rycerz, L.; Gaune-Escard, M. *Journal of Nuclear Science and Technology* **2002**, *39*, 632–634.

(34) Dienstbach, v. F.; Blachnik, R. *Zeitschrift für anorganische und allgemeine Chemie* **1975**, *412*, 97–109.

(35) Papatheodorou, G. N.; Waernes, O.; Østvold, T.; Holm, A.; Toubro, N.; Krantz, A.; Laureni, J. *Acta Chemica Scandinavia* **1979**, 173–178.

(36) Gaune-Escard, M.; Bogacz, A.; Rycerz, L.; Szczepaniak, W. *Thermochimica Acta* **1994**, *236*, 67–80.

(37) Rycerz, L.; Gaune-Escarda, M. *Zeitschrift für Naturforschung A* **2002**, *57*, 136–142.

(38) Chojnacka, I.; Rycerz, L.; Kapala, J.; Gaune-Escard, M. *Journal of Molecular Liquids* **2020**, *319*, 113935.

(39) Rycerz, L.; Kapala, J.; Gaune-Escard, M. *Journal of Molecular Liquids* **2021**, *342*, 116963.

(40) Enninga, E.; Alberts, G.; Blachnik, R. *Thermochimica Acta* **1983**, *64*, 317–325.

(41) Blachnik, R.; Alberts, G.; Enninga, E. *Zeitschrift fur Anorganische und Allgemeine Chemie* **1985**, *522*, 207–216.

(42) Hatem, G.; Gaune-Escard, M.; Pelton, A. *The Journal of Physical Chemistry* **1982**, *86*, 3039–3046.

(43) Gaune-Escard, M. *Pure and Applied Chemistry* **1983**, *55*, 505–514.

(44) Lukas, H.; Fries, S. G.; Sundman, B., *Computational thermodynamics: the Calphad method*; Cambridge university press: 2007.

(45) Centre for Research in Computational Thermochemistry FactSage 8.2.

(46) Pelton, A. D.; Chartrand, P.; Eriksson, G. *Metallurgical and Materials Transactions A* **2001**, *32*, 1409–1416.

(47) Kohler, F.; Findenegg, G. *Monatshefte für Chemie und verwandte Teile anderer Wissenschaften* **1965**, *96*, 1228–1251.

(48) Toop, G. *Trans. TMS-AIME* **1965**, *223*, 850–855.

(49) Beneš, O. Joint Research Centre Molten Salt Database - JRCMSD, data retrieved from Joint Research Centre: EU Science Hub, https://joint-research-centre.ec.europa.eu/joint-research-centre-molten-salt-database-jrcmsd_en, 2021.

(50) Alders, D. C.; Cette, D. J.; Konings, R. J. M.; Smith, A. L. *Physical Chemistry, Chemical Physics* **2024**, *26*, 24041–24057.

(51) Rand, M.; Mompean, F. J.; Perrone, J.; Illemassène, M. *(No Title)* **2008**.

(52) Barin, I.; Platzki, G., *Thermochemical data of pure substances*; 334; Wiley Online Library: 1989; Vol. 304.

(53) Roki, F.-Z.; Ohnet, M.-N.; Fillet, S.; Chatillon, C.; Nuta, I. *The Journal of Chemical Thermodynamics* **2014**, *70*, 46–72.

(54) Chartrand, P.; Pelton, A. D. *Canadian Metallurgical Quarterly* **2001**, *40*, 13–32.

(55) Dumaire, T.; Ocádiz-Flores, J. A.; Konings, R. J. M.; Smith, A. L. *Calphad* **2022**, *79*, 102496.

(56) Alders, D. C.; Rooijakkers, B. A.; Konings, R. J.; Smith, A. L. *The Journal of Physical Chemistry C* **2025**, *129*, 2726–2738.

(57) Alders, D. C.; Sacristán-Civera, A.; Wolff, M.; Capelli, E.; Bright, E.; Hennig, C.; Konings, R.; Smith, A. *Dalton Transactions (under review)* **2025**.

# 3

# SIMULANT CHEMISTRY IN MOLTEN CHLORIDE FUEL

*To achieve the goal of this work, i.e. investigate the effects of fission products on molten salt fuel thermochemistry, a thermodynamic model of the fuel in combination with relevant fission products is necessary. To achieve this, simulant systems that mimic the behaviour of $PuCl_3$ systems are used when no experimental data for $PuCl_3$ are available. In this chapter an analysis of simulant chemistry for $PuCl_3$ is presented through the comparison of systems $NaCl–MCl_3$, $CsCl–MCl_3$ and $MgCl_2–MCl_3$ (M = Ce, Nd, U, Pu). The aim of this analysis is to find the simulant element that is most suited for modelling the behaviour of Pu in the molten salt.*

*As part of this study, new insights into the solid state chemistry of the systems $NaCl–RECl_3$ (RE = Ce, Nd) are presented, in which the intermediate compound suggested in the literature, $Na_3RE_5Cl_{18}$, is investigated more closely. Our studies have revealed a homogeneity range around the intermediate compound in the form of the $Na_{3x}RE_{2-x}Cl_6$, as opposed to a stoichiometric compound, and have allowed us to revisit the phase diagrams of the $NaCl–RECl_3$ (RE = Ce, Nd) systems accordingly.*

*In addition, the binary systems $NaCl–MgCl_2$ and $MgCl_2–MCl_3$ (M = Ce, Nd, U, Pu) are revisited based on existing data in the literature and estimated mixing enthalpies. With the binary subsystems in the $NaCl–MgCl_2–MCl_3$ (M = Ce, Nd, Pu, U) ternary systems modelled, extrapolations to the ternary systems were calculated and compared to the available data in the literature.*

Parts of this chapter have been published in in "Alders et al., Dalton Transactions 54.44 (2025): 16475-16491".

The aim of this work is to model molten fuel salt systems that contain plutonium. However the necessary experimental data are not always available, and work with Pu is not possible at TU Delft. In view of safety, cost and regulations related to the handling of Pu, an approach using simulant systems was used. This approach was based on the elements that show behaviour close to that of Pu in molten salt systems, but which can be handled more easily. Cerium has often been cited as actinide surrogate in the literature [1–4], but other rare earth elements show comparable behaviour. Cerium is commonly used for the fact that its stable oxidation states (*i.e.* 3+ and 4+) mirror that of plutonium in oxide systems, where $CeO_2$ and $Ce_2O_3$ can be used as simulant for $PuO_2$ and $Pu_2O_3$, respectively. In a molten salt environment, Pu is mostly stable in its 3+ oxidation state (*i.e.* $PuCl_3$), but can oxidize to 4+ in case oxychlorides form (*i.e.* $PuOCl_2$). Only a few lanthanides are stable in the 4+ oxidation state, among which Ce, which is why Ce seems like the most logical choice at first glance. However, when looking at the melting behaviour, it may not be the most suitable lanthanide to fill the role of simulant element, thus a simulant analysis must be performed in this work.

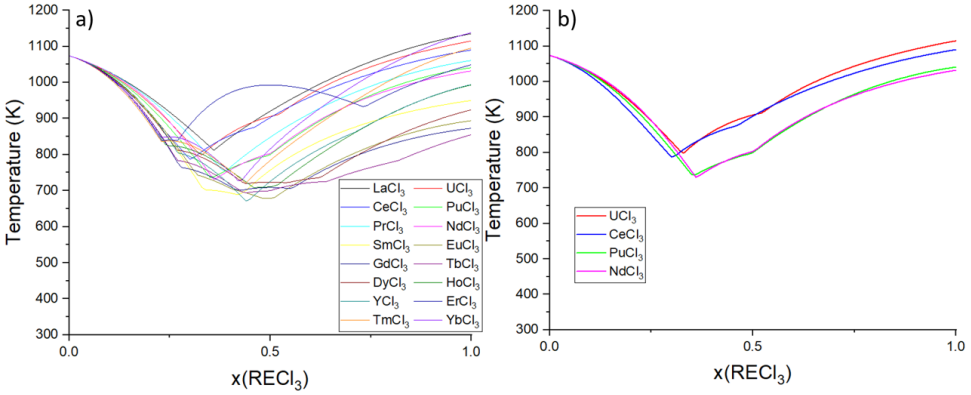


Figure 3.1: Liquidus lines of NaCl−$MCl_3$ systems (M = La-Yb, Y, U, Pu) reported in the literature [3, 5–23] (a), and selected liquidus lines for potential simulant systems (b).

A simulant analysis using every rare earth chloride, however, is a strenuous task, and therefore a pre-selection of simulant candidates is made. For this, a comparison of the melting behaviour of different lanthanide chloride-alkali chloride systems is made. To remain within the scope of this dissertation, *i.e.* the effect of fission products on melting behaviour and fission product retention, the melting behaviour is the metric that is used to judge simulant performance. Experimental liquidus data reported in the literature have been collected for the systems NaCl−$MCl_3$ [3, 5–23] and CsCl−$MCl_3$ (M = La-Yb, U, Pu) [6, 7, 10, 11, 14, 24–27]. The decision on which potential simulants to consider is based on the data shown in Figures 3.1 and 3.2, which allows for a pre-selection based on similarity with Pu at first glance. Shown in these figures is the melting behaviour of ACl−$MCl_3$ (A = Na, Cs; M = La-Yb, Pu, U) mixtures as a function of x($MCl_3$), *i.e.* the molar fraction of the $MCl_3$ species. The systems with NaCl were chosen because NaCl is part of the base fuel salt, whereas Cs, and by extension its chloride CsCl, is an important fission

product.

As seen in Figure 3.1b, the liquidus line of the NaCl−$NdCl_3$ system is almost perfectly overlapping with that of the NaCl−$PuCl_3$ system. Also shown in this figure is the liquidus line of the NaCl−$CeCl_3$ system, which has been cited as simulant for Pu and U in the literature [1–4], and NaCl−$UCl_3$ system, which is potentially interesting as simulant because uranium is an actinide like plutonium. The same comparison is drawn in Figure 3.2 for the CsCl−$MCl_3$ systems, and again the CsCl−$NdCl_3$ liquidus is closest to that of the corresponding $PuCl_3$ system. Moreover, while there is a difference in the absolute value of the liquidus temperatures compared to the $PuCl_3$ based system, the progression of the liquidus in the CsCl−$CeCl_3$ and CsCl−$UCl_3$ systems is again very similar.



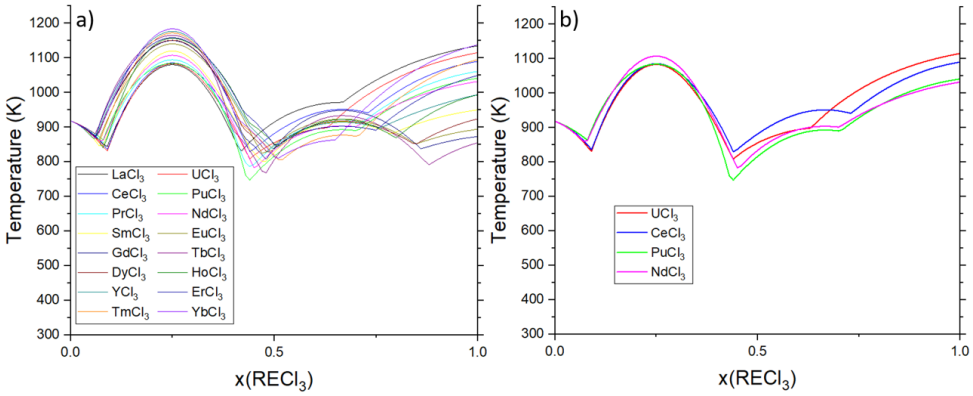


Figure 3.2: Liquidus lines of CsCl−$MCl_3$ systems (M = La-Yb, Y, U, Pu) reported in the literature [6, 7, 10, 11, 14, 24–27] (a), and selected liquidus lines for potential simulant systems (b).

After detailing the process of selecting the most suitable simulant element, this chapter will show an updated thermodynamic description of the base fuel NaCl−$MgCl_2$−$PuCl_3$ that will be considered in the rest of this dissertation.

## 3.1. SIMULANT SYSTEMS

The accuracy with which each simulant selected in Figures 3.1 and 3.2 describes the equivalent $PuCl_3$ systems is investigated in this section. This is done by comparing the models of $CeCl_3$, $NdCl_3$ and $UCl_3$ with the experimental data for $PuCl_3$ based salt systems. One of the main interests of this work is investigating the melting behaviour of a molten salt fuel upon addition of fision products, so the main criterion for a good simulant is the ability to reproduce the melting behaviour of $PuCl_3$ in a mixture. Initially, the comparison will be based on the NaCl−$MCl_3$ and CsCl−$MCl_3$ systems (M = Ce, Nd, U, Pu). In Section 3.3, this study will be expanded upon by adding the comparison with the $MgCl_2$−$MCl_3$ (M = Ce, Nd, U, Pu) systems. Later on in Chapter 5, the comparison will be extended further to include also the $SrCl_2$−$MCl_3$ and $BaCl_2$−$MCl_3$ systems.

The performance of the selected simulants in the NaCl−$MCl_3$ systems is shown in Figure 3.3. This figure shows that the liquidus of the NaCl−$PuCl_3$ system is very close

to that of the NaCl−$NdCl_3$ system. The systems NaCl−$CeCl_3$ and NaCl−$UCl_3$ show a similar slope of the liquidus to the $PuCl_3$ and $NdCl_3$ systems, but the difference in melting point between these simulants and $PuCl_3$ leads to a significant deviation of the melting temperature. The observed eutectic composition is similar for all four systems, as shown in Table 3.1. The eutectic composition and temperature of the NaCl−$NdCl_3$ system is closest to that of the NaCl−$PuCl_3$ system, though the latter can be once more explained by the aforementioned difference in melting point of the end-members.



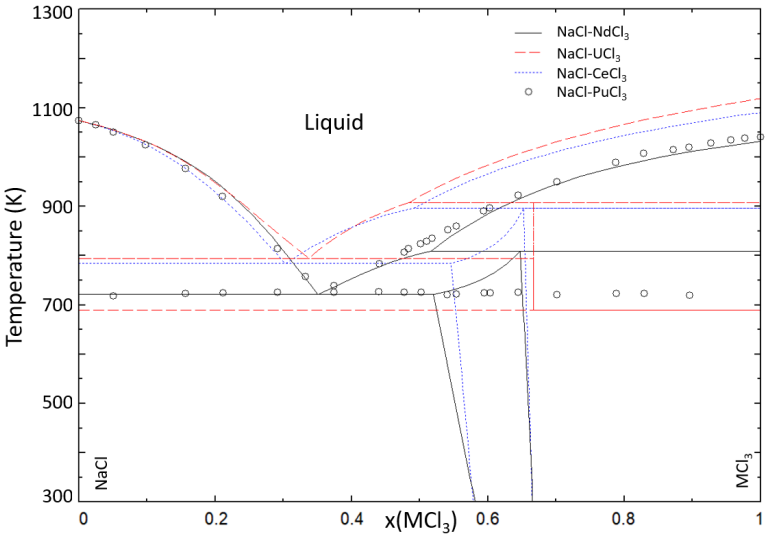


Figure 3.3: Calculated phase diagrams of the systems NaCl−$NdCl_3$ (solid black line), NaCl−$CeCl_3$ (dashed blue line) and NaCl−$UCl_3$ (dashed red line) using the thermodynamic models developed in this work, compared to the experimental data on the NaCl−$PuCl_3$ system (open black circles) presented by Bjorklund et al. [16].

| System | $x_1$ | $T_1$ (K) | Source |
|---|---|---|---|
| $PuCl_3$ | 0.385 | 725 | Dumaire et al. [28] |
| $NdCl_3$ | 0.355 | 718 | This work |
| $CeCl_3$ | 0.303 | 778 | This work |
| $UCl_3$ | 0.337 | 794 | This work |

Table 3.1: Eutectic equilibria in the NaCl−$MCl_3$ (M = Ce, Nd, U, Pu) systems as calculated with the thermodynamic models presented in this chapter.

The comparison between the systems CsCl−$MCl_3$ (M = Ce, Nd, U, Pu) is shown in Figure 3.4. Here it is observed that, like in the NaCl systems, the liquidus of the CsCl−$NdCl_3$ system most closely resembles the melting behaviour of the CsCl−$PuCl_3$ system. Also like in the NaCl−$MCl_3$ systems, this difference is most pronounced at the $MCl_3$-rich side, owing to a difference in melting point between the end-members. The eutectic compositions and temperatures of these systems are given in Table 3.2. The eutectic compositions of all four systems are very similar at $x(MCl_3) \leq 0.5$, but the eutectic at $x(NdCl_3) =$

0.703 is closest to that of the CsCl−$PuCl_3$ system.

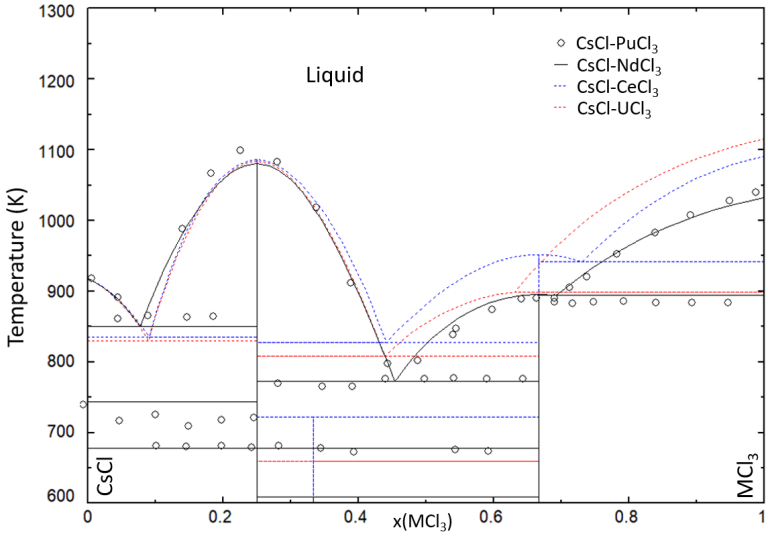


Figure 3.4: Calculated phase diagrams of the systems CsCl−$NdCl_3$ (solid black line), CsCl−$CeCl_3$ (dashed blue line) and CsCl−$UCl_3$ (dashed red line) using the thermodynamic models developed in this work, compared to the experimental data on the CsCl−$PuCl_3$ system (open black circles) presented by Benz et al. [24].

| System | $x_1$ | $T_1$ (K) | $x_2$ | $T_2$ (K) | $x_3$ | $T_3$ (K) |
|---|---|---|---|---|---|---|
| $PuCl_3$ | 0.077 | 861 | 0.454 | 751 | 0.700 | 886 |
| $NdCl_3$ | 0.078 | 849 | 0.456 | 770 | 0.703 | 895 |
| $CeCl_3$ | 0.091 | 834 | 0.441 | 826 | 0.730 | 940 |
| $UCl_3$ | 0.090 | 823 | 0.439 | 806 | - | - |

Table 3.2: Eutectic equilibria in the CsCl−$MCl_3$ (M = Nd, Ce, U, Pu) systems as calculated with the thermodynamic models presented in this chapter.

Based on the above observations, $NdCl_3$ seems to be the most promising simulant for the melting behaviour of $PuCl_3$ based systems. $CeCl_3$ on the other hand seems like a more suitable simulant for $UCl_3$. This comparison between these four chlorides will be extended to the $MgCl_2$−$MCl_3$ (M = Ce, Nd, U, Pu) systems in Section 3.3, and to the $SrCl_2$−$MCl_3$ and $BaCl_2$−$MCl_3$ systems in Chapter 5 for a more thorough analysis.

## 3.2. NaCl-$MCl_3$ (M = Nd, Ce, U, Pu) systems

An experimental investigation and re-assessment of the salt systems NaCl−$NdCl_3$ and NaCl−$CeCl_3$ was carried out in this work. Notably, this was done to gain more insights into the intermediate compound reported in the literature on these systems.

### 3.2.1. $NaCl–NdCl_3$

Experimental data have been reported in the literature on the $NaCl–NdCl_3$ system by Seifert et al. in 1988 [29], who performed DTA and XRD analyses. They found by XRD that an intermediate compound exists, which they assigned to $Na_3Nd_5Cl_{18}$, also written as $Na_{0.67}(Na_{0.33}Nd_{1.67})Cl_6$ (space group P63/m [29]). Sato et al. [8] presented an experimental investigation of this system in 1998 using DTA and XRD, and they retain the intermediate compound found by Seifert et al., $Na_3Nd_5Cl_{18}$ in their assessment. They suggest that a homogeneity range exists at elevated temperatures, specifically between $x(NdCl_3) = 0.59$ and $x(NdCl_3) = 0.7$ and T = [573-873] K. According to the sketched phase diagram Sato et al. report, the homogeneity range is only stable at elevated temperatures, while the room temperature composition remains $Na_3Nd_5Cl_{18}$. However, neither Sato et al. nor Seifert et al. report detailed crystallographic information on the intermediate compound, notably the atomic positions in the crystal structure. Earlier assessments by Igarashi et al. (1990) [13] and Sharma et al. (1992) [9] agree about the existence of an intermediate, but suggest the intermediate $NaNd_3Cl_{10}$ instead, and indicate no homogeneity range. In view of the discrepancies between the literature studies, new investigations of the crystal structures of this compound were performed in this work to address the remaining questions.

In addition to the phase diagram studies found in the literature, single-crystal studies of the intermediate compound by Lissner et al. (1994) [30] dived more in detail into the crystal structure chemistry. They reported a structure of $Na_{0.698}(Na_{0.35}Ce_{1.65})Cl_6$, corresponding to a general stoichiometry of $Na_x(Na_{\frac{x}{2}}Nd_{1-\frac{x}{2}})Cl_3$ (space group P63/m). The existence of this compound is confirmed in our work with new experimental investigations, and the description of Lissner et al. is thus retained. Moreover, the extend of the homogeneity range is investigated in detail for the first time. While the $Na_x(Na_{\frac{x}{2}}Nd_{1-\frac{x}{2}})Cl_3$ notation gives an insight into the crystallography (*e.g.* the shared Na/Nd position), in this work we will use the simpler notation $Na_{3x}Nd_{2-x}Cl_6$. Based on the atomic positions they reported for a sample of stoichiometry $Na_{0.608}(Na_{0.304}Nd_{1.696})Cl_6$, we can define a general description for the $Na_{3x}Nd_{2-x}Cl_6$ phase that has been used in this work (see Table 3.4, Figure 3.5). Several samples were prepared in this work with varying ($NaCl:NdCl_3$) ratios as detailed in Chapter 2, with the aim of confirming the crystal structure model, and defining the limits of the homogeneity range. Mixtures were prepared within the expected homogeneity range, as well as in the two-phase domains. The mixtures were subjected to thermal treatment at T = 693 K for at least 48 hours. The aim of these experiments was to investigate the behaviour of this compound both at elevated temperatures and at room temperature, following the hints in the literature by Sato et al. [8] and Lissner et al. [30].

Shown in Figure 3.7 is the profile refinement of the composition $x(NdCl_3) = 0.65$, collected at room temperature using sXRD. This refinement shows that a single phase exists at this composition, with no traces of the end members NaCl and $NdCl_3$. The same was observed for the compositions $x(NdCl_3) = 0.55$, 0.6 and 0.625 in the same binary system, confirming the existence of an intermediate with a considerable homogeneity range. The $Na_{3x}Nd_{2-x}Cl_6$ phase adopts the same crystal structure symmetry as $NdCl_3$

(also hexagonal, in space group P63/m [31]). Upon addition of sodium to the $NdCl_3$ structure, partial substitution of sodium on the Nd site (2c) occurs, while the rest of the sodium is located on the (0,0,0) position (2b) with an occupancy equal to 2y. The shared Nd/Na2 site is nine-fold coordinated (same as in the $NdCl_3$), while the Na1 site is six-fold coordinated. The crystal structures of $Na_{3x}Nd_{2-x}Cl_6$ and $NdCl_3$ are shown in Figures 3.5 and 3.6, respectively to illustrate this. The atomic positions obtained from the refinements of the intermediates $Na_{3x}RE_{2-x}Cl_6$ are presented in Table 3.4.



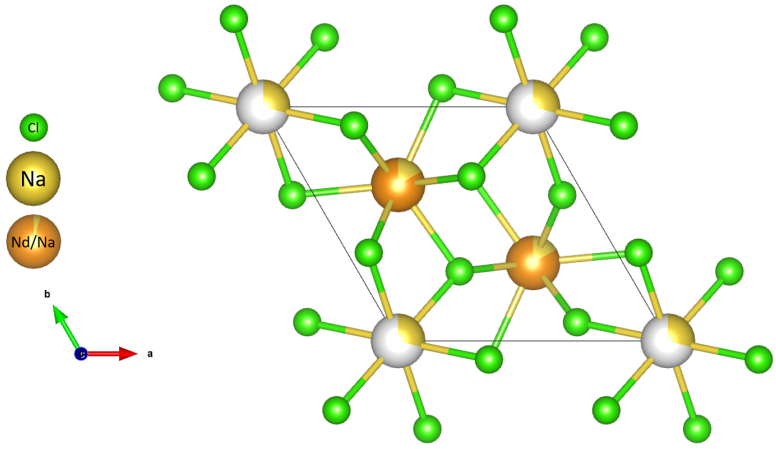


Figure 3.5: Crystal structure of the $Na_{0.848}(Na_{0.167}Nd_{1.832})Cl_6$ compound obtained in this work viewed along the *c*-axis, with the elements Na, Nd and Cl indicated in yellow, orange and green respectively. The corresponding atomic parameters are listed in Table 3.4.

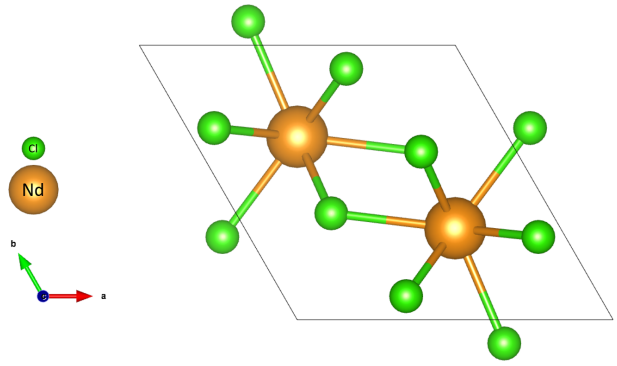


Figure 3.6: Crystal structure of $NdCl_3$ as reported by Meyer et al. [31] viewed along the *c*-axis, with the elements Nd and Cl indicated in orange and green respectively.

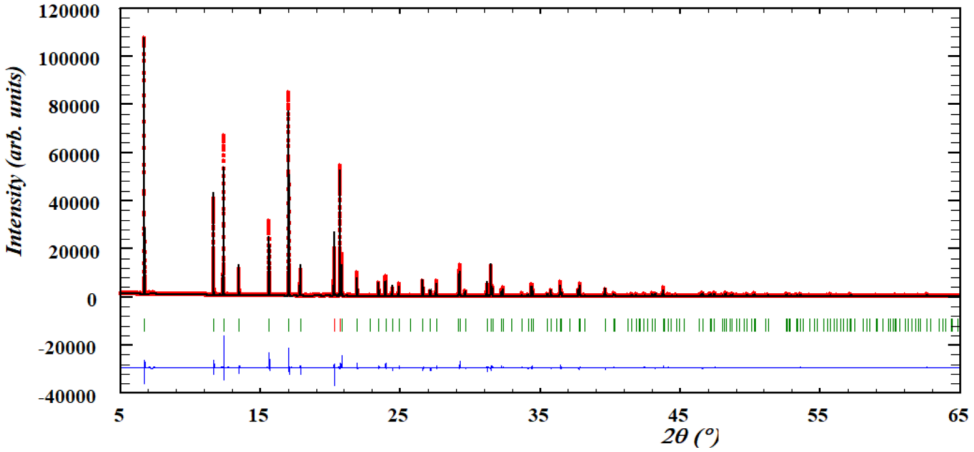


Figure 3.7: Profile refinement of the sXRD ($\lambda$ = 0.7653 Å) at x($NdCl_3$) = 0.623 in the NaCl−$NdCl_3$ system, showing the single phase $Na_{0.335}(Na_{0.168}Nd_{1.848})Cl_6$. The observed intensity (red circles) is shown alongside the calculated intensity (black line), and the difference between the two is shown (blue line). The angles at which reflections occur, i.e. the bragg positions, are shown as well (green, vertical lines).

At composition x($NdCl_3$) = 0.70, as shown in Figure 3.8, the first traces of the end member $NdCl_3$ become apparent, showing that the limiting composition of the homogeneity range lies between x($NdCl_3$) = 0.65 and x($NdCl_3$) = 0.70. Similarly, the other limiting composition, *i.e.* that on the NaCl-rich side, was found between x($NdCl_3$) = 0.50 and x($NdCl_3$) = 0.55. Contrary to the assessments of Seifert et al. [32] and Sato et al. [8], the solid solution in this system was observed to be stable at room temperature, rather than exclusively at elevated temperatures.

The stability of the solid solution at elevated temperatures was moreover investigated through quenching experiments, where three samples at compositions x($NdCl_3$) = 0.6, 0.625 and 0.65 were heated up to 773 K and subsequently quenched to preserve the crystal structures stable at high temperatures. These experiments showed that at T = 773 K, the crystal structure was still that of the single-phase solid solution. Furthermore, to rule out kinetic effects that limit the formation of the solid solution, we performed a synthesis experiment at x($NdCl_3$) = 0.75 with two different heating durations (48 h and 96 h). No appreciable difference was observed between the two experiments, thus we conclude that 48 h is enough time for the synthesis experiment to reach thermodynamic equilibrium.

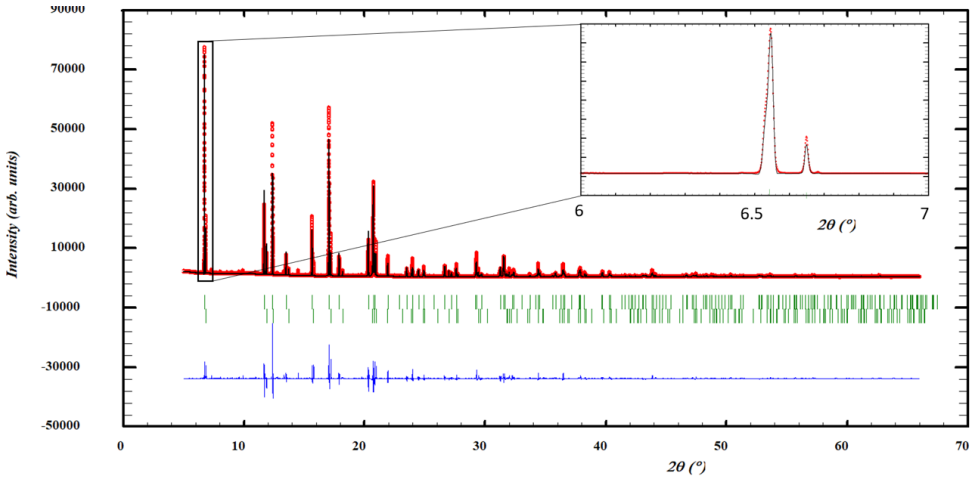


Figure 3.8: Profile refinement of the sXRD ($\lambda$ = 0.7653) at x($NdCl_3$) = 0.70 in the NaCl−$NdCl_3$ system, with phases $Na_{3x}Nd_{2-x}Cl_6$ [30] and $NdCl_3$ [31] included in the refinement. The zoomed part of the figure shows the distinct separation of the $Na_{3x}Nd_{2-x}Cl_6$ peak (left) and the $NdCl_3$ peak (right). The observerd intensity (red circles) is shown alongside the calculated intensity (black line), and the difference between the two is shown (blue line). The angles at which reflections occur, i.e. the bragg positions, are shown as well (green, vertical lines).

The progression of the cell volume of the intermediate compound $Na_{3x}Nd_{2-x}Cl_6$ is shown in Figure 3.10 as a function of composition, and the values are reported in Table 3.3. On the left side of the single-phase region (*i.e.* from x($NdCl_3$) = 0.55-0.65), a mixture of NaCl and $Na_{3x}Nd_{2-x}Cl_6$ is found, and the solid solution reaches the volume at its limiting composition. On the right side of the solubility range, a mixture of $NdCl_3$ and $Na_{3x}Nd_{2-x}Cl_6$ is found, but the size of the unit cell of the intermediate keeps shrinking as the $NdCl_3$ fraction increases. We would expect the volume of the intermediate compound to remain constant and equal to that at the limiting composition of the homogeneity range instead. The reason for this is as of yet not known, and should be subjected to further investigation. As shown before in Figures 3.7 and 3.8, several samples in the NaCl−$NdCl_3$ system were measured with synchrotron-XRD ($\lambda$ = 0.765 Å), labelled (ESRF) in Figure 3.10, whie others were measured by conventional laboratory XRD. The aim of the synchrotron experiments was to investigate the possible presence of end-members at compositions x($NdCl_3$) = 0.55 and 0.7, given the higher resolution of s-XRD compared to lab-XRD, as well as obtain a high-resolution XRD of the single-phase $Na_{3x}Nd_{2-x}Cl_6$. The results of the synchrotron-XRD are very similar to the measurements carried out using lab XRD, confirming the reliability of the results.

The phase diagram has then been optimized based on the experimental DTA data from Sato et al. [8], shown in solid black circles in Figure 3.9. The data from Sato et al. largely agree with the work of Seifert et al. [29], with the exception of the peritectic equilibrium. Seifert et al. measure two sub-liquidus equilibria between x($NdCl_3$) = 0.5 and x($NdCl_3$) = 0.95, whereas Sato et al. only measure one. This single peritectic equilibrium is also reported by Igarashi et al. [13] and Sharma et al. [9]. Moreover, the work of Sharma

et al. and Igarashi et al. report the eutectic equilibrium up to x($NdCl_3$) = 0.8, while Sato et al. and Seifert et al. report the eutectic up to x($NdCl_3$) = 0.5 and 0.6, respectively. A possible explanation for the fact that Sharma et al. and Igarashi et al. measure the eutectic equilibrium up to higher $NdCl_3$ content could be a contamination (Sharma et al. report a minor NdOCl contamination), or a subcooling effect (Igarashi et al. analysed the measured cooling curves).

Additionally, the limits of the homogeneity range and the stability at room temperature of the intermediate $Na_{3x}Nd_{2-x}Cl_6$ have been included in the optimisation using the experimental data obtained in this work. The mixing enthalpy of this system has been measured by Gaune-Escard et al. [33] at T = 1124 K and has been optimized based on these experimental data. The calculated mixing enthalpy of this system in Figure 3.14. The intermediate compound $Na_{3x}Nd_{2-x}Cl_6$ has been included in the thermodynamic model as a solid solution between NaCl and $NaNd_2Cl_7$ (corresponding to $Na_{0.571}(Na_{0.286}Nd_{1.714})Cl_6$ at x($NdCl_3$) = 0.66) as end-members to account for the limiting composition on the right side of the solubility range. Furthermore, the NaCl end-member had to be destabilized with a positive enthalpic term to obtain the desired phase diagram.

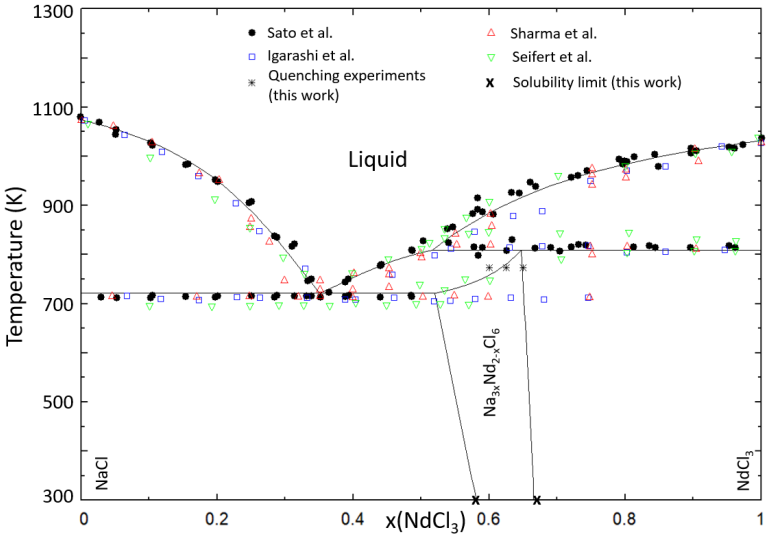


Figure 3.9: Phase diagram of the NaCl−$NdCl_3$ system calculated with the thermodynamic model presented in this work. Experimental data from Sato et al. [8] (closed black circles), Igarashi et al. [13] (open blue squares), Sharma et al. [9] (open upward green triangles) and Seifert et al. [29] (open downward red triangles).

### 3.2.2. NaCl−$CeCl_3$

Similarly, the salt system NaCl−$CeCl_3$ has been investigated experimentally by various authors in the literature. Most authors have interpreted the system as a simple binary eutectic system [34–37], with Storonkin et al. [38] suggesting solubility of NaCl in a hypothetical low-temperature polymorphic phase of $CeCl_3$. Since $CeCl_3$ does not have a

low-temperature phase, that interpretation is discarded. Kramer and Meyer (1990) [39] and Lissner et al. (1992) [30] reported single-crystal studies of $Na_{0.76}(Na_{0.38}Ce_{1.62})Cl_6$ and $Na_{0.698}(Na_{0.35}Ce_{1.65})Cl_6$, respectively, again corresponding to a general stoichiometry of $Na_{3x}Nd_{2-x}Cl_6$ (space group P63/m). Seifert et al. [32] suggested, based on DTA and XRD, that a solid solution between $CeCl_3$ and an intermediate compound of composition $Na_3Ce_5Cl_{18}$ existed.



In addition to the data found in the literature, an experimental investigation of the intermediate compound $Na_{3x}Ce_{2-x}Cl_6$ was performed, like in the NaCl−$NdCl_3$ system, mostly to gain further insight into the composition of the intermediate and possible existence of a homogeneity range. Synthesis experiments at several compositions were performed to identify the solubility limits of this intermediate compound. A single-phase intermediate compound was found at compositions x($CeCl_3$) = 0.60, 0.625 and 0.65, while NaCl was observed at compositions x($CeCl_3$) ≤ 0.55 and $CeCl_3$ was observed at compositions x($CeCl_3$) ≥ 0.70. Based on these results, we conclude that the limiting concentrations of this solid solution are between x($CeCl_3$) = 0.55 and 0.60 on the NaCl-rich side, and x($CeCl_3$) = 0.65 and 0.70 on the $CeCl_3$-rich side. The progression of the cell volume of the intermediate compound $Na_{3x}Ce_{2-x}Cl_6$, obtained from the refinements performed in this work, is shown in Figure 3.10 and reported in Table 3.3. The compositions at which a single phase solid solution is observed obey the expected linear trend, in agreement with Vegard's Law. Furthermore, like in the $Na_{3x}Nd_{2-x}Cl_6$ intermediate, the limiting composition on the left side of the solubility range shows that the cell volume reaches a maximum at compositions x($CeCl_3$) ≤ 0.59. The same trend in the cell volume decreasing beyond the solubility limit of the rare earth chloride (that was also seen in the NaCl−$NdCl_3$ system), is observed here.

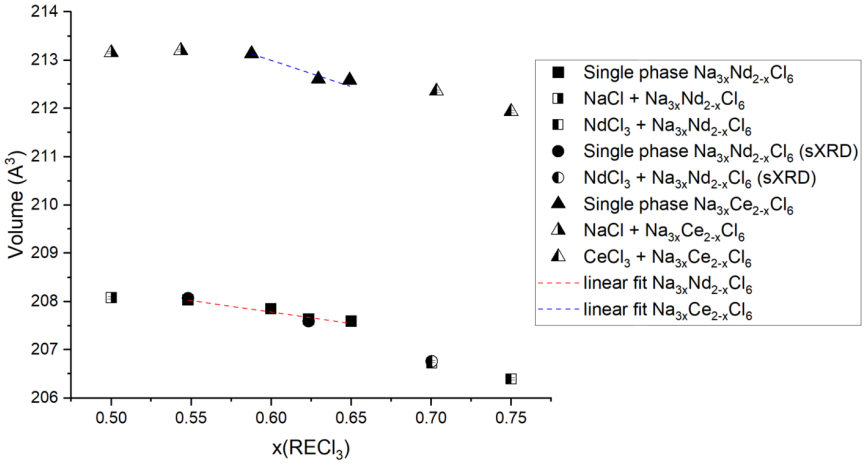


Figure 3.10: Cell volumes calculated from the profile refinements carried out in this work in the NaCl−RECl$_3$ (RE = Ce, Nd) systems. The data are both from synchrotron XRD and lab XRD, and the results obtained with these techniques are in good agreement with each other. A linear trend is visible in the single-phase solid solution following the insertion of the $Na^+$ cation in the interstitial sites of the $Na_{3x}RE_{2-x}Cl_6$ crystal structure. The refined values are also given in Table 3.3.

| x(RECl$_3$) | a,b (Å) | c (Å) | Volume (Å$^3$) | Method |
|---|---|---|---|---|
| **NaCl−NdCl$_3$** | | | | |
| 0.500 | 7.5343(4) | 4.2326(5) | 208.1(3) | XRD |
| 0.548 | 7.5340(5) | 4.2321(3) | 208.0(2) | XRD |
| 0.548 | 7.5345(4) | 4.2322(5) | 208.1(3) | sXRD |
| 0.600 | 7.5385(6) | 4.2294(3) | 208.0(3) | XRD |
| 0.625 | 7.5279(3) | 4.2307(3) | 207.6(2) | XRD |
| 0.625 | 7.5269(4) | 4.2310(5) | 207.6(3) | sXRD |
| 0.650 | 7.5210(3) | 4.2300(3) | 207.2(2) | XRD |
| 0.700 | 7.5130(5) | 4.2304(5) | 206.8(3) | XRD |
| 0.700 | 7.5134(4) | 4.2293(5) | 206.8(2) | sXRD |
| 0.750 | 7.5069(4) | 4.2291(5) | 206.4(3) | XRD |
| **NaCl−CeCl$_3$** | | | | |
| 0.500 | 7.5596(4) | 4.3070(4) | 213.2(2) | XRD |
| 0.543 | 7.5593(4) | 4.3082(4) | 213.2(2) | XRD |
| 0.588 | 7.5584(2) | 4.3078(2) | 213.1(1) | XRD |
| 0.630 | 7.5550(5) | 4.3057(4) | 212.8(2) | XRD |
| 0.649 | 7.5513(8) | 4.3078(7) | 212.7(4) | XRD |
| 0.700 | 7.5470(4) | 4.3052(4) | 212.4(2) | XRD |
| 0.750 | 7.5392(6) | 4.3056(8) | 211.9(3) | XRD |

Table 3.3: Refined lattice parameters of all investigated samples in the NaCl−RECl$_3$ (RE = Nd, Ce) systems, also shown in Figure 3.10.

| x($RECl_3$) | Intermediate Stoichiometry | Site | Element | Wyckoff position | x | y | z | Occupancy |
|---|---|---|---|---|---|---|---|---|
| All | - | Na1 | Na | 2*b* | 0 | 0 | 0 | x |
| All | - | RE1 | RE | 2*c* | $\frac{1}{3}$ | $\frac{2}{3}$ | $\frac{1}{4}$ | 1-$\frac{x}{2}$ |
| All | - | Na2 | Na | 2*c* | $\frac{1}{3}$ | $\frac{2}{3}$ | $\frac{1}{4}$ | $\frac{x}{2}$ |
| **RE = Nd** | | | | | | | | |
| 0.500 | $Na_{0.429}(Na_{0.214}Nd_{1.786})Cl_6$ | | | | 0.38158(59) | 0.29672(64) | | |
| 0.548 | $Na_{0.429}(Na_{0.214}Nd_{1.786})Cl_6$ | | | | 0.3760(6) | 0.2926(6) | | |
| 0.548* | $Na_{0.429}(Na_{0.214}Nd_{1.786})Cl_6$ | | | | 0.3872(1) | 0.3027(1) | | |
| 0.600 | $Na_{0.364}(Na_{0.182}Nd_{1.818})Cl_6$ | | | | 0.3783(8) | 0.2937(9) | | |
| 0.623 | $Na_{0.335}(Na_{0.168}Nd_{1.832})Cl_6$ | | | | 0.3826(6) | 0.2986(7) | | |
| 0.623* | $Na_{0.335}(Na_{0.168}Nd_{1.832})Cl_6$ | Cl1 | Cl | 6*h* | 0.3902(2) | 0.3032(2) | $\frac{1}{4}$ | 1 |
| 0.650 | $Na_{0.304}(Na_{152}Nd_{1.848})Cl_6$ | | | | 0.3736(7) | 0.2938(7) | | |
| 0.700 | $Na_{0.304}(Na_{0.152}Nd_{1.848})Cl_6$ | | | | 0.3915(2) | 0.3049(2) | | |
| 0.700* | $Na_{0.304}(Na_{0.152}Nd_{1.848})Cl_6$ | | | | 0.3763(6) | 0.2918(2) | | |
| 0.750 | $Na_{0.304}(Na_{0.152}Nd_{848})Cl_6$ | | | | 0.3752(7) | 0.2903(7) | | |
| **RE = Ce** | | | | | | | | |
| 0.500 | $Na_{0.379}(Na_{0.190}Ce_{1.810})Cl_6$ | | | | 0.37583(60) | 0.29484(62) | | |
| 0.543 | $Na_{0.379}(Na_{0.190}Ce_{1.810})Cl_6$ | | | | 0.3754(6) | 0.2920(6) | | |
| 0.588 | $Na_{0.379}(Na_{0.190}Ce_{1.810})Cl_6$ | | | | 0.3736(5) | 0.2914(5) | | |
| 0.630 | $Na_{0.328}(Na_{0.164}Ce_{1.834})Cl_6$ | Cl1 | Cl | 6*h* | 0.3737(4) | 0.2908(4) | $\frac{1}{4}$ | 1 |
| 0.649 | $Na_{0.305}(Na_{0.153}Ce_{1.847})Cl_6$ | | | | 0.3768(6) | 0.2942(6) | | |
| 0.703 | $Na_{0.305}(Na_{0.153}Ce_{1.847})Cl_6$ | | | | 0.3804(6) | 0.2974(7) | | |
| 0.750 | $Na_{0.305}(Na_{0.153}Ce_{1.847})Cl_6$ | | | | 0.3732(6) | 0.2913(6) | | |

Table 3.4: Crystallographic data of the $Na_{3x}RE_{2-x}Cl_6$ solid solution (SGR $P6_3m$; RE = Ce, Nd) obtained from the refinements of the XRD data in this work. Compositions at which sXRD data was used are marked with an asterisk. The occupancy is treated as variable in this work, and is based on molar fraction of $RECl_3$ in the solid solution: x = $\frac{1-x(RECl_3)}{x(RECl_3)+\frac{1}{2}}$.

The NaCl−$CeCl_3$ system was optimized based on the DTA data from Seifert et al. [32]. The measurement of the eutectic equilibrium past x($CeCl_3$) = 0.55 could be due to contaminations. Kojima et al. [37] and Nishihara et al. [36] report $CeCl_3$ purities ≤ 98%, and Storonkin et al. [38] measure what they interpret as a polymorphic transition in $CeCl_3$, which is an indication that they also had impurities in their $CeCl_3$ batch. Baev et al. [34] and Korshunov et al. [35] do not specify their measurement method or end-member purity, so it is difficult to say what could have gone wrong.

The extent and stability of the intermediate compound $Na_{3x}Ce_{2-x}Cl_6$ along with its solubility range was optimized based on the experimental data obtained in this work. The phase diagram of this system is presented in Figure 3.11. The mixing enthalpy of this system was optimized based on the experimental data from Papatheodorou et al. [40], and is shown in Figure 3.14. Like in the NaCl−$NdCl_3$ system, the intermediate compound $Na_{3x}Ce_{2-x}Cl_6$ has been included in the thermodynamic model as a solid solution between NaCl and $NaCe_2Cl_7$ end-members.

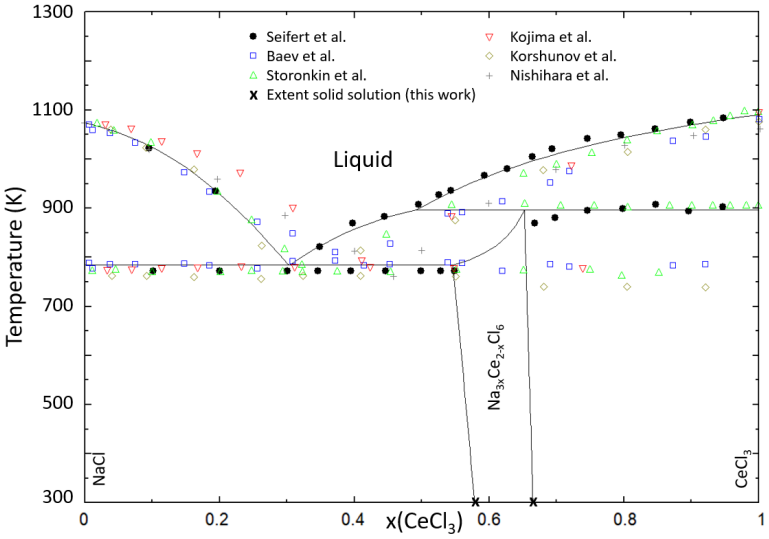


Figure 3.11: Phase diagram of the NaCl−$CeCl_3$ system calculated with the thermodynamic model presented in this work. Experimental data from Seifert et al. [32] (closed black circles), Baev et al. [34] (open blue squares), Storonkin et al. [41] (open upward green triangles), Kojima et al. [37] (open downward red triangles), Korshunov et al. [35] (open gold diamonds) and Nishihara et al. [36] (grey pluses).

### 3.2.3. NaCl–$UCl_3$

The system NaCl−$UCl_3$ has been investigated experimentally by Kraus et al. [42], Sooby et al. [3] and Yingling et al. [15]. The former reported the use of thermal analysis to obtain their results without further specifying their measurement method, whereas Sooby et al. and Yingling et al. used DSC. Both Kraus et al. and Sooby et al. interpret this system as a simple binary eutectic system. Yingling et al., however, suggest that an intermediate compound with the composition $NaU_2Cl_7$ (or $Na_3U_5Cl_{18}$) exists at elevated temperatures, based on their XRD measurements. Yingling et al. fit their thermodynamic model to the liquidus and eutectic equilibria of Kraus et al. and Sooby et al., rather than those they measured themselves.

In this work, the interpretation of this system by of Yingling et al. [15] has been retained. However, Yingling et al. use two different end-members for $UCl_3$ (*i.e.* $UCl_3$ and $U_2Cl_6$), which we do not. Therefore, our CALPHAD model was optimized to agree with the interpretation by Yingling et al., with the caveat that we use only $UCl_3$ as end-member. Given the results obtained in this work in the $NdCl_3$ and $CeCl_3$ systems, we hypothesize that a similar homogeneity range exists (*i.e.* $Na_{3x}U_{2-x}Cl_6$), although it is modelled as stable only at high temperatures to match with the DSC data. Therefore, we propose an alternative phase diagram, shown alongside the interpretation of Yingling et al. in Figure 3.12. The mixing enthalpy of this system is shown in Figure 3.14 and has been optimized to fit the experimental data measured by Matsuura et al. [43] at T = 1113 K.

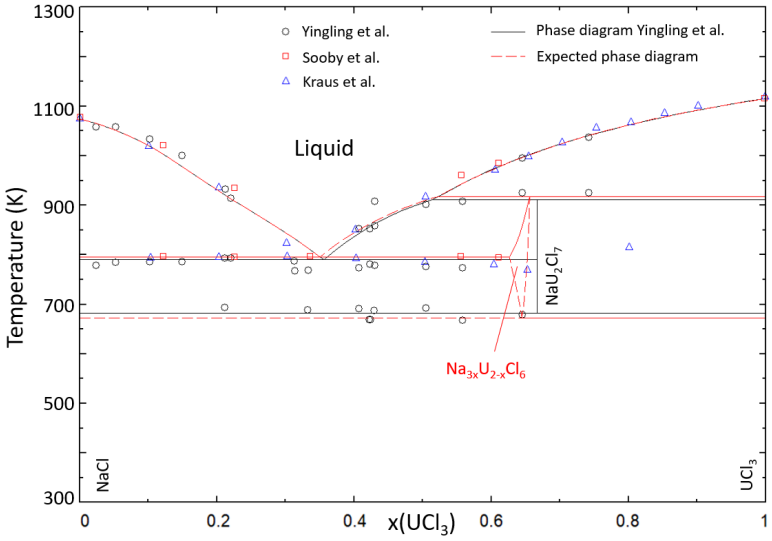


Figure 3.12: Phase diagram of the NaCl−$UCl_3$ system calculated with the thermodynamic model presented by Yingling et al. [15] (solid black line), as well as an expected phase diagram based on the available experimental data and our findings in the NaCl−$NdCl_3$ and NaCl−$CeCl_3$ systems (dashed red line). Experimental data from Yingling et al. [15] (open black circles), Sooby et al. [3] (open red squares) and Kraus et al. [42] (open blue triangles).

### 3.2.4. NaCl−$PuCl_3$

The available experimental data for the NaCl−$PuCl_3$ system is much less abundant than for the other NaCl−$MCl_3$ systems (M = Ce, Nd, U). Bjorklund et al. [16] used a combination of TA and DTA to investigate the system, and concluded that it is a simple binary eutectic system with no intermediates or solid solubility. Additionally, since there is no experimental data available for the mixing enthalpy of this system, Davis' method [44] was used to obtain an estimate of the mixing enthalpy.

Dumaire et al. [28] presented a thermodynamic assessment of this system using the same formalism as used in this work. Their assessment of this binary system is therefore retained here as well, and the phase diagram is shown in Figure 3.13. The mixing enthalpy of this system is shown in Figure 3.14. What should be noted is that this phase diagram requires further study by DSC and XRD: given the similarities between the $NdCl_3$ and $PuCl_3$ systems, it could be expected that a similar intermediate ($Na_{3x}Pu_{2-x}Cl_6$) exists in this system as well.

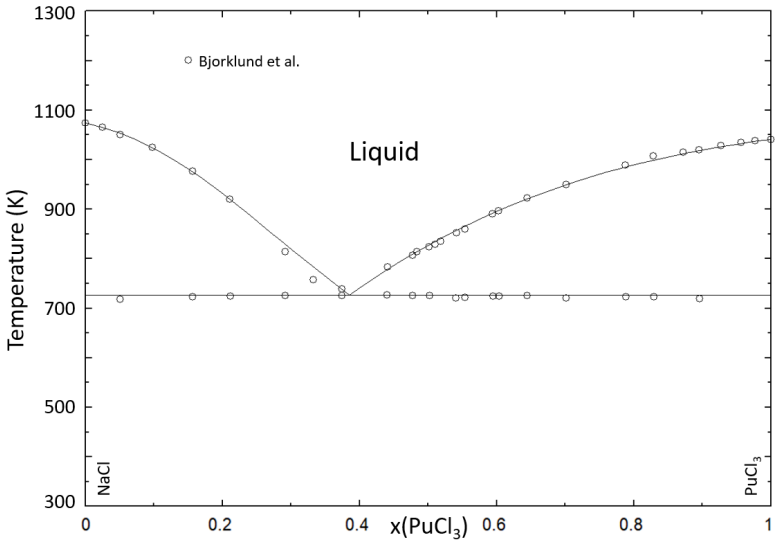


Figure 3.13: Phase diagram of the NaCl−$PuCl_3$ system calculated with the thermodynamic model presented by Dumaire et al. [28]. Experimental data from Bjorklund et al. [16] (open black circles).

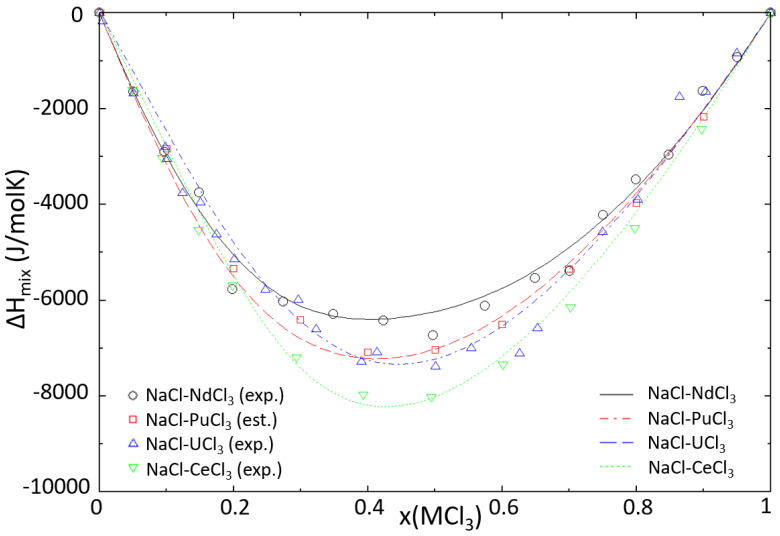


Figure 3.14: Calculated mixing enthalpies of the NaCl−$MCl_3$ (M = Ce, Nd, U, Pu) systems at T = 1125 K using the thermodynamic model presented in this work. Experimental data from Gaune-Escared et al. [33] (NaCl−$NdCl_3$, open black circles) at T = 1124 K, Papatheodorou et al. [40] (NaCl−$CeCl_3$, open downward green triangles) at T = 1118 K and Matsuura et al. [43] (NaCl−$UCl_3$, open blue upward triangles) at T = 1113 K. Data of the NaCl−$PuCl_3$ system (open red squares) were estimated using Davis' method.

## 3.3. BINARY SYSTEMS WITH $MgCl_2$

### 3.3.1. $NaCl-MgCl_2$

Four intermediates in the $NaCl-MgCl_2$ system have been identified in the literature, and their crystallographic information has been reported by Seifert et al. [45], van Loon et al. [46] and Kanno et al. [47]. These intermediates are $NaMgCl_3$ (SGR $R\bar{3}h$), $Na_2MgCl_4$ (SGR $Pbam$), $Na_6MgCl_8$ (SGR $Fm\bar{3}m$) and $Na_2Mg_3Cl_8$ (SGR $R\bar{3}mh$).

The invariant equilibria in the $NaCl-MgCl_2$ system have been investigated abundantly in the literature [48–55] and a CALPHAD model using the quadruplet approximation in the quasichemical formalism has been presented by Chartrand et al. [56] based on the data in the literature. However, in the model by Chartrand et al. the intermediate $Na_2MgCl_4$ is unstable at room temperature, which is not consistent with the corresponding crystallographic literature [45–47]. Furthermore, the assessment by Chartrand et al. [56] does not include the intermediates $Na_6MgCl_8$ and $Na_2Mg_3Cl_8$, although crystal structures have been reported in the literature [45, 46]. In this work, we have identified the intermediate $Na_6MgCl_8$ from XRD measurements in the quaternary system. For these reasons, the $NaCl-MgCl_2$ system is re-assessed in this work.

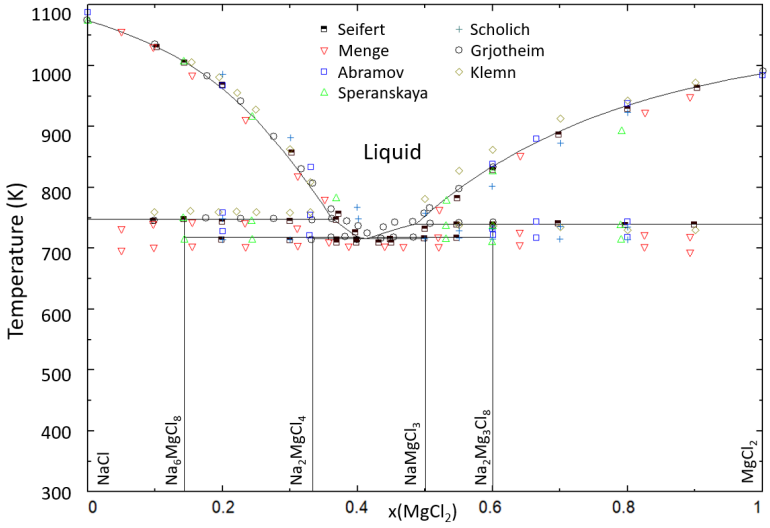


Figure 3.15: Phase diagram of the $NaCl-MgCl_2$ system, calculated with the CALPHAD model presented in this work. Experimental data from Seifert et al. [45] (black, half-filled squares), Menge et al. [55] (red, open downward triangles), Abramov et al. [53] (blue, open squares), Speranskaya et al. [54] (lime green, upward open triangles), Scholich et al. [48] (azure, crosses), Grjotheim et al. [51] (black, open circles) and Klemn et al. [49] (khaki, open diamonds) are shown for comparison with the calculated phase diagram.

The optimized phase diagram of the $NaCl-MgCl_2$ system is presented in Figure 3.15. The thermodynamic model is in good agreement with most of the available experimental data. An exception is the data from Menge et al. [55], who measured a single eutectic equilibrium across the entire composition range using thermal analysis on their cooling

curves. However, Menge et al. also report a contamination of their $MgCl_2$ with up to 7% MgO, which could explain their results. Moreover, several authors report two transitions at $x(MgCl_2) \geq 0.6$ between 700 and 750 K, which is in contrast with what our model predicts. However, since the most recent publications, those being the work of Grjotheim et al. [51] and Seifert et al. [45] do not report these equilibria, we decided to follow Seifert's interpretation of this section of the phase diagram.



The thermodynamic model was moreover optimized to fit the experimental mixing enthalpy data. The calculated mixing enthalpy of this system is given in Figure 3.16, and is compared to the experimental data from Kleppa and McCarthy [57], who measured the mixing enthalpy at 1083 K with high-temperature reaction calorimetry using the break-off ampoule method [58].

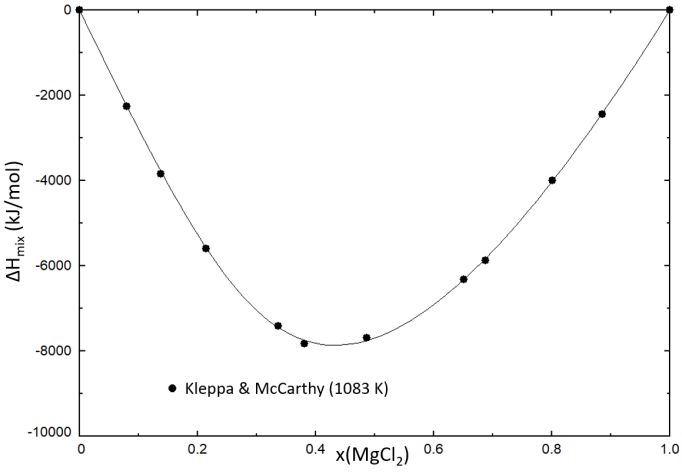


Figure 3.16: Mixing enthalpy of the NaCl−$MgCl_2$ system, calculated at T = 1083 K, compared to experimental data from Kleppa and McCarthy [57], measured at T = 1083 K.

A comparison between the invariant equilibria presented in the literature, and those calculated with the thermodynamic model is given in Table 3.5. The CALPHAD model reproduces the experimental data for the melting points of the end members well, as well as the eutectic temperatures. There is a slight deviation from most literature in the peritectic equilibria of $Na_2MgCl_4$ and $NaMgCl_3$, which are modelled lower than reported. This is due to the fact that the peritectic equilibria of $Na_2MgCl_4$ and $NaMgCl_3$ in the literature, are interpreted here as the peritectics of $Na_6MgCl_8$ and $Na_2Mg_3Cl_8$ in accordance with Seifert et al. [45].

| $x(MgCl_2)$ | Modelling (T (K)) | | Experimental data (T (K)) | | | | | | | Equilibrium | Invariant reaction |
|---|---|---|---|---|---|---|---|---|---|---|---|
| | This work | Chartrand | Grjotheim | Seifert | Menge | Sperenskaya | Scholich | Abramov | Klemm | | |
| 0 | 1073 | 1074 | 1073 | - | - | 1072 | - | 1086 | - | Congruent Melting | $NaCl = L$ |
| 0.143 | 751 | 748[a] | 747[a] | 747 | 742[a] | 749[a] | 747[a] | 757[a] | 760[a] | Peritectic | $Na_6MgCl_8 = NaCl + L'$ |
| 0.333 | 723 | - | - | 715 | - | - | - | - | - | Peritectic | $Na_2MgCl_4 = Na_6MgCl_8 + L'$ |
| 0.415 | 720 | 732 | 724 | 709 | 702 | 714 | 713 | 721 | - | Eutectic | $Na_2MgCl_4 + NaMgCl_3 = L$ |
| 0.5 | 722 | 739 | 740 | 716 | 717 | 735 | 728 | 730 | 734 | Peritectic | $NaMgCl_3 = Na_2Mg_3Cl_8 + L'$ |
| 0.6 | 743 | - | - | 740 | - | - | - | - | - | Peritectic | $Na_2Mg_3Cl_8 = MgCl_2 + L'$ |
| 1 | 987 | 987 | 991 | - | - | - | - | 984 | - | Congruent Melting | $MgCl_2 = L$ |

Table 3.5: Calculated invariant equilibria in the $NaCl-MgCl_2$ system, as well as experimentally measured values of these invariants from Seifert et al. [45], Grjotheim et al [51], Menge et al. [55], Speranskaya et al. [54], Scholich et al. [48], Abramov et al. [53] and Klemm et al. [49], as well as the thermodynamic assessment of Chartrand et al. [56].
[a] Reported temperatures were interpreted as the peritectic reaction $Na_2MgCl_4 = NaCl + L'$ in the literature.



## 3.3.2. $MgCl_2-MCl_3$ (M = Nd, Ce, U, Pu)

### THERMODYNAMIC MODELS

All systems $MgCl_2-MCl_3$ (M = Ce, Nd, U, Pu) modelled in this section are simple binary eutectic systems, with no reported intermediates or solid solubility. The $MgCl_2-NdCl_3$ system has been investigated experimentally by Vogel et al. [59] using DTA. Sun et al. [60] measured the $MgCl_2-CeCl_3$ system using thermal analysis, without further specifying their measurement technique. The system $MgCl_2-UCl_3$ was investigated by Desyatnik et al. [61] using differential thermal analysis (DTA), and they did not detect any solid solubility using XRD. Finally, the $MgCl_2-PuCl_3$ system has been modeled based on the experimental investigation by Johnson et al. [62]. In the absence of experimental mixing enthalpy data for any of the systems, the mixing enthalpy of these systems has been estimated with the method of Davis and Rice [44].

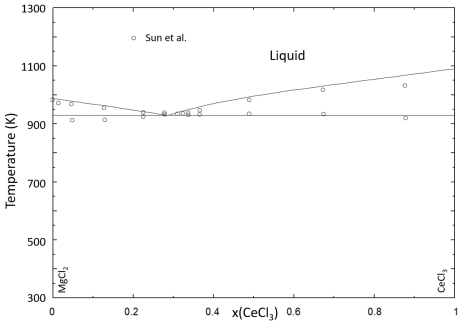


Figure 3.17: Phase diagram of the $MgCl_2-CeCl_3$ system, calculated with the thermodynamic model presented in this work and compared to the experimental data from Sun et al. [60].

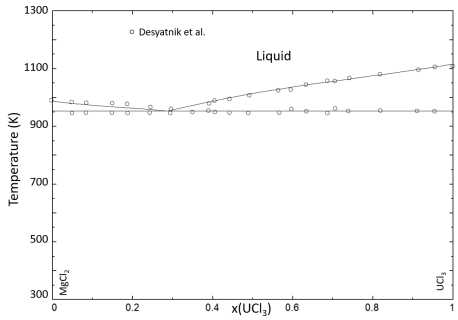


Figure 3.18: Phase diagram of the $MgCl_2-UCl_3$ system calculated with the thermodynamic model presented in this work, compared to the experimental data from Desyatnik et al. [61].

The systems $MgCl_2-UCl_3$ and $MgCl_2-PuCl_3$ have been modelled previously by Beneš et al. [63]. However, Beneš et al. did not include mixing enthalpy data in their assessment, so in order to have our thermodynamic model agree with the estimated mixing enthalpy data, these systems have been reoptimized in this work. The phase diagrams of the systems $MgCl_2-CeCl_3$, $MgCl_2-UCl_3$, $MgCl_2-NdCl_3$ and $MgCl_2-PuCl_3$ are presented in Figures 3.17, 3.18, 3.19 and 3.20, respectively. The calculated mixing en-

thalpies of these systems are given in Figure 3.21, along with the estimated data using Davis' method. Good agreement was obtained between the CALPHAD model and the experimental phase diagram data, as well as the estimated mixing enthalpies for the systems.

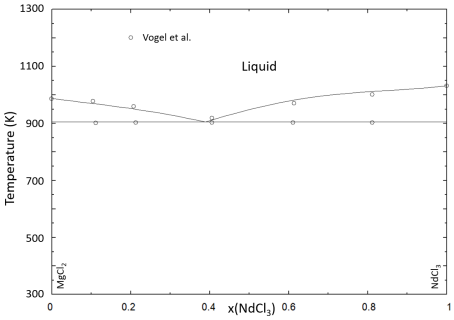


Figure 3.19: Phase diagram of the $MgCl_2-NdCl_3$ system, calculated with the thermodynamic model presented in this work and compared to the experimental data from Vogel et al. [59].

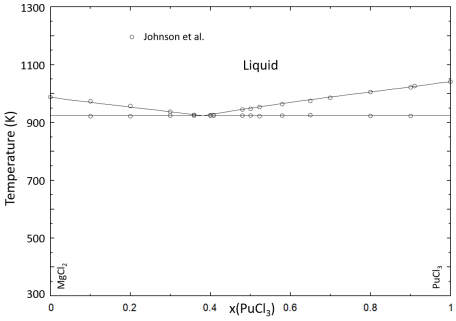


Figure 3.20: Phase diagram of the $MgCl_2-PuCl_3$ system calculated with the thermodynamic model presented in this work, compared to the experimental data from Johnson et al. [62].

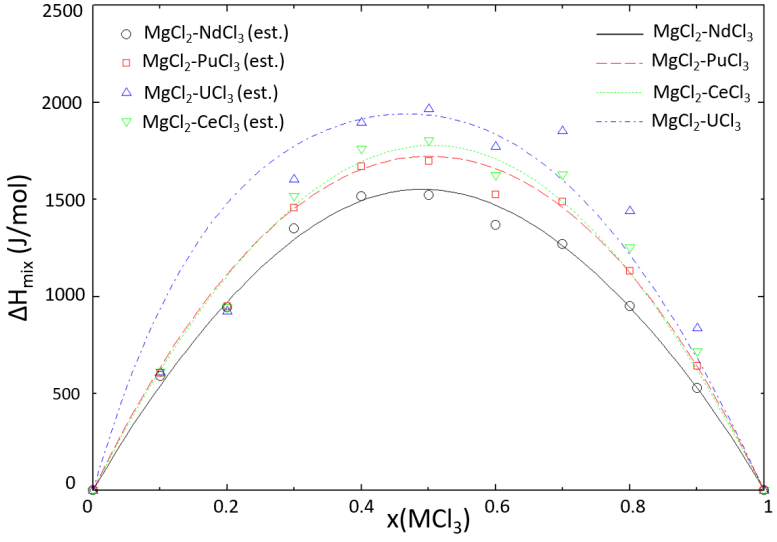


Figure 3.21: Mixing enthalpy of the $MgCl_2-MCl_3$ systems (M = Ce, Nd, U, Pu) calculated at T = 1123 K, compared to data estimated using Davis' method [44].

### 3.3.3. SIMULANT ANALYSIS

With the optimized phase diagrams in Figures 3.17-3.20, we can continue the assessment of the simulant of choice in this work. Figure 3.22 shows the comparison between

the experimental data for the $MgCl_2$−$PuCl_3$ system, and the thermodynamic models for the $MgCl_2$−$MCl_3$ (M = Ce, Nd, U) systems, like in Section 3.1 for the NaCl-$MCl_3$ and CsCl-$MCl_3$ (M = Ce, Nd, U, Pu) systems. Like in the aforementioned systems with NaCl and CsCl, the difference in melting point of the $MCl_3$ (M = Ce, U) end-member causes a difference in melting behaviour compared to the $PuCl_3$ system on the $MCl_3$-rich side of the phase diagram, which is not the case for the $NdCl_3$ system. The eutectic compositions and temperatures of the $MgCl_2$−$MCl_3$ systems are given in Table 3.6. This table shows that while the eutectic temperature of the $CeCl_3$ system is marginally closer to that of the $PuCl_3$ system, the composition of the $NdCl_3$ system is almost identical to that of the $PuCl_3$ system.



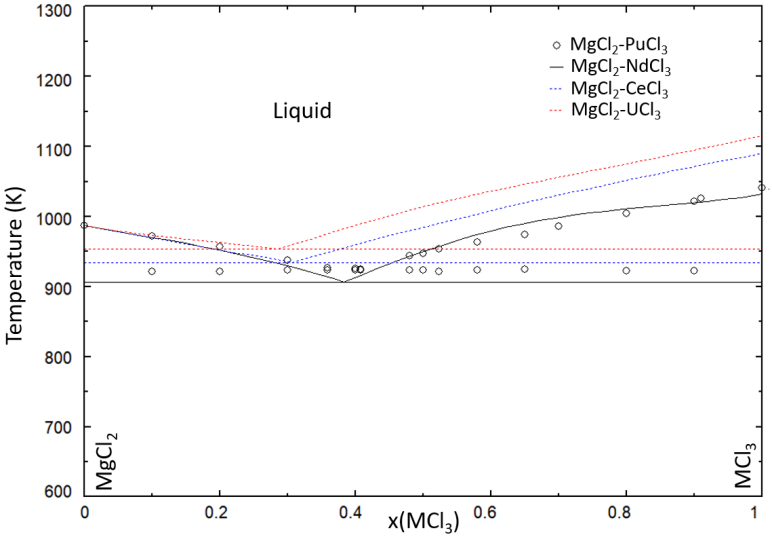


Figure 3.22: Calculated phase diagrams of the systems $MgCl_2$−$NdCl_3$ (solid black line), $MgCl_2$−$CeCl_3$ (dashed blue line) and $MgCl_2$−$UCl_3$ (dashed red line) compared to the experimental data on the $MgCl_2$−$PuCl_3$ system (open black circles) presented by Johnson et al. [62].

| System | $x_1$ | $T_1$ (K) |
|---|---|---|
| $PuCl_3$ | 0.382 | 922 |
| $NdCl_3$ | 0.383 | 906 |
| $CeCl_3$ | 0.308 | 934 |
| $UCl_3$ | 0.285 | 953 |

Table 3.6: Eutectic equilibria in the $MgCl_2$−$MCl_3$ (M = Ce, Nd, U, Pu) systems as calculated with the thermodynamic models presented in this chapter.

## 3.4. TERNARY SYSTEMS NaCl–$MgCl_2$–$MCl_3$ (M = Ce, Nd, U, Pu)

Extrapolations to ternary systems NaCl–$MgCl_2$–$MCl_3$ (M = Ce, Nd, U, Pu) have been made without the addition of ternary excess parameters. This was done because there are no experimental data in the ternary system available, and to be consistent with Beneš et al. [63] who did not introduce ternary interaction terms either. The projected liquidus surface of the ternary systems NaCl–$MgCl_2$–$NdCl_3$ and NaCl–$MgCl_2$–$PuCl_3$ are presented in Figures 3.23 and 3.24.



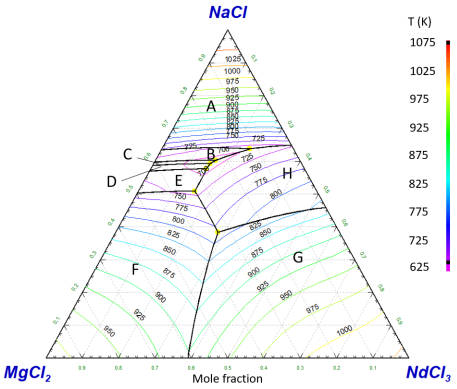


Figure 3.23: Projected liquidus surface of the NaCl–$MgCl_2$–$NdCl_3$ system, calculated with the thermodynamic model presented in this work. Phases listed on the ternary diagram A-H are the primary crystallization phases. Phases listed are NaCl (A), $Na_6MgCl_8$ (B), $Na_2MgCl_4$ (C), $NaMgCl_3$ (D), $Na_2Mg_3Cl_8$ (E), $MgCl_2$ (F), $NdCl_3$ (G) and $Na_{3x}Nd_{2-x}Cl_6$ (H). The calculated ternary eutectic equilibria are presented in Table 3.7.

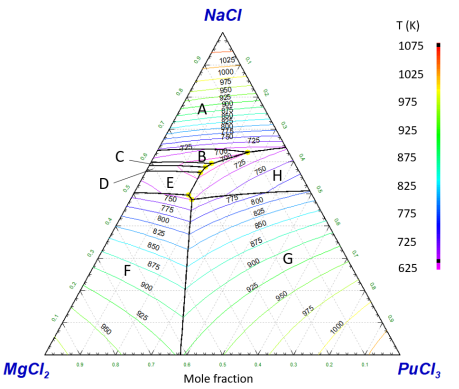


Figure 3.24: Projected liquidus surface of the NaCl–$MgCl_2$–$PuCl_3$ system, calculated with the thermodynamic model presented in this work. Phases listed on the ternary diagram A-H are the primary crystallization phases. Phases listed are NaCl (A), $Na_6MgCl_8$ (B), $Na_2MgCl_4$ (C), $NaMgCl_3$ (D), $Na_2Mg_3Cl_8$ (E), $MgCl_2$ (F) and $PuCl_3$ (G). The calculated ternary eutectic equilibria are presented in Table 3.7.

As seen in Figures 3.23 and 3.24, the projected liquidus surface of the NaCl–$MgCl_2$–$NdCl_3$ and NaCl–$MgCl_2$–$PuCl_3$ systems are quite similar. This is also seen in Table 3.7, where the ternary equilibria are presented. Also shown in Table 3.7 is that there is a difference in the amount of ternary invariant compositions found using our thermodynamic model, compared to that of Beneš et al. This is because in our assessment of the NaCl–$MgCl_2$ system, we used four intermediate compounds ($Na_6MgCl_8$, $Na_2MgCl_4$, $NaMgCl_3$ and $Na_2Mg_3Cl_8$), whereas Beneš et al. used two ($Na_2MgCl_4$ and $NaMgCl_3$). However, the compositions and temperatures of the ternary invariant equilibria predicted by Beneš et al. are close to compositions at which our thermodynamic model also predicts invariant equilibria.

| x(NaCl) | x($MgCl_2$) | x($MCl_3$) | T (K) | Invariant equilibrium |
|---|---|---|---|---|
| **NaCl−$MgCl_2$−$NdCl_3$ - This work** | | | | |
| 0.419 | 0.328 | 0.252 | 782 | $MgCl_2$ + $NdCl_3$ + $Na_{3x}Nd_{2-x}Cl_6$ |
| 0.499 | 0.336 | 0.165 | 714 | $MgCl_2$ + $Na_{3x}Nd_{2-x}Cl_6$ + $Na_2Mg_3Cl_8$ |
| 0.635 | 0.121 | 0.244 | 702 | NaCl + $Na_6MgCl_8$ + $Na_{3x}Nd_{2-x}Cl_6$ |
| 0.569 | 0.275 | 0.156 | 692 | $Na_2Mg_3Cl_8$ + $NaMgCl_3$ + $Na_{3x}Nd_{2-x}Cl_6$ |
| 0.596 | 0.236 | 0.167 | 688 | $NaMgCl_3$ + $Na_2MgCl_4$ + $Na_{3x}Nd_{2-x}Cl_6$ |
| 0.585 | 0.257 | 0.158 | 688 | $Na_2MgCl_4$ + $Na_6MgCl_8$ + $Na_{3x}Nd_{2-x}Cl_6$ |
| **NaCl−$MgCl_2$−$PuCl_3$ - This work** | | | | |
| 0.487 | 0.405 | 0.107 | 724 | $MgCl_2$ + $PuCl_3$ + $PuCl_3$ |
| 0.608 | 0.125 | 0.267 | 700 | NaCl + $Na_6MgCl_8$ + $PuCl_3$ |
| 0.554 | 0.310 | 0.136 | 692 | $Na_2Mg_3Cl_8$ + $NaMgCl_3$ + $PuCl_3$ |
| 0.570 | 0.282 | 0.148 | 687 | $NaMgCl_3$ + $Na_2MgCl_4$ + $PuCl_3$ |
| 0.580 | 0.255 | 0.165 | 688 | $Na_2MgCl_4$ + $Na_6MgCl_8$ + $PuCl_3$ |
| **NaCl−$MgCl_2$−$PuCl_3$ - Beneš et al. [63]** | | | | |
| 0.632 | 0.171 | 0.196 | 697 | NaCl + $PuCl_3$ + $Na_2MgCl_4$ |
| 0.582 | 0.295 | 0.124 | 706 | $NaMgCl_3$ + $Na_2MgCl_4$ + $PuCl_3$ |
| 0.521 | 0.389 | 0.090 | 722 | $MgCl_2$ + $PuCl_3$ + $NaMgCl_3$ |

Table 3.7: Calculated ternary invariant equilibria in the NaCl−$MgCl_2$−$MCl_3$ systems (M = Nd, Pu).



Furthermore, the liquidus projections of the ternary systems NaCl−$MgCl_2$−$CeCl_3$ and NaCl−$MgCl_2$−$UCl_3$ are presented in Figures 3.25 and 3.26. The ternary invariant equilibria shown on the liquidus projections in these figures are also listed in Table 3.8, along with the predicted invariant equilibria presented by Beneš et al. [63]. Like in Table 3.7, the difference in the amount of invariant equilibria found by Beneš et al. and our model is explained by the different amount of intermediate compounds present in the models. Again, like in the NaCl−$MgCl_2$−$PuCl_3$ system, the invariant equilibria calculated by Beneš et al. are also obtained with our thermodynamic model. Additionally, when comparing the liquidus surfaces of all NaCl−$MgCl_2$−$MCl_3$ (M = Ce, Nd, U, Pu) systems, it reinforces the idea that Nd is more accurate as a simulant for Pu than either Ce or U. The behaviour of $CeCl_3$ in the molten salt systems presented in this chapter is a lot closer to that of $UCl_3$, hence Ce could be used as a simulant for U instead.

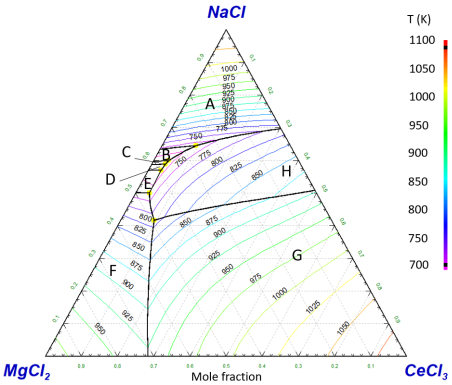


Figure 3.25: Projected liquidus surface of the $NaCl-MgCl_2-CeCl_3$ system, calculated with the thermodynamic model presented in this work. Phases listed on the ternary diagram A-H are the primary crystallization phases at that composition. Phases listed are NaCl (A), $Na_6MgCl_8$ (B), $Na_2MgCl_4$ (C), $NaMgCl_3$ (D), $Na_2Mg_3Cl_8$ (E), $MgCl_2$ (F), $CeCl_3$ (G) and $Na_{3x}Ce_{2-x}Cl_6$ (H). The calculated ternary equilibria are presented in Table 3.8.

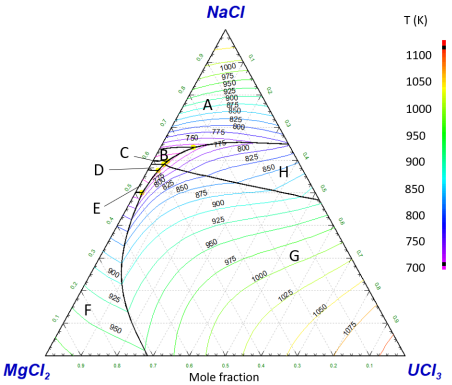


Figure 3.26: Projected liquidus surface of the $NaCl-MgCl_2-UCl_3$ system, calculated with the thermodynamic model presented in this work. Phases listed on the ternary diagram A-H are the primary crystallization phases at that composition. Phases listed are NaCl (A), $Na_6MgCl_8$ (B), $Na_2MgCl_4$ (C), $NaMgCl_3$ (D), $Na_2Mg_3Cl_8$ (E), $MgCl_2$ (F), $UCl_3$ (G) and $NaU_2Cl_7$ (H). The calculated ternary eutectic equilibria are presented in Table 3.8.

| x(NaCl) | x($MgCl_2$) | x($MCl_3$) | T (K) | Invariant equilibrium |
|---|---|---|---|---|
| **NaCl−$MgCl_2$−$CeCl_3$ - This work** | | | | |
| 0.417 | 0.490 | 0.093 | 787 | $MgCl_2$ + $CeCl_3$ + $Na_{3x}Ce_{2-x}Cl_6$ |
| 0.645 | 0.261 | 0.095 | 733 | $MgCl_2$ + $Na_{3x}Ce_{2-x}Cl_6$ + $Na_2Mg_3Cl_8$ |
| 0.499 | 0.462 | 0.039 | 730 | NaCl + $Na_6MgCl_8$ + $Na_{3x}Ce_{2-x}Cl_6$ |
| 0.570 | 0.394 | 0.036 | 710 | $Na_2Mg_3Cl_8$ + $NaMgCl_3$ + $Na_{3x}Ce_{2-x}Cl_6$ |
| 0.599 | 0.359 | 0.042 | 708 | $NaMgCl_3$ + $Na_2MgCl_4$ + $Na_{3x}Ce_{2-x}Cl_6$ |
| 0.588 | 0.374 | 0.038 | 706 | $Na_2MgCl_4$ + $Na_6MgCl_8$ + $Na_{3x}Ce_{2-x}Cl_6$ |
| **NaCl−$MgCl_2$−$UCl_3$ - This work** | | | | |
| 0.639 | 0.260 | 0.101 | 735 | $MgCl_2$ + $UCl_3$ + $Na_xU_{2-2x}Cl_{6-5x}$ |
| 0.500 | 0.481 | 0.020 | 733 | $MgCl_2$ + $NaU_2Cl_7$ + $Na_2Mg_3Cl_8$ |
| 0.568 | 0.402 | 0.029 | 711 | NaCl + $Na_6MgCl_8$ + $NaU_2Cl_7$ |
| 0.597 | 0.360 | 0.043 | 709 | $Na_2Mg_3Cl_8$ + $NaMgCl_3$ + $NaU_2Cl_7$ |
| 0.596 | 0.361 | 0.042 | 707 | $NaMgCl_3$ + $Na_2MgCl_4$ + $NaU_2Cl_7$ |
| 0.587 | 0.378 | 0.036 | 707 | $Na_2MgCl_4$ + $Na_6MgCl_8$ + $NaU_2Cl_7$ |
| **NaCl−$MgCl_2$−$UCl_3$ - Beneš et al. [63]** | | | | |
| 0.637 | 0.251 | 0.112 | 719 | NaCl + $UCl_3$ + $Na_2MgCl_4$ |
| 0.578 | 0.356 | 0.066 | 720 | $NaMgCl_3$ + $Na_2MgCl_4$ + $UCl_3$ |
| 0.520 | 0.433 | 0.047 | 731 | $MgCl_2$ + $UCl_3$ + $NaMgCl_3$ |

Table 3.8: Calculated ternary invariant equilibria in the $NaCl-MgCl_2-MCl_3$ systems (M = Ce, U).

## 3.5. CONCLUSIONS

In this chapter, a simulant analysis for the approximation of the behaviour of $PuCl_3$ in molten chlorides is presented. By comparing the phase diagrams of the $NaCl-MCl_3$, $CsCl-MCl_3$ and $MgCl_2-MCl_3$ systems (M = Ce, Nd, U, Pu), $NdCl_3$ was found to be the best simulant for approximating the melting behaviour of multicomponent systems con-

taining $PuCl_3$.

Furthermore, a structural investigation of the intermediate compounds in the systems $NaCl-NdCl_3$ and $NaCl-CeCl_3$ has been performed. The intermediate compound $Na_{3x}RE_{2-x}Cl_6$ (RE = Ce, Nd) has been found as well as the solubility limits. This solid solubility has been included in the re-assessment of the thermodynamic model. The system $NaCl-UCl_3$ has been re-optimized based on the assessment of Yingling et al. [15], and the model of the $NaCl-PuCl_3$ system has been taken from the work Dumaire et al. [28]. Further experimental investigation is necessary to investigate the possible intermediate compounds $Na_{3x}Ac_{2-x}Cl_6$ (Ac = U, Pu).

Moreover, the re-optimized thermodynamic model of the base fuel $NaCl-MgCl_2-PuCl_3$ is presented. This molten salt system is the basis for all other systems and calculations performed in this work. The $NaCl-MgCl_2$ system was re-optimized to include four intermediates: $NaMgCl_3$, $Na_2MgCl_4$, $Na_2Mg_3Cl_8$ and $Na_6MgCl_8$. Contrary to previous assessments of this system [48, 49, 51, 53–56], in which only two of the aforementioned intermediates were included, we retain the interpretation of Seifert et al. [45] that all four compounds are stable. The simple binary eutectic systems $MgCl_2-MCl_3$ (M = Ce, Nd, U, Pu) have been optimized based on the experimental data reported in the literature. Additionally, the mixing enthalpy of these systems has been estimated using Davis' method, and the CALPHAD model has been optimized to fit the estimated data. Finally, ternary extrapolations to the systems $NaCl-MgCl_2-MCl_3$ (M = Ce, Nd, U, Pu) have been made and compared to values reported in the literature, showing a good agreement between the two. The thermodynamic model for the base fuel $NaCl-MgCl_2-PuCl_3$ that has been compiled from the assessed binaries, and fission products can be added as will be discussed in subsequent chapters to investigate their effect on the solid-liquid equilibria.

# BIBLIOGRAPHY


(1) Darab, J. G.; Li, H.; Bucher, J. J.; Icenhower, J. P.; Allen, P. G.; Shuh, D. K.; Vienna, J. D. *Journal of the American Ceramic Society* **2022**, *105*, 6627–6639.

(2) Marra, J. C. *Cerium as a surrogate in the plutonium immobilized form*; tech. rep.; Savannah River Site (SRS), Aiken, SC (United States), 2001.

(3) Sooby, E.; Nelson, A.; White, J.; McIntyre, P. *Journal of Nuclear Materials* **2015**, *466*, 280–285.

(4) Quemet, A.; Buravand, E.; Catanese, B.; Huot, P.; Dalier, V.; Ruas, A. *Journal of Radioanalytical and Nuclear Chemistry* **2020**, *326*, 255–260.

(5) Seifert, H. J.; Fink, H.; Thiel, G. *Journal of the Less Common Metals* **1985**, *110*, 139–147.

(6) Seifert, H. *Journal of Thermal Analysis and Calorimetry* **2002**, *67*, 789–826.

(7) Seifert, H.; Sandrock, J.; Uebach, J. *Zeitschrift für anorganische und allgemeine Chemie* **1987**, *555*, 143–153.

(8) Sato, T.; Ogawa, T. *Journal of Thermal Analysis* **1998**, *52*, 363–371.

(9) Sharma, R. A.; Rogers, R. A. *Journal of the American Ceramic Society* **1992**, *75*, 2484–2490.

(10) Yimin, S.; Xiangzhen, M.; Jun, L.; Shunxiang, Y.; Zhisen, M.; Zhiyu, Q. *Journal of Rare Earths* **2007**, *25*, 36–41.

(11) Meng, X.; Sun, Y.; Yuan, S.; Ma, Z.; Wang, Y.; Qiao, Z. *Calphad* **2006**, *30*, 301–307.

(12) Ma, Z.; Sun, Y.; Ding, Y.; Wang, Y.; Qiao, Z.; Ye, X. *Calphad* **2006**, *30*, 88–94.

(13) Igarashi, K.; Kosaka, M.; Iwadate, Y.; Hattori, T.; Mochinaga, J. *Denki Kagaku oyobi Kogyo Butsuri Kagaku* **1990**, *58*, 469–470.

(14) Korshunov, B.; Drobot, D.; Bukhtiyarov, V.; Shevtsova, Z. *ZHURNAL NEORGANICH-ESKOI KHIMII* **1964**, *9*, 1427–1430.

(15) Yingling, J.; Schorne-Pinto, J.; Aziziha, M.; Ard, J.; Mofrad, A.; Christian, M.; Dixon, C.; Besmann, T. *The Journal of Chemical Thermodynamics* **2023**, *179*, 106974.

(16) Bjorklund, C.; Reavis, J.; Leary, J.; Walsh, K. *The Journal of Physical Chemistry* **1959**, *63*, 1774–1777.

(17) Sun, Y.; Ma, Z.; Ding, Y.; Wang, Y.; Qiao, Z. *Journal of solution chemistry* **2005**, *34*, 1197–1209.

(18) Baglio, J.; Brock, L.; Struck, C. *Thermochimica Acta* **2002**, *386*, 27–34.

(19) Yimin, S.; Yongxiang, Y.; Juan, H.; Xiangzhen, M.; Tianyi, G.; Zhiyu, Q. *Journal of Rare Earths* **2008**, *26*, 552–557.

(20) Hu, J.; Sun, Y.; Gao, T.; Meng, X.; Yao, Y.; Qiao, Z. *Journal of phase equilibria and diffusion* **2008**, *29*, 398–404.

(21) Seifert, H.-J.; Sandrock, J.; Uebach, J. *Acta Chemica Scandinavica* **1995**, *49*, 653–657.

(22) Chojnacka, I.; Rycerz, L.; Kapala, J.; Gaune-Escard, M. *Journal of Molecular Liquids* **2020**, *319*, 113935.

(23) Mochinaga, J.; Irisawa, K. *Bulletin of the Chemical Society of Japan* **1974**, *47*, 364–367.

(24) Benz, R.; Douglass, R. *The Journal of Physical Chemistry* **1961**, *65*, 1461–1463.

(25) Zheng, C.; Seifert, H. J. *Journal of Solid State Chemistry* **1998**, *135*, 127–131.

(26) Mitra, S.; Uebach, J.; Seifert, H. J. *Journal of Solid State Chemistry* **1995**, *115*, 484–489.

(27) Blachnik, R.; Alberts, G.; Enninga, E. *Zeitschrift fur Anorganische und Allgemeine Chemie* **1985**, *522*, 207–216.

(28) Dumaire, T.; Ocádiz-Flores, J. A.; Konings, R. J. M.; Smith, A. L. *Calphad* **2022**, *79*, 102496.

(29) Seifert, H.; Fink, H.; Uebach, J. *Journal of Thermal Analysis and Calorimetry* **1988**, *33*, 625–632.

(30) Lissner, F.; Krämer, K.; Schleid, T.; Meyer, G.; Hu, Z.; Kaindl, G. *Zeitschrift für anorganische und allgemeine Chemie* **1994**, *620*, 444–450.

(31) Meyer, G.; Schleid, T. *Journal of the Less Common Metals* **1986**, *116*, 187–197.

(32) Seifert, H.; Sandrock, J.; Thiel, G. *Journal of Thermal Analysis* **1986**, *31*, 1309–1318.

(33) Gaune-Escard, M.; Rycerz, L.; Szczepaniak, W.; Bogacz, A. *Thermochimica Acta* **1994**, *236*, 59–66.

(34) Baev, A.; Novikov, G. *Russian Journal of Inorganic Chemistry* **1960**, *6*, 1320.

(35) Korshunov, B.; Morozov, I.; Ionov, V. *Izvestiya vysshikh uchebnykh zavedeniy, Tsvetnaya mettalurgiya* **1960**, 402.

(36) Nishihara, K.; Shimizu, Y.; Morita, N. *Electrochemistry* **1950**, *19*, 105–106.

(37) Kojima, T. *Electrochemistry* **1951**, *20*, 173–176.

(38) Storonkin, I.; Vasilkova, O.; Kozhina, I. *Vestnik, Leningrad University* **1973**, *4*, 80–83.

(39) Krämer, K.; Meyer, G. *Zeitschrift für anorganische und allgemeine Chemie* **1990**, *589*, 96–100.

(40) Papatheodorou, G.; Kleppa, O. *The Journal of Physical Chemistry* **1974**, *78*, 178–181.

(41) Storonkin, I.; Vasilkova, I.; Grebrennikova, O.; Kozhina, I. *Bulletin of Leningrad University* **1973**, *22*, 84–88.

(42) Kraus, C. *Phase Diagram of Some Complex Salts of Uranium with Halides of the Alkali and Alkaline Earth Metals*; tech. rep.; This report was produced in 1943, well before there was an Atomic Energy . . ., 1943.

(43) Matsuura, H.; Takagi, R.; Rycerz, L.; Gaune-Escard, M. *Journal of Nuclear Science and Technology* **2002**, *39*, 632–634.

(44) Davis, H. T.; Rice, S. A. *The Journal of Chemical Physics* **1964**, *41*, 14–24.

(45) Seifert, H.; Fink, H. *Revue de Chimie Minerale* **1975**, *12*, 466–475.

(46) Van Loon, C.; IJdo, D. *Acta Crystallographica Section B: Structural Crystallography and Crystal Chemistry* **1975**, *31*, 770–773.

(47) Kanno, R.; Takeda, Y.; Murata, K.; Yamamoto, O. *Solid State Ionics* **1990**, *39*, 233–244.

(48) Scholich, K. *Neues Jahrb. Mineral. Geol.* **1920**, *43*, 269.

(49) Klemn, W.; Beyersdorfer, K.; Oryschkewitsch, J. *Zeitschrift für anorganische Chemie* **1948**, *256*, 25–36.

(50) Seifert, H. et al. *Revue de Chimie Minerale* **1980**, 147–157.

(51) Grjotheim, K.; Holm, J. L.; Malmo, J. *Acta Chem. Scand* **1970**, *24*, 6.

(52) Matiašovskỳ, K. *Chemical Papers* **1959**, *13*, 69–77.

(53) Abramov, G. A. *Metallurg (Leningrad)* **1935**, *10*, 82–105.

(54) Speranskaya, E. *Ivz. Akad. Nauk. SSSR, Ser. Khim* **1938**, 463.

(55) Menge, O. *Zeitschrift fur Anorganische und Allgemeine Chemie* **1911**, *72*, 162–219.

(56) Chartrand, P.; Pelton, A. D. *Canadian Metallurgical Quarterly* **2001**, *40*, 13–32.

(57) Kleppa, O.; McCarty, F. *The Journal of Physical Chemistry* **1966**, *70*, 1249–1255.

(58) Hersh, L. S.; Kleppa, O. *The Journal of Chemical Physics* **1965**, *42*, 1309–1322.

(59) Vogel, G.; Schneider, A. *Inorganic and Nuclear Chemistry Letters* **1972**, *8*, 513–521.

(60) Sun, I.-C.; Morozov, I. *Zhurnal Neorganicheskoi Khimii* **1958**, *3*, 1914–1924.

(61) Desyatnik, V.; Izmodenov, Y.; Melnikov, Y.; Nichkov, I.; Raspopin, S. *Soviet Atomic Energy* **1969**, *26*, 634–635.

(62) Johnson, K. W.; Kahn, M.; Leary, J. *The Journal of Physical Chemistry* **1961**, *65*, 2226–2229.

(63) Beneš, O. Joint Research Centre Molten Salt Database - JRCMSD, data retrieved from Joint Research Centre: EU Science Hub, https://joint-research-centre.ec.europa.eu/joint-research-centre-molten-salt-database-jrcmsd_en, 2021.

# 4

# CHEMISTRY OF Sr AND Ba IN SIMULANT SYSTEMS

*The behaviour of the fission products strontium and barium, which are produced with a high yield in nuclear fuels, has been investigated in simulant systems for $NaCl-PuCl_3$, in the $NaCl-CeCl_3$ and $NaCl-NdCl_3$ systems. The thermochemical properties of the molten salt system $AECl_2-RECl_3$ (AE = Sr, Ba; RE = Ce, Nd) have been investigated using an experimental and modelling approach. These molten salt systems include intermediate compounds, i.e. $Ba_3Ce_2Cl_{12}$, $Ba_3Nd_2Cl_{12}$ and $Sr_9Nd_5Cl_{33}$, whose structure has been investigated using X-ray (XRD) and neutron diffraction (ND). Additionally, the intermediate compound $Sr_9Ce_5Cl_{33}$ has been observed in mixtures, but has not been isolated. Furthermore, these systems exhibit solubility of $RECl_3$ (RE = Ce, Nd) in $SrCl_2$ and the high-temperature polymorph $\beta$-$BaCl_2$. Moreover, our measurements show solubility of $BaCl_2$ and $SrCl_2$ in $RECl_3$. The investigation of these solid solutions has been performed using quenching experiments and subsequent post-characterisation by X-ray diffraction. Phase diagram equilibria have also been investigated using differential scanning calorimetry (DSC). Using the aforementioned information on phase transitions, intermediate compound stability, and mutual solid solubility, a thermodynamic assessment of the systems has been performed using the CALPHAD method. The model for the Gibbs energy of the liquid solution is the quasi-chemical formalism in the quadruplet approximation, while the model for the Gibbs energy of the solid solutions is a two-sublattice polynomial model.*

Parts of this chapter have been published in "Alders et al., Physical Chemistry Chemical Physics **26**, 36 (2024) [1]" and "Alders et al., Journal of Molecular Liquids **396**, (2024) [2]".

The phase diagram of the molten salt system $BaCl_2$−$CeCl_3$ has been studied by Morozov et al. using thermal analysis [3]. Morozov et al. reported a single eutectic system with one intermediate compound of composition $Ba_3CeCl_9$, but the existence of this intermediate has not been reported elsewhere. However, another structure containing both barium, cerium and chloride was reported by Meyer et al. [4] as $Ba_9Ce_6Cl_{34}O$. Meyer et al. reported the $Ba_9Ce_6Cl_{34}X$ composition based on X-ray powder diffraction, with X corresponding to an interstitial space for an interstitial atom. From an electroneutrality perspective, Meyer et al. argued that this must be an oxygen anion, though they mentioned that a chloride ion would be more feasible considering the size of the hole. We suspect that there are in fact two chloride anions present in the structure, satisfying the electroneutrality condition, rather than one oxygen anion, corresponding to the chemical formula $Ba_3Ce_2Cl_{12}$ ($x_{CeCl_3}$ = 0.4). Morozov et al. do not report measuring the eutectic equilibrium at compositions $x(CeCl_3) \leq 0.4$, which indicates a possible intermediate compound at this composition rather than $Ba_3CeCl_9$ ($x(CeCl_3)$ = 0.333). This system was also investigated by Storonkin et al. using a thermographic method [5]. They postulated that there may be solid solutions existing at compositions near $BaCl_2$ and $CeCl_3$. The $SrCl_2$−$CeCl_3$ system has been investigated by Morozov et al. [3] using DTA. No intermediates are reported in the literature on this system.

No intermediates have been reported in the literature for the $BaCl_2$−$NdCl_3$ system. However, Meyer et al. [4] have reported a compound with the chemical formula $Ba_9Nd_6Cl_{34}O$. This compound could correspond to the intermediate $Ba_3Nd_2Cl_{12}$ instead, as is the case in the analogous $BaCl_2$−$CeCl_3$ system [2]. Measurements of invariant equilibria have been reported by Morozov et al. [3] and Vogel et al. [6]. In the $SrCl_2$−$NdCl_3$ system, the intermediates $Sr_4NdCl_{11}$ (space group $P2_1/m$) and $Sr_9Nd_5Cl_{33}$ (space group $R\bar{3}$), as well as a solid solution $Sr_{1-x}Nd_xCl_{2+x}$, have been identified by Hodorowicz et al. [7]. Experimental measurements of invariant equilibria have been reported by Morozov et al. [3] and Vogel et al. [6].

## 4.1. $BaCl_2$–$RECl_3$ SYSTEMS (RE = Ce, Nd)

### 4.1.1. STRUCTURAL INVESTIGATIONS

The systems $BaCl_2$−$RECl_3$ both contain an intermediate of composition $Ba_3RE_2Cl_{12}$. The intermediates $Ba_3RE_2Cl_{12}$ have not been reported in the literature before, but Meyer et al. [4] do suggest the existence of compounds with the same stoichiometric ratio of barium to rare earth metal, i.e. $Ba_9RE_6Cl_{34}O$. There was still debate about the existence and stoichiometry of this intermediate, as Meyer et al. suggest it contains oxygen. The crystal structure was determined using X-ray powder diffraction to be tetragonal, in space group I4/m (87), with cell parameters $a,b$ = 11.348(3) Å and $c$ = 21.729(5) Å. Our work, as detailed hereafter, suggests to discard the presence of oxygen in this structure, and instead suggests the presence of two chlorine ions, which also satisfies the charge condition.

### $Ba_3Ce_2Cl_{12}$

In order to investigate this intermediate, a synthesis was performed as described in Chapter 2 using a solid state route by heating the miture of end-members to 750 °C (50 K below the peritectic) and equilibrating at this temperature for 48 hours. The synthesised material was subsequently investigated using XRD and ND, and the profile refinements of this material are shown in Figure 4.1 (XRD) and Figure 4.2 (ND), respectively. For this refinement, the structure of $Ba_9Ce_6Cl_{34}O$ as identified by Meyer et al. was used as a starting structural model. The oxygen ion they suggest to balance the charge is not present in the crystallographic data they reported. The refinements performed here also lack two chlorine atoms.



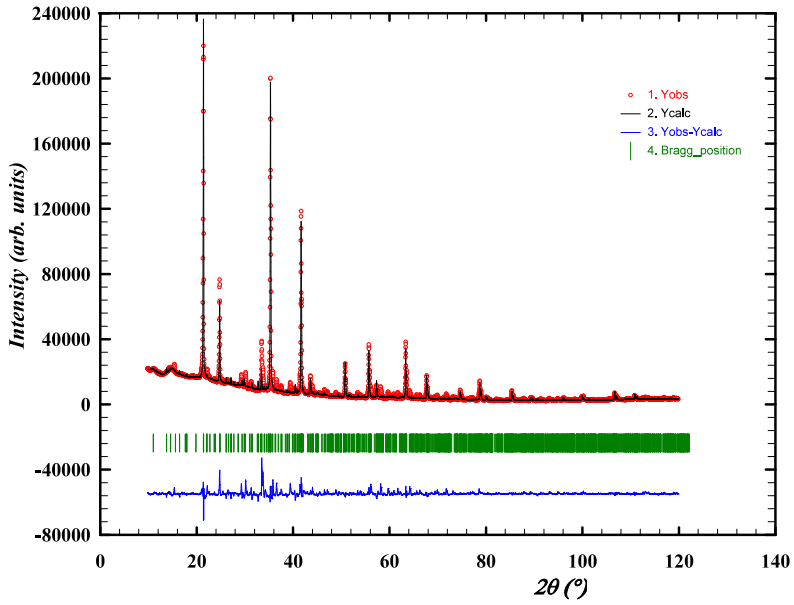


Figure 4.1: Profile refinement [8] of X-ray diffraction data using the crystal structure of $Ba_9Ce_6Cl_{34}O$ as reported by Meyer et al. [4] as structural model. The observed intensity (Yobs, red) is plotted along with the calculated intensity from the refinement (Ycalc, black), and the difference between the two is shown (Yobs-Ycalc, blue). The angles at which reflections occurr are shown as well (Bragg positions, vertical lines). Measurement at $\lambda$ = Cu-K$\alpha$.

The profile refinements in Figures 4.1 and 4.2 show good agreement between the observed and the calculated patterns, indicating that the synthesis was a success. The refined crystal structure of this salt, does not account for a possible presence of oxygen.

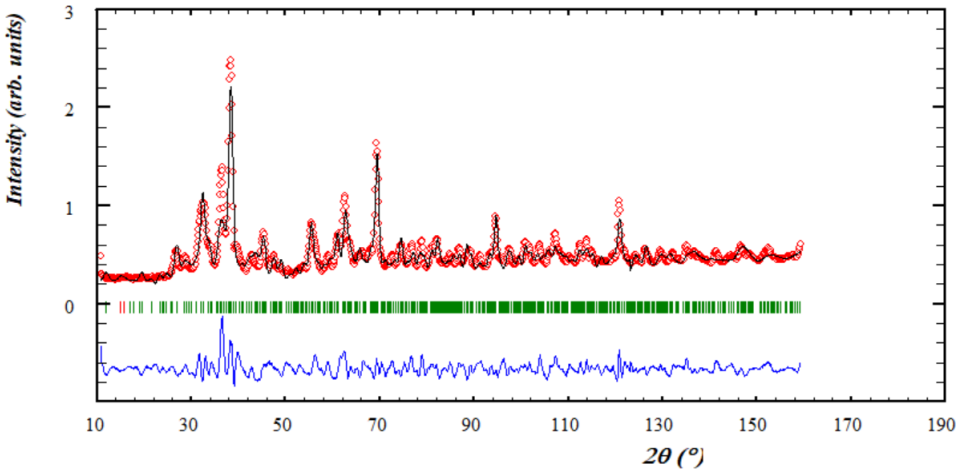


Figure 4.2: Profile refinement of the neutron diffraction data. The observed intensity (red circles) is plotted along with the calculated intensity from the refinement (black line), and the difference between the two is shown (blue line). Bragg positions at which reflections occur are also shown (green lines). Measurement at $\lambda$ = 1.667 Å.

### $Ba_3Nd_2Cl_{12}$

The intermediate $Ba_3Nd_2Cl_{12}$ was synthesised in the same way as $Ba_3Ce_2Cl_{12}$. The obtained profile refinement of this synthesis is shown in Figure 4.3. This figure shows that, like in the $BaCl_2$−$CeCl_3$ system, the crystal structure reported by Meyer et al. is in good agreement with our measurements.

A comparison between the lattice parameters proposed by Meyer et al., the refinement of the XRD pattern and the refinement of the ND pattern is given in Table 4.1. No large discrepancies were observed that would suggest a vastly different crystal structure from what Meyer et al. report.

| Source | Compound | a,b (Å) | c (Å) | V (Å$^3$) |
|---|---|---|---|---|
| This work | $Ba_3Nd_2Cl_{12}$ | 11.304(7) | 21.635(3) | 2765(2) |
| Meyer et al. [4] | $Ba_9Nd_6Cl_{34}O$ | 11.329(5) | 21.676(7) | 2782(4) |
| This work (XRD) | $Ba_3Ce_2Cl_{12}$ | 11.363(1) | 21.547(6) | 2782(2) |
| This work (ND) | $Ba_3Ce_2Cl_{12}$ | 11.336(9) | 21.529(4) | 2767(6) |
| Meyer et al. [4] | $Ba_9Ce_6Cl_{34}O$ | 11.348(3) | 21.729(5) | 2798(2) |

Table 4.1: Comparison between cell parameters obtained for intermediates $Ba_3RE_2Cl_{12}$ (RE = Ce, Nd) (space group I4/m) in this work and the literature.

### SOLID SOLUTIONS - $Ba_{1-x}RE_xCl_{2+x}$ (CUB.)

In the systems $BaCl_2$−$RECl_3$ (RE = Ce, Nd) solid solubility is present at the end-members. In both systems, on the $BaCl_2$-rich side, a high-temperature solid solution is formed in the $\beta$-phase of $BaCl_2$ (space group $Fm\bar{3}m$), namely the cubic phase $Ba_{1-x}RE_xCl_{2+x}$ (RE = Ce, Nd; space group $Fm\bar{3}m$). The existence and structural parameters of solid-solutions

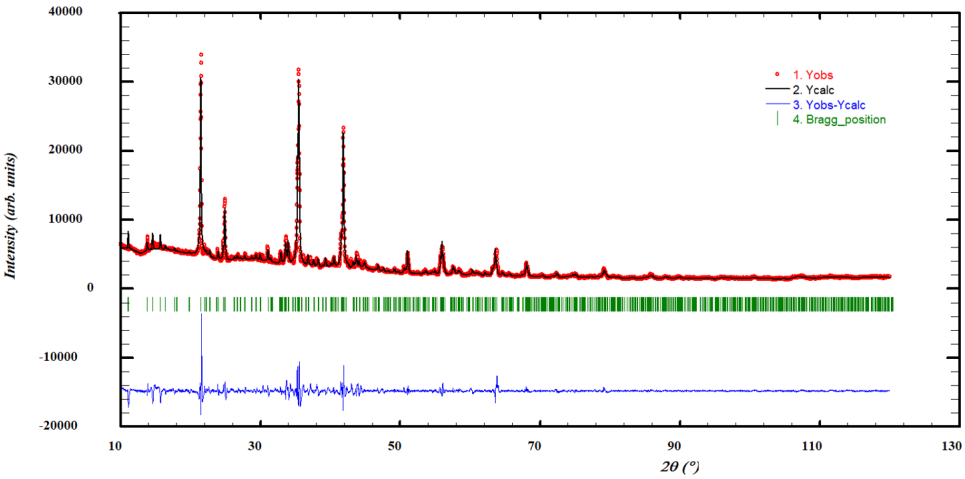


Figure 4.3: Profile refinement of the intermediate salt $Ba_3Nd_2Cl_{12}$, using the structure of $Ba_9Nd_6Cl_{34}O$ as reported by Meyer et al. as crystal structure. The observed intensity (Yobs, red) is plotted along with the calculated intensity from the refinement (Ycalc, black), and the difference between the two is shown (Yobs-Ycalc, blue). The angles at which reflections occurr are shown as well (Bragg positions, vertical lines). Measurement at $\lambda$ = Cu-K$\alpha$.

in this binary system have been investigated through the use of quecning experiments followed by XRD. The compositions at which quenching experiments were performed are x($CeCl_3$) = [0.05, 0.075, 0.15, 0.2, 0.3], quenched from T = 1025 K, and x($CeCl_3$) = 0.1, quenched from 1275 K, in the $BaCl_2$–$CeCl_3$ system. Furthermore, in the $NdCl_3$ system, quenching experiments were carried out at compositions x($NdCl_3$) = [0.05, 0.1, 0.15], quenched from 923 K. In both cases the solid solution, $Ba_{1-x}RE_xCl_{2+x}$, is identical in crystal structure to that of the $\beta$-phase of $BaCl_2$ (both are cubic, in space group $Fm\bar{3}m$), and a shift in cell parameters is visible with increasing $RECl_3$-content. This shift is due to the insertion of the smaller $RE^{3+}$ cation ($R_{crystal,Ce}$ = 1.15 Å, $R_{crystal,Nd}$ = 1.123 Å [9]) instead of the larger $Ba^{2+}$ ($R_{crystal}$ = 1.49 Å [9]) cation in the crystal structure of $\beta$-$BaCl_2$. The formation of this solid solution is also visible by DSC, as shown in Section 4.1.3. The evolution of the cell volume with composition is shown in Figures 4.4a and 4.5. In all single-phase solid solutions observed in these systems, a linear trend in the cell volume is apparent.

### SOLID SOLUTIONS - $Ba_yRE_{1-y}Cl_{3-y}$ (HEX.)

In addition to the $Ba_{1-x}RE_xCl_{2+x}$ (cub.) solid solution, solid solubility of $BaCl_2$ in the hexagonal crystal structure of $CeCl_3$ (space group $P6_3m$) has been observed. Structurally, this solid solution is different from the $Ba_{1-x}Ce_xCl_{2+x}$ (cub.) solution, as it has a hexagonal crystal structure, denoted as $Ba_yCe_{1-y}Cl_{3-y}$ (hex.) (space group $P6_3m$). In this case, the solid solution was investigated through quenching experiments at x($CeCl_3$) = [0.9, 0.95, 0.975, 0.99], quenched from 973 K (all compositions except x($CeCl_3$ = 0.9) or 1023 K (x($Cecl_3$) = 0.9). Given the crystal sizes of the $Ce^{3+}$ and $Ba^{2+}$ cations respoectively, an

increase in cell volume with increasing $BaCl_2$ content is expected. This is also shown in Figure 4.4b, where the single-phase solid solution obeys the expected linear trend, increasing in size as the $BaCl_2$-content increases. Additionally, a drop in the measured eutectic temperature, shown in Section 4.1.3, was observed for compositions $x(CeCl_3) \geq 0.95$, which also serves as an indication that a solid solution forms. Similar experiments have not been performed to verify the existence of the $Ba_yNd_{1-y}Cl_{3-y}$ (hex.) solid solution, but based on the similarity between the $CeCl_3$ and $NdCl_3$ systems, the fact that the aforementioned decrease in eutectic temperature is also measured in the $BaCl_2$–$NdCl_3$ system at compositions $x(NdCl_3) \geq 0.95$, and the Tammann diagram shown in Figure 4.9, this solid solution was included in the thermodynamic assessment of this system.



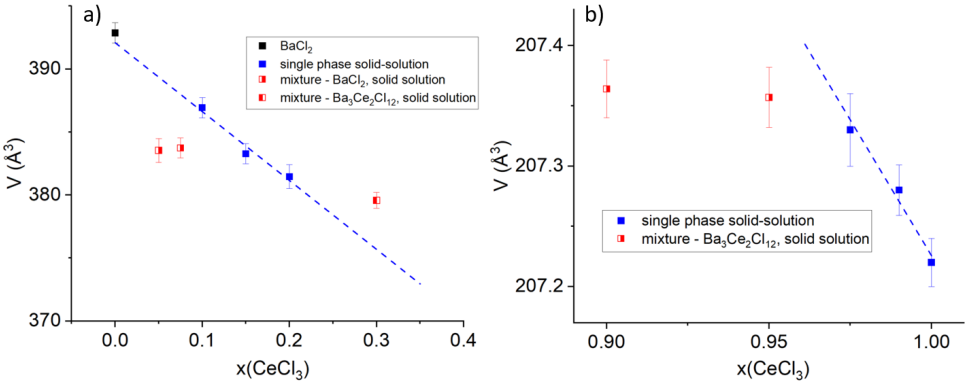


Figure 4.4: Refined cell volumes of the samples, quenched from 1025 K, containing solid solutions on the $BaCl_2$-rich side, as well as the refined cell parameters of the cubic solid solution $Ba_{1-x}Ce_xCl_{2+x}$ (a, left) and refined cell volumes of the samples, quenched from 973 and 1023 K, containing solid solutions on the $CeCl_3$-rich side, as well as the hexagonal solid solution $Ce_{1-y}Ba_yCl_{3-y}$ (b, right).

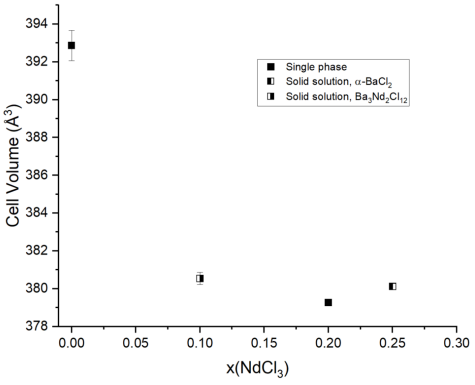


Figure 4.5: Refined cell volumes of the samples, quenched from 923 K, containing solid solutions on the $BaCl_2$-rich side, as well as the refined cell parameters of the cubic solid solution $Ba_{1-x}Nd_xCl_{2+x}$.

| entry | reaction | $\Delta_{sln}H(298.15K)$ (kJ·mol$^{-1}$) | source |
|---|---|---|---|
| 1 | $Ba_3Ce_2Cl_{12}$ (cr) + $H_2O$ = 3 $BaCl_2$(sln) + 2 $CeCl_3$(sln) | -290.19 ± 0.62[a] | this work |
| 2 | 3 $BaCl_2$ (cr) + 2 $CeCl_3$ (cr) + $H_2O$ = 3 $BaCl_2$(sln) + 2 $CeCl_3$(sln) | -316.93 ± 0.80[a] | this work |
| **entry** | **reaction** | $\Delta_f H^o_m(298.15K)$ (kJ·mol$^{-1}$) | **source** |
| 3 | Ba(cr) + $Cl_2$(g) = $BaCl_2$(cr) | -855.2 ± 1.7 | [10] |
| 4 | Ce(cr) + 3/2 $Cl_2$(g) = $CeCl_3$(cr) | -1059.7 ± 1.5 | [11] |
| 5 | 3 Ba(cr) + 2 Ce(cr) + 6 $Cl_2$(g) = $Ba_3Ce_2Cl_{12}$(cr) | -4711.7 ± 6.0 | this work |

Table 4.2: Thermochemical cycle used to determine the standard enthalpy of formation of $Ba_3Ce_2Cl_{12}$. Measurements performed in the temperature interval T = 298.15 ± 0.3 K. The enthalpy of formation of $Ba_3Ce_2Cl_{12}$ was calculated using the relation $\Delta_f H^o_m(5) = -\Delta_{sln}H(1) + \Delta_{sln}H(2) + 3\Delta_f H^o_m(3) + 2\Delta_f H^o_m(4)$.
[a]Expanded uncertainty $U$ with a coverage factor $k = 2$, corresponding to a 95% confidence interval.

### 4.1.2. INVESTIGATION OF THERMODYNAMIC PROPERTIES

The standard enthalpy of formation of $Ba_3Ce_2Cl_{12}$ was measured in this work using the thermochemical cycles shown in Table 4.2 in 25 mL $H_2O$. The dissolution reactions reported in Eqs. 4.1 and 4.2 were performed successively. The amounts of $Ba_3Ce_2Cl_{12}$ and {$BaCl_2$ + $CeCl_3$} were adjusted so tht the solutions obtained as products of reactions 4.1 and 4.2 had the same final concentrations of dissolved ions.

$$Ba_3Ce_2Cl_{12}(cr) + H_2O(l) = 3BaCl_2(sln) + 2CeCl_3(sln) \qquad \Delta_{sln}H_1 \qquad (4.1)$$

$$3BaCl_2(cr) + 2CeCl_3(cr) + H_2O(l) = 3BaCl_2(sln) + 2CeCl_3(sln) \qquad \Delta_{sln}H_2 \qquad (4.2)$$

The dissolution of the salts $BaCl_2$, $CeCl_3$ and $Ba_3Ce_2Cl_{12}$ was in all cases instantaneous. The details of the calorimetric results are given in Table 4.3. The enthalpy of the formation reaction from the consituting binary chloride salts can be expressed as in Eq 4.3. The standard enthalpy of formation has been calculated using Equation 4.4. The obtained value for the standard enthalpy of formation of $Ba_3Ce_2Cl_{12}$ is -4711.7 ± 6.0 kJ·mol$^{-1}$.

$$\Delta_r H^o_m = -\Delta_{sln}H_1 + \Delta_{sln}H_2 \qquad (4.3)$$

$$\Delta_f H^o_m(5) = -\Delta_{sln}H_1 + \Delta_{sln}H_2 + 3\Delta_f H^o_m(3) + 2\Delta_f H^o_m(4) \qquad (4.4)$$

| entry | m($Ba_3Ce_2Cl_{12}$) (mg) | ΔT (mK) | $C_p$ (J·K$^{-1}$) | Q (J) | $\Delta_r H^o_m$(298.15 K) (kJ·mol$^{-1}$) |
|---|---|---|---|---|---|
| 1 | 56.00 | 162.420 | 117.683 | -14.552 | -290.453 |
| 2 | 56.05 | 121.729 | 117.691 | -14.542 | -289.968 |
| 3 | 55.71 | 121.309 | 117.345 | -14.449 | -289.882 |
| **entry** | **m($BaCl_2$ + $CeCl_3$)** (mg) | **ΔT (mK)** | **$C_p$ (J·K$^{-1}$)** | **Q (J)** | **$\Delta_r H^o_m$(298.15 K) (kJ·mol$^{-1}$)** |
| 1 | 31.79 + 25.37 | 129.699 | 117.823 | -16.157 | -317.430 |
| 2 | 31.40 + 25.56 | 128.567 | 117.065 | -16.763 | -316.424 |
| 3 | 30.83 + 24.40 | 133.421 | 117.469 | 15.673 | -317.026 |

Table 4.3: Measured dissolution enthalpies at 298.15 K for $Ba_3Ce_2Cl_{12}$(cr) (M = 1117.65 g·mol$^{-1}$) in 25 mL $H_2O$.

### 4.1.3. PHASE EQUILIBRIA AND THERMODYNAMIC ASSESSMENT

A list of mixtures measured by DSC, along with the temperatures of invariant transitions and associated invariant reactions, is presented in Appendix D, Tables D.1 and D.2 for the $BaCl_2$−$CeCl_3$ and $BaCl_2$−$NdCl_3$ systems, respectively. The phase equilibria are also shown on the optimized phase diagrams in Figures 4.7 and 4.6, respectively.



#### $BaCl_2$−$CeCl_3$

The CALPHAD model displayed in Figure 4.6 shows good agreement with the measured invariant points. Figure 4.8 shows that the calculated mixing enthalpy also reproduces the mixing enthalpy as estimated with Davis' method well. A few differences between the data obtained in this work and the phase equilibria as interpreted by Morozov et al. [3] and Storonkin et al. [5] are worth pointing out. First, the liquidus that is measured here is rather flat between the compositions $x_{CeCl_3} = 0.025$ and $x_{CeCl_3} = 0.3$. This could be related to the formation of a solid-solution in this composition range, as the equilibrium between $Ba_{1-x}Ce_xCl_{2+x}$ and $\{Ba_{1-x}Ce_xCl_{2+x} + L\}$ is not observable. Also in this composition range, thermal events were detected around T = 950 K in contrast to the previous works, which according to the present model, correspond to the formation of this solid solution. The peritectic decomposition of the intermediate $Ba_3Ce_2Cl_{12}$ observed near T = 1100 K is also reported in the literature, though Morozov et al. identified this intermediate as $Ba_3CeCl_9$. The eutectic composition that was measured in this work ($x(CeCl_3) = 0.67$) is approximately at the same composition as measured by Morozov et al. ($x(CeCl_3) = 0.68$) and Storonkin et al. ($x(CeCl_3) = 0.65$). Finally, Storonkin et al. observed a solid-solution on the $CeCl_3$-rich side of the phase diagram, and the DSC data obtained in this work corroborates that. The solubility limit of $BaCl_2$ in $CeCl_3$ is around 5% at temperatures above 970 K, while that of $CeCl_3$ in $BaCl_2$ has a maximum of about 25% at 1060 K. The invariant equilibria calculated with this CALPHAD model are presented in Table 4.4, compared to the experimental values measured in this work, and reported in the literature [3, 5].

| **$x(CeCl_3)$** | **T (K)** | | | | **Equilibrium** | **Invariant reaction** |
|---|---|---|---|---|---|---|
| | CALPHAD | Morozov | Storonkin | This work (DSC) | | |
| 0 | 1198 | 1200 | 1199 | 1197 ± 5 | $\alpha$-$\beta$ transition | $\alpha$-$BaCl_2$ = $\beta$-$BaCl_2$ |
| | 1234 | 1243 | 1239 | 1235 ± 5 | Congruent melting | $\beta$-$BaCl_2$ = L |
| 0.18 | 940 | | | 944 ± 10 | Eutectoid | $BaCl_2 + Ba_3Ce_2Cl_{12} = Ba_{1-x}Ce_xCl_{2+x}$ |
| 0.4 | 1068 | 1071 | 1069 | 1062 ± 10 | Peritectic | $Ba_3Ce_2Cl_{12} = Ba_{1-x}Ce_xCl_{2+x} + L'$ |
| 0.66 | 966 | 972 | 970 | 971 ± 10 | Eutectic | $Ba_3Ce_2Cl_{12} + Ce_{1-y}Ba_yCl_{3-y} = L$ |
| 1 | 1089 | 1093 | 1101 | 1093 ± 5 | Congruent melting | $CeCl_3$ = L |

Table 4.4: Calculated invariant equilibria in the $BaCl_2$−$CeCl_3$ system using the model presented in this work (CALPHAD), as well as measured values of these invariants from Morozov et al. [3], Storonkin et al. [5] and this work (DSC).

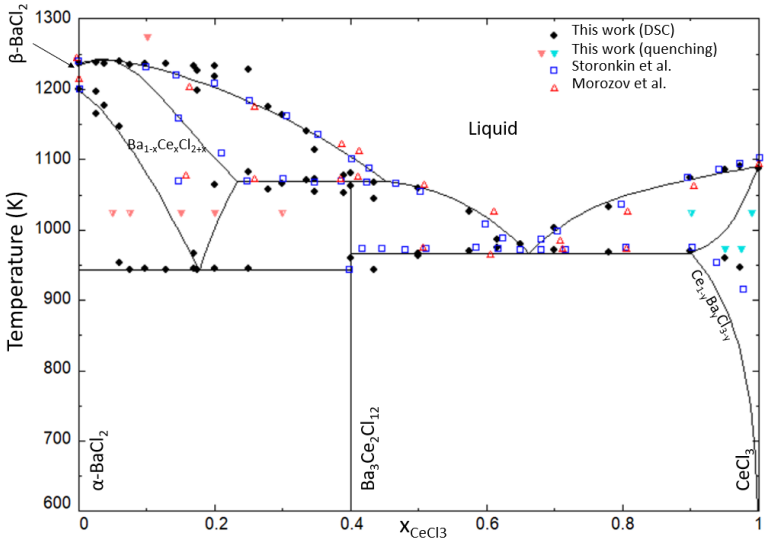


Figure 4.6: Phase diagram of the $BaCl_2$-$CeCl_3$ binary system, as calculated with the optimized thermodynamic model. Data from Morozov et al. [3] (empty orange triangles), Storonkin et al. [5] (empty blue squares) and this work (filled black circles). Labels for the quenching experiments are completely filled (pure solid-solution), right-filled (mixture of solid-solution and $BaCl_2$) and left-filled (mixture of solid-solution and $Ba_3Ce_2Cl_{12}$).

## $BaCl_2$–$NdCl_3$

The CALPHAD model displayed in Figure 4.7 was optimized to fit the measured invariant points, as well as the estimated mixing enthalpy as shown in Figure 4.8. The DSC data between $0.05 \leq x(NdCl_3) \leq 0.3$ at T = 935 K that were not observed by Morozov et al. [3] or Vogel et al. [6] are explained well by the addition of a solid solution phase $Ba_{1-x}Nd_xCl_{2+x}$, stable only at elevated temperatures. The temperature of the peritectic, as well as the temperature and composition of the eutectic, are reproduced accurately by the model. While both Morozov et al. and Vogel et al. reported an intermediate of composition $Ba_3NdCl_9$ to be stable in this system, the absence of a eutectic event at compositions $x(NdCl_3) \leq 0.39$ indicates that the intermediate $Ba_3Nd_2Cl_{12}$ is more likely, as is corroborated by the XRD analysis presented in this work, and the limiting composition of x = 0.4 in the Tammann diagram, as seen in Figure 4.9. The invariant equilibria calculated with this CALPHAD model are presented in Table 4.5, compared to the experimental values measured in this work, and reported in the literature [3, 6].

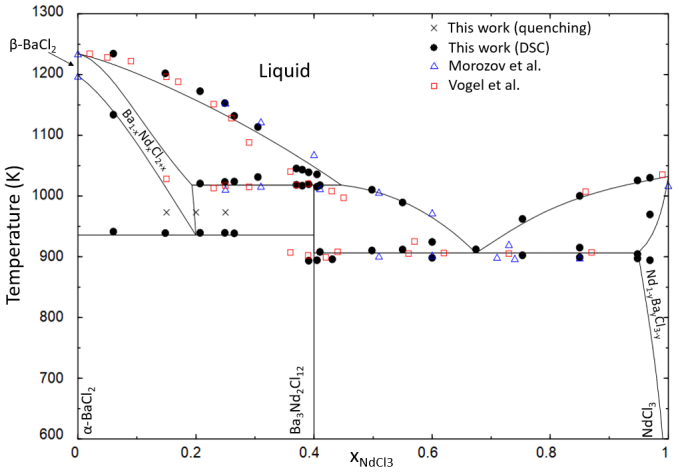


Figure 4.7: Phase diagram of the $BaCl_2$—$NdCl_3$ binary system, as calculated with the optimized thermodynamic model. Data from Morozov et al. [3] (empty blue triangles), Vogel et al. [6] (empty red squares) and this work (filled black circles). The compositions and temperatures at which quenching experiments have been performed are marked with black crosses.

| x($NdCl_3$) | T (K) | | | | Equilibrium | Invariant reaction |
|---|---|---|---|---|---|---|
| | CALPHAD | Morozov | Vogel | This work (DSC) | | |
| 0 | 1198 | 1200 | 1199 | 1197 ± 5 | $\alpha$-$BaCl_2$ = $\beta$-$BaCl_2$ | |
| | 1234 | 1243 | 1239 | 1235 ± 5 | Congruent melting | $\beta$-$BaCl_2$ = L |
| 0.2 | 935 | | | 939 ± 10 | Eutectoid | $\alpha$-$BaCl_2$ + $Ba_3Nd_2Cl_{12}$ = $Ba_{1-x}Nd_xCl_{2+x}$ |
| 0.4 | 1017 | 1011 | 1020 | 1015 ± 10 | Peritectic | $Ba_3Nd_2Cl_{12}$ = $Ba_{1-x}Nd_xCl_{2+x}$ + L′ |
| 0.676 | 906 | 902[a] | 901[b] | 912 ± 10[c] | Eutectic | $Ba_3Nd_2Cl_{12}$ + $Nd_{1-y}Ba_yCl_{3-y}$ = L |
| 1 | 1030 | 1016 | - | 1031 ± 5 | Congruent melting | $NdCl_3$ = L |

Table 4.5: Calculated invariant equilibria in the $BaCl_2$—$NdCl_3$ system, as well as experimentally measured values of these invariants from Morozov et al. [3], Vogel et al [6] and this work (DSC).
[a] x($NdCl_3$, eutectic) = 0.710
[b] x($NdCl_3$, eutectic) = 0.620
[c] x($NdCl_3$, eutectic) = 0.674

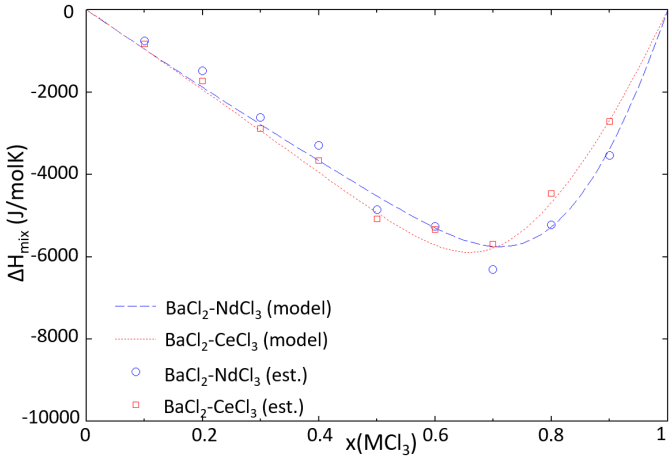


Figure 4.8: Mixing enthalpy of the $BaCl_2$−$NdCl_3$ (dashed line) and $BaCl_2$−$CeCl_3$ (dotted line) binary systems at T = 1273 K, as calculated with the thermodynamic model presented in this section. The mixing enthalpy data were obtained with the mixing enthalpy estimation method presented by Davis and Rice [12] for the $BaCl_2$−$NdCl_3$ (open blue circles) and $BaCl_2$−$CeCl_3$ (open red squares) systems.

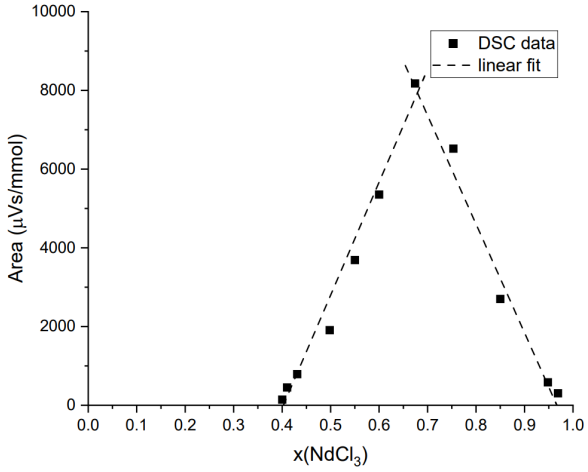


Figure 4.9: Tammann-diagram calculated from the DSC data obtained in this work on the $BaCl_2$−$NdCl_3$ system. The intersection of the linear fits (dashed lines) is the predicted composition of the eutectic in this system. the limiting compositions are x = 0.4 (intermediate $Ba_3Nd_2Cl_{12}$) and x = 0.96 (solid solution $Nd_{1-y}Ba_yCl_{3-y}$).

## 4.2. $SrCl_2$–$RECl_3$ SYSTEMS (RE = Ce, Nd)

### 4.2.1. STRUCTURAL INVESTIGATIONS

#### $Sr_9RE_5Cl_{33}$ (RE = Ce, Nd)

In the $SrCl_2$–$NdCl_3$ system, the intermediates $Sr_4NdCl_{11}$ (space group $P2_1/m$) and $Sr_9Nd_5Cl_{33}$ (space group $R\bar{3}$), as well as a solid solution $Sr_{1-x}Nd_xCl_{2+x}$, have been identified by Hodorowicz et al. [7]. No crystallographic data in the $SrCl_2$–$CeCl_3$ system have been reported in the literature thus far.

In the $SrCl_2$–$NdCl_3$ system, the intermediate $Sr_9Nd_5Cl_{33}$ (hexagonal in space group $R\bar{3}$) was succesfully synthesised, and the profile refinement is shown in Figure 4.10. The obtained refined cell parameters are compared to those presented by Hodorowicz et al. in Table 4.6, and these are in good agreement with each other.



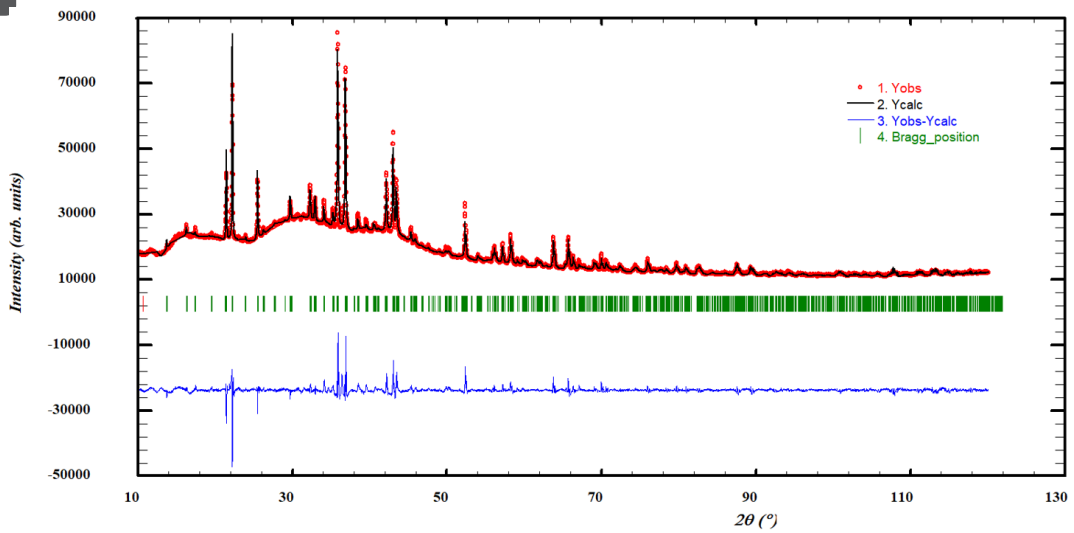


Figure 4.10: Profile refinement of the intermediate salt $Sr_9Nd_5Cl_{33}$ using the structural model by Hodorowicz et al. [7]. The observed intensity (Yobs, red) is plotted along with the calculated intensity from the refinement (Ycalc, black), and the difference between the two is shown (Yobs-Ycalc, blue). The angles at which reflections occurr are shown as well (Bragg positions, vertical lines). Measurement at $\lambda$ = Cu-K$\alpha$.

| Source | Compound | a,b (Å) | c (Å) | V (Å$^3$) |
|---|---|---|---|---|
| This work (XRD) | $Sr_9Nd_5Cl_{33}$ | 12.899(1) | 24.858(2) | 4136(2) |
| Hodorowicz et al. [7] | $Sr_9Nd_5Cl_{33}$ | 12.908(6) | 24.82(1) | 4135(5) |
| This work (XRD) | $Sr_9Ce_5Cl_{33}$ | 13.003(1) | 25.045(3) | 4235(2) |

Table 4.6: Comparison between cell parameters obtained for the intermediate $Sr_9RE_5Cl_{33}$ (RE = Nd, Ce) (space group $R\bar{3}$) in this work and in the literature.

Because of our successful synthesis of $Sr_9Nd_5Cl_{33}$, we attempted to synthesise an analogous compound in the $SrCl_2$–$CeCl_3$ system. These syntheses were largely unsuc-

cessful, and we did not manage to isolate the compound. However, we have observed the crystal structure of $Sr_9Ce_5Cl_{33}$ in mixtures, as shown in Figure 4.11. The calculated cell parameters for this intermediate, using the crystal structure of $Sr_9Nd_5Cl_{33}$ as starting model, are $a,b = 12.9394(5)$ Å and $c = 24.883(1)$ Å. These parameters are slightly larger than the ones measured in this work and reported by Hodorowicz et al. [7] for $Sr_9Nd_5Cl_{33}$, as shown in Table 4.6. This is to be expected since the size of $Ce^{3+}$ cation ($R_{crystal}$ = 1.15 [9]) is slightly larger than that of the $Nd^{3+}$ cation ($R_{crystal}$ = 1.123 [9]). Furthermore, based on our DSC measurements shown in Section 4.2.2, we believe that the intermediate $Sr_9Ce_5Cl_{33}$ does exist, and is therefore incorporated in the CALPHAD model.

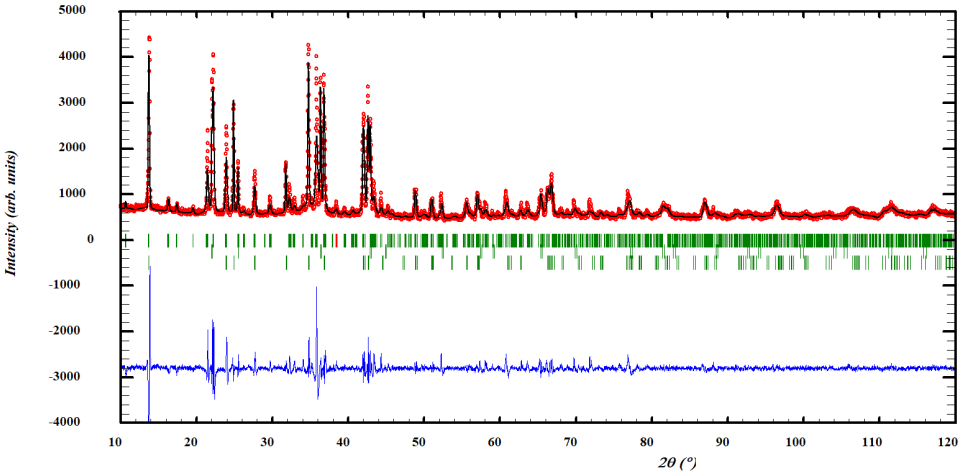


Figure 4.11: Profile refinement of the sample at composition x($CeCl_3$) = 0.55 in the $SrCl_2$–$CeCl_3$ system. The crystal structure of the intermediate salt $Sr_9Nd_5Cl_{33}$ [7] is used as structural model for the $Sr_9Ce_5Cl_{33}$ intermediate compound. Additionally, the phases NaCl and $CeCl_3$ are used in the refinement. The observed intensity (Yobs, red) is plotted along with the calculated intensity from the refinement (Ycalc, black), and the difference between the two is shown (Yobs-Ycalc, blue). The angles at which reflections occurr are shown as well (Bragg positions, vertical lines). Measurement at $\lambda$ = Cu-K$\alpha$.

### SOLID SOLUTIONS - $Sr_{1-x}Nd_xCl_{2+x}$ (CUB.)

Two crystal structures, corresponding to two polymorphic phases, of $SrCl_2$ have been reported in the literature: a simple cubic structure (space group $Fm\bar{3}m$) for $\alpha$-$SrCl_2$ [13], and a slightly distorted cubic structure (also space group $Fm\bar{3}m$) for $\beta$-$SrCl_2$ [13]. The transition from the $\alpha$-phase to the $\beta$-phase, however, is a second-order transition that occurs around 1000 K, that is not measured as an invariant equilibrium by DSC [1]. For this reason, the transition was discarded in the thermodynamic model.

In their investigation of the $SrCl_2$–$NdCl_3$ system, Hodorowicz et al. [7] found that $NdCl_3$ is soluble in the cubic crystal structure of $SrCl_2$ (space group $Fm\bar{3}m$) with a maximum solubility of approximately 18% $NdCl_3$. The solid solution that is formed with $SrCl_2$, namely $Sr_{1-x}Nd_xCl_{2+x}$ (space group $Fm\bar{3}m$) is analogous to the solid solution in the high-temperature phase of $BaCl_2$, namely $Ba_{1-x}Nd_xCl_{2+x}$. The existence of this solid solution is confirmed in this work with quenching and post-XRD measurements. Stoi-

chiometric mixtures of $SrCl_2$ and $NdCl_3$ of compositions x($NdCl_3$) = 0, 0.05, 0.1 and 0.15 were quenched from 923 K. All mixtures showed a single phase solid solution. The profile refinements of the collected XRD data are reported in the Appendix, and the evolution of the lattice parameters in Figure 4.13.



In Figure 4.12, a refinement of the post-XRD at x($NdCl_3$) = 0.1, quenched from 850 K, is shown, indicating a single-phase solid solution at this composition. In contrast to the findings of Hodorowicz et al., the cell volumes calculated with the refined lattice parameters from the profile refinements do not obey a decreasing linear trend, but instead seem to fluctuate around an average value, as seen in Figure 4.13. Based on the DSC data obtained in this work, shown in Section 4.2.2, we are inclined to conclude that the solid solution is stable up to approximately 20 % $NdCl_3$, as the peritectic transition observed at approximately 890 K disappears at lower concentrations (see Figure 4.14). This is in line with the 18% solubility limit as reported by Hodorowicz et al. [7].

The solid solution on the $NdCl_3$-rich side of the system has not been characterized by XRD, but based on the results we found when calculating the Tammann diagram shown in Figure 4.16, we have reason to believe that a narrow solubility range of $SrCl_2$ in $NdCl_3$ exists. Therefore, the solid solution $Sr_yNd_{1-y}Cl_{3-y}$ (hexagonal in space group $P6_3m$) has been included in the CALPHAD model.

The solid solutions we have observed between $SrCl_2$ and $NdCl_3$ have not been observed consistently in the $SrCl_2$−$CeCl_3$ system. However, based on our findings in the $SrCl_2$−$NdCl_3$ system and the similarity between the $BaCl_2$−$RECl_3$ (RE = Ce, Nd) systems, we have included the same solid solutions, to wit $Sr_{1-x}Ce_xCl_{2+x}$ (cub.) and $Sr_yCe_{1-y}Cl_{3-y}$ (hex.), in our thermodynamic assessment of the $SrCl_2$−$CeCl_3$ system.

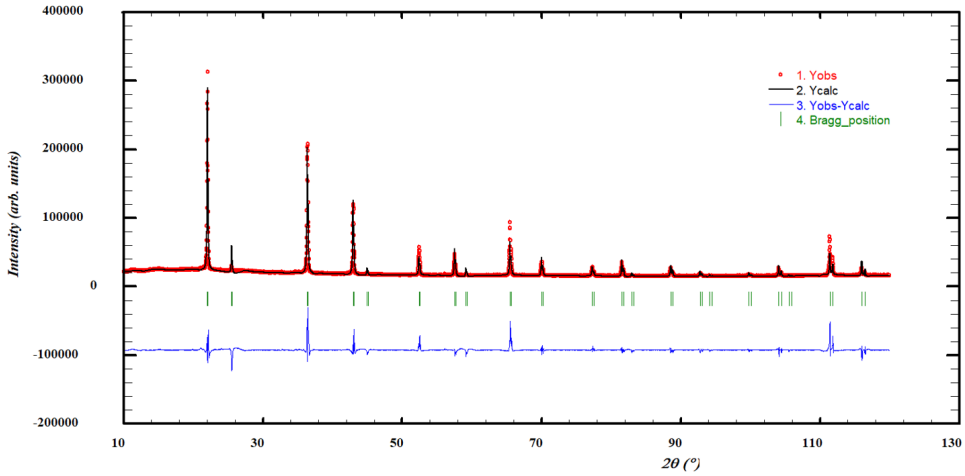


Figure 4.12: Profile refinement of a quenched sample with x($NdCl_3$) = 0.1, showing solid solution $Sr_{1-x}Nd_xCl_{2+x}$, quenched from 850 K. The observed intensity (Yobs, red) is plotted along with the calculated intensity from the refinement (Ycalc, black), and the difference between the two is shown (Yobs-Ycalc, blue). The angles at which reflections occur are shown as well (Bragg positions, vertical lines). Measured at $\lambda$ = Cu-K$\alpha$.

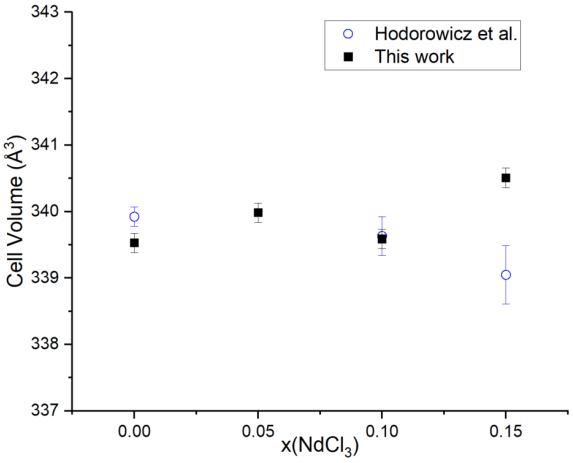


Figure 4.13: Cell volumes of the cubic $Sr_{1-x}Nd_xCl_{2+x}$ (space group $Fm\bar{3}m$) phase, calculated from the profile refinements of the solid solutions quenched in the $SrCl_2$–$NdCl_3$ system for T = 923 K.

### 4.2.2. PHASE EQUILIBRIA AND THERMODYNAMIC ASSESSMENT

Experimental measurement of invariant equilibria in the $SrCl_2$–$NdCl_3$ system has been reported by Morozov et al. [3] and Vogel et al. [6], both using Differential Thermal Analysis (DTA) and analyzing the cooling curves. Morozov et al. also investigated the $SrCl_2$–$CeCl_3$ system with DTA [3].

The results of our DSC investigation of these systems are reported in Appendix D, Tables D.3 and D.4 for the $NdCl_3$ and $CeCl_3$ systems, respectively. The measured invariant equilibria are also shown on the phase diagrams of these systems in Figures 4.14 and 4.17, respectively.

### $SrCl_2$–$NdCl_3$

With the thermodynamic descriptions of the parameters in the system as described in Chapter 2, the phase diagram and mixing enthalpy of the system were calculated. The optimized phase diagram is shown in Figure 4.14, and the enthalpy of mixing is reported in Figure 4.15. The CALPHAD model has been optimized to fit the invariant equilibria measured in this work, as opposed to the data available in the literature. There is a significant discrepancy between the calculated liquidus between x($NdCl_3$) = 0.2 and x($NdCl_3$) = 0.6 when comparing to the data from Morozov et al. [3] and Vogel et al. [6]. Given the fact that the data from these sources are not in agreement with each other, and that the actual liquidus we measure is in between the reported sets of data, we are confident in the accuracy of our experimental measurements and model in this composition range. The eutectic composition calculated by the model is in good agreement with the predicted composition from the Tammann-diagram in Figure 4.16, where the heat flow area of the eutectic transition is plotted against composition.

The composition of the intermediate compound that we identified is also different from that reported by Morozov et al. and Vogel et al., but its existence is supported by the XRD data obtained in this work, as well as the work of Hodorowicz et al. [7]. It is also consistent with the limiting composition obtained at x = 0.357 in the Tammann diagram. The existence of mutual solid solubility of $NdCl_3$ and $SrCl_2$ was suggested previously by Vogel et al. and Hodorowicz et al., which our data corroborate. Moreover, the solubility of $SrCl_2$ in $NdCl_3$ is up to 5% $SrCl_2$ at 900 K. This is again in line with the Tammann diagram in Figure 4.16 where the area of the eutectic peak goes to zero at approximately x($NdCl_3$) = 0.95, indicating that there is a solid solution at higher compositions.

| x($NdCl_3$) | T (K) | | | | Equilibrium | Invariant reaction |
|---|---|---|---|---|---|---|
| | CALPHAD | Morozov | Vogel | This work (DSC) | | |
| 0 | 1146 | 1142 | 1151 | 1147 ± 5 | Congruent melting | $SrCl_2 = L$ |
| 0.357 | 890 | 893 | 873 | 894 ± 10 | Peritectic | $Sr_9Nd_5Cl_{33} = Sr_{1-x}Nd_xCl_{2+x} + L'$ |
| 0.535 | 878 (0.530) | 872 (0.560) | 853 (0.420) | 885 ± 10 (0.535) | Eutectic | $Sr_9Nd_5Cl_{33} + Nd_{1-y}Sr_yCl_{3-y} = L$ |
| 1 | 1030 | 1016 | - | 1031 ± 5 | Congruent melting | $NdCl_3 = L$ |

Table 4.7: Calculated invariant equilibria in the $SrCl_2$–$NdCl_3$ system, as well as experimentally measured values of these invariants from Morozov et al. [3], Vogel et al [6] and this work (DSC). The numbers in parentheses are the respective compositions of the eutectic.

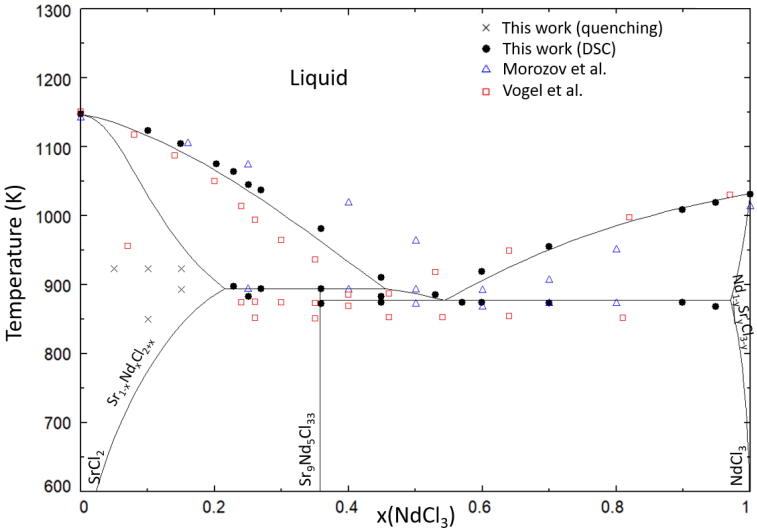


Figure 4.14: Phase diagram of the $SrCl_2$−$NdCl_3$ salt system calculated with the thermodynamic model presented in this section. Experimental data from this work (closed black circles), Morozov et al. [3] (open blue triangles) and Vogel et al. [6] (open red squares). Compositions and temperatures at which quenching experiments were performed are marked with a black x.

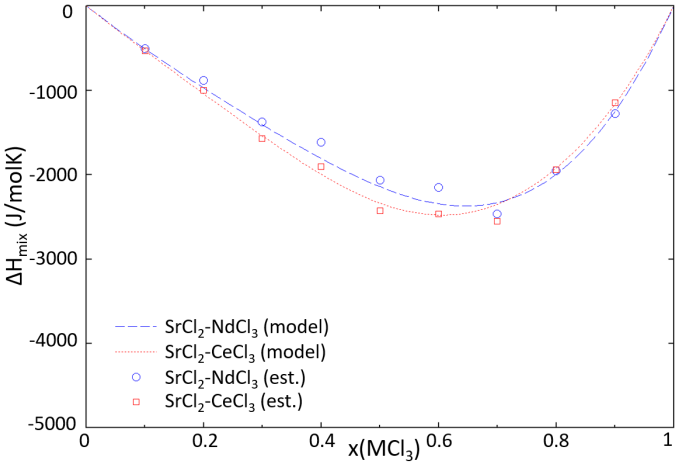


Figure 4.15: Mixing enthalpy of the $SrCl_2$−$NdCl_3$ (dashed line) and $SrCl_2$−$CeCl_3$ (dotted line) salt systems calculated at T = 1200 K with the thermodynamic model presented in this section, and compared with mixing enthalpy estimated using the method of Davis and Rice [12] of the $SrCl_2$−$NdCl_3$ (open blue circles) and $SrCl_2$−$CeCl_3$ (open red squares) systems.

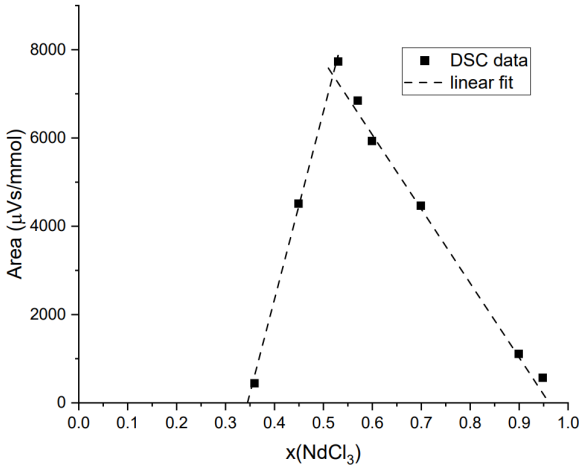


Figure 4.16: Tammann-diagram showing the heat flow area of the eutectic transition versus composition, obtained in this work on the $SrCl_2-NdCl_3$ system. The intersection of the linear fits (dashed lines) is the predicted composition of the eutectic in this system, and the diagram matches with the composition of the intermediate.

### $SrCl_2-CeCl_3$

The calculated phase diagram of the $SrCl_2-CeCl_3$ system is presented in Figure 4.17, and the mixing enthalpy is shown in Figure 4.15. The calculated invariant equilibria are given in Table 4.8, where they are compared to the values measured in this work by DSC, and the values measured by Morozov et al. [3]. The composition of the intermediate in this system is assumed to be the same as in the $SrCl_2-NdCl_3$ system, *i.e.* $Sr_9RE_5Cl_{33}$ (RE = Ce, Nd), since this phase has been observed in mixtures using XRD. The existence of the cubic solid solution $Sr_{1-x}Ce_xCl_{2+x}$ has been confirmed by XRD, while the hexagonal solid solution $Ce_{1-y}Sr_yCl_{3-y}$ has been based on the existence of the solid solution $Nd_{1-y}Sr_yCl_{3-y}$ in the $SrCl_2-NdCl_3$ system.

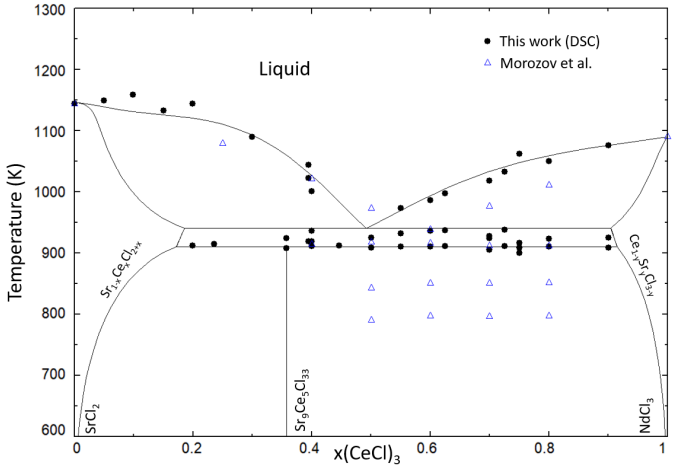


Figure 4.17: Phase diagram of the $SrCl_2$−$CeCl_3$ salt system calculated with the thermodynamic model presented in this section. Experimental data obtained in this work (closed black circles) and from Morozov et al. [3] (open blue squares).

| x($NdCl_3$) | T (K) | | | Equilibrium | Invariant reaction |
|---|---|---|---|---|---|
| | CALPHAD | Morozov | This work (DSC) | | |
| 0 | 1146 | 1142 | 1147 ± 5 | Congruent melting | $SrCl_2$ = L |
| 0.357 | 915 | - | 914 ± 5 | Peritectic | $Sr_9Ce_5Cl_{33}$ = $Sr_{1-x}Ce_xCl_{2+x}$ + L′ |
| 0.5 | 939 (0.492) | 916 (0.600) | 926 ± 10 (0.500) | Eutectic | $Sr_{1-x}Ce_xCl_{2+x}$ + $Ce_{1-y}Sr_yCl_{3-y}$ = L |
| 1 | 1089 | 1090 | 1093 ± 5 | Congruent melting | $NdCl_3$ = L |

Table 4.8: Calculated invariant equilibria in the $SrCl_2$−$CeCl_3$ system, as well as experimentally measured values of these invariants from Morozov et al. [3] and this work (DSC). The numbers in parentheses are the respective compositions of the eutectic.

## 4.3. CONCLUSIONS

A thermodynamic assessment of the molten salt systems $AECl_2$−$RECl_3$ (AE = Sr, Ba; RE = Ce, Nd) is presented in this work based on the quasi-chemical formalism in the quadruplet approximation for the liquid solution. The mixing enthalpy of these systems has been estimated with Davis' method over the entire composition range, and these estimations were used to optimize the CALPHAD model.

The $BaCl_2$−$CeCl_3$ system is characterized by: i) a single eutectic, ii) a peritectic decomposition of the intermediate $Ba_3Ce_2Cl_{12}$, iii) a $Ba_{1-x}Ce_xCl_{2+x}$ (cubic) solid-solution stable at high temperature in the composition range x($CeCl_3$) = [0.05-0.25], iv) a $Ce_{1-y}Ba_yCl_{3-y}$ (hexagonal) solid-solution stable at high temperatures in the composition range x($CeCl_3$) = [0.925-1]. The structures of the solid-solutions in this system have been characterised using XRD, and the intermediate $Ba_3Ce_2Cl_{12}$ has been characterised with XRD and ND.

The system $BaCl_2$−$NdCl_3$ is very similar to the $BaCl_2$−$CeCl_3$ system, and is characterised by: i) a single eutectic, ii) a peritectic decomposition of the intermediate $Ba_3Nd_2Cl_{12}$,

iii) a $Ba_{1-x}Nd_xCl_{2+x}$ (cubic) solid solution in the composition range x($NdCl_3$) = [0-0.2], stable only at temperatures above 940 K, iv) a $Nd_{1-y}Sr_yCl_{3-y}$ (hexagonal) solid solution in the composition range x($NdCl_3$) $\geq$ 0.95. The structure of the intermediate $Ba_3Nd_2Cl_{12}$ has been determined using XRD, and the solid solution $Ba_{1-x}Nd_xCl_{2+x}$ has been investigated with quenching experiments and post-XRD characterisation.

Furthermore, the system $SrCl_2$−$CeCl_3$ is made up of: 1) a single eutectic, ii) a peritectic decomposition of the intermediate $Sr_9Ce_5Cl_{33}$, iii) a $Sr_{1-x}Ce_xCl_{2+x}$ (cubic) solid solution, iv) a $Ce_{1-y}Sr_yCl_{3-y}$ (hexagonal) solid solution. The existence of the intermediate compound and the cubic solid solution $Sr_{1-x}Ce_xCl_{2+x}$ were verified by XRD.

The system $SrCl_2$−$NdCl_3$ is similarly characterised by: i) a single eutectic, ii) a peritectic decomposition of the intermediate $Sr_9Nd_5Cl_{33}$, iii) a $Sr_{1-x}Nd_xCl_{2+x}$ (cubic) solid solution in the composition range x($NdCl_3$) = [0-0.2], iv) a $Nd_{1-y}Sr_yCl_{3-y}$ (hexagonal) solid solution in the composition range x($NdCl_3$) $\geq$ 0.95. The structure of the intermediate $Sr_9Nd_5Cl_{33}$ has been characterised with XRD, and the solid solution $Sr_{1-x}Nd_xCl_{2+x}$ has been investigated with quenching experiments and post-XRD characterisation.

In conclusion, the compositions of the stable intermediate compounds in the $AECl_2$−$RECl_3$ (AE = Sr, Ba; RE = Ce, Nd) systems have been identified, and mutual solid solubility has been incorporated in the thermodynamic model. Due to the nature of $NdCl_3$ and $CeCl_3$ as potential simulants for $PuCl_3$ and $UCl_3$ respectively, it is likely that the observations made in this chapter can be extended to these actinide systems as well, as we will see in Chapter 5.

# BIBLIOGRAPHY


(1) Alders, D. C.; Cette, D. J.; Konings, R. J. M.; Smith, A. L. *Physical Chemistry, Chemical Physics* **2024**, *26*, 24041–24057.

(2) Alders, D. C.; Vlieland, J.; Thijs, M.; Konings, R. J. M.; Smith, A. L. *Journal of Molecular Liquids* **2024**, *396*, 123997.

(3) Morozov, I.; T'en, F. N. *Russian Journal of Inorganic Chemistry* **1971**, *16*, 1215–1217.

(4) Meyer, G.; Masselmann, S. *Chemistry of Materials* **1998**, *10*, 2994–3004.

(5) Storonkin, I.; Vasilkova, O.; Kozhina, I. *Vestnik, Leningrad University* **1973**, *4*, 80–83.

(6) Vogel, G.; Schneider, A. *Inorganic and Nuclear Chemistry Letters* **1972**, *8*, 513–521.

(7) Hodorowicz, S. A.; Olejak-Chodan, M.; Eick, H. A. *Journal of Solid State Chemistry* **1987**, *71*, 205–213.

(8) Rietveld, H. M. *Journal of applied Crystallography* **1969**, *2*, 65–71.

(9) Shannon, R. D. *Acta crystallographica section A: crystal physics, diffraction, theoretical and general crystallography* **1976**, *32*, 751–767.

(10) Chase Jr, M. W. *Journal of Physical and Chemical Reference Data, Monograph* **1998**, *9*.

(11) Konings, R. J. M.; Kovács, A. *Handbook on the physics and chemistry of rare earths* **2003**, *33*, 147–247.

(12) Davis, H. T.; Rice, S. A. *The Journal of Chemical Physics* **1964**, *41*, 14–24.

(13) Hull, S.; Norberg, S. T.; Ahmed, I.; Eriksson, S. G.; Mohn, C. E. *Journal of Solid State Chemistry* **2011**, *184*, 2925–2935.

# 5

# CHEMISTRY OF Sr AND Ba IN ACTINIDE CHLORIDE MOLTEN SALT SYSTEMS

*As proven in the previous chapters, the behaviour of $PuCl_3$ in molten salt systems is very well described by $NdCl_3$, and the same is true for $UCl_3$ and $CeCl_3$. However, to further cement the potential of simulant chemistry in the area of molten salt research, we wanted to put the application of it to the test. Based on our understanding of the $BaCl_2$–$CeCl_3$ system, we investigated the system with $UCl_3$ to show the potential of the use of simulants in molten salt research.*

*In the $BaCl_2$–$UCl_3$ system, a high-temperature solid solution of $UCl_3$ in $\beta$-$BaCl_2$ is expected to be stable, which has the composition $Ba_{1-x}U_xCl_{2+x}$. Additionally, the intermediate compound $Ba_3U_2Cl_{12}$ was detected by XRD, indicating that the chemistry of this system is very similar indeed to that of the simulant system $BaCl_2$–$CeCl_3$.*

Parts of this chapter are currently under review in "Alders et al., Nuclear Materials and Energy (2026)

This chapter is dedicated to the phase equilibria of fission products Sr and Ba in binary salt systems with actinide chlorides $UCl_3$ and $ThCl_4$. The reason for this is twofold: first, it is important to have an accurate thermodynamic description of these systems for the application calculations in Chapter 9, but also to stress the importance of the studies on the simulant systems presented in Chapter 4. The latter goal was addressed by targeted experiments carried out to show the similar behaviour of $BaCl_2$–$UCl_3$ compared to the systems $BaCl_2$–$RECl_3$ (RE = Ce, Nd) shown in Chapter 4. By including $UCl_3$ in the thermodynamic model of the fuel system, other base fuels such as NaCl–$UCl_3$–$PuCl_3$ can be used in the application calculations (Chapter 9).

The $BaCl_2$–$UCl_3$ and $SrCl_2$–$UCl_3$ systems have been investigated experimentally by Desyatnik et al. [1] using DTA. In their assessment of the $SrCl_2$–$UCl_3$ system, Desyatnik et al. [1] suggested the existence of an intermediate compound with the composition $SrUCl_5$ based on the disappearance of their measured eutectic event at compositions $x(UCl_3) \leq 0.5$. In the $BaCl_2$–$UCl_3$ system, Desyatnik et al. proposed the existence of an intermediate compound with stoichiometry $Ba_2UCl_7$ based on the disappearance of the measured eutectic event at compositions $x(UCl_3) \leq 0.35$. Additionally, Desyatnik et al. observed a series of events at T = 950 K between $x(UCl_3)$ = 0.5 and 0.85, for which no explanation is offered in the original work.

The systems $SrCl_2$–$ThCl_4$ and $BaCl_2$–$ThCl_4$ have been investigated by Gorbunov et al. [2] using DTA. Based on their measurements, Gorbunov et al. conclude that the $SrCl_2$–$ThCl_4$ system is a simple binary eutectic system. The invariant equilibria that the authors measured in the $BaCl_2$–$ThCl_4$ system indicate two possible intermediate compounds, namely $Ba_3ThCl_{10}$ and $Ba_3Th_2Cl_{14}$. No crystallographic data on these compounds have been reported in the literature.

## 5.1. SYSTEMS WITH $UCl_3$

### 5.1.1. $SrCl_2$–$UCl_3$

$SrCl_2$ The system $SrCl_2$–$UCl_3$ has been studied by Desyatnik et al. [1] using DTA. In their discussion of this system, Desyatnik et al suggest an intermediate compound with the composition $SrUCl_5$ to account for the disappearance of the eutectic event at compositions $x(UCl_3) \leq 0.5$, as well as the appearance of a peritectic event at these compositions.

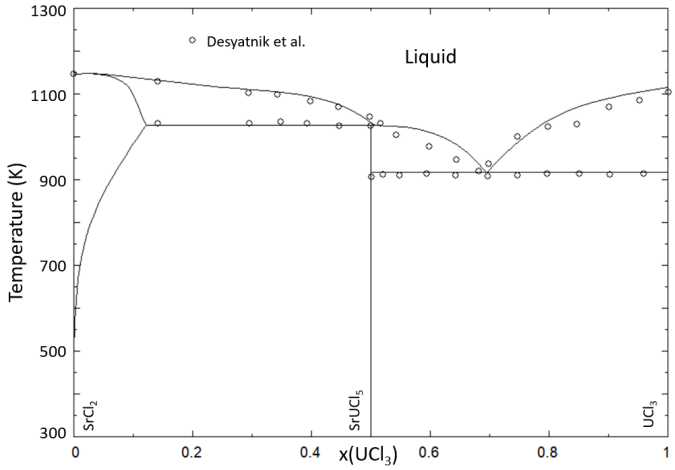


Figure 5.1: Phase diagram of the $SrCl_2-UCl_3$ binary system, as calculated with the optimized thermodynamic model. Data from Desyatnik et al. [1] (open black circles).



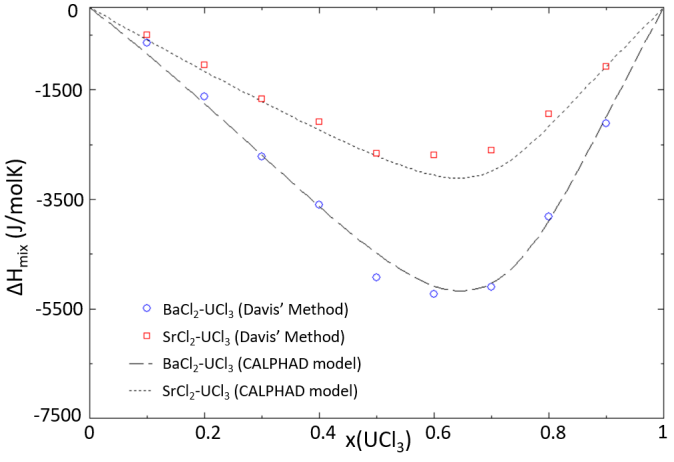


Figure 5.2: Mixing enthalpy of the $SrCl_2-UCl_3$ system at T = 1200 K (dotted line) and $BaCl_2-UCl_3$ system calculated at T = 1273 K (dashed line), as calculated with the thermodynamic model. The thermodynamic model well reproduces the data estimated using Davis' method [3] of $SrCl_2-UCl_3$ (open red squares) and $BaCl_2-UCl_3$ (open blue circles).

The CALPHAD model displayed in Figure 5.1 was optimized to fit the measured invariant points by Desyatnik et al., as well as the estimated mixing enthalpy shown in Figure 5.2. A comparison between the invariant equilibria calculated with the CALPHAD model and the experimental data from Desyatnik et al. [1] is presented in Table 5.1, showing a good agreement. Furthermore, the eutectic composition in this system corresponds with the minimum of the mixing enthalpy curve. Based on the analogous system $SrCl_2-NdCl_3$ and $SrCl_2-CeCl_3$, presented in Chapter 5, a solid solution on the $SrCl_2$-rich

side of the phase diagram was also included. It is worth pointing out that this solid solution helps accounting for the very flat liquidus line Desyatnik et al. [1] measured in this system at low $UCl_3$ content. Desyatnik et al. did not include this solid solution in their interpretation of the system. However, due to the lack of DTA experiments below $x(UCl_3) = 0.15$ and the fact that they did not perform crystallographic measurements in this system, it is possible that they simply did not observe it.

| $x_{NdCl3}$ | T (K) | | Equilibrium | Invariant reaction |
|---|---|---|---|---|
| | CALPHAD | Desyatnik et al. [1] | | |
| 0 | 1146 | 1147 | Congruent melting | $SrCl_2 = L$ |
| 0.5 | 1125 | 1115 | Peritectic | $SrUCl_5 = Sr_{1-x}U_xCl_{2+x} + L'$ |
| 0.697 | 915 | 908 (0.690) | Eutectic | $SrUCl_5 + UCl_3 = L$ |
| 1 | 1113 | 1106 | Congruent melting | $UCl_3 = L$ |

Table 5.1: Calculated invariant equilibria in the $SrCl_2-UCl_3$ system, as well as experimentally measured values of these invariants from Desyatnik et al. [1]. The number in parentheses is the respective composition of the eutectic from Desyatnik et al.

5

### 5.1.2. $BaCl_2-UCl_3$

The system $BaCl_2-UCl_3$ has been investigated experimentally by Desyatnik et al. [1] using DTA, and identified an intermediate at composition $x(UCl_3) = 0.33$ with the stoichiometry $Ba_2UCl_7$. This is also the stoichiometry that was reported in the literature on the $BaCl_2-CeCl_3$ system by Storkonkin et al. [4], but as shown in Chapter 4 this is likely to correspond to the intermediate $Ba_3Ce_2Cl_{12}$ instead. Additionally, in the $BaCl_2-RECl_3$ (RE = Ce, Nd) systems, a high-temperature solid solution with the composition $Ba_{1-x}RE_xCl_{2+x}$ (RE = Ce, Nd) is formed at low molar fractions of $RECl_3$ ($\leq 0.25$). For the same reasons, we presume that such a solid solution also exists in the $BaCl_2-UCl_3$ system. To investigate this further, an experimental investigation was conducted with targeted experiments.

#### EXPERIMENTAL INVESTIGATION

In order to investigate the existence of a solid solution at high temperature (with composition $Ba_{1-x}U_xCl_{2+x}$) a DSC measurement was performed at $x(UCl_3) = 0.2$. This DSC measurement is shown on the phase diagram in Figure 5.4. This measurement confirms the formation of the solid solution at elevated temperature through the measured equilibrium at T = 920 K. Moreover, the measured liquidus is in good agreement with the work of Desyatnik et al. [5]. Additionally, on the first cycle of the measurement, a small peak was detected at T = 1060 K, where Desyatnik et al. also measure an equilibrium. This peak disappeared on subsequent cycles, however, leading to its exclusion from the measured data.

Furthermore, post-DSC XRD measurement was performed on the same sample to investigate the existence of the intermediate $Ba_3U_2Cl_{12}$. The profile refinement of this XRD is presented in Figure 5.3. This refinement shows the presence of the low-temperature polymorph $\alpha$-$BaCl_2$ (SGR *Pnma*), as well as the intermediate compound $Ba_3U_2Cl_{12}$. No crystal structure has been reported for the latter compound, so the structure of the analogous compounds $Ba_3Ce_2Cl_{12}$ and $Ba_3Nd_2Cl_{12}$, suggested by Alders et al. [6, 7] and based

on the crystal structures by Meyer et al. [8], was used. A good agreement between the measured data and the calculated refinement is obtained, corroborating that the intermediate compound $Ba_3U_2Cl_{12}$ exists in this binary system. The cell parameters of $Ba_3U_2Cl_{12}$ obtained from the refinement are presented in Table 5.2 and compared to the measured values for $Ba_3Ce_2Cl_{12}$ and $Ba_3Nd_2Cl_{12}$ (Chapter 4). The increase in cell volume of the intermediate compounds $Ba_3Nd_2Cl_{12}$, $Ba_3Ce_2Cl_{12}$ and $Ba_3U_2Cl_{12}$ shown in Table 5.2 is as expected, considering the ionic radii of the $M^{3+}$ cations (*i.e.* r($Nd^{3+}$, VI) < r($Ce^{3+}$, VI) < r($U^{3+}$, VI) [9]).

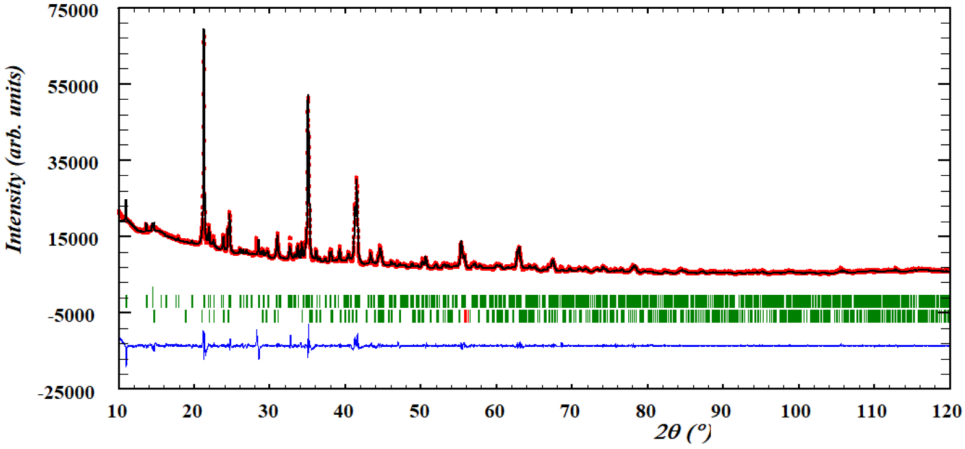


Figure 5.3: Profile refinement of the XRD of the post-DSC sample at x($UCl_3$) = 0.2. The phases included in the refinement are $\alpha$-$BaCl_2$ (SGR *Pnma*, Hull et al. [10]) and $Ba_3U_2Cl_{12}$ (based on $Ba_3Ce_2Cl_{12}$, SGR *I4/m*, Alders et al. [6]). The observed intensity (Yobs, red) is plotted along with the calculated intensity from the refinement (Ycalc, black), and the difference between the two is shown (Yobs-Ycalc, blue). The angles at which reflections occurr are shown as well (Bragg positions, vertical lines). Measurement at $\lambda$ = Cu-K$\alpha$.

| Source | Compound | a,b (Å) | c (Å) | V (Å$^3$) |
|---|---|---|---|---|
| This work | $Ba_3U_2Cl_{12}$ | 11.397(2) | 21.797(4) | 2831.2(6) |
| This work | $Ba_3Nd_2Cl_{12}$ | 11.304(7) | 21.635(3) | 2764.5(25) |
| This work (XRD) | $Ba_3Ce_2Cl_{12}$ | 11.363(1) | 21.547(6) | 2782.1(8) |
| This work (ND) | $Ba_3Ce_2Cl_{12}$ | 11.336(9) | 21.529(4) | 2766.5(31) |

Table 5.2: Comparison between cell parameters obtained for intermediates $Ba_3M_2Cl_{12}$ (M = Ce, Nd, U) (space group I4/m) in this work.

### THERMODYNAMIC MODELLING

The thermodynamic model of this system was fitted to the experimental data of Desyatnik et al. [1] and, in the absence of experimental data, the mixing enthalpy as estimated with Davis' method [3]. The phase diagram of the $BaCl_2$−$UCl_3$ system is shown in Figure 5.4, and the mixing enthalpy in Figure 5.2. A comparison between the invariant equilibria calculated with the CALPHAD model and the experimental data from Desyatnik et al. [1] is presented in Table 5.3. The thermodynamic model reproduces the experimental

data well, with the exception of the measured invariant equilibria between $x(UCl_3) = 0.5$ and $x(UCl_3) = 0.85$ at T = 950 K. These equilibria have not been interpreted by Desyatnik et al., either. Without further information on the nature of these equilibria, we have been unable to incorporate them in the CALPHAD model. Additionally, the high-temperature solubility limit of $UCl_3$ in $\beta$-$BaCl_2$ must be investigated to further improve the thermodynamic model.

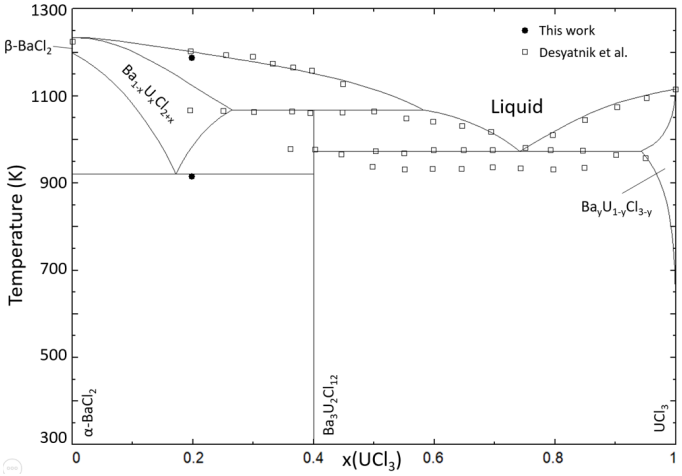


Figure 5.4: Phase diagram of the $BaCl_2-UCl_3$ system calculated with the thermodynamic model presented in this work. Experimental data by Desyatnik et al. (open black squares) and this work (closed black circles).

| $x_{NdCl3}$ | T (K) | | Equilibrium | Invariant reaction |
|---|---|---|---|---|
| | CALPHAD | Desyatnik et al. [1] | | |
| 0 | 1235 | 1233 | Congruent melting | $BaCl_2 = L$ |
| 0.172 | 921 | - | Eutectoid | $\alpha\text{-}BaCl_2 + Ba_3U_2Cl_{12} = Ba_{1-x}U_xCl_{2+x}$ |
| 0.4 | 1067 | 1058 | Peritectic | $Ba_3U_2Cl_{12} = Ba_{1-x}U_xCl_{2+x} + L'$ |
| 0.742 | 970 | 973 (0.750) | Eutectic | $Ba_3U_2Cl_{12} + U_{1-y}Ba_yCl_{3-y} = L$ |
| 1 | 1113 | 1106 | Congruent melting | $UCl_3 = L$ |

Table 5.3: Calculated invariant equilibria in the $BaCl_2-UCl_3$ system, as well as experimentally measured values of these invariants from Desyatnik et al. [1]. The number in parentheses is the respective composition of the eutectic from Desyatnik et al.

## 5.2. SIMULANT ANALYSIS

A simulant analysis of the systems $NaCl-MCl_3$, $CsCl-MCl_3$ and $MgCl_2-MCl_3$ was presented in Chapter 3. Here, upon completion of the investigations of the systems $AECl_2-MCl_3$ (AE = Sr, Ba; M = Ce, Nd, U), a simulant analysis of the systems containing Sr and Ba is also presented. The comparison of the thermodynamic models of the $SrCl_2-MCl_3$ (M = Ce, Nd, U) with the experimental data of the $SrCl_2-PuCl_3$ system presented by Johnson et al. [11] is shown in Figure 5.5. The calculated and measured invariant equilibria used in the comparison are presented in Table 5.4.

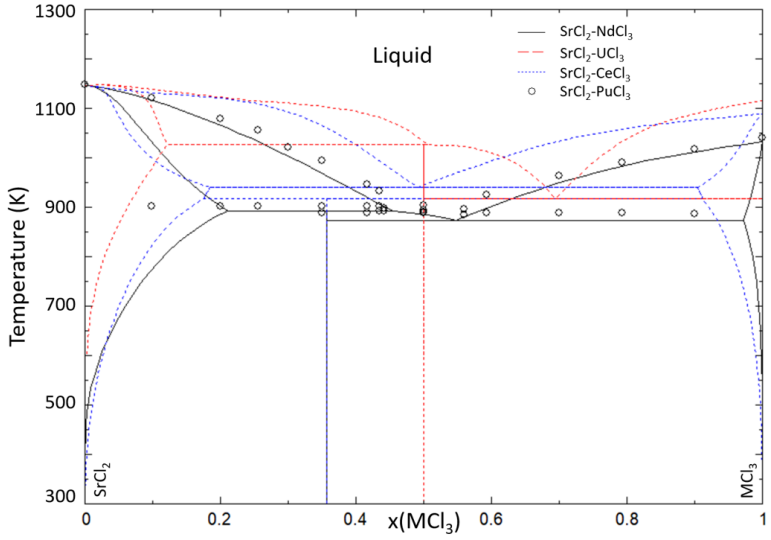


Figure 5.5: Calculated phase diagrams of the systems $SrCl_2-NdCl_3$ (solid black line), $SrCl_2-CeCl_3$ (dashed blue line) and $SrCl_2-UCl_3$ (dashed red line) compared to the experimental data on the $SrCl_2-PuCl_3$ system (open black circles) presented by Johnson et al. [11].

| $MCl_3$ | $x_1$ | $T_1$ (K) | $x_2$ | $T_2$ (K) | $x_3$ | $T_3$ (K) |
|---|---|---|---|---|---|---|
| **$BaCl_2-MCl_3$ (M = Ce, Nd, U, Pu)** | | | | | | |
| $PuCl_3$ | - | - | 0.4 | 1023 | 0.64 | 921 |
| $NdCl_3$ | 0.20 | 936 | 0.4 | 1017 | 0.67 | 906 |
| $CeCl_3$ | 0.18 | 940 | 0.4 | 1068 | 0.66 | 966 |
| $UCl_3$ | 0.17 | 964 | 0.4 | 1064 | 0.73 | 960 |
| **$SrCl_2-MCl_3$ (M = Ce, Nd, U, Pu)** | | | | | | |
| $PuCl_3$ | 0.25 | 903 | 0.51 | 892 | - | - |
| $NdCl_3$ | 0.357 | 890 | 0.535 | 939 | - | - |
| $CeCl_3$ | 0.357 | 915 | 0.492 | 878 | - | - |
| $UCl_3$ | 0.50 | 1125 | 0.697 | 915 | - | - |

Table 5.4: Invariant equilibria in the $AECl_2-MCl_3$ (AE = Sr, Ba; M = Ce, Nd, U, Pu) systems as calculated with the thermodynamic models presented in this work.

As seen in Figure 5.5, the melting behaviour of the $SrCl_2-UCl_3$ system is markedly different from that of the other investigated systems. The main reason for this difference is the different intermediate that forms in these systems: $Sr_9M_5Cl_{33}$ (M = Ce, Nd) in the systems with $CeCl_3$ and $NdCl_3$, and the intermediate compound $SrUCl_5$ in the $UCl_3$ system. Further experimental investigation is necessary to verify the data from Desyatnik et al. [1] in the $SrCl_2-UCl_3$ system, and investigate the stable intermediate compound. Furthermore, as seen in Figure 5.5 and Table 5.4, the $NdCl_3$ system once more shows the greatest agreement with the $PuCl_3$ system, as was shown in Chapter 3 for the NaCl, CsCl and $MgCl_2$ systems as well.

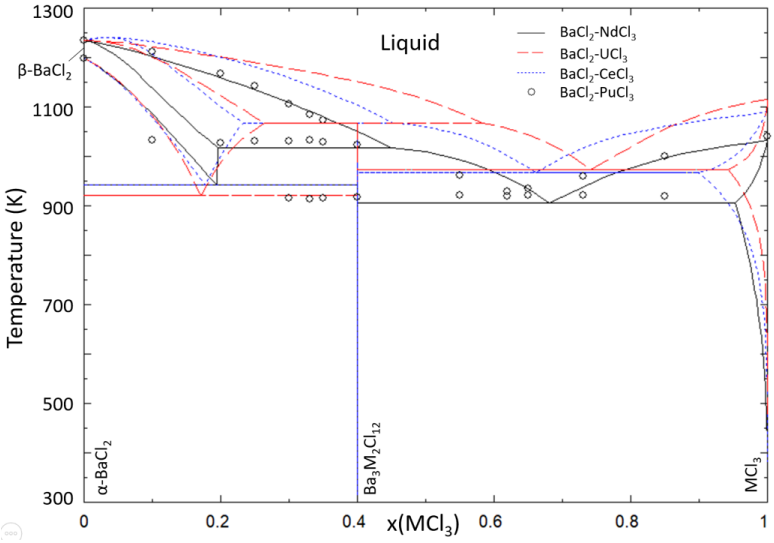


Figure 5.6: Calculated phase diagrams of the systems $BaCl_2-NdCl_3$ (solid black line), $BaCl_2-CeCl_3$ (dashed blue line) and $BaCl_2-UCl_3$ (dashed red line) compared to the experimental data on the $BaCl_2-PuCl_3$ system (open black circles) presented by Johnson et al. [11].

Figure 5.6 shows the comparison between the $BaCl_2-MCl_3$ (M = Ce, Nd, U, Pu) systems. As seen in most other simulant analyses in this work, the melting point of the eutectics of the $BaCl_2-UCl_3$ and $BaCl_2-CeCl_3$ systems is slightly higher than that of the $BaCl_2-NdCl_3$ and $BaCl_2-PuCl_3$ systems. The temperatures of the eutectic and peritectic in the $BaCl_2-NdCl_3$ and $BaCl_2-PuCl_3$ systems are in good agreement with each other. The composition of the eutectic is slightly different ($x(NdCl_3) = 0.67$ and $x(PuCl_3) = 0.63$, respectively), but the melting behaviour is still reproduced relatively accurately. Given the good performance of $NdCl_3$ as a simulant for the melting behaviour of $PuCl_3$ in the systems with NaCl, CsCl and $MgCl_2$ (Chapter 3), as well as the systems with $SrCl_2$ and $BaCl_2$ (this chapter), Nd is selected as the premier simulant for Pu, and will be used as such in this work, notably as simulant in iodide systems (Chapters 7-8) and for the application calculations (Chapter 9).

## 5.3. SYSTEMS WITH $ThCl_4$

In addition to the molten salt fuel systems $NaCl-MgCl_2-PuCl_3$ and $NaCl-UCl_3-PuCl_3$, other fuel salt systems have potential application in a molten salt reactor. Of particular interest are systems with $ThCl_4$, *e.g.* in the $NaCl-ThCl_4-PuCl_3$ fuel system [12], because of the possibility of thorium breeding and large natural abundance. To this end, the interactions between fission products and $ThCl_4$ were modelled, so that fuel systems on a thorium basis may also be investigated through application calculations in Chapter 10.

### 5.3.1. $SrCl_2$–$ThCl_4$

The thermodynamic assessment of the $SrCl_2$–$ThCl_4$ system is based on the experimental data by Gorbunov et al. [2]. In their work, Gorbunov et al. measured the system using DTA and found it to be a simple binary eutectic. A comparison between the invariant equilibria calculated with the CALPHAD model and the experimental data from Gorbunov et al. [2] is presented in Table 5.5. The thermodynamic model is in good agreement with the measured invariant equilibria. No experimental mixing enthalpy data have been reported in the literature, and due to the lack of information from systems that are similar to $ThCl_4$-systems, no mixing enthalpy could be estimated either. The phase diagram of this system is presented in Figure 5.7, and the calculated mixing enthalpy is given in Figure 5.10. Due to the low boiling point of $ThCl_4$, the gas phase is also visible on the phase diagram on the $ThCl_4$-rich side.

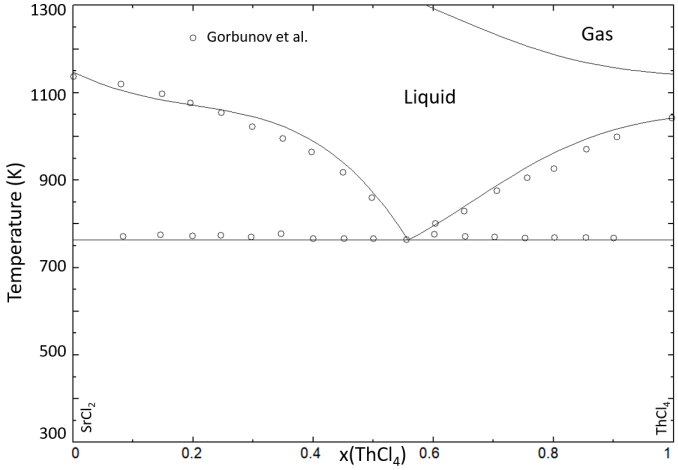


Figure 5.7: Phase diagram of the system $SrCl_2$–$ThCl_4$ calculated with the thermodynamic model presented in this work. Experimental data from Gorbunov et al. [2] (open black circles).

| $x_{ThCl4}$ | T (K) | | Equilibrium | Invariant reaction |
|---|---|---|---|---|
| | CALPHAD | Gorbunov et al. [2] | | |
| 0 | 1146 | 1143 | Congruent melting | $SrCl_2$ = L |
| 0.56 | 761 | 769 (0.560) | Eutectic | $ThCl_4$ + $SrCl_2$ = L |
| 1 | 1040 | 1040 | Congruent melting | $ThCl_4$ = L |

Table 5.5: Calculated invariant equilibria in the $SrCl_2$–$ThCl_4$ system, as well as experimentally measured values of these invariants from Gorbunov et al. [2]. The number in parentheses is the respective composition of the eutectic from Gorbunov et al.

### 5.3.2. $BaCl_2$–$ThCl_4$

In addition to the work Gorbunov et al. [2] present on the $SrCl_2$–$ThCl_4$ system, they report an experimental investigation of the system $BaCl_2$–$ThCl_4$. This system is more complex than the $SrCl_2$-system, and contains two intermediate compounds with compositions $Ba_3ThCl_{10}$ and $Ba_3Th_2Cl_{12}$, respectively. Gorbunov et al. based the existence

of these intermediates on the disappearance of the eutectic and peritectic events below certain compositions (*i.e.* x($ThCl_4$) = 0.4 and x($ThCl_4$) = 0.25, respectively). As is the case for the $SrCl_2$−$ThCl_4$ system, no experimentaly mixing enthalpy data have been reported, and no mixing enthalpy could be estimated. The phase diagram for this system is presented in Figure 5.8, and the calculated mixing enthalpy is given in Figure 5.10. A comparison between the invariant equilibria calculated with the CALPHAD model and the experimental data from Gorbunov et al. [2] is presented in Table 5.6. The CALPHAD model is in good agreement with the available experimental data, with the exception of the liquidus in the $BaCl_2$-rich region. The underestimation of the liquidus in this part of the phase diagram by the CALPHAD model could be an indication of a high-temperature solid solution of $ThCl_4$ in $\beta$-$BaCl_2$, but due to a lack of experimental data this solid solution was not included in the model.

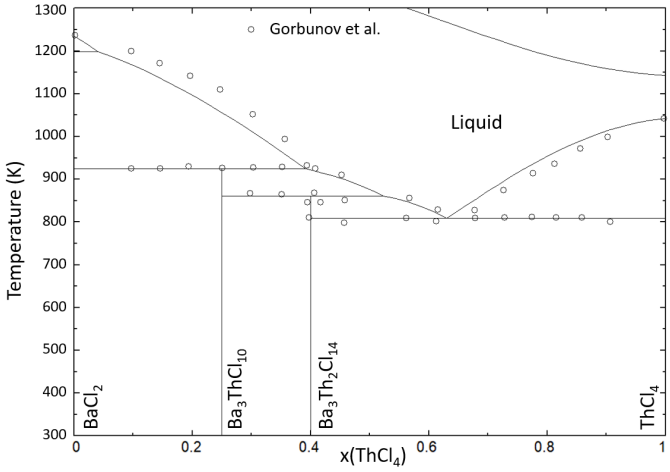


Figure 5.8: Phase diagram of the system $BaCl_2$−$ThCl_4$ calculated with the thermodynamic model presented in this work. Experimental data from Gorbunov et al. [2] (open black circles).

| $x_{ThCl4}$ | T (K) | | Equilibrium | Invariant reaction |
|---|---|---|---|---|
| | CALPHAD | Gorbunov et al. [2] | | |
| 0 | 1235 | 1234 | Congruent melting | $SrCl_2$ = L |
| 0.25 | 924 | 923 | Peritectic | $Ba_3ThCl_{10}$ = $\alpha$-$BaCl_2$ + L′ |
| 0.40 | 860 | 858 | Peritectic | $Ba_3Th_2Cl_{12}$ = $Ba_3ThCl_{10}$ + L′ |
| 0.63 | 810 | 808 (0.64) | Eutectic | $ThCl_4$ + $Ba_3Th_2Cl_{12}$ = L |
| 1 | 1040 | 1040 | Congruent melting | $ThCl_4$ = L |

Table 5.6: Calculated invariant equilibria in the $BaCl_2$−$ThCl_4$ system, as well as experimentally measured values of these invariants from Gorbunov et al. [2]. The number in parentheses is the respective composition of the eutectic from Gorbunov et al.

## 5.4. THE SYSTEM $UCl_3$–$ThCl_4$

The system $UCl_3$−$ThCl_4$ has been investigated experimentally by Desyatnik et al. [13] by DTA. Based on the disappearance of the eutectic event below the composition x($ThCl_4$)

= 0.25, Desyatnik et al. concluded that an intermediate of composition $U_3ThCl_{13}$ forms in the system. A thermodynamic model was constructed based on the interpretation by Desyatnik et al., and the calculated phase diagram is shown in Figure 5.9, showing very good agreement with the experimental data. A comparison between the invariant equilibria calculated with the CALPHAD model and the experimental data from Desyatnik et al. [13] is presented in Table 5.7. As for the other systems containing $ThCl_4$, the mixing enthalpy data have not been reported in the literature, and no estimation could be made based on similar systems. The mixing enthalpy of this system as calculated with the thermodynamic model is given in Figure 5.10.

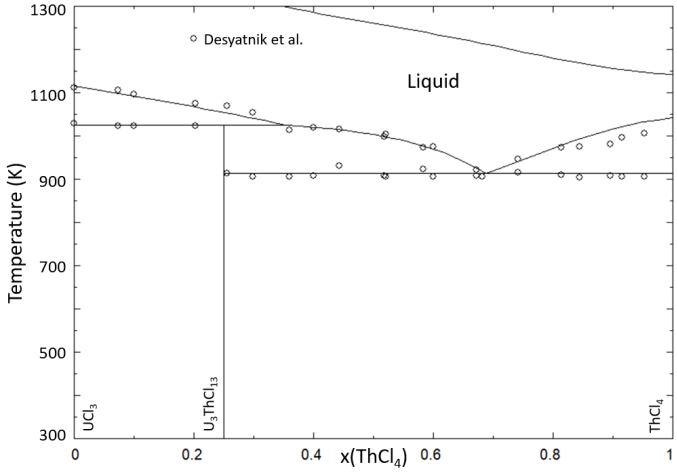


Figure 5.9: Phase diagram of the $UCl_3$–$ThCl_4$ system as calculated with the thermodynamic model presented in this work. Experimental data by Desyatnik et al. [13] (open black circles).

| $x_{ThCl4}$ | T (K) | | Equilibrium | Invariant reaction |
|---|---|---|---|---|
| | CALPHAD | Desyatnik et al. [13] | | |
| 0 | 1113 | 1110 | Congruent melting | $UCl_3 = L$ |
| 0.25 | 1023 | 1023 | Peritectic | $U_3ThCl_{13} = UCl_3 + L'$ |
| 0.69 | 912 | 905 (0.70) | Eutectic | $ThCl_4 + U_3ThCl_{13} = L$ |
| 1 | 1040 | 1040 | Congruent melting | $ThCl_4 = L$ |

Table 5.7: Calculated invariant equilibria in the $UCl_3$–$ThCl_4$ system, as well as experimentally measured values of these invariants from Desyatnik et al. [13]. The number in parentheses is the respective composition of the eutectic from Desyatnik et al.

The mixing enthalpies of the systems with $ThCl_4$ shown in Figure 5.10 show that the mixing enthalpy of the $SrCl_2$–$ThCl_4$ system is less negative than that of the $BaCl_2$–$ThCl_4$ system. This is in line with the trend observed in Figure 5.2 as well as in Chapter 5, where the same was shown for the systems with $CeCl_3$ and $NdCl_3$. Additionally, the minima of the mixing enthalpy curves are close to the lowest eutectic compositions of each system.

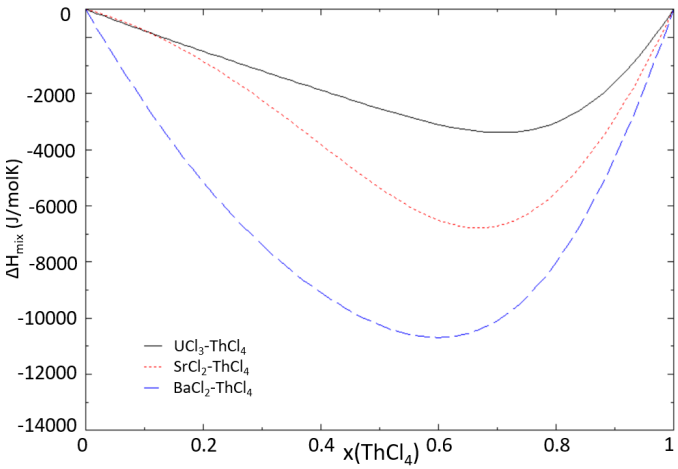


Figure 5.10: Mixing enthalpies of the systems $SrCl_2-ThCl_4$ (dotted red line), $BaCl_2-ThCl_4$ (dashed blue line) and $UCl_3-ThCl_4$ (solid black line) calculated at T = 1200 K with the thermodynamic model presented in this work.

5

## 5.5. SUMMARY AND CONCLUSION

In this chapter, the thermochemical behaviour of $SrCl_2$ and $BaCl_2$ in actinide chloride systems with uranium and thorium has been modelled. As seen in Sections 5.1.1 and 5.1.2, the behaviour of the systems $AECl_2-UCl_3$ (AE = Sr, Ba) is very similar to that of the systems $AECl_2-RECl_3$ (RE = Ce, Nd). As shown in Section 5.1.2, the behaviour of the $BaCl_2-UCl_3$ system could be predicted from the behaviour of the simulant systems for a large part. In particular, the existence of the solid solution $Ba_{1-x}U_xCl_{2+x}$ and intermediate $Ba_3U_2Cl_{12}$ were hypothesised based on the simulant chemistry observed in $BaCl_2-RECl_3$ systems (RE = Ce, Nd), and subsequently confirmed experimentally.

In addition to the models of the fission products with $UCl_3$, the interactions of fission products $SrCl_2$ and $BaCl_2$ (as well as $UCl_3$) with $ThCl_4$ have been modelled. With these models, the effect of fission products Sr and Ba on fuel systems containing $ThCl_4$ (or a mixture of $ThCl_4$ and $UCl_3$) can be investigated through application calculations.

In addition to the phase diagrams presented in this section, phase diagrams of other systems containing $ThCl_4$ are necessary to perform the desired application calculations on thorium-based systems in Chapter 9. These systems were based exclusively on experimental data from the literature, and there is no chapter dedicated to these types of systems. For this reason, the thermochemical models of $ThCl_4$ with other fission product chlorides, as well as other molten fuel matrix constituents, are given in Appendix A.

# BIBLIOGRAPHY


(1) Desyatnik, V.; Dubinin, B.; Melnikov, Y.; Raspopin, S. *Russian Journal of Inorganic Chemistry* **1975**, *20*, 1085–1087.

(2) Gorbunov, L.; Desyatnik, V.; Raspopin, S.; Trifonov, K. *Russian Journal of Inorganic Chemistry* **1974**, *19*, 3093–3095.

(3) Davis, H. T.; Rice, S. A. *The Journal of Chemical Physics* **1964**, *41*, 14–24.

(4) Storonkin, I.; Vasilkova, O.; Kozhina, I. *Vestnik, Leningrad University* **1973**, *4*, 80–83.

(5) Desyatnik, V.; Izmodenov, Y.; Melnikov, Y.; Nichkov, I.; Raspopin, S. *Soviet Atomic Energy* **1969**, *26*, 634–635.

(6) Alders, D. C.; Vlieland, J.; Thijs, M.; Konings, R. J. M.; Smith, A. L. *Journal of Molecular Liquids* **2024**, *396*, 123997.

(7) Alders, D. C.; Cette, D. J.; Konings, R. J. M.; Smith, A. L. *Physical Chemistry, Chemical Physics* **2024**, *26*, 24041–24057.

(8) Meyer, G.; Masselmann, S. *Chemistry of Materials* **1998**, *10*, 2994–3004.

(9) Shannon, R. D. *Acta crystallographica section A: crystal physics, diffraction, theoretical and general crystallography* **1976**, *32*, 751–767.

(10) Hull, S.; Norberg, S. T.; Ahmed, I.; Eriksson, S. G.; Mohn, C. E. *Journal of Solid State Chemistry* **2011**, *184*, 2925–2935.

(11) Johnson, K. W.; Kahn, M.; Leary, J. *The Journal of Physical Chemistry* **1961**, *65*, 2226–2229.

(12) Dumaire, T.; Ocádiz-Flores, J. A.; Konings, R. J. M.; Smith, A. L. *Calphad* **2022**, *79*, 102496.

(13) Desyatnik, V.; V., N. *Russian Journal of Inorganic Chemistry* **1975**, 101–103.

# 6

# CHEMISTRY OF IODINE IN MOLTEN $NaCl$-$MgCl_2$

*Thus far, the thermodynamic modelling in this work has been exclusively on mixed-cation systems with a common anion. However, when moving to higher order systems such as the quaternary system described in this chapter, the behaviour of the molten salts get a little more complicated. To include the effect of iodine on the thermochemical properties of the molten salt systems investigated in this work, we must look at mixed-anion systems with a common cation, and mixed-cation mixed-anion systems. The latter especially is more challenging than simple binary common-cation systems but, as this chapter shows, not impossible by any means.*

*The thermochemistry of the quaternary molten salt system $NaCl-NaI-MgCl_2-MgI_2$ was studied using an experimental and thermodynamic modelling approach. The binary system $NaCl-NaI$ was re-assessed based on existing data in the literature. The binary subsystem $NaI-MgI_2$ was subjected to a renewed experimental investigation, to complement and revisit the data in the literature. The subsystem $MgCl_2-MgI_2$ was investigated for the first time in this work using Differential Scanning Calorimetry (DSC). Furthermore, the phase equilibria in the pseudo-binary phase diagrams $NaCl-MgI_2$ and $NaI-MgCl_2$ in the quaternary system were investigated by DSC, while the condensed phases in the quaternary system were investigated using X-Ray Diffraction (XRD). A thermodynamic model of the quaternary system was developed using the CALPHAD (CALculation of PHase Diagrams) method with the quadruplet approximation in the modified quasichemical model for the liquid phase, and two-sublattice polynomial models for the solid solution phases. With this model, the liquidus surface of the $NaCl-NaI-MgCl_2-MgI_2$ quaternary system has been described for the first time.*

The contents of this chapter have been published in "Alders et al., The Journal of Physical Chemistry C **129**, 5 (2025) [1]".

This chapter is dedicated to the effect of fission product iodine on the melting behaviour of the base fuel matrix $NaCl-MgCl_2$. To describe this effect, a thermodynamic model of the quaternary system $NaCl-NaI-MgCl_2-MgI_2$ was constructed. This quaternary system consists of four binary systems, $NaCl-MgCl_2$, $NaCl-NaI$, $NaI-MgI_2$ and $MgCl_2-MgI_2$, and two pseudo-binary systems in $NaCl-MgI_2$ and $NaI-MgCl_2$. The model of the system $NaCl-MgCl_2$ was already presented in Chapter 3, and the rest of the thermodynamic models will be presented in this chapter. The investigations of these systems are presented here in sections 6.1.1 ($NaI-MgI_2$), 6.1.2 ($NaCl-NaI$), and 6.1.3 ($MgCl_2-MgI_2$).

The system $NaI-MgI_2$ has been investigated previously by Klemn et al. [2], and in this work we have aimed to complement that data. Seifert et al. assumed the existence of a eutectic system with wide solid solutions at both end-members [3]. No intermediates have been reported in the literature on this binary system.

The full system $NaCl-NaI$ has been investigated experimentally by Johnson et al. [4] previously. The eutectic has been measured as well by Amadori et al. [5] and Ilyasov et al. [6], at a slightly different composition and temperature. Furthermore, Amadori et al. report solidus data at x(NaI) = 0.83 and 0.9, which they attributed to the formation of a solid solution. Johnson et al. did not find any evidence of solid solubility between NaCl and NaI in their XRD and thermal analyses. Oonk et al. [7, 8] suggest that negligible solid solubility in the Na(Cl,I) system can indeed be expected, which is in agreement with Amadori et al. [5].



## 6.1. BINARY SYSTEMS

### 6.1.1. $NaI-MgI_2$

The system $NaI-MgI_2$ has been investigated previously by Klemn et al. [2], and in this work we have aimed to complement that data. The experimental data on invariant equilibria obtained in this work is given in Appendix D, Table D.5. Seifert et al. assumed a eutectic system with wide solid solutions at both end-members, which seems to be disproven by our data, as evidenced by the eutectic event that is measured at compositions $0.1 \leq x(MgI_2) \leq 0.7$. Based on the measured eutectic events, a Tammann diagram was drawn up that corroborates the eutectic composition and the existence of a mutual solid solution. The limiting compositions of this solid solution are $x(MgI_2) = 0.04$ and 0.87. The optimized phase diagram is shown in Figure 6.1, and the Tammann diagram is given in Figure 6.2.

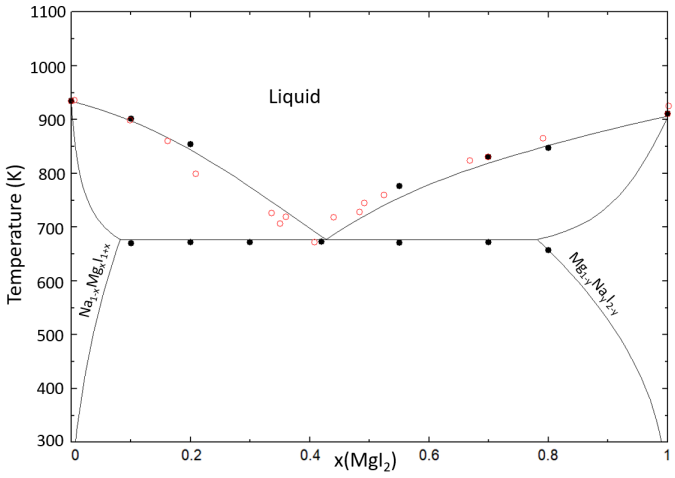


Figure 6.1: Phase diagram of the NaI−$MgI_2$ system as calculated with the CALPHAD model presented in this work. Experimental data from Klemn et al. [2] (red, open circles) and this work (black, closed circles).



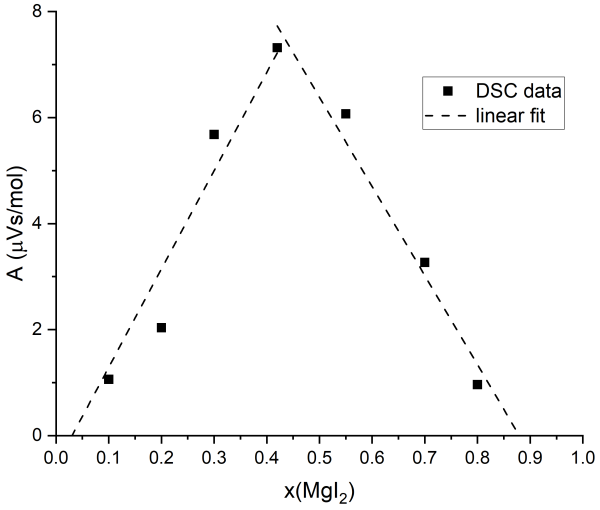


Figure 6.2: Tammann diagram of the NaI−$MgI_2$ system, calculated using the areas of the eutectic equilibria measured in this work by DSC.

The Tammann diagram shown in Figure 6.2 shows that the composition of the eutectic is x($MgI_2$) = 0.40, and the limits of the solid solution are approximately x($MgI_2$) = 0.07 and 0.87, respectively. This is in good agreement with the thermodynamic model. The calculated mixing enthalpy of this system is shown in Figure 6.3. No data was avail-

able in the literature for the mixing enthalpy of the liquid in this system. To obtain an estimate of the mixing enthalpy to which the model could be fit, the empirical method of Davis and Rice [9] was used. This method is based on the size difference between the cations in a molten salt system, as discussed in the work of Alders et al. [10]. The invariant equilibria measured in this work are compared to the data from Klemn et al. [2] and the thermodynamic model in Table 6.1.

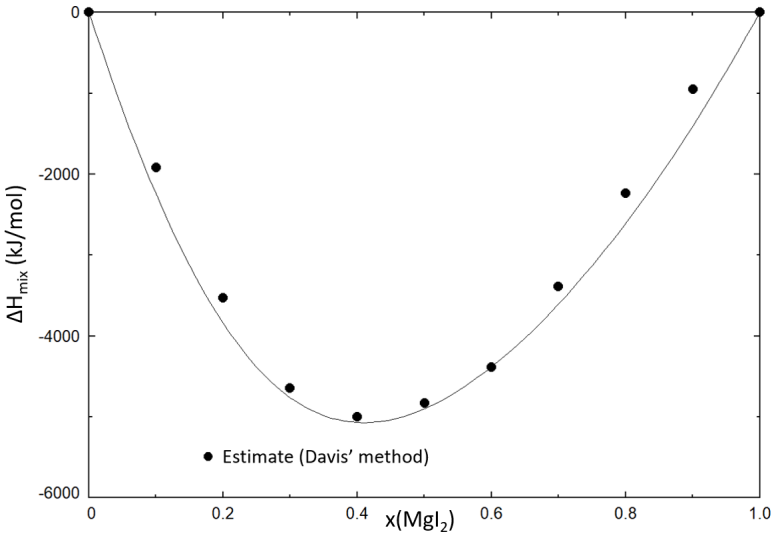


Figure 6.3: Mixing enthalpy of the NaI−$MgI_2$ system, calculated at T = 1000 K, compared to the estimated mixing enthalpy obtain using the estimation method of Davis and Rice [9].

| x($MgCl_2$) | T (K) | | | Equilibrium | Invariant reaction |
|---|---|---|---|---|---|
| | CALPHAD | This work (DSC) | Klemn | | |
| 0 | 933 | 934 ± 5 | 932 | Congruent Melting | NaI = L |
| 0.4 | 671 | 665 ± 10 | 669 | Eutectic | $Na_{1-x}Mg_xCl_{1+x}$ + $Na_yMg_{1-y}Cl_{2-y}$ = L |
| 1 | 905 | 911 ± 5 | 909 | Congruent Melting | $MgI_2$ = L |

Table 6.1: Calculated invariant equilibria in the NaI−$MgI_2$ system compared to experimentally measured values in this work using DSC, as well as the data from Klemn et al. [2].

### 6.1.2. NaCl-NaI

The full system NaCl−NaI has been previously investigated experimentally by Johnson et al. [4]. The eutectic has been measured as well by Amadori et al. [5] and Ilyasov et al. [6], at a slightly different composition and temperature. Furthermore, Amadori et al. report solidus data at x(NaI) = 0.83 and 0.9, which they attributed to the formation of a solid solution. Johnson et al. did not find any evidence of solid solubility between NaCl and NaI in their XRD and thermal analyses. Oonk et al. [7, 8] suggest that negligible solid solubility in the Na(Cl,I) system can be expected, which is in agreement with Amadori et al. [5], and for this reason solid solubility has been included in the thermodynamic model shown in Figure 6.4. Table 6.2 shows the comparison between the invariant equi-

libria calculated with the thermodynamic model, and those reported in the literature. This table shows good agreement with the eutectic equilibria reported in the literature.

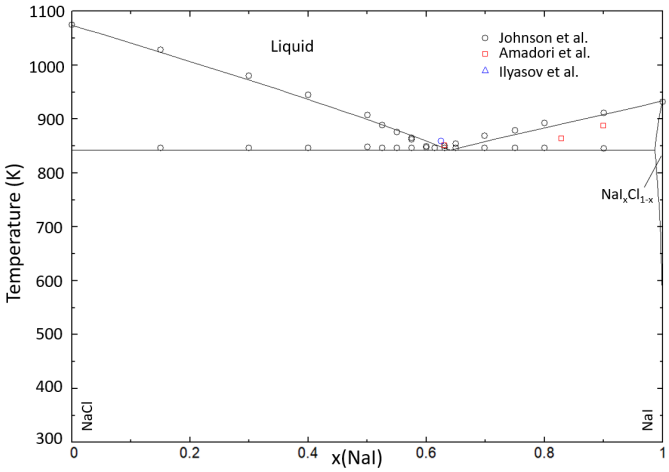


Figure 6.4: Phase diagram of the NaCl-NaI system calculated with the thermodynamic model presented in this work. Experimental data from Johnson et al. [4] (black, open circles), Amadori et al. [5] (red, open squares) and Ilyasov et al. (blue, open triangle) are compared to the calculated phase equilibria.



The mixing enthalpy of this system has been measured experimentally by Melnichak et al. [11]. The CALPHAD model presented in this work has been optimized to fit the mixing enthalpy, and the agreement between the model and the experimental data is shown in Figure 6.5.

| x(NaI) | T (K) | | | | Equilibrium | Invariant reaction |
|---|---|---|---|---|---|---|
| | CALPHAD | Johnson | Amadori | Ilyasov | | |
| 0 | 1074 | 1073 | - | - | Congruent Melting | NaCl = L |
| 0.622 | 848 | 845 | 850 | 858 | Eutectic | NaCl + NaI = L |
| 1 | 933 | 931 | - | - | Congruent Melting | NaI = L |

Table 6.2: Calculated invariant equilibria in the NaCl−NaI system compared to experimentally measured values from Johnson et al. [4], Amadori et al. [5] and Ilyasov et al. [12].

### 6.1.3. $MgCl_2$–$MgI_2$

The system $MgCl_2$−$MgI_2$ has been investigated experimentally for the first time in this work, and a CALPHAD model of this system has been constructed, as shown in Figure 6.6. The invariant equilibria measured experimentally by DSC are given in Appendix D, Table D.6. A Tammann diagram of this system is presented in Figure 6.7. The Tammann diagram, as well as the absence of the eutectic event at compositions x($MgI_2$) ≥ 0.85, indicate that a solid solution in the $MgI_2$-rich region of the phase diagram is stable, with the composition $MgI_{2-2y}Cl_{2y}$. Moreover, the invariant equilibria measured in this work, and those calculated with the thermodynamic model, are shown in Table 6.3.

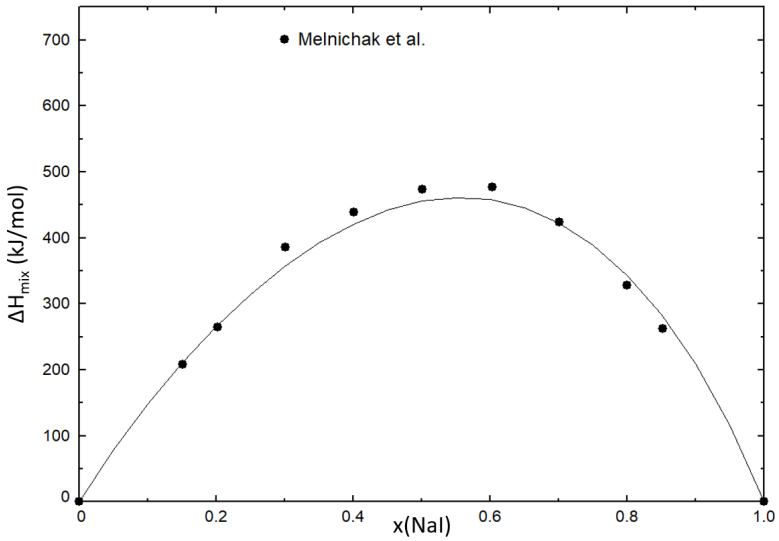


Figure 6.5: Mixing enthalpy of the NaCl−NaI system, calculated at 1084 K, compared to the experimental data from Melnichak et al. [11] obtained at 1084 K.



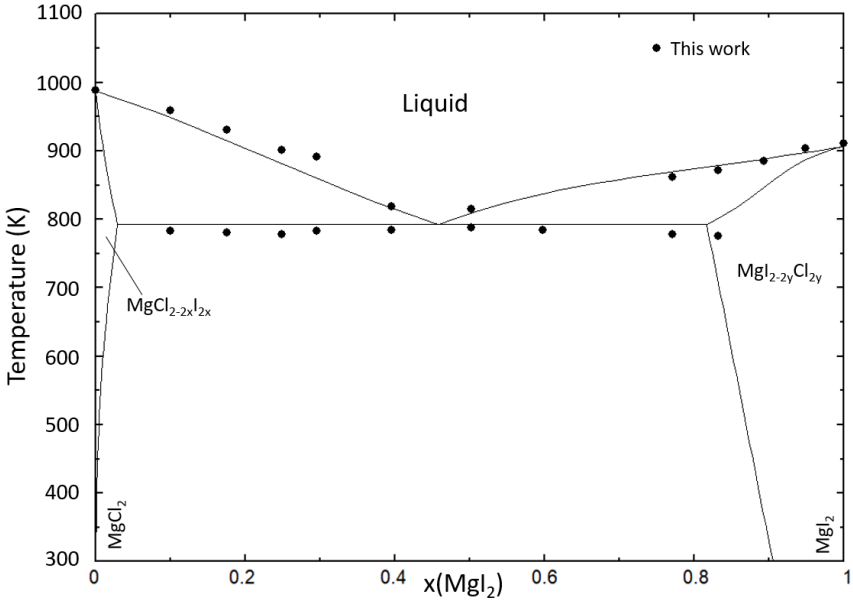


Figure 6.6: Phase diagram of the $MgCl_2-MgI_2$ system calculated with the thermodynamic model presented in this work. Experimental data obtained in this work (black circles) are compared to the calculated equilibria.

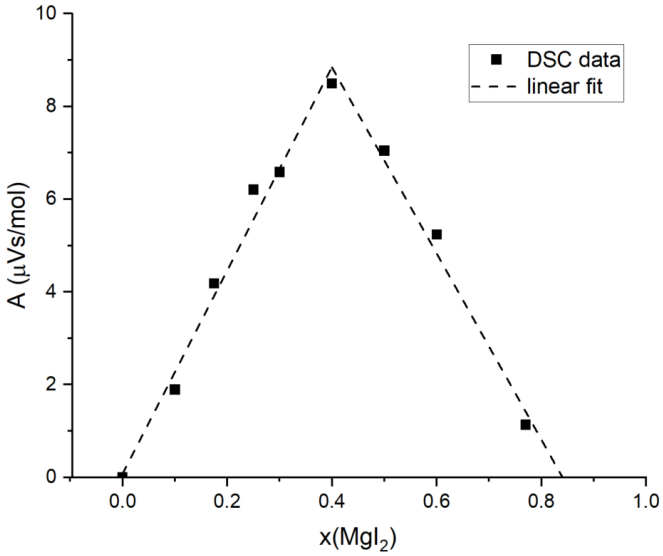


Figure 6.7: Tammann diagram of the $MgCl_2-MgI_2$ system, calculated using the area of the eutectic equilibria measured in this work by DSC (black circles).



There is no experimental data on the mixing enthalpy of the $MgCl_2-MgI_2$ system available in the literature. Additionally, no experimental data has been reported on similar systems $MCl_2-MI_2$ either, to the best of our knowledge, which makes estimating the mixing enthalpy using Davis' method impossible. The calculated enthalpy of mixing obtained using the CALPHAD model presented in this work is given in Figure 6.8. This figure shows a positive deviation from ideality, which is also observed for the mixed chloride-iodide systems with alkali metals [11] (ACl−AI, A = Li, Na, K, Rb, Cs).

| **x($MgI_2$)** | **T (K)** | | **Equilibrium** | **Invariant reaction** |
|---|---|---|---|---|
| | CALPHAD | This work (DSC) | | |
| 0 | 987 | 988 ± 5 | Congruent Melting | $MgCl_2$ = L |
| 0.452 | 786 | 784[a] ± 10 | Eutectic | $MgCl_{2-2x}I_{2x}$ + $MgI_{2-2y}Cl_{2y}$ = L |
| 1 | 905 | 911 ± 5 | Congruent Melting | $MgI_2$ = L |

Table 6.3: Calculated invariant equilibria in the $MgCl_2-MgI_2$ system compared to experimentally measured values from Johnson et al. [4], Amadori et al. [5] and Ilyasov et al. [12].
[a] Average value of measured eutectic equilibria shown in Figure 6.6.

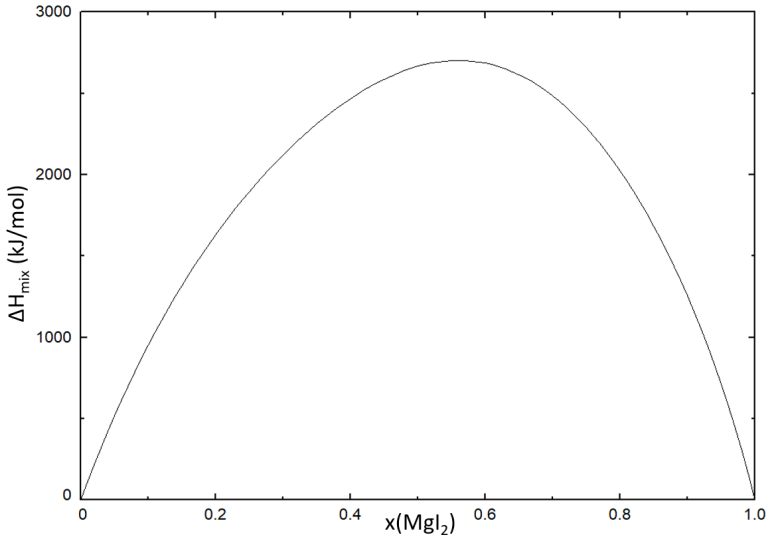


Figure 6.8: Mixing enthalpy of the $MgCl_2-MgI_2$ system calculated using the CALPHAD method presented in this work.



## 6.2. PSEUDO-BINARY AND QUATERNARY SYSTEMS

In order to assess the accuracy of the thermodynamic model, an experimental investigation of the quaternary system $NaCl-NaI-MgCl_2-MgI_2$ has been performed of the systems along the quaternary diagonals $NaCl-MgI_2$ and $NaI-MgCl_2$. The investigation of these pseudo-binary systems is discussed in Section 6.2.1 and 6.2.2 respectively.

### 6.2.1. $NaCl-MgI_2$

The $NaCl-MgI_2$ binary system has been investigated using DSC and XRD. The DSC measurements of the invariant equilibria are shown on the phase diagram in Figure 6.9 and reported in Appendix D, Table D.7. In order to improve the agreement between the extrapolated phase diagram of the $NaCl-MgI_2$ system and the experimental data, reciprocal terms were added to the CALPHAD model. The CALPHAD model describes the measured invariant equilibria well, though there are discrepancies at x($MgI_2$) = 0.098, which can be due to some currently unexplained sub-solidus behaviour.

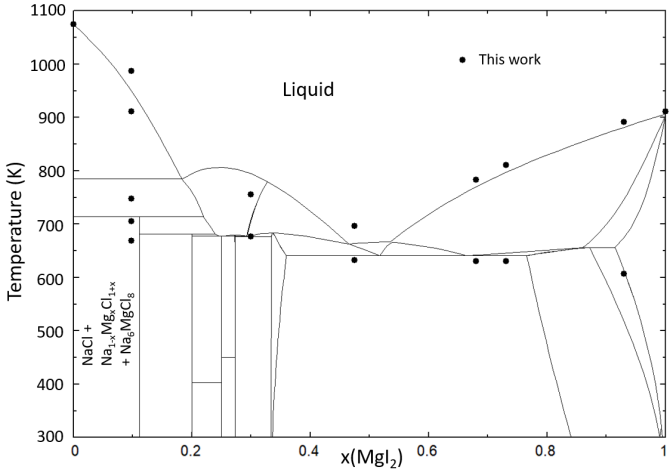


Figure 6.9: Phase diagram of the system NaCl-$MgI_2$ calculated with the optimized quaternary model presented in this work. Experimental data obtained in this work (black circles). The labelled phase fields correspond to phase fields where post-DSC XRD measurements have been performed.

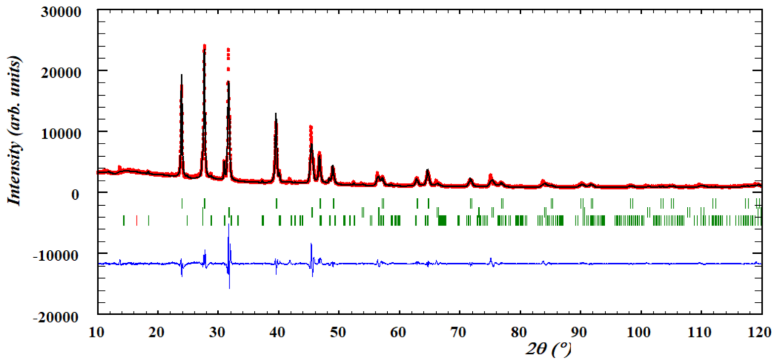


Figure 6.10: Profile refinement of the XRD obtained from the post-DSC sample at x($MgI_2$) = 0.1 in the NaCl−$MgI_2$ system. Phases used in the refinement are NaCl, NaI, $NaMgCl_3$ and $Na_6MgCl_8$. The observerd intensity (red circles) is shown alongside the calculated intensity (black line), and the difference between the two is shown (blue line). The angles at which reflections occur, i.e. the bragg positions, are shown as well (green, vertical lines).

XRD measurements have been performed on the post-DSC samples at composition x($MgI_2$) = 0.1, and a profile refinement has been performed using the method of Rietveld, Loopstra and van Laar [13, 14]. The refinement of the sample at x($MgI_2$) = 0.1 is shown in Figure 6.10. The phases found with this refinement are NaCl (36.69 $_{wt}$%), NaI (29.02 $_{wt}$%), $NaMgCl_3$ (7.21 $_{wt}$%) and $Na_6MgCl_8$ (27.08 $_{wt}$%). The expected phases at equilibrium from the thermodynamic model are NaCl, NaI and $Na_6MgCl_8$. While a sample at full thermodynamic equilibrium should consist of only three phases, it could be that the formation kinetics of these phases were not favourable during cooling in the DSC exper-

iment. This could be the case here, given that the presence of $NaMgCl_3$ in the sample is minor. This experiment also shows that iodine prefers associating with Na over Mg, as evidenced by the fact that NaI is present in the final sample.

### 6.2.2. $NaI-MgCl_2$

The $NaI-MgCl_2$ binary system has also been investigated using DSC and XRD. The DSC measurements of the invariant equilibria are shown on the phase diagram in Figure 6.11 and are reported in Appendix D, Table D.8. The model agrees well with the measured invariant equilibria, with the exception of two points at $x(MgCl_2) = 0.2$, around T = 630 K. These measured equilibria could be due to some currently unexplained sub-solidus behaviour.

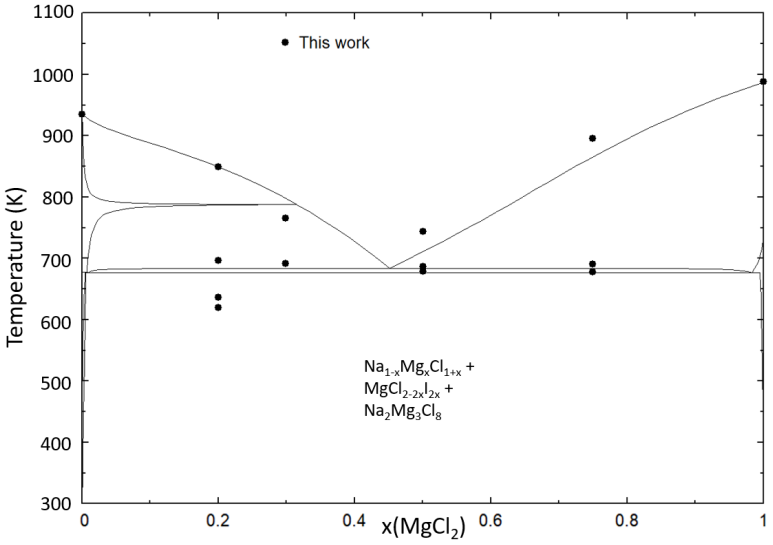


Figure 6.11: Phase diagram of the system NaI-$MgCl_2$ calculated with the optimized quaternary model presented in this work. Experimental data obtained in this work (black circles). The labelled phase field corresponds to the phase field where post-DSC XRD measurements have been performed.

Post-DSC XRD analysis of some samples in the $NaI-MgCl_2$ system has been performed in order to investigate how well the thermodynamic model predicts the stable solid phases. The refinement of the DSC sample taken at $x(MgCl_2) = 0.3$ is shown in Figure 6.12. The refinement shows that the dominant phases at this composition are $Na_{1-x}Mg_xI_{1+x}$ and $MgCl_2$, which is in agreement with the thermodynamic model predictions. In the thermodynamic model, $Na_2Mg_3Cl_8$ is also predicted to be stable at room temperature, however only at a concentration of $1.05{\cdot}10^{-5}$ mole per mole $NaI-MgCl_2$ mixture. This is expected to be below the detection limit of this XRD, hence it explains that it is not measured here.

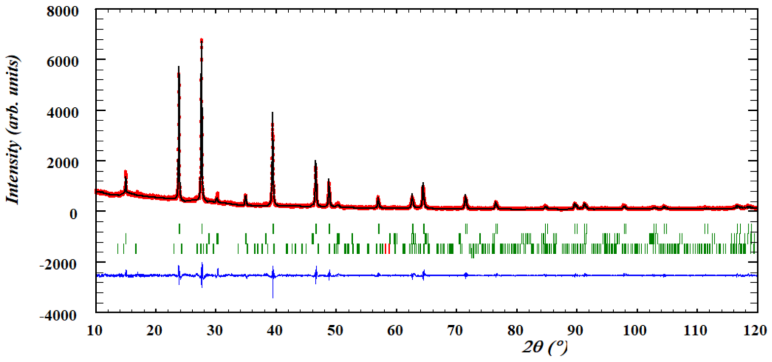


Figure 6.12: Profile refinement of the XRD obtained from the post-DSC sample at x($MgCl_2$) = 0.3 in the NaI−$MgCl_2$ system. Phases used in the refinement are $MgCl_2$, NaI and $Na_3Mg_2Cl_8$. The observerd intensity (red circles) is shown alongside the calculated intensity (black line), and the difference between the two is shown (blue line). The angles at which reflections occur, i.e. the bragg positions, are shown as well (green, vertical lines).

### 6.2.3. QUATERNARY LIQUIDUS PROJECTION

The liquidus projection of this quaternary system is presented in Figure 6.13. The optimization of this quaternary system was done based on the pseudo-binary systems NaCl−$MgI_2$ and NaI−$MgCl_2$, as detailed in Sections 6.2.1 and 6.2.2. The calculated invariant equilibria in the quaternary system are shown in Table 6.4.



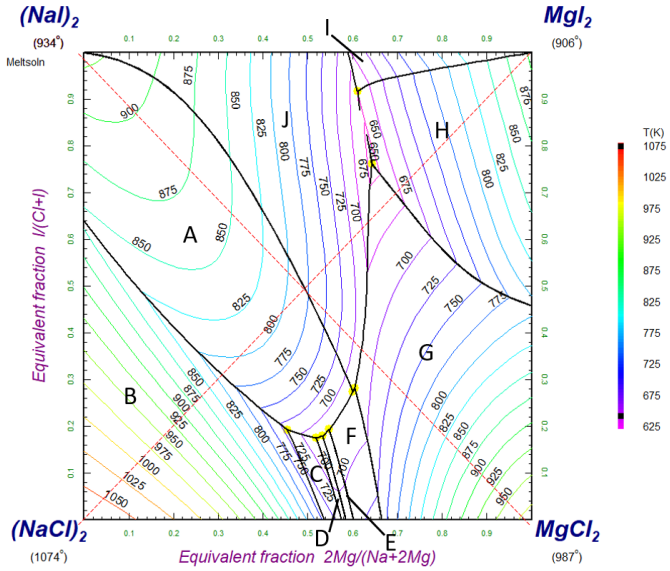


Figure 6.13: Liquidus projection of the Na-Mg-Cl-I quaternary system. Primary crystallization phases labelled A-I are: $Na_{1-x}I_xCl_{1-x}$ (A), NaCl (B), $Na_6MgCl_8$ (C), $Na_2MgCl_4$ (D), $NaMgCl_3$ (E), $Na_2Mg_3Cl_8$ (F), $MgI_{2-2x}Cl_{2x}$ (G), $MgCl_{2-2y}I_{2y}$ (H), $Na_yMg_{1-y}Cl_{2-y}$ (I), $Na_{1-x}Mg_xCl_{1+x}$ (J). Dashed red lines indicate the pseudo-binary sections NaCl−$MgI_2$ and NaI−$MgCl_2$, also shown in Figure 6.9 and 6.11 respectively.

| Fraction 2Mg/(Na + 2Mg) | Fraction I/(Cl + I) | T(K) | Invariant Reaction |
|---|---|---|---|
| 0.45 | 0.19 | 713 | NaCl, $Na_6MgCl_8$, $Na_{1-x}Mg_xI_{1+x}$ |
| 0.52 | 0.17 | 681 | $Na_2MgCl_4$, $Na_6MgCl_8$, $Na_{1-x}Mg_xI_{1+x}$ |
| 0.60 | 0.27 | 677 | $MgI_{2-2y}Cl_{2y}$, $Na_2Mg_3Cl_8$, $Na_{1-x}Mg_xI_{1+x}$ |
| 0.55 | 0.19 | 677 | $Na_2Mg_3Cl_8$, NaMgCl, $Na_{1-x}Mg_xI_{1+x}$ |
| 0.53 | 0.18 | 677 | $Na_2MgCl_4$, $NaMgCl_3$, $Na_{1-x}Mg_xI_{1+x}$ |
| 0.61 | 0.91 | 677 | $MgI_{2-2y}Cl_{2y}$, $MgCl_{2-2x}I_{2x}$, $Na_{1-x}Mg_xI_{1+x}$ |
| 0.64 | 0.77 | 641 | $MgI_{2-2y}Cl_{2y}$, $Mg_{1-y}Na_yI_{2-y}$, $Na_{1-x}Mg_xI_{1+x}$ |

Table 6.4: Calculated invariant equilibria in the $NaCl-NaI-MgCl_2-MgI_2$ system.

## 6.3. CONCLUSION

A thermodynamic model of the quaternary fused salt system $NaCl-NaI-MgCl_2-MgI_2$ has been presented in this chapter using the CALPHAD method with the quasi-chemical formalism in the quadruplet approximation for the liquid solution. Two of the binary subsystems of this quaternary system have been re-optimized based on data from the literature. The first system is NaCl−NaI, which has been assessed as a simple binary eutectic. Based on the assessment by Oonk et al. [8], limited solubility of NaCl in NaI has been included in the model. Second is the $NaCl-MgCl_2$ system, which was described in detail in Chapter 3.

The $MgCl_2-MgI_2$ system has been investigated experimentally for the first time in this work. This system is characterised by: i) a single eutectic at $x(MgI_2)$ = 0.43 and T = 790 ± 10 K, ii) a solid solution $MgCl_{2-2x}I_{2x}$ (rhombohedral) in the composition range $x(MgI_2) \leq 0.1$, iii) a solid solution $MgI_{2-2y}Cl_{2y}$ (rhombohedral) in the composition range $x(MgI_2) \geq 0.85$. Additionally, the system $NaI-MgI_2$ has been re-assessed based on our own experimental data in addition to the data from the literature. We have shown with our measurements of invariant equilibria that the solubility ranges of NaI in $MgI_2$ and vice versa are much narrower than previously assumed. Furthermore, using a Tammann diagram we have determined the composition of the eutectic and optimized our thermodynamic model accordingly.

Moreover, the pseudo-binary systems $NaCl-MgI_2$ and $NaI-MgCl_2$ have been investigated experimentally for the first time. Based on the DSC measurements, the quaternary system was optimized further. Post-DSC XRD measurements were performed to investigate the accuracy of the model predictions on the solid phase, and the obtained experimental results were in agreement with the thermodynamic model.

# BIBLIOGRAPHY


(1) Alders, D. C.; Rooijakkers, B. A.; Konings, R. J.; Smith, A. L. *The Journal of Physical Chemistry C* **2025**, *129*, 2726–2738.

(2) Klemn, W.; Beyersdorfer, K.; Oryschkewitsch, J. *Zeitschrift für anorganische Chemie* **1948**, *256*, 25–36.

(3) Seifert, H. et al. *Revue de Chimie Minerale* **1980**, 147–157.

(4) Johnson, C. E.; Hathaway, E. J. *Journal of The Electrochemical Society* **1971**, *118*, 631.

(5) Amadori, M. *Atti della Accademia Nazionale dei Lincei. Memorie. Classe di Scienze Fisiche, Matematiche e Naturali. Serie VIII. Sezione II* **1912**, *21*, 467.

(6) Ilyasov, I. I.; Bergman, A. G. *Russian Journal of Inorganic Chemistry* **1964**, *9*, 768–771.

(7) Oonk, H.; Blok, K.; van de Koot, B.; Brouwer, N. *Calphad* **1981**, *5*, 55–74.

(8) Oonk, H. *Pure and Applied Chemistry* **2001**, *73*, 807–823.

(9) Davis, H. T.; Rice, S. A. *The Journal of Chemical Physics* **1964**, *41*, 14–24.

(10) Alders, D. C.; Vlieland, J.; Thijs, M.; Konings, R. J. M.; Smith, A. L. *Journal of Molecular Liquids* **2024**, *396*, 123997.

(11) Melnichak, M.; Kleppa, O. *The Journal of Chemical Physics* **1972**, *57*, 5231–5241.

(12) Ilyasov, I.; Bostandzhiyan, A. *Soviet Research in Fused Salts, 1956, in English Translation* **1958**, 768–771.

(13) Rietveld, H. M. *Journal of applied Crystallography* **1969**, *2*, 65–71.

(14) Van Laar, B.; Schenk, H. *Acta Crystallographica Section A: Foundations and Advances* **2018**, *74*, 88–92.

# 7

# CHEMISTRY OF IODINE IN BASE FUEL $NaCl\text{-}MgCl_2\text{-}PuCl_3$

*This chapter is, in a way, the continuation of Chapter 7. Where in the previous chapter the effect of iodine on the $NaCl-MgCl_2$ fuel matrix was investigated, this chapter investigates the effect of the same fission product on the base fuel $NaCl-MgCl_2-PuCl_3$. To do so, a thermodynamic model of the $NaCl-NaI-MgCl_2-MgI_2-PuCl_3-PuI_3$ system is needed. Before this model is obtained, however, some binary subsystems in this higher order senary system must be investigated. The binary system $NaI-PuI_3$ model was first developed in this work based on the experimental data of the $NaI-NdI_3$ system, reported in the literature.*

*In addition, experimental investigations of the systems $NdCl_3-NdI_3$ and $MgI_2-NdI_3$, as simulant systems for the analogous Pu-system, are presented in this chapter. These systems have not been reported in the literature thus far. By DSC and XRD, the invariant equilibria and crystallographic composition of the solid phase were investigated. Both systems were found to be binary eutectic systems, with solid solutions $NdCl_{3-3x}I_{3x}$ (hexagonal) and $NdCl_{3y}I_{3-3y}$ (orthorhombic) in the $NdCl_3-NdI_3$ system.*

*Additionally, the reciprocal systems $NaCl-NaI-NdCl_3-NdI_3$ and $MgCl_2-MgI_2-NdCl_3-NdI_3$ were investigated by DSC and XRD. This was done by investigating the diagonals in these reciprocal systems: $NaCl-NdI_3$, $NaI-NdCl_3$, $MgCl_2-NdI_3$ and $MgI_2-NdCl_3$, respectively. For these reciprocal binary systems, higher order excess Gibbs energy parameters have been added to the thermodynamic model to fit the the measurements of the invariant equilibria and the compositions of the solid phase. Finally, the experimental data obtained in this work and in the literature were used as simulant data for the respective Pu-systems.*

To investigate the effect of iodine on the molten fuel salt $NaCl-MgCl_2-PuCl_3$, the higher order system $NaCl-NaI-MgCl_2-MgI_2-PuCl_3-PuI_3$ must be investigated. The first part of this system was already covered in the previous chapter, where the thermodynamic model of the quaternary system $NaCl-NaI-MgCl_2-MgI_2$ was presented. For the addition of $PuCl_3$ and $PuI_3$ to this system, several other common-ion binary systems must be investigated. These are the systems $NaI-PuI_3$, $MgI_2-PuI_3$ and $PuCl_3-PuI_3$. Additionally, information in the pseudo-binary systems, such as $NaCl-PuI_3$ and $NaI-PuCl_3$ can be used to further optimize the models.

In the absence of experimental data involving plutonium iodides, this chapter relies on simulant systems containing $NdI_3$ instead, as explained in Chapter 3. The system $NaI-NdI_3$ was investigated by Kutscher et al. [1], who used DTA to investigate the invariant equilibria in the system. Kutscher et al. found a single intermediate $Na_7NdI_{10}$, based on their DTA data, which undergoes a polymorphic phase transition at 650 K. Moreover, the mixing enthalpy of the $NaI-NdI_3$ system was investigated experimentally by Rycerz et al. [2]. The minimum of the mixing enthalpy they measure is in good agreement with the composition of the eutectic as measured by Kutscher et al.

To the best of our knowledge, data have not been reported for any of the binary or reciprocal systems $MgI_2-NdI_3$, $NdCl_3-NdI_3$, $NaCl-MgI_2$, $NaI-Mgcl_2$, $NaI-NdCl_3$, $NaCl-NdI_3$, $MgCl_2-NdI_3$ and $MgI_2-NdCl_3$ in the literature.

In this chapter, the binary simulant systems with Nd are first presented in Sections 7.1.1-7.2.4. The quaternary systems $NaCl-NaI-NdCl_3-NdI_3$ and $MgCl_2-MgI_2-NdCl_3-NdI_3$ calculated with the thermodynamic model are presented in Chapter 2. The aim of this chapter is to obtain thermodynamic models that describe the fuel salt $NaCl-MgCl_2-PuCl_3$ upon addition of iodine to this system, so the thermodynamic models of the systems containing Pu, based on the Nd-systems, are presented in Section 7.4. Finally, the thermodynamic functions that underlie the CALPHAD model are presented in Chapter 2.



## 7.1. BINARY SYSTEMS

### 7.1.1. $NaI-NdI_3$

The $NaI-NdI_3$ system was investigated by Kutscher et al. [3], who found a single intermediate $Na_7NdI_{10}$ based on their DTA measurements. Kutscher et al. also report a polymorphic transition on this intermediate at T = 658 K. Crystallographic data for this compound have not been reported in the literature.

The calculated phase diagram of this system is presented in Figure 7.1. The mixing enthalpy of the $NaI-NdI_3$ system was measured by Rycerz et al. [2], and this data was used to fit the CALPHAD model. The calculated mixing enthalpy of the $NaI-NdI_3$ system is shown in Figure 7.2 along with the experimental data [2] and the mixing enthalpies of the $MgI_2-NdI_3$ and $NdCl_3-NdI_3$ systems. Good agreement between the experimental data and the thermodynamic model was achieved through optimization. The calculated equilibrium at T = 850 K corresponds to a polymorphic phase transition in $NdI_3$, however this transition was not measured by Rycerz et al. Since this transition has been measured

in this work and in other sources in the literature, it is possible that Rycerz et al. had a small contamination in their $NdI_3$ that inhibited the polymorphic transition.

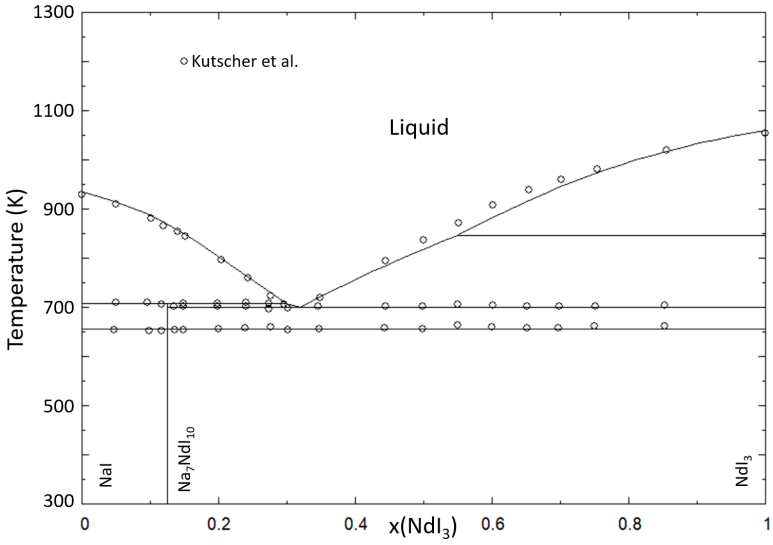


Figure 7.1: Phase diagram of the NaI−$NdI_3$ system calculated with the thermodynamic model presented in this work. Experimental data from Kutscher et al. [3] (black open circles).



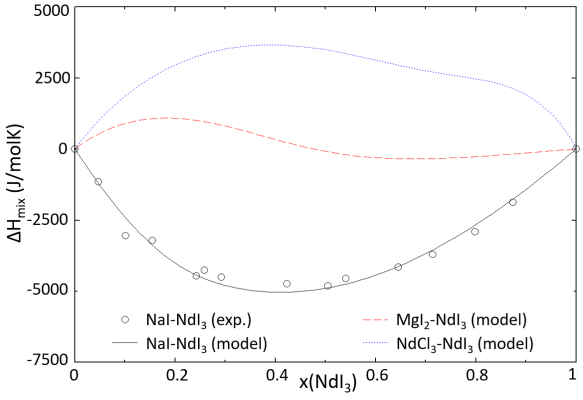


Figure 7.2: Calculated mixing enthalpy of the NaI−$NdI_3$ system (solid black line, T = 1068 K), $MgI_2$−$NdI_3$ system (dashed red line, T = 1068 K) and $NdCl_3$−$NdI_3$ system (dotted blue line, T = 1068 K), as well as experimental of the NaI−$NdI_3$ system reported by Rycerz et al. [2] (solid black circles, T = 1068 K).

| $x_{NdCl3}$ | T (K) | | Equilibrium | Invariant reaction |
|---|---|---|---|---|
| | CALPHAD | Kutscher | | |
| 0 | 934 | 927 ± 8 | Congruent melting | NaI = L |
| 0.32 | 702 | 702 ± 8 | Eutectic | $Na_7NdI_{10} + NdI_3 = L$ |
| 0.125 | 716 | 706 ± 8 | Peritectic | $Na_7NdI_{10} = NaCl + L'$ |
| 1 | 1049 | 1053 ± 8 | Congruent melting | $NdI_3 = L$ |

Table 7.1: Calculated invariant equilibria in the $NaI-NdI_3$ system as well as experimentally measured values of these invariants from Kutscher et al. [3].

### 7.1.2. $MgI_2-NdI_3$

The binary system $MgI_2-NdI_3$ was investigated experimentally in this work. XRD experiments were conducted to investigate the possible formation of intermediate compounds or solid solutions, and the temperatures of the invariant equilibria were investigated using DSC.

A sample at composition $x(NdI_3) = 0.5$ was mixed in a mortar and subjected to thermal treatment to investigate the crystal structure in this binary system. The profile refinement of this XRD is shown in Figure 7.3. This profile refinement shows the presence of both end-members, and no additional peaks. The cell volumes of the end-members obtained from the profile refinement are given in Table 7.2 compared to the values reported in the literature. These results give no indication that a solid solution forms in this system, and no intermediates are present.



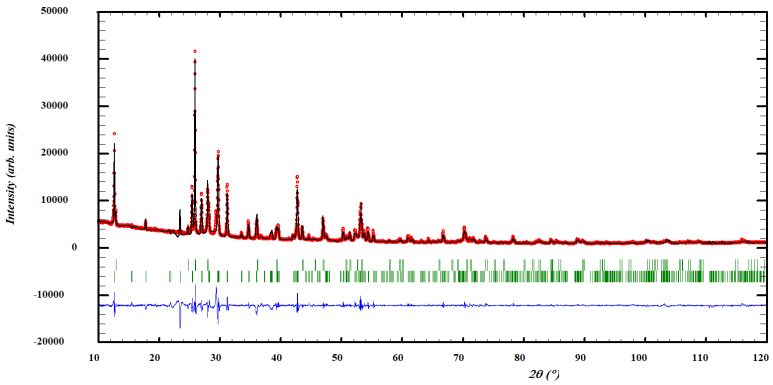


Figure 7.3: Profile refinement of the synthesised sample as $x(NdI_3) = 0.5$ in the $MgI_2-NdI_3$ system using the phases $MgI_2$ and $NdI_3$ as reported by Brogan et al. [4] and Beck et al. [5] respectively. The observed intensity (red circles) is shown alongside the calculated intensity (black line), and the difference between the two is shown (blue line). The angles at which reflections occur, i.e. the bragg positions, are shown as well (green, vertical lines).

| **Compound** | Source | Volume (Å$^3$) |
|---|---|---|
| $MgI_2$ | Brogan et al. [4] | 102.5(4) |
| | This work | 102.6(3) |
| $NdI_3$ | Beck et al. [5] | 599.9(3) |
| | This work | 599.9(2) |

Table 7.2: Refined cell volumes of $MgI_2$ and $NdI_3$ after thermal treatment of a mixture at x($NdI_3$) = 0.5, compared with reported literature values.

Moreover, a DSC study of this system was conducted as reported in Figure 7.4 and in Appendix D, Table D.9. The XRD investigation of this system gave no indication that a solid solution is stable at room temperature. However, the disappearance of the eutectic equilibrium at compositions x($NdI_3$) ≤ 0.2 indicates that there could be a solid solution at elevated temperatures in this system. Additionally, inspecting the peak areas recorded for every eutectic transition shows that there is a linear decrease in peak area magnitude from x($NdI_3$) = 0.42 to x($NdI_3$) = 0.2, approaching zero at x($NdI_3$) = 0.13. This is also an indication that there could indeed be solid solubility of $NdI_3$ in $MgI_2$. Because of this, solid solubility of $NdI_3$ in $MgI_2$ at elevated temperatures has been incorporated in the thermodynamic model. The mixing enthalpy of this system is presented in Figure 7.2. There are no experimental data available on the mixing enthalpy of this system, nor is there any data available to estimate the mixing enthalpy. Based on the behaviour of the chloride systems presented in Chapter 3, the mixing enthalpy of the Mg-system is expected to be more positive than the mixing enthalpy of the Na-system, which is indeed seen in Figure 7.2.



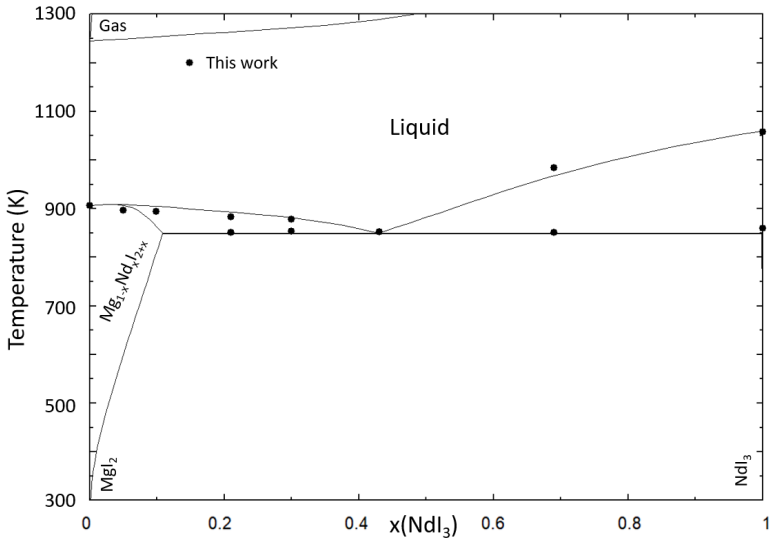


Figure 7.4: Phase diagram of the $MgI_2$−$NdI_3$ system calculated with the thermodynamic model presented in this work. Experimental data from this work (black closed circles).

| $x_{NdCl3}$ | T (K) | | Equilibrium | Invariant reaction |
|---|---|---|---|---|
| | CALPHAD | This work (DSC) | | |
| 0 | 1040 | 1030 ± 5 | Congruent melting | $MgI_2$ = L |
| 0.43 | 846 | 848 ± 10 | Eutectic | $MgI_2$ + $NdI_3$ = L |
| 1 | 1049 | 1053 ± 5 | Congruent melting | $NdI_3$ = L |

Table 7.3: Calculated invariant equilibria in the $MgI_2-NdI_3$ system as well as experimentally measured values of these invariant equilibria in this work (DSC).

### 7.1.3. $NdCl_3-NdI_3$

To investigate the existence of possible solid solutions or intermediate salts, a sample of composition x($NdI_3$) = 0.5 was synthesised and characterised with XRD. The profile refinement of this experiment is shown in Figure 7.5. Additionally, to investigate the possibility of solid solutions forming in this binary system, a comparison was made between the calculated cell volumes of the individual phases, obtained from the profile refinement, and those values as reported in the literature. This comparison is shown in Table 7.4.

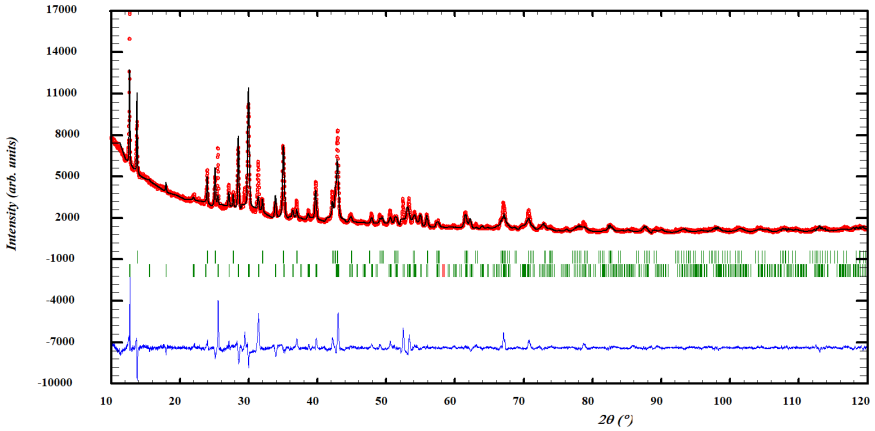


Figure 7.5: Profile refinement of the synthesised sample as x($NdI_3$) = 0.5 in the $NdCl_3-NdI_3$ system. The phases used for this refinement are $NdCl_3$ [6] and $NdI_3$ [5], with an additional position for iodine (in $NdCl_3$) and chlorine (in $NdI_3$) respectively. The observed intensity (red circles) is shown alongside the calculated intensity (black line), and the difference between the two is shown (blue line). The angles at which reflections occur, i.e. the bragg positions, are shown as well (green, vertical lines).

Shown in Table 7.4 are the cell volumes obtained from the refinement in Figure 7.5, compared to those reported in the literature by Meyer et al. [6] and Beck et al. [5] for $NdCl_3$ and $NdI_3$, respectively. It is clear that the calculated cell volume of the $NdCl_3$ end-member is close to the value reported in the literature. The calculated cell volume of $NdI_3$, however, deviates significantly from the value reported in the literature. This indicates that a solid solution of composition $NdCl_{3-3x}I_{3x}$ is likely formed in this binary system.

| **Compound** | Source | Volume (Å$^3$) |
|---|---|---|
| $NdCl_3$ | Meyer et al. [6] | 201.4(5) |
| | This work | 201.5(4) |
| $NdCl_{3-3x}I_{3x}$ | This work | 202.4(12) |
| $NdI_3$ | Beck et al. [5] | 599.9(3) |
| | This work | 599.9(2) |
| $NdCl_{3y}I_{3-3y}$ | This work | 582.4(6) |

Table 7.4: Refined cell volumes of $NdCl_3$ and $NdI_3$ compared with reported literature values, as well as the solid solutions obtained after thermal treatment of a mixture at x($NdI_3$) = 0.5.

The results of the DSC investigation of the $NdCl_3$−$NdI_3$ system are given on the phase diagram in Figure 7.6, and are reported in Appendix D, Table D.10. There is good agreement between the measured equilibria and the CALPHAD model, which is also shown in Table 7.5. The mixing enthalpy of this system is presented in Figure 7.2, but no experimental data have been reported to fit the thermodynamic model to. However, as seen in the NaCl−NaI and $MgCl_2$−$MgI_2$ systems, it is not unexpected that the mixing of a common-cation system between a chloride and an iodide shows a positive deviation from ideality. This is in agreement with Sangster et al. [7], who show that the mixing enthalpies in binary alkali-halide systems with chlorine and iodine are positive for all alkali metals.



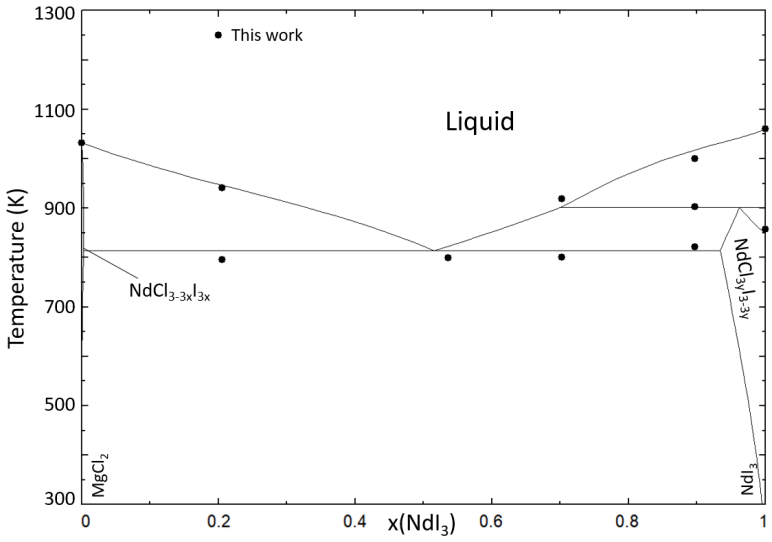


Figure 7.6: Phase diagram of the $NdCl_3$−$NdI_3$ system calculated with the thermodynamic model presented in this work. Experimental data from this work (black closed circles).

| $x_{NdCl3}$ | T (K) | | Equilibrium | Invariant reaction |
|---|---|---|---|---|
| | CALPHAD | This work (DSC) | | |
| 0 | 1040 | 1030 ± 5 | Congruent melting | $NdCl_3 = L$ |
| 0.533 | 808 | 799 ± 10 | Eutectic | $NdCl_{3-3x}I_{3x} + NdI_{3-3y}Cl_{3y} = L$ |
| 1 | 1049 | 1053 ± 5 | Congruent melting | $NdI_3 = L$ |

Table 7.5: Calculated invariant equilibria in the $NdCl_3-NdI_3$ system as well as experimentally measured values of these invariant equilibria in this work (DSC).

## 7.2. PSEUDO-BINARY SYSTEMS

To fully characterise the thermochemical behaviour of this higher order system, it is necessary to look beyond the binary systems alone. For this purpose, the diagonal pseudo-binaries in the quaternary systems $NaCl-NaI-NdCl_3-NdI_3$ and $MgCl_2-MgI_2-NdCl_3-NdI_3$ were investigated, in addition to the work on the $NaCl-NaI-MgCl_2-MgI_2$ system already reported in Chapter 6.

### 7.2.1. NaI–$NdCl_3$

The phase diagram of the $NaI-NdCl_3$ system, along with the measured invariant equilibria, is shown in Figure 7.7. There is good agreement between the measured invariant equilibria and the thermodynamic model optimized in this work, especially regarding the liquidus behaviour. The decomposition of the intermediate $Na_7NdI_{10}$ as calculated by the model at T = 520 K is not observed by DSC. This could be because the decomposition reaction has a small associated energy, but further experiments will have to be performed to ascertain if this is the case.



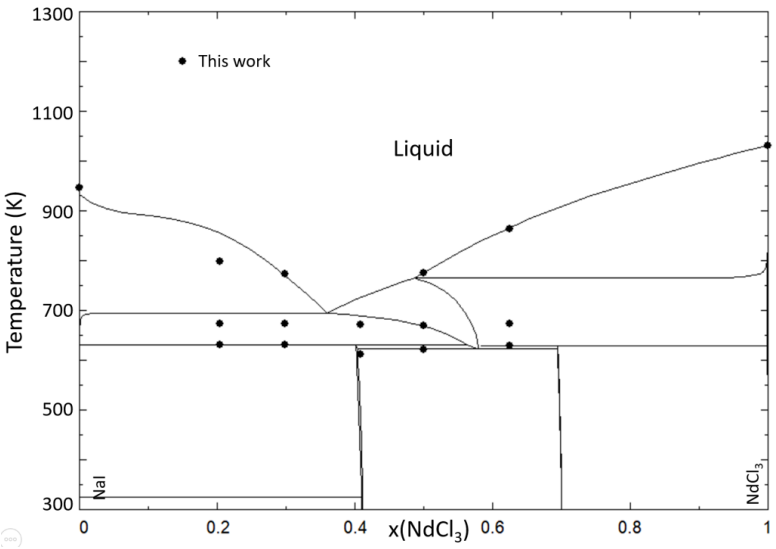


Figure 7.7: Calculated phase diagram of the $NaI-NdCl_3$ system, compared to experimental data obtained in this work (closed black circles).

### 7.2.2. $NaCl–NdI_3$

The thermodynamic model of the $NaCl–NdI_3$ system was optimized based on the experimental data obtained in this work. The calculated phase diagram of this system is presented in Figure 7.8. The thermodynamic model reproduces the measured equilibria well.

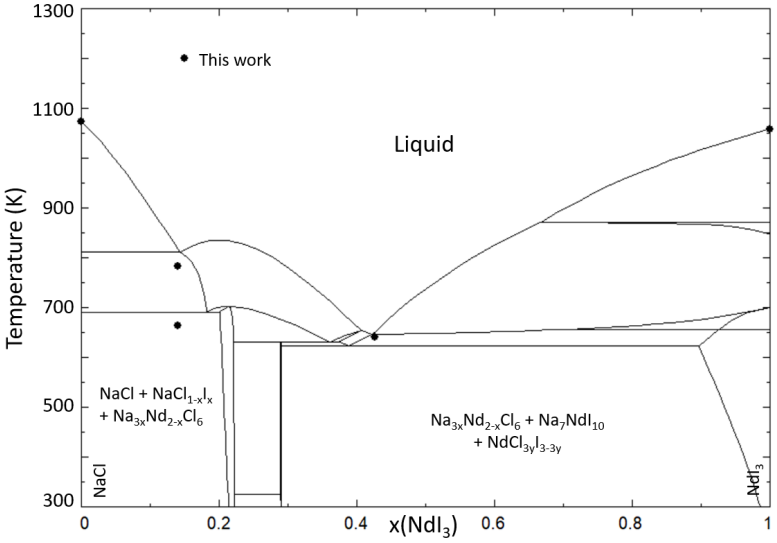


Figure 7.8: Calculated phase diagram of the $NaCl–NdI_3$ system, compared to experimental data obtained in this work (closed black circles).

### 7.2.3. $MgI_2–NdCl_3$

The model of the $MgI_2–NdCl_3$ system was optimized to fit the experimental data on the invariant equilibria measured in this work, as seen in Figure 7.9.

In this system, part of the quaternary $MgCl_2–MgI_2–NdCl_3–NdI_3$ system, two XRD measurements were carried out to investigate the phases stable at room temperature. These experiments were conducted at $x(NdCl_3) = 0.2$ and 0.42 in the pseudo-binary system. The Le Bail fits of these XRD measurements are presented in Appendix C. The phases that could be identified in these refinements are in good agreement with the expected phases from the CALPHAD model. While the CALPHAD model predicts that the stable phases at composition $x(NdCl_3) = 0.42$ are $MgCl_{2-2x}I_{2x}$, $NdCl_{3-3x}I_{3x}$ and $NdI_{3y}Cl_{3-3y}$, only the former two are observed in the XRD pattern. The reason for this could be that the fraction of $NdI_{3y}Cl_{3-3y}$ that forms is so small that it is below the detection capacity of the measurement (molar fraction $\leq 3{\cdot}10^{-4}$, according to the CALPHAD model).

### 7.2.4. $MgCl_2–NdI_3$

The measured invariant equilibria and the calculated phase diagram of this system are presented in Figure 7.10.

XRD measurement were carried out in this sytem to verify that the compositions at room temperature as predicted by the model are correct. The profile refinements of

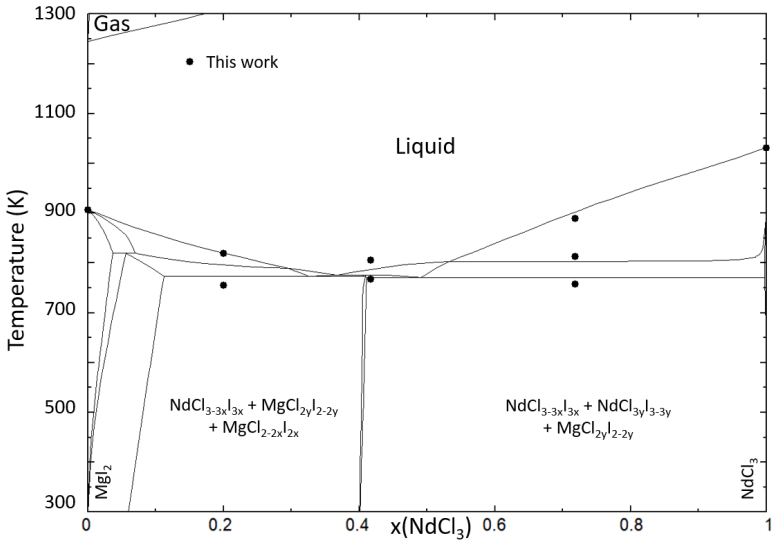


Figure 7.9: Calculated phase diagram of the $MgI_2$−$NdCl_3$ system, compared to the experimental data (solid black circles) measured in this work.

7

samples at compositions x($NdI_3$) = 0.40 and 0.7 are shown in Appendix C. The identified phases, $MgCl_{2-2x}I_{2x}$ and $NdCl_{3-3y}I_{3y}$, are in good agreement with the thermodynamic model shown in Figure 7.10. The third phase listed on the phase diagram, $MgCl_{2y}I_{2-2y}$ is present only in minor amounts according to the thermodynamic model, thus that could explain why it is not observed by XRD.

## 7.3. QUATERNARY SYSTEMS

The optimization of the quaternary systems NaCl−NaI−$NdCl_3$−$NdI_3$ and $MgCl_2$−$MgI_2$−$NdCl_3$−$NdI_3$ was done through the optimization of the reciprocal systems, as shown in Sections 7.2.1-7.2.4. Based on these optimizations, the quaternary liquidus projections can be calculated. These are shown in Figure 7.11 and 7.12 for the NaCl−NaI−$NdCl_3$−Nd and $MgCl_2$−$MgI_2$−$NdCl_3$−$NdI_3$ systems, respectively.

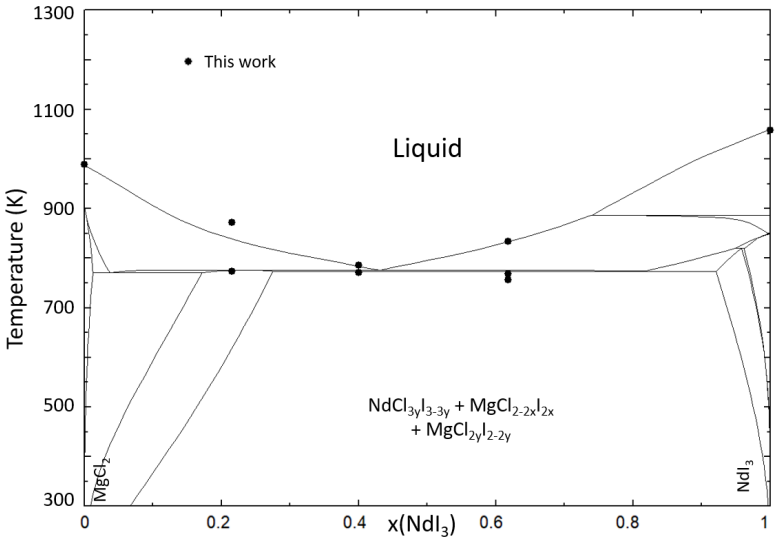


Figure 7.10: Calculated phase diagram of the $MgCl_2-NdI_3$ system, compared to the experimental data measured in this work (closed black circles).

| $NaCl-NaI-NdCl_3-NdI_3$ | | | |
|---|---|---|---|
| **Fraction I/(Cl + I)** | **Fraction 3Nd/(3Nd + 2Mg)** | **T(K)** | **Invariant reaction** |
| 0.582 | 0.129 | 691 | $NaI_xCl_{1-x} + NaCl + Na_{3x}Nd_{2-x}Cl_6 = L$ |
| 0.673 | 0.675 | 655 | $NaI_xCl_{1-x} + \alpha\text{-}Na_7NdI_{10} + \beta\text{-}Na_7NdI_{10} = L$ |
| 0.681 | 0.714 | 655 | $NdCl_{3y}I_{3-3y} + \alpha\text{-}Na_7NdI_{10} + \beta\text{-}Na_7NdI_{10} = L$ |
| 0.686 | 0.594 | 631 | $NaI_xCl_{1-x} + \alpha\text{-}Na_7NdI_{10} + Na_{3x}Nd_{2-x}Cl_6 = L$ |
| 0.708 | 0.606 | 628 | $\alpha\text{-}Na_7NdI_{10} + Na_{3x}Nd_{2-x}Cl_6 + NdCl_{3-3x}I_{3x} = L$ |
| 0.701 | 0.616 | 623 | $Na_{3x}Nd_{2-x}Cl_6 + NdCl_{3-3x}I_{3x} + NdCl_{3y}I_{3-3y} = L$ |
| $MgCl_2-MgI_2-NdCl_3-NdI_3$ | | | |
| **Fraction I/(Cl + I)** | **Fraction 3Nd/(3Nd + 2Mg)** | **T(K)** | **Invariant reaction** |
| 0.346 | 0.535 | 779 | $MgCl_{2y}I_{2-2y} + MgCl_{2-2x}I_{2x} + NdCl_{3y}I_{3-3y} = L$ |
| 0.457 | 0.841 | 819 | $MgCl_{2-2x}I_{2x} + NdCl_{3y}I_{3-3y} + NdCl_{3-3x}I_{3x} = L$ |
| 0.705 | 0.482 | 771 | $MgCl_{2-2x}I_{2x} + NdCl_{3y}I_{3-3y} + Mg_{1-x}Nd_xI_{2+x} = L$ |

Table 7.6: Calculated quaternary invariant equilibria in the $NaCl-NaI-NdCl_3-NdI_3$ and $MgCl_2-MgI_2-NdCl_3-NdI_3$ systems.

## 7.4. TRANSPOSITION ON Pu-BASED SYSTEMS

Using the obtained experimental data, as well as the data from the literature, from the Nd-based systems, the optimization of the Pu-based systems $NaI-PuI_3$, $MgI_2-PuI_3$, $PuCl_3-PuI_3$, $NaCl-PuI_3$, $NaI-PuCl_3$, $MgCl_2-PuI_3$, and $MgI_2-PuCl_3$ was performed. As elaborated on in Chapter 3, Nd is used as a simulant for Pu in the absence of experimental data and the Pu system was optimized to fit the experimental data of the corresponding Nd system.

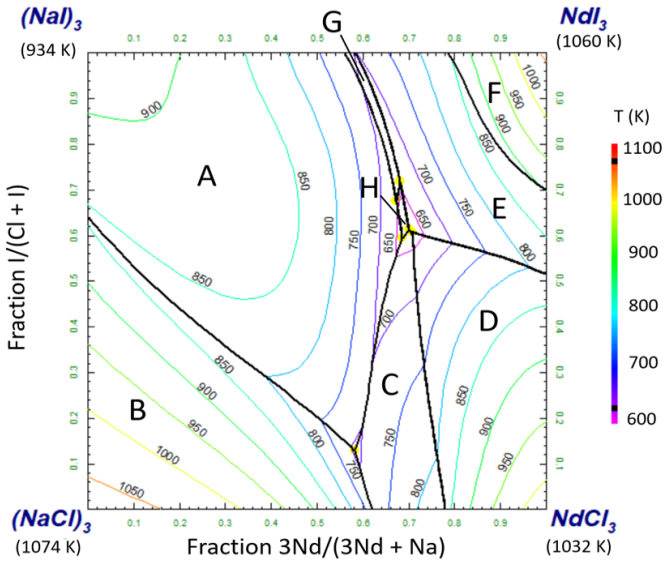


Figure 7.11: Liquidus surface of the NaCl−NaI−$NdCl_3$−$NdI_3$ quaternary system. Primary crystallization phases labelled A-F are: $NaI_xCl_{1-x}$ (A), NaCl (B), $Na_{3x}Nd_{2-x}Cl_6$ (C), $NdCl_{3-3x}I_{3x}$ (D), $NdCl_{3y}I_{3-3y}$ (E), $\beta$-$NdI_3$ (F), $\beta$-$Na_7NdI_{10}$ (G) and $\alpha$-$Na_7NdI_{10}$ (H). The calculated quaternary eutectic equilibria are shown in Table 7.6.



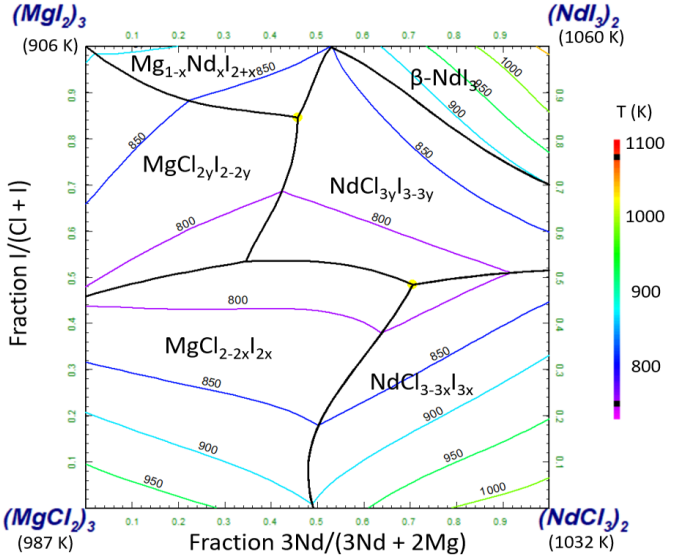


Figure 7.12: Liquidus surface of the $MgCl_2$−$MgI_2$−$NdCl_3$−$NdI_3$ quaternary system. Phases labelled on the liquidus surface are the primary crystallization phases in that area. The calculated quaternary eutectic equilibria are shown in Table 7.6.

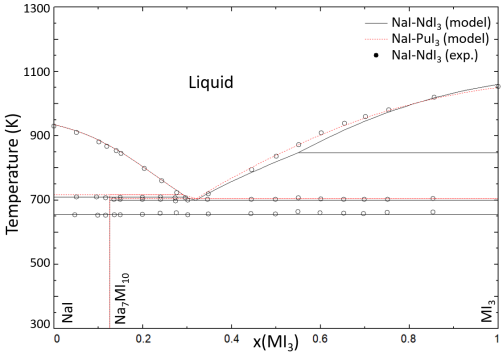


Figure 7.13: Phase diagram of the NaI−$PuI_3$ system (dotted red line) compared to the thermodynamic model (solid black line) and experimental data from the NaI−$NdI_3$ system measured by Kutscher et al. [3] (open black circles).

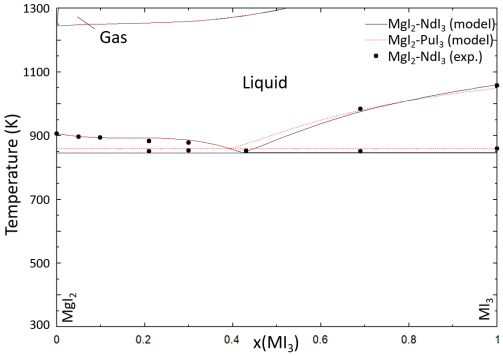


Figure 7.14: Phase diagram of the $MgI_2$−$PuI_3$ system (dotted red line) compared to the thermodynamic model (solid black line) and experimental data from the $MgI_2$−$NdI_3$ system measured in this work (black circles).

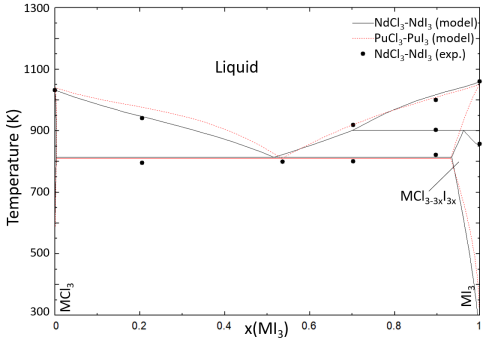


Figure 7.15: Phase diagram of the $PuCl_3$−$PuI_3$ system (dotted red line) compared to the thermodynamic model (solid black line) and experimental data from the $NdCl_3$−$NdI_3$ system measured in this work (black circles).

Figures 7.13-7.15 show the phase diagrams of the common-anion or common-cation systems with Pu, compared to the experimental data of the analogous Nd system. In all cases, good agreement between the simulant data and the thermodynamic model is achieved. The mixed-anion, mixed-cation systems with plutonium are presented in Figures 7.16-7.19. These figures also show a good agreement between the simulant data and the calculated phase diagram.

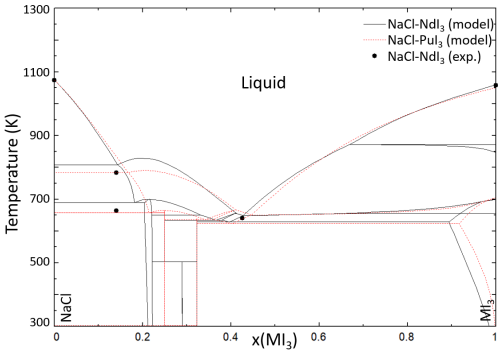


Figure 7.16: Phase diagram of the $NaCl-PuI_3$ system (dotted red line) compared to the thermodynamic model (solid black line) and experimental data from the $NaCl-NdI_3$ system measured in this work (black circles).

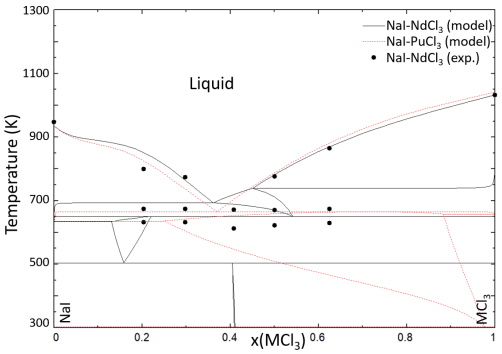


Figure 7.17: Phase diagram of the $NaI-PuCl_3$ system (dotted red line) compared to the thermodynamic model (solid black line) and experimental data from the $NaI-NdCl_3$ system measured in this work (black circles).

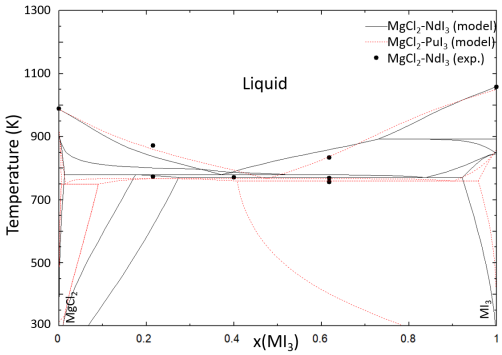


Figure 7.18: Phase diagram of the $MgCl_2-PuI_3$ system (dotted red line) compared to the thermodynamic model (solid black line) and experimental data from the $MgCl_2-NdI_3$ system measured in this work (black circles).

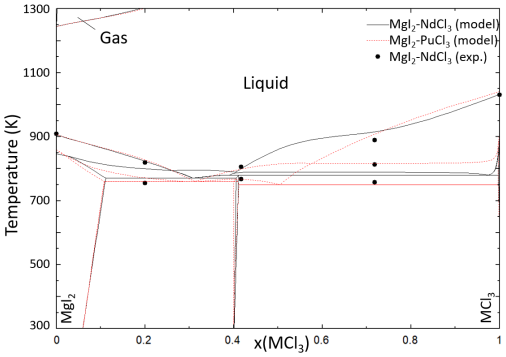


Figure 7.19: Phase diagram of the $MgI_2-PuCl_3$ system (dotted red line) compared to the thermodynamic model (solid black line) and experimental data from the $MgI_2-NdCl_3$ system measured in this work (black circles).

The liquidus projections of the systems $NaCl-NaI-PuCl_3-PuI_3$ and $MgCl_2-MgI_2-PuCl_3-PuI_3$ are presented in Figures 7.20 and 7.21, and the calculated quaternary eutectic equilibria are given in Table 7.7.

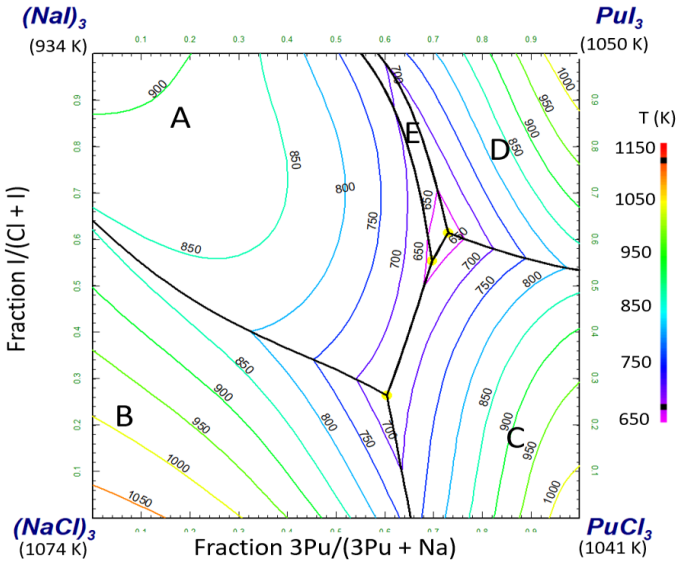


Figure 7.20: Liquidus surface of the NaCl−NaI−$PuCl_3$−$PuI_3$ quaternary system. Primary crystallization phases labelled A-F are: $NaI_xCl_{1-x}$ (A), NaCl (B), $PuCl_{3-3x}I_{3x}$ (C), $PuCl_{3y}I_{3-3y}$ (D), $Na_7PuI_{10}$ (E). The calculated quaternary eutectic equilibria are shown in Table 7.7.

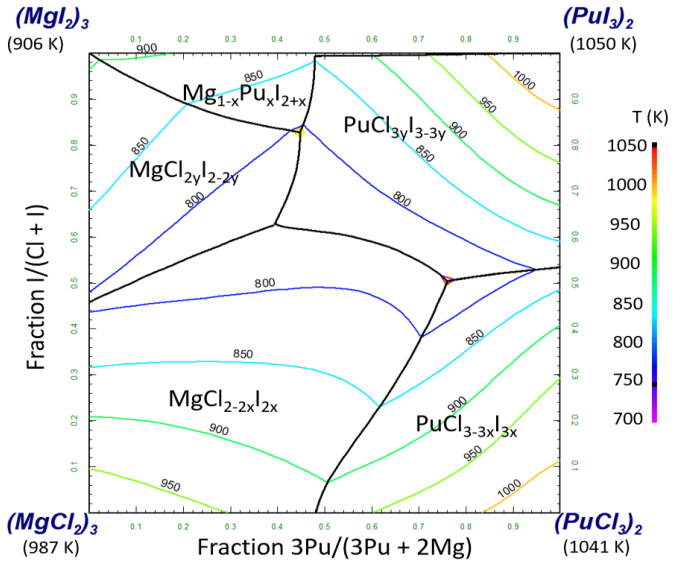


Figure 7.21: Liquidus surface of the $MgCl_2$−$MgI_2$−$PuCl_3$−$PuI_3$ quaternary system. Phases labelled on the liquidus surface are the primary crystallization phases in that area. The calculated quaternary eutectic equilibria are shown in Table 7.7.

| $NaCl-NaI-PuCl_3-PuI_3$ | | | |
|---|---|---|---|
| **Fraction I/(Cl + I)** | **Fraction 3Pu/(3Pu + Na)** | **T(K)** | **Invariant reaction** |
| 0.234 | 0.587 | 660 | $NaI_xCl_{1-x} + NaCl + PuCl_{3-3x}I_{3x} = L$ |
| 0.513 | 0.691 | 624 | $NaI_xCl_{1-x} + PuCl_{1-x}I_x + Na_7PuI_{10} = L$ |
| 0.584 | 0.726 | 613 | $PuCl_{3-3x}I_{3x} + PuCl_{3y}I_{3-3y} + Na_7PuI_{10} = L$ |
| $MgCl_2-MgI_2-PuCl_3-PuI_3$ | | | |
| **Fraction I/(Cl + I)** | **Fraction 3Pu/(3Pu + 2Mg)** | **T(K)** | **Invariant reaction** |
| 0.394 | 0.629 | 753 | $MgCl_{2y}I_{2-2y} + MgCl_{2-2x}I_{2x} + PuCl_{3y}I_{3-3y} = L$ |
| 0.448 | 0.882 | 795 | $Mg_{1-x}Nd_xI_{2+x} + PuCl_{3y}I_{3-3y} + PuCl_{3-3x}I_{3x} = L$ |
| 0.761 | 0.502 | 746 | $MgCl_{2-2x}I_{2x} + PuCl_{3y}I_{3-3y} + PuCl_{3-3x}I_{3x} = L$ |

Table 7.7: Calculated quaternary invariant equilibria in the $MgCl_2-MgI_2-PuCl_3-PuI_3$ and $NaCl-NaI-PuCl_3-PuI_3$ systems.

## 7.5. CONCLUSIONS

The binary systems $MgI_2-NdI_3$ and $NdCl_3-NdI_3$ have been optimized based on the experimental data measured in this work. These systems are both simple binary eutectic systems, with the $NdCl_3-NdI_3$ system exhibiting appreciable solid solubility of $NdCl_3$ in $NdI_3$ in the form of $NdCl_{3y}I_{3-3y}$ (orthorhombic), and negligible solid solubility of $NdI_3$ in $NdCl_3$ in the form of $NdCl_{3-3x}I_{3x}$ (hexagonal). No intermediates are present in either of these systems.

The reciprocal pseudo-binary systems $NaCl-NdI_3$, $NaI-NdCl_3$, $MgCl_2-NdI_3$ and $MgI_2-NdCl_3$ have been modelled based on the experimental data measured in this work. The thermodynamic models are in good agreement with the measured invariant equilibria. Additionally, XRD measurements were carried out to investigate the composition of the solid phase in these systems, and these measurements again show a good agreement between the thermodynamic model and the experimental results.

Based on the results obtained with the simulant systems containing Nd, the analogous systems with Pu were also modelled. Good agreement between the thermodynamic models of the Pu-based systems and the experimental data of the Nd-based systems was achieved through optimization.

As summarised above, this chapter presents the thermodynamic models for the $NaCl-NaI-PuCl_3-PuI_3$ and $MgCl_2-MgI_2-PuCl_3-PuI_3$ salt systems. In combination with Chapter 7, where the model for the $NaCl-NaI-MgCl_2-MgI_2$ system is presented, these quaternary systems provide the thermodynamic model for the full higher order system $NaCl-NaI-MgCl_2-MgI_2-PuCl_3-PuI_3$, with all individual interactions between end-members modelled. In doing so, the thermodynamic model of the base fuel $NaCl-MgCl_2-PuCl_3$ upon the inclusion of the fission product iodine has been completed.

# BIBLIOGRAPHY


(1) Blachnik, R.; Alberts, G.; Enninga, E. *Zeitschrift fur Anorganische und Allgemeine Chemie* **1985**, *522*, 207–216.

(2) Rycerz, L.; Gaune-Escarda, M. *Zeitschrift für Naturforschung A* **2002**, *57*, 136–142.

(3) Kutscher, J.; Schneider, A. *Zeitschrift für anorganische und allgemeine Chemie* **1971**, *386*, 38–46.

(4) Brogan, M. A.; Blake, A. J.; Wilson, C.; Gregory, D. H. *Acta Crystallographica Section C: Crystal Structure Communications* **2003**, *59*, i136–i138.

(5) Beck, H.; Gladrow, E. *Zeitschrift für anorganische und allgemeine Chemie* **1979**, *453*, 79–92.

(6) Meyer, G.; Schleid, T. *Journal of the Less Common Metals* **1986**, *116*, 187–197.

(7) Sangster, J.; Pelton, A. D. *Journal of physical and chemical reference data* **1987**, *16*, 509–561.

# 8

# CHEMISTRY OF CESIUM AND IODINE IN BASE FUEL $NaCl\text{-}MgCl_2\text{-}PuCl_3$

*Following the previous two chapters on the inclusion of iodine as a fission product in the thermodynamic model of the base fuel $NaCl-MgCl_2-PuCl_3$, this chapter investigates the effect of adding cesium. Starting from the quaternary system $NaCl-NaI-MgCl_2-MgI_2$ introduced in chapter 7, chapter 8 introduced the senary system (Na,Mg,Pu)(Cl,I). This chapter aims to take it one step further to an octonary system: (Na,Mg,Pu,Cs)(Cl,I). This is the necessary basis to assess the effect that the potentially volatile CsI has on the fuel matrix $NaCl-MgCl_2-PuCl_3$.*

*First, the effect of adding CsCl to the base fuel $NaCl-MgCl_2-NdCl_3$ is investigated by crafting thermodynamic models of the constituting binary systems $NaCl-CsCl$, $CsCl-MgCl_2$ and $CsCl-NdCl_3$. Subsequently, the same is done for the corresponding iodide systems $NaI-CsI$, $CsI-MgI_2$ and $CsI-NdI_3$.*

*Finally, the reciprocal systems $NaCl-NaI-CsCl-CsI$, $CsCl-CsI-MgCl_2-MgI_2$ and $CsCl-CsI-NdCl_3-NdI_3$ are investigated based on experimental data from the literature, or obtained in this work. The reciprocal systems NaCl-CsI, NaI-CsCl, and $CsI-MgCl_2$ are modelled based on data from the literature, while the systems $CsCl-MgI_2$, $CsCl-NdI_3$ and $CsI-NdCl_3$ are investigated experimentally in this work. The experimental data obtained in this work is furthermore used as simulant data for the respective Pu-systems. In conclusion, a thermodynamic description of the octonary system $NaCl-NaI-MgCl_2-MgI_2-NdCl_3-NdI_3-CsCl-CsI$ is obtained, to be used in application calculations with the purpose of assessing CsI retention and volatility in molten chlorides.*

Parts of this chapter are currently under review in "Alders et al., Journal of Physical Chemistry B (2026)

The need to add Cs to the thermodynamic models presented in this work stems from the question of whether CsI formation during the fission process will cause poor retention of Cs and I in the molten fuel salt, leading to potential vaporization of these elements. From an environmental point of view, both Cs and I pose a large risk due to their high radiotoxicity and high fission yield. In case of an accident, it is important to know what will happen to these species. In the literature, it has been shown that in fluoride-based molten salts there is limited solubility of CsI, leading to a high volatility of this species in the molten salt [1, 2].

Whereas the addition of iodine to the molten fuel salt $NaCl-MgCl_2-PuCl_3$ has already been covered in the previous chapter, this chapter focuses on including cesium in the thermodynamic model as well. To do this, first the interaction of cesium with the base fuel is investigated by modelling the systems $CsCl-NaCl$, $CsCl-MgCl_2$ and $CsCl-PuCl_3$, as well as the simulant system $CsCl-NdCl_3$. This alone leads to a thermodynamic description of the molten salt fuel that includes just the fission product Cs, *i.e.* the quaternary system $NaCl-MgCl_2-PuCl_3-CsCl$ presented in Section 8.1.1. However, as Beneš et al. [1] and Capelli et al. [3] showed for molten fluoride salts, it is the formation of CsI that influences the volatility of Cs and I considerably. To this end, the effects of the presence of both cesium and iodine must be modelled for molten chloride salts as well.

The addition of iodine to the aforementioned molten salt system gives a complex, higher order system: $NaCl-NaI-MgCl_2-MgI_3-PuCl_3-PuI_3-CsCl-CsI$. While large parts of this octonary system, *i.e.* the senary system $NaCl-NaI-MgCl_2-MgI_2-PuCl_3-PuI_3$ (Chapter 8), has already been modelled, the inclusion of Cs in this system is nevertheless a significant task. In addition to the aforementioned quaternary chloride system $NaCl-MgCl_2-PuCl_3-CsCl$, the corresponding quaternary iodide system $NaI-MgI_2-PuI_3^-$ $-CsI$ must be modelled as well, which is shown in Section 8.1.2. Furthermore, the mixed-anion mixed-cation reciprocal systems $NaCl-NaI-CsCl-CsI$, $CsCl-CsI-MgCl_2-MgI_2$ and $CsCl-CsI-PuCl_3-PuI_3$ must be investigated to complete the octonary system.



As has been the case throughout this entire dissertation, Nd is used as a simulant for Pu in the experimental investigations of these systems. For this chapter that means that, with the exception of the $CsCl-PuCl_3$ system [4], all thermodynamic models of plutonium systems are optimized based on the experimental data of the corresponding neodymium system.

## 8.1. BINARY SYSTEMS

### 8.1.1. CESIUM IN THE BASE FUEL

#### $CsCl-NaCl$

The system CsCl-NaCl has been investigated in the literature by Murgulescu et al. [5] by DTA. Their investigation of this system led to the conclusion that it is a simple binary eutectic, and in this work has been modelled as such, as shown in Figure 8.1. The mixing enthalpy of this system has been measured experimentally by Hersh et al. [6] at T = 1083 K, and the thermodynamic model was optimized to fit this data, as shown in Figure 8.4.

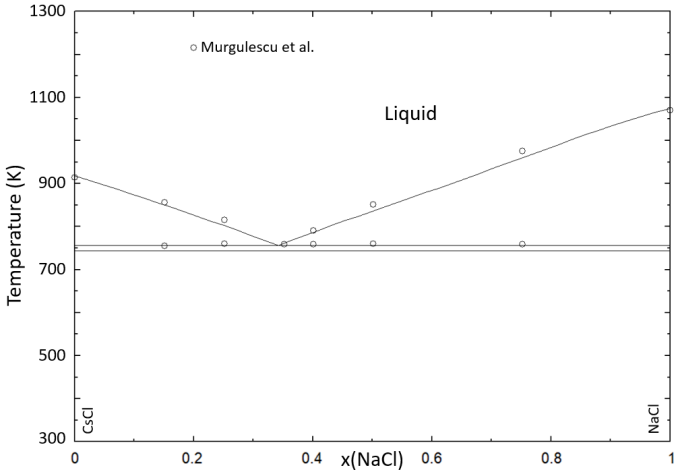


Figure 8.1: Calculated phase diagram of the NaCl−CsCl system compared to the experimental work of Murgulescu et al. [5] (open black circles).

Good agreement is achieved between the CALPHAD model and the experimental phase diagram and mixing enthalpy data.

### $CsCl-MgCl_2$

The system $CsCl-MgCl_2$ has been investigated experimentally by Markov et al. [7], who identified four intermediate compounds, namely $CsMgCl_3$ (space group $P6_3/mmc$ [8]), $Cs_2MgCl_4$ (space group Pnma [9]), $Cs_3MgCl_5$ (space group I4/mcm [10]) and $CsMg_3Cl_7$ (no crystallographic data). The existence of these intermediates has later been supported by Seifert et al. [11], with the exception of $CsMg_3Cl_7$. Seifert et al. performed solution calorimetry and proposed a phase diagram based on Markov et al.'s data. Seifert et al. did suggest the existence of another intermediate in this system $Cs_2Mg_3Cl_8$ [10], which they suggest decomposes peritectically. Recent publications involving this system [12, 13] have erroneously interpreted the phase diagram by Seifert et al. [11] as experimental data, and have fit their thermodynamic models to this phase diagram. However, as the only available experimental data on the invariant equilibria in this system is from Markov et al. [7], this work offers a re-optimization of the thermodynamic model based on their experimental data. The phase diagram of this system is presented in Figure 8.2. Additionally, based on the reported data by Markov et al., the intermediate compound $CsMg_3Cl_7$ seems more likely to exist than $Cs_2Mg_3Cl_8$. The difference in composition between these intermediates (*i.e.* $x(MgCl_2) = 0.75$ for $CsMg_3Cl_7$, $x(MgCl_2) = 0.6$ for $Cs_2Mg_3Cl_8$) means that the peritectic equilibrium measured by Markov et al. [7] at $x(MgCl_2) = 0.74$, 0.77 and 0.80, T = 795 K, can only be explained with the former intermediate. Due to the absence of experimental data for $x(MgCl_2) \geq 0.8$, however, the intermediate compound that decomposes peritectically at the previously mentioned temperature could be even richer in $MgCl_2$. This would have to be verified by additional experiments, however.

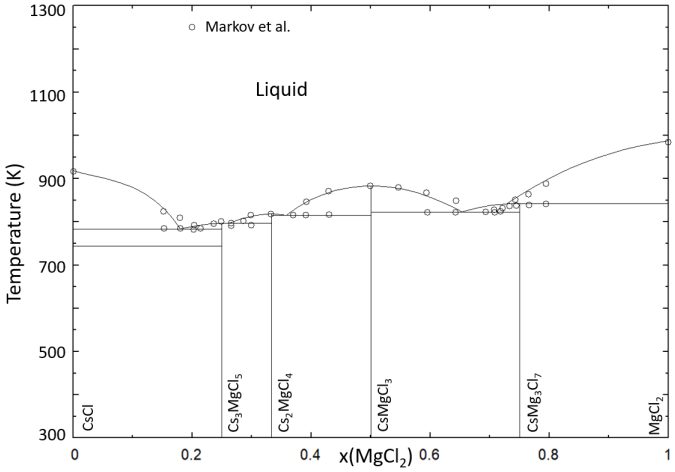


Figure 8.2: Phase diagram of the CsCl−$MgCl_2$ system calculated with the thermodynamic model presented in this work, compared to the experimental data from Markov et al. [7].

The mixing enthalpy of the CsCl−$MgCl_2$ system has been measured by Kleppa et al. [14] at T = 1003 K, and the model was optimized to fit this data. The calculated and experimental mixing enthalpies in this system are presented in Figure 8.4.

8

## CsCl−$NdCl_3$

Seifert et al. [15] investigated this system by DTA, identifying three intermediate compounds $Cs_3NdCl_6$, $Cs_2NdCl_5$ and $CsNd_2Cl_7$. The former, $Cs_3NdCl_6$, has a low-temperature $\alpha$ phase and a high-temperature $\beta$ phase, with a transition at T = 765 K [16, 17]. Both phases have been characterised by XRD by Reuter et al. [17]. There is no crystal structure known for the intermediate compound $CsNd_2Cl_7$, but analogous compounds $CsLn_2Cl_7$ (Ln = Pr, Sm-Lu) have been identified for other lanthanides [18]. The crystal structure of the intermediate compound $Cs_2NdCl_5$ has also not been reported in the literature, but analogous compounds $Cs_2RECl_5$ (RE = Pr, Eu-Lu) have been reported. The mixing enthalpy of this system has been measured by Gaune-Escard et al. [19] at T = 1122K.

The phase diagram of the CsCl−$NdCl_3$ as calculated with our thermodynamic model is presented in Figure 8.3, and the mixing enthalpy is shown in Figure 8.4.

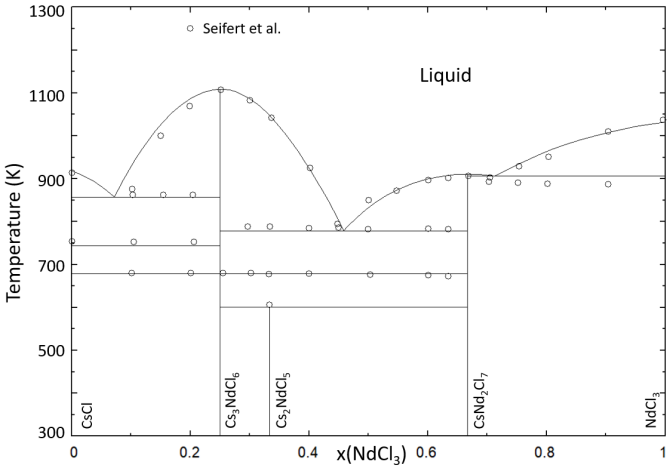


Figure 8.3: Phase diagram of the CsCl−$NdCl_3$ system, calculated with the thermodynamic model presented in this work and compared to the experimental data from Seifert et al. [15].

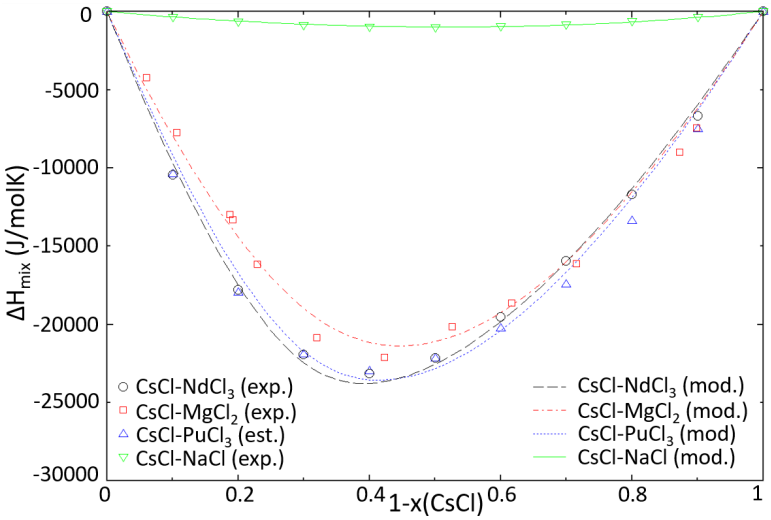


Figure 8.4: Calculated mixing enthalpies of the liquid in the systems CsCl−NaCl (solid green line, 1083 K), CsCl−$MgCl_2$ (red dashed-dotted line, 1003 K), CsCl−$PuCl_3$ (blue dotted line, 1122 K) and CsCl−$NdCl_3$ (black dashed line, 1122 K). The thermodynamic model well reproduces the experimental data from Hersh et al. [6] (open green upward triangles, NaCl−CsCl), Kleppa et al. [14] (open red squares, CsCl−$MgCl_2$) and Gaune-Escard et al. [19] (open black circles, CsCl−$NdCl_3$), as well as the data estimated using Davis' method [20] for the CsCl−$PuCl_3$ system (open upward blue traingles).

### 8.1.2. CESIUM IN IODIDE SYSTEMS

To model the effect of both volatile elements, Cs and I, in the molten salt fuel, the interactions of cesium in the corresponding iodide systems must also be modelled. To this

end, this section presents the results of the investigation of the binary subsystems in the $NaI-MgI_2-PuI_3-CsI$ quaternary system.

### CsI−NaI

Experimental investigations of the NaI−CsI system have been reported by Ilyasov et al. [21] and Scuro et al. [22]. Both authors report a simple binary eutectic system, and this interpretation has been retained in this work. The phase diagram of this system is presented in Figure 8.5. The mixing enthalpy of this system was measured by Kleppa et al. [14] at T = 973 K. The calculated mixing enthalpy is presented in Figure 8.8, along with the experimental data from Kleppa et al. it was based on.

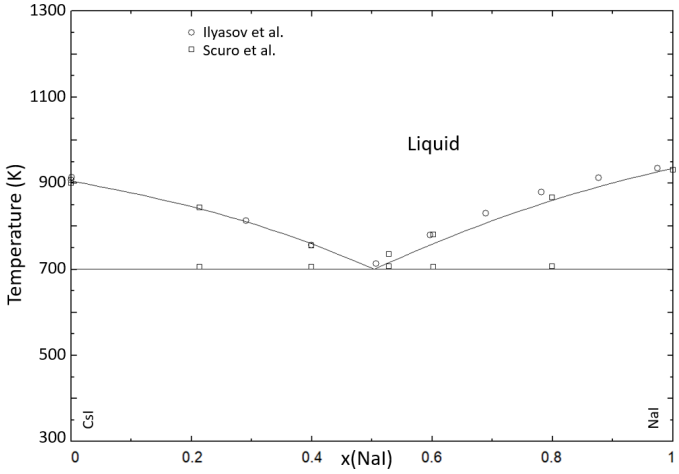


Figure 8.5: Phase diagram of the NaI−CsI system as calculated with the thermodynamic model presented in this work. Experimental data from Ilyasov et al. [21] (open black circles) and Scuro et al. [22] (open black squares).



### $CsI-MgI_2$

The system $CsI-MgI_2$ has been investigated by Seifert et al. [23], who identified 3 intermediates, namely $CsMgI_3$ (space group $P6_3/mmc$ [23, 24]), $Cs_2MgI_4$ (space group Pnma [23]) and $Cs_3MgI_5$ (space group I4/mcm [23]). In addition to the experimental data by Seifert et al., DSC experiments have been carried out in this work to substantiate the existing data, showing very good agreement with the previous study by Seifert et al. [23]. The phase diagram of this system is presented in Figure 8.6.

Experimental data available in the literature for the mixing enthalpy of the $CsI-MgI_2$ system have not been reported. Using the available experimental data of the $AX-MgX_2$ (A = Li, Na, K, Rb; X = F, Cl, Br) [14, 25, 26] systems, extrapolations could be made to the systems $CsX-MgX_2$ (X = F, Cl, Br) and $AI-MgI_2$ (A = Li, Na, K, Rb), respectively, using Davis' method, as explained in Chapter 2. From these systems, the mixing enthalpy of the $CsI-MgI_2$ system could be estimated, and was used as a fitting basis for the mixing enthalpy. The estimated mixing enthalpy of this system, along with the calculated mixing

enthalpy from the CALPHAD model, is shown in Figure 8.8.

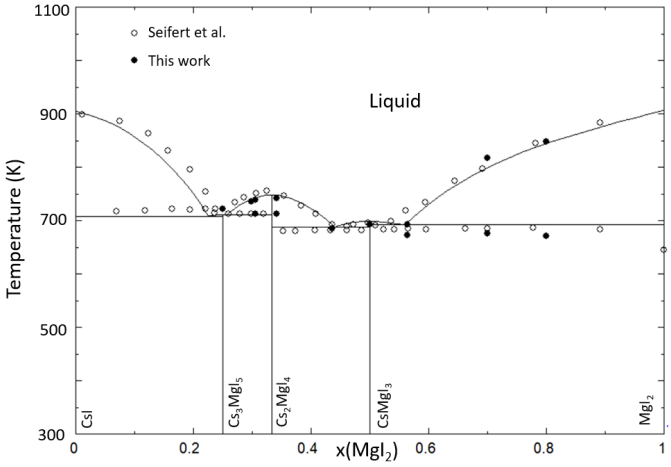


Figure 8.6: Phase diagram of the CsI−$MgI_2$ system, calculated with the thermodynamic model presented in this work. Experimental data from Seifert et al. [23] (open black circles) and this work (closed black circles).



## CsI−$NdI_3$

The CsI−$NdI_3$ system has been investigated by Kutscher et al. [27] by DTA. They identified three intermediates in $Cs_3NdI_6$, $Cs_3Nd_2I_9$ and $CsNd_4I_{13}$ based on their measured invariant equilibria. No crystal structures have been reported in the literature for any of these intermediate compounds. Crystal structures have been reported for analogous compounds $Cs_3M_2I_9$ (M = Er, Tm, Y, Sc, Bi) [28–31], but whether this is true for the CsI−$NdI_3$ system as well must be investigated experimentally.

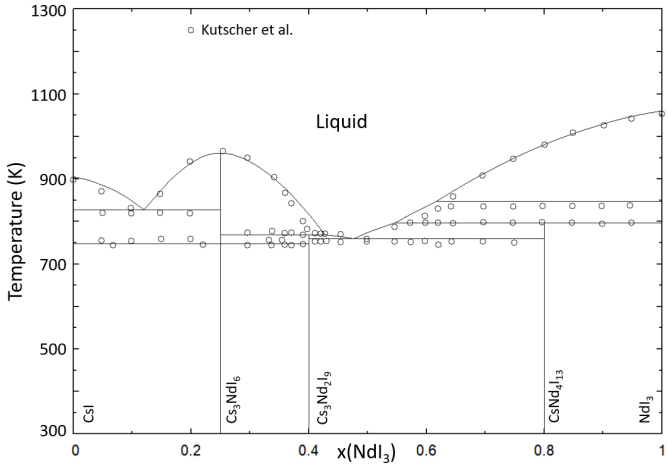


Figure 8.7: Phase diagram of the $CsI-NdI_3$ system calculated with the thermodynamic model presented in this work, compared to the experimental data reported by Kutscher et al. [27] (open black circles).

The mixing enthalpy of this system has been measured experimentally by Gaune-Escard et al. [32] at T = 1183 K. The data have been used as a basis to optimize the mixing enthalpy of the CALPHAD model. Both the calculated mixing enthalpy, and the measured values by Gaune-Escard et al. [32] are presented in Figure 8.8.

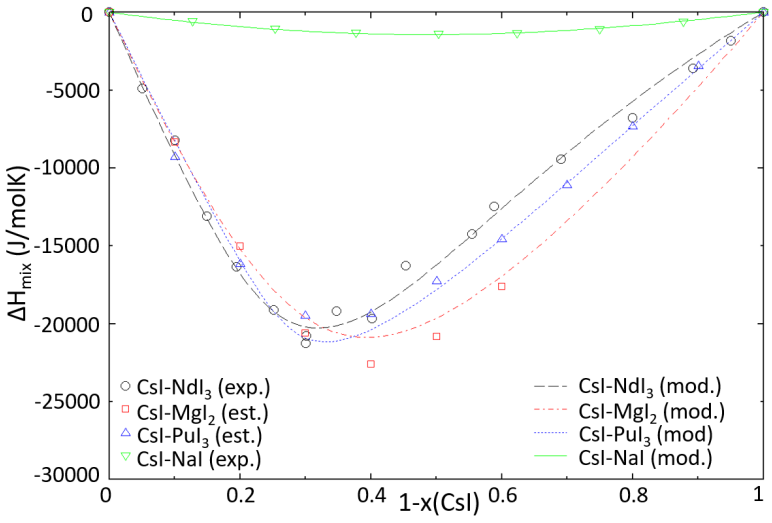


Figure 8.8: Calculated mixing enthalpies of the liquid in the systems CsI−NaI (solid green line, 1013 K), $CsI-MgI_2$ (red dashed-dotted line, 1000 K), $CsI-PuI_3$ (blue dotted line, 1183 K) and $CsI-NdI_3$ (black dashed line, 1183 K). The thermodynamic model well reproduces the experimental data from Kleppa et al. [14] (open purple upward triangles, NaI−CsI) and Gaune-Escard et al. [32] (open black circles, $CsI-NdI_3$), as well as the data estimated using Davis' method [20] for the $CsI-MgI_2$ (open red squares) and the $CsI-PuI_3$ systems (open upward blue traingles).

## 8.2. PSEUDO-BINARY AND QUATERNARY SYSTEMS

The results of the previous sections, *i.e.* the effect of cesium on the chloride fuel and the corresponding iodide systems, can be coupled with the results of Chapter 8 to create a model for the full system (Na, Mg, Pu, Cs)(Cl, I). To complete this model, however, the quaternary systems $NaCl-MgCl_2-PuCl_3-CsCl$ and $NaI-MgI_2-PuI_3-CsI$ must be coupled. This means that the interactions between the mixed-anion mixed-cation systems must be investigated, as is done in this section.

### 8.2.1. CsI IN CHLORIDE FUEL

#### CsCl–CsI

The system CsCl–CsI has been investigated in the literature by Ilyasov et al. [21] and Weyand et al. [33]. While there are no intermediates present in the system, Weyand et al. [33] did identify three areas with solid solubility: $CsCl_{1-x}I_x$ (Pm-3m) and $CsCl_{1-x}I_x$ (Fm-3m), given on the phase diagram in Figure 8.9 as $\alpha$-$CsCl_{1-x}I_x$ and $\beta$-$CsCl_{1-x}I_x$, respectively, and $CsI_{1-y}Cl_y$. The mixing enthalpy of the liquid in this system has been measured experimentally by Melnichak et al. [34] at T = 973 K, and the CALPHAD model was optimized to agree with this. The mixing enthalpy of the CsCl-CsI system is presented in Figure 8.10.

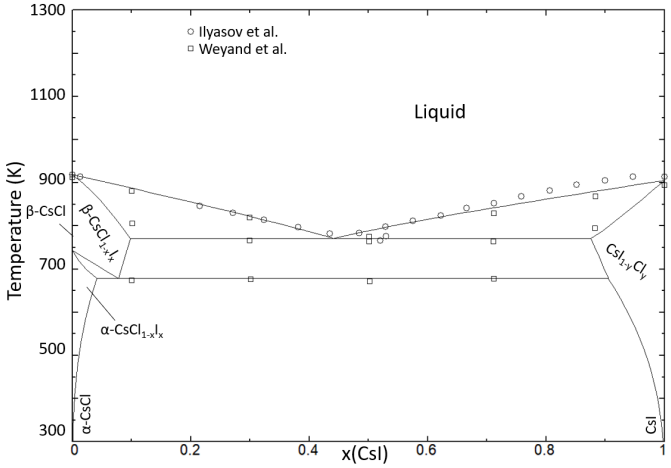


Figure 8.9: Phase diagram of the CsCl–CsI system calculated with the thermodynamic model presented in this work compared to the experimental liquidus data reported by Ilyasov et al. [21] (open black circles) and Weyand et al. [33] (open black squares).

#### (Na,Cs)(Cl,I) SYSTEMS

The melting behaviour of the CsCl–NaI and CsI–NaCl systems has been investigated experimentally by Ilyasov et al. [21], who measured the liquidus surface of the quaternary system. The calculated phase diagrams of these systems, based on the optimization of the binary systems only, are presented in Figures 8.11 and 8.12.

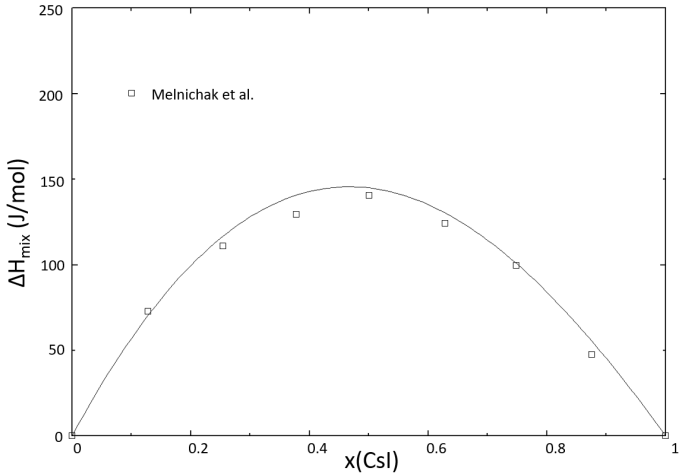


Figure 8.10: Mixing enthalpy of the CsCl-CsI system calculated at T = 971 K with the CALPHAD model presented in this work. Experimental data from Melnichak et al. [34] measured at the same temperature.

The liquidus of the reciprocal systems CsCl−NaI and NaCl−CsI is accurately depicted by the thermodynamic model presented in this work without the need for higher order excess Gibbs energy parameters.



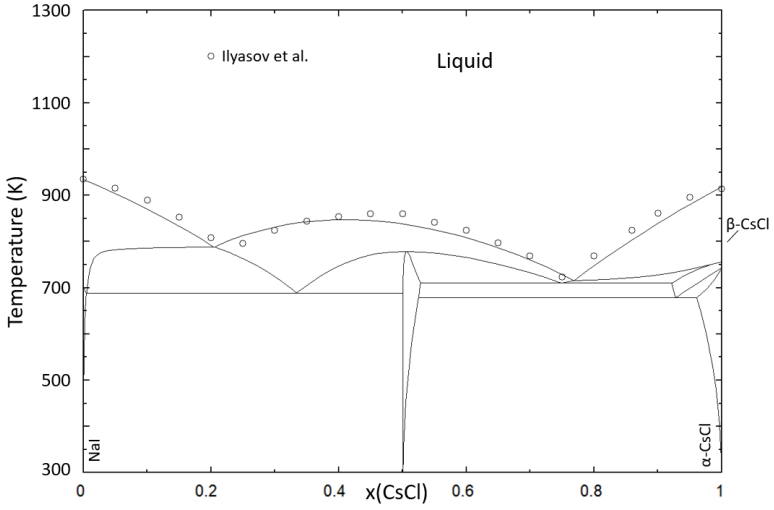


Figure 8.11: Phase diagram of the NaI−CsCl system calculated with the thermodynamic model presented in this work compared to the experimental liquidus data reported by Ilyasov et al. [21] (open black circles).

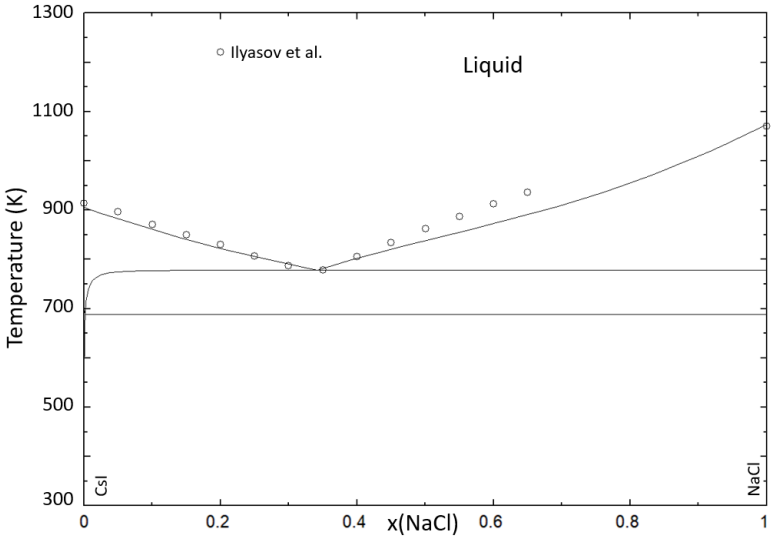


Figure 8.12: Phase diagram of the NaCl−CsI system calculated with the thermodynamic model presented in this work compared to the experimental liquidus data reported by Ilyasov et al. [21] (open black circles).

In their assessment of the quaternary system (Na,Cs)(Cl,I), Ilyasov et al. [21] identified two quaternary eutectic equilibria. These quaternary eutectics are in good agreement with the eutectics calculated using the CALPHAD model used in this work, as shown in Table 8.1.

| **This work** | | | |
|---|---|---|---|
| **Fraction I/(Cl + I)** | **Fraction Cs/(Cs + Na)** | **T(K)** | **Invariant reaction** |
| 0.781 | 0.261 | 710 | $NaI_{1-y}Cl_y + NaCl + CsI_{1-y}Cl_y = L$ |
| 0.465 | 0.923 | 688 | $NaCl + CsI_{1-y}Cl_y + \beta\text{-}CsCl_{1-x}I_x = L$ |
| **Ilyasov et al. [35]** | | | |
| **Fraction I/(Cl + I)** | **Fraction Cs/(Cs + Na)** | **T(K)** | **Invariant reaction** |
| 0.771 | 0.311 | 706 | $NaI_{1-y}Cl_y + NaCl + CsI_{1-y}Cl_y = L$ |
| 0.472 | 0.918 | 693 | $NaCl + CsI_{1-y}Cl_y + \beta\text{-}CsCl_{1-x}I_x = L$ |

Table 8.1: Calculated quaternary eutectic equilibria in the NaCl−NaI−CsCl−CsI system with the thermodynamic model presented in this work (top) and the equilibria measured by Ilyasov et al. [21].

### (Cs,Mg)(Cl,I) SYSTEMS

The thermochemical behaviour of the system CsCl−$MgI_2$ has been investigated in this work by DSC and XRD. The phase diagram of this system is presented in Figure 8.13. The system CsI−$MgCl_2$ has been investigated by Dixon et al. [36] using DSC, and the phase diagram of this system is presented in Figure 8.14. The liquidus and most of the sub-liquidus equilibria in this system are very well reproduced with the thermodynamic

model.

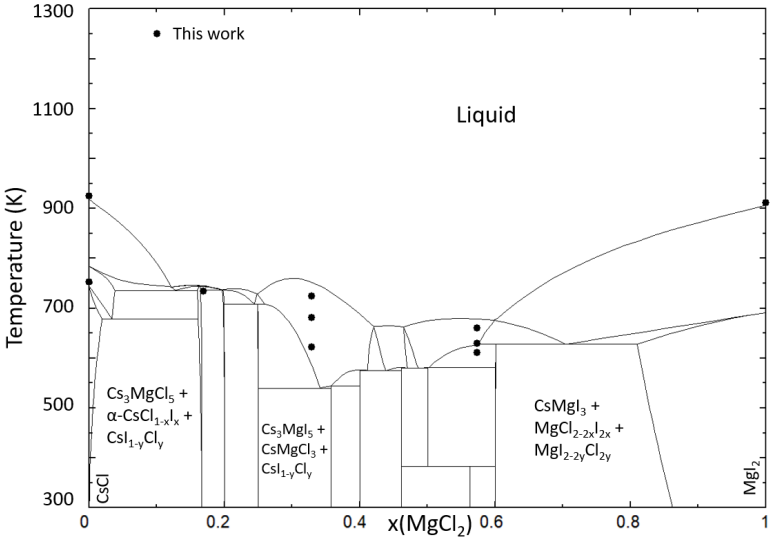


Figure 8.13: Calculated phase diagram of the $CsCl-MgI_2$ system using the thermodynamic model presented in this work. Experimental data measured by DSC in this work.

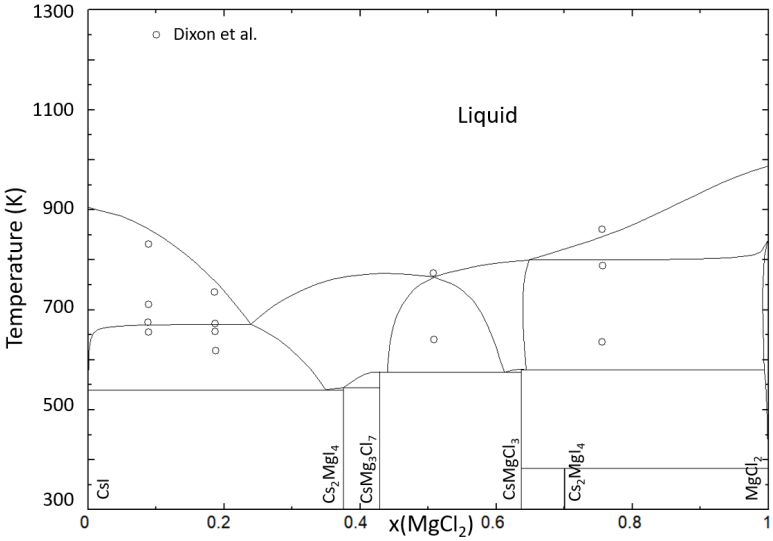


Figure 8.14: Calculated phase diagram of the $CsI-MgCl_2$ system using the thermodynamic model presented in this work. Experimental data measured by Dixon et al. [36]

In addition to the investigation of invariant equilibria in these systems, XRD measurements have been performed to investigate the stable phases at room temperature.

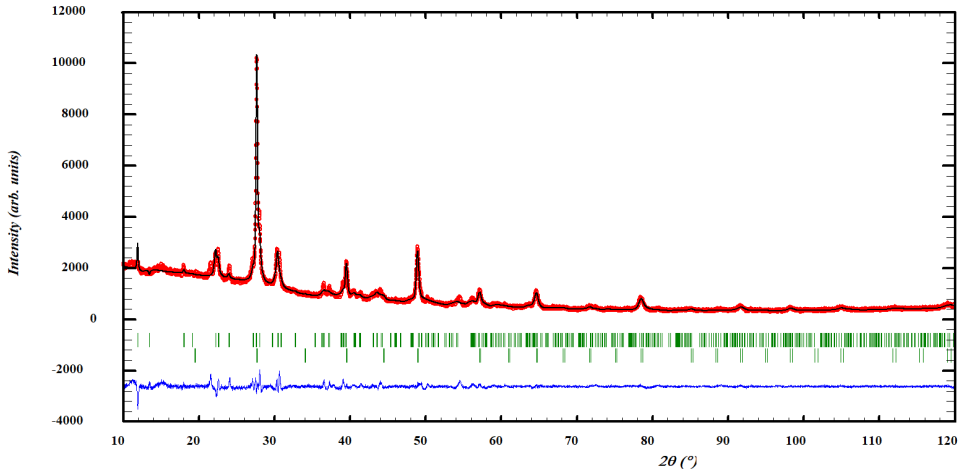


Figure 8.15: Le Bail fit of the post-DSC sample at x($MgI_2$) = 0.15 in the CsCl−$MgI_2$ system. The phases included in the refinement are $CsI_{1-y}Cl_y$ (based on the structure of CsI [37]) and $Cs_3MgCl_5$ as reported by Seifert et al. [10]. The observed intensity (red circles) is shown alongside the calculated intensity (black line), and the difference between the two is shown (blue line). The angles at which reflections occur, i.e. the Bragg positions, are shown as well (green, vertical lines).

Due to the fact that not all crystal structures of the intermediate compounds encountered in these systems are known, analysing the XRD patterns was challenging. However, for the sample at x($MgI_2$) = 0.15 the dominant phases in the pattern were identifiable, as seen in Figure 8.15. Two of the expected phases, $CsI_{1-y}Cl_y$ and $Cs_3MgCl_5$, were identified from the XRD pattern. The third phase expected from the CALPHAD model, $\alpha$-$CsCl_{1-x}I_x$, was not observed. This can be explained by the fact that the molar fraction is very small (x($\alpha$-$CsCl_{1-x}I_x$) ≤ 0.05) according to the CALPHAD model.

8

### (Cs,Nd)(Cl,I) SYSTEMS

The pseudo-binary systems CsCl−$NdI_3$ and CsI−$NdCl_3$ have been investigated experimentally to provide an experimental basis for optimizing the quaternary system CsCl−CsI−$NdCl_3$−$NdI_3$. The invariant equilibria were investigated by DSC, and are shown on the calculated phase diagrams in Figures 8.16 and 8.17, respectively. A good agreement between the experimental data and the thermodynamic model is achieved through optimization. Slight differences in the melting point in the CsX (X = Cl, I) rich regions in these reciprocal systems remain, however. Many of the sub-liquidus equilibria are likewise explained by the thermodynamic model.

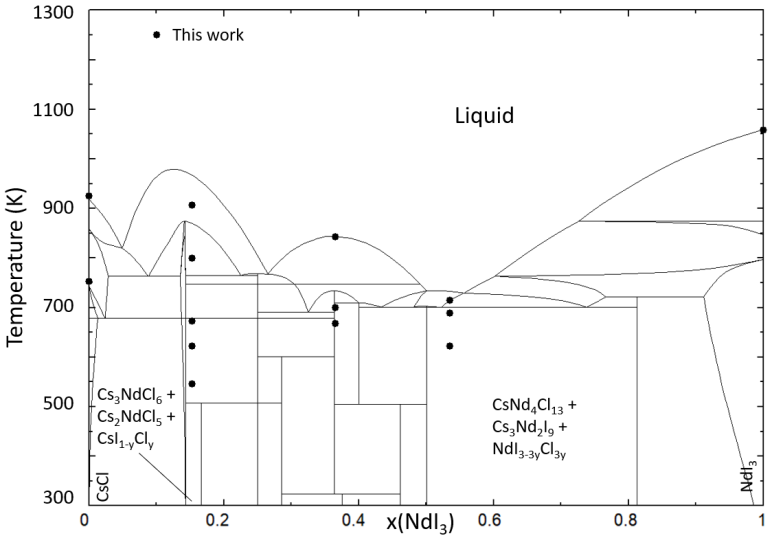


Figure 8.16: Calculated phase diagram of the CsCl−$NdI_3$ system using the thermodynamic model presented in this work. Experimental data measured by DSC in this work.

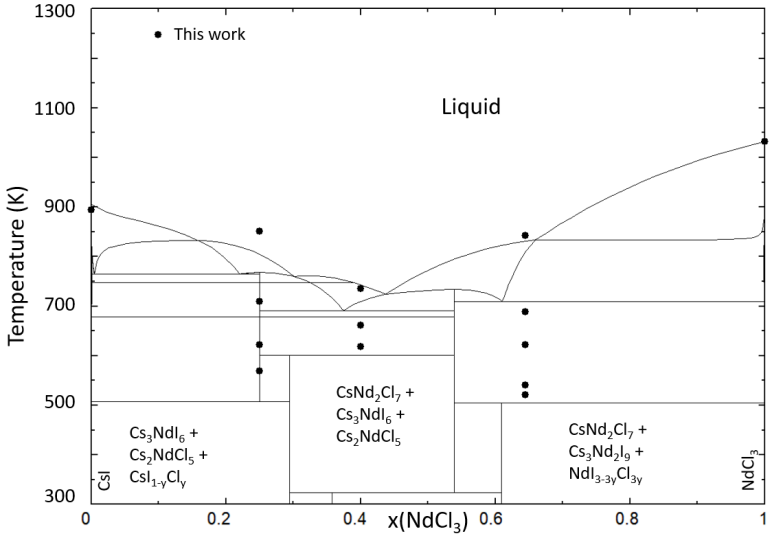


Figure 8.17: Calculated phase diagram of the CsI−$NdCl_3$ system using the thermodynamic model presented in this work. Experimental data measured by DSC in this work.

An XRD measurement was performed in the pseudo-binary system CsCl−$NdI_3$ at x($NdI_3$) = 0.15 to investigate the phases stable at room temperature. The profile refinement of this XRD is shown in Figure 8.18. The crystal structures used for this refinement are $Cs_3NdCl_6$ [17], CsI as reported by Balamurugan et al. [37], but with a shared I/Cl po-

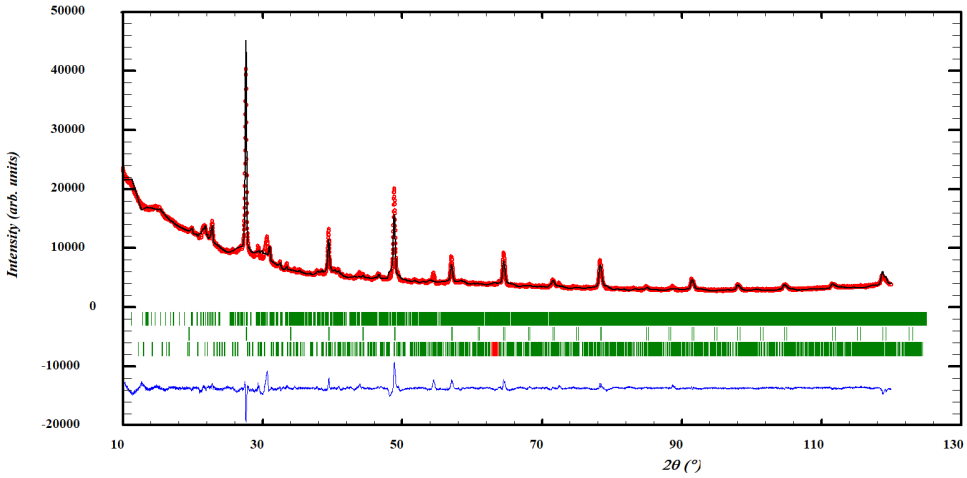


Figure 8.18: Profile refinement of the post-DSC sample at x($NdI_3$) = 0.15 in the CsCl−$NdI_3$ system. The phases included in the refinement are $CsI_{1-y}Cl_y$ (based on the structure of CsI [37]), $Cs_3NdCl_6$ (Reuter et al. [17]) and $Cs_2NdCl_5$ (based on the structure of $Cs_2PrCl_5$ [38]). The observed intensity (red circles) is shown alongside the calculated intensity (black line), and the difference between the two is shown (blue line). The angles at which reflections occur, i.e. the Bragg positions, are shown as well (green, vertical lines).



sition, and $Cs_2PrCl_5$ [38], but with Nd in the Pr position. The observation of these phases in the XRD pattern is in good agreement with the thermodynamic model.

### 8.2.2. QUATERNARY SYSTEMS

The quaternary systems CsCl−CsI−$MgCl_2$−$MgI_2$ and CsCl−CsI−$NdCl_3$−$NdI_3$ have been investigated in this chapter, and the liquidus projections of these systems are shown in Figures 8.20 and 8.19, respectively. Also shown in Table 8.2 are the quaternary invariant equilibria in these systems.

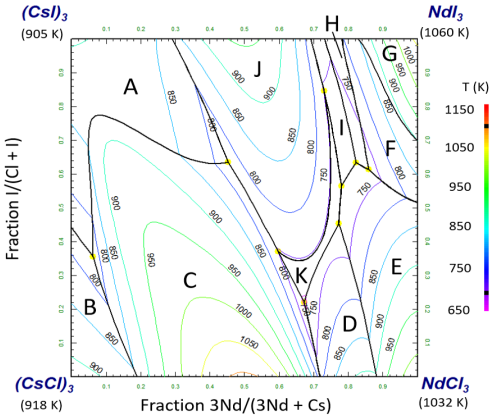


Figure 8.19: Liquidus surface of the CsCl−CsI−$NdCl_3$−$NdI_3$ quaternary system. Primary crystallization phases labelled A-K are: $CsI_{1-y}Cl_y$ (A), $\beta$-$CsCl_{1-x}I_x$ (B), $\beta$-$Cs_3NdCl_6$ (C), $CsNd_2Cl_7$ (D), $NdCl_{3-3x}I_{3x}$ (E), $NdCl_{3y}I_{3-3y}$ (F), $\beta$-$NdI_3$ (G), $CsNd_4I_{13}$ (H), $Cs_3Nd_2I_9$ (I), $\beta$-$Cs_3NdI_6$ (J) and $\alpha$-$Cs_3NdI_6$ (K). The calculated quaternary invariant equilibria are shown in Table 8.2.

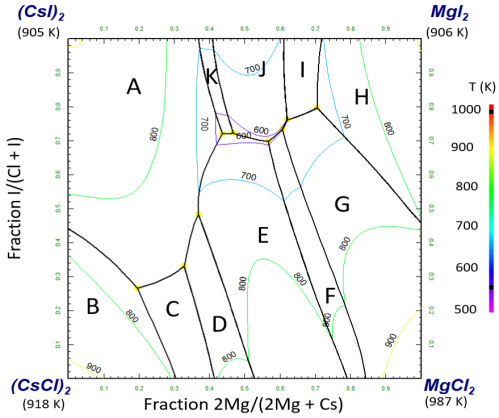


Figure 8.20: Liquidus surface of the CsCl−CsI−$MgCl_2$−$MgI_2$ quaternary system. Primary crystallization phases labelled A-K are: $CsI_{1-y}Cl_y$ (A), $\beta$-$CsCl_{1-x}I_x$ (B), $Cs_3MgCl_5$ (C), $Cs_2MgCl_4$ (D), $CsMgCl_3$ (E), $CsMg_3Cl_7$ (F), $MgCl_{2-2x}I_{2x}$ (G), $MgCl_{2y}I_{2-2y}$ (H), $CsMgI_3$ (I), $Cs_2MgI_4$ (J) and $Cs_3MgI_5$ (K). The calculated quaternary invariant equilibria are shown in Table 8.2.

| Fraction I/(Cl + I) | Fraction 2Mg/(2Mg + Cs) | T(K) | Invariant reaction |
|---|---|---|---|
| **$CsCl-CsI-MgCl_2-MgI_2$** | | | |
| 0.327 | 0.331 | 736 | $CsI_{1-y}Cl_y + Cs_3MgCl_5 + Cs_2MgCl_4 = L$ |
| 0.196 | 0.262 | 735 | $CsI_{1-y}Cl_y + \beta\text{-}CsCl_{1-x}I_x + Cs_3MgCl_5 = L$ |
| 0.368 | 0.483 | 708 | $CsI_{1-y}Cl_y + Cs_2MgCl_4 + CsMgCl_3 = L$ |
| 0.705 | 0.794 | 635 | $MgCl_{2-2x}I_{2x} + MgCl_{2y}I_{2-2y} + CsMgI_3 = L$ |
| 0.621 | 0.765 | 599 | $MgCl_{2-2x}I_{2x} + CsMgI_3 + Cs_2MgI_4 = L$ |
| 0.606 | 0.735 | 597 | $MgCl_{2-2x}I_{2x} + Cs_2MgI_4 + CsMg_3Cl_7 = L$ |
| 0.567 | 0.697 | 591 | $CsMgCl_3 + Cs_2MgI_4 + CsMg_3Cl_7 = L$ |
| 0.467 | 0.728 | 563 | $CsMgCl_3 + Cs_2MgI_4 + Cs_3MgI_5 = L$ |
| 0.436 | 0.729 | 557 | $CsI_{1-y}Cl_y + CsMgCl_3 + Cs_3MgI_5 = L$ |
| **$CsCl-CsI-NdCl_3-NdI_3$** | | | |
| 0.452 | 0.631 | 764 | $CsI_{1-y}Cl_y + Cs_2NdCl_7 + \beta\text{-}Cs_3NdI_6 = L$ |
| 0.062 | 0.352 | 763 | $CsI_{1-y}Cl_y + \beta\text{-}CsCl_{1-x}I_x + \beta\text{-}Cs_3NdCl_6 = L$ |
| 0.730 | 0.843 | 747 | $Cs_3Nd_2I_9 + \beta\text{-}Cs_3NdI_6 + \alpha\text{-}Cs_3NdI_6 = L$ |
| 0.597 | 0.374 | 747 | $\beta\text{-}Cs_3NdCl_6 + \beta\text{-}Cs_3NdI_6 + \alpha\text{-}Cs_3NdI_6 = L$ |
| 0.859 | 0.615 | 721 | $NdCl_{3-3x}I_{3x} + NdCl_{3y}I_{3-3y} + CsNd_4I_{13} = L$ |
| 0.772 | 0.456 | 709 | $Cs_2NdCl_7 + NdCl_{3-3x}I_{3x} + \alpha\text{-}Cs_3NdI_6 = L$ |
| 0.780 | 0.567 | 701 | $NdCl_{3-3x}I_{3x} + Cs_3Nd_2I_9 + \alpha\text{-}Cs_3NdI_6 = L$ |
| 0.823 | 0.633 | 700 | $NdCl_{3-3x}I_{3x} + CsNd_4I_{13} + Cs_3Nd_2I_9 = L$ |
| 0.672 | 0.220 | 690 | $\beta\text{-}Cs_3NdCl_6 + \alpha\text{-}Cs_3NdI_6 + Cs_2NdCl_7 = L$ |

Table 8.2: Calculated quaternary invariant equilibria in the $CsCl-CsI-MgCl_2-MgI_2$ and $CsCl-CsI-NdCl_3-NdI_3$ systems.

## 8.3. SYSTEMS CONTAINING Pu

### $CsX-PuX_3$(X=Cl,I)

The system $CsCl-PuCl_3$ has been modelled based on the experimental data presented by Benz et al. [4], who found two stable intermediate compounds, $Cs_3PuCl_6$ and $CsPu_2Cl_7$, in this system. The latter compound has been found to undergo a polymorphic transition at T = 683 K. No crystal structures have been reported for these intermediates, but analogous compounds $Cs_3RECl_6$ (RE = Nd, Sm-Yb, space group Pbcm) [39] and $CsRE_2Cl_7$ (RE = Pr, Sm-Lu, space group Pnma) [18, 38] have been identified in the literature. The polymorphic transition Benz et al. have observed in $Cs_3PuCl_6$ is also present in the $Cs_3RECl_6$ compounds [17]. The calculated phase diagram of this system is presented in Figure 8.21 alongside the experimental data from Benz et al. [4] that has been used for the optimization. The calculated mixing enthalpy is presented in Figure 8.4, compared to the estimated mixing enthalpy using Davis' method.

Experimental data have not been reported for the $CsI-PuI_3$ system, so the $CsI-NdI_3$ experimental data have been used as simulant for the $PuI_3$ system. The main difference is that the polymorphic transition of $Cs_3NdI_6$ has not been included for $Cs_3PuI_6$, as there is no experimental evidence to support it. The phase diagram of this system is reported in Figure 8.22. Additionally, no experimental mixing enthalpy data are available for this

system, so the method of Davis [20] was used to estimate the mixing enthalpy. The calculated mixing enthalpy is shown in Figure 8.8, and fits well with the experimental data.

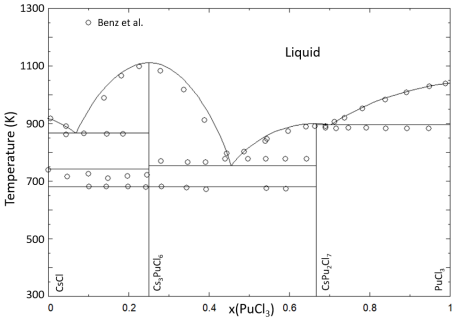


Figure 8.21: Phase diagram of the $CsCl-PuCl_3$ system, calculated with the thermodynamic model presented in this work and compared to the experimental data from Benz et al. [4].

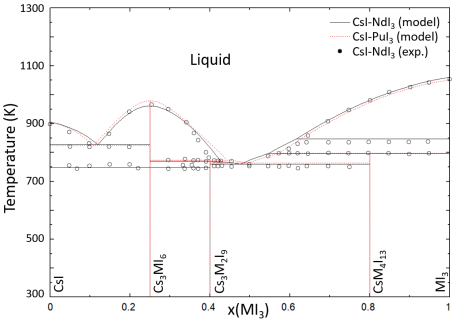


Figure 8.22: Phase diagram of the $CsI-PuI_3$ system (dotted red line) compared to the thermodynamic model (solid black line) and experimental data on the $CsI-NdI_3$ system reported by Kutscher et al. [27].

## (Cs,Pu)(Cl,I) SYSTEMS

The reciprocal pseudo-binary systems $CsCl-PuI_3$ and $CsI-PuCl_3$ have been optimized in this work based on the measured invariant equilibria in the corresponding Nd-systems. The calculated phase diagrams of the Pu-systems are presented here to shown the good agreement with the experimental data from the simulant systems.

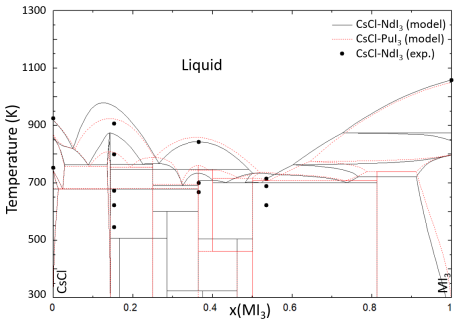


Figure 8.23: Phase diagram of the $CsCl-PuI_3$ system (dotted red line) compared to the thermodynamic model (solid black line) and experimental data from the $CsCl-NdI_3$ system (solid black circles) measured by DSC in this work.

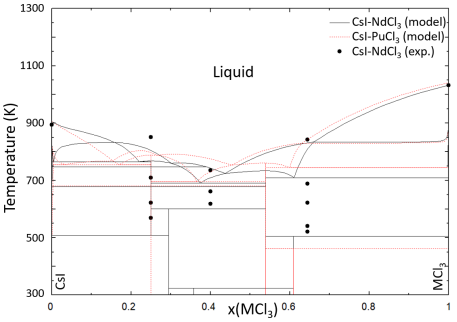


Figure 8.24: Phase diagram of the $CsI-PuCl_3$ system (dotted red line) compared to the thermodynamic model (solid black line) and experimental data from the $CsI-NdCl_3$ system (solid black circles) measured by DSC in this work.

In addition to the pseudo-binary systems shown above, the liquidus surface of the $CsCl-CsI-PuCl_3-PuI_3$ quaternary system has been calculated, as shown in Figure 8.25. The calculated invariant equilibria of this quaternary system are presented in Table 8.3.

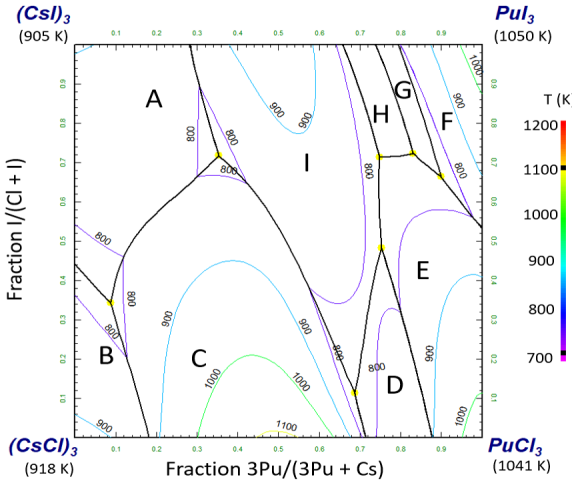


Figure 8.25: Liquidus surface of the CsCl−CsI−$PuCl_3$−$PuI_3$ quaternary system. Primary crystallization phases labelled A-I are: $CsI_{1-y}Cl_y$ (A), $\beta$-$CsCl_{1-x}I_x$ (B), $\beta$-$Cs_3PuCl_6$ (C), $CsPu_2Cl_7$ (D), $PuCl_{3-3x}I_{3x}$ (E), $PuCl_{3y}I_{3-3y}$ (F), $CsPu_4I_{13}$ (H), $Cs_3Pu_2I_9$ (I), and $Cs_3PuI_6$ (J). The calculated quaternary invariant equilibria are shown in Table 8.3.

| CsCl−CsI−$PuCl_3$−$PuI_3$ | | | |
|---|---|---|---|
| 0.352 | 0.712 | 770 | $CsI_{1-y}Cl_y + Cs_2NdCl_7 + \beta$-$Cs_3NdI_6$ = L |
| 0.087 | 0.342 | 759 | $CsI_{1-y}Cl_y + \beta$-$CsCl_{1-x}I_x + \beta$-$Cs_3PuCl_6$ = L |
| 0.753 | 0.483 | 759 | $CsPu_2Cl_7 + Cs_3PuI_6 + PuCl_{3-3x}I_{3x}$ = L |
| 0.899 | 0.664 | 740 | $PuCl_{3-3x}I_{3x} + PuCl_{3-3x}I_{3x} + CsPu_4I_{13}$ = L |
| 0.748 | 0.715 | 727 | $Cs_3PuI_6 + PuCl_{3-3x}I_{3x} + Cs_3Pu_2I_9$ = L |
| 0.831 | 0.725 | 714 | $PuCl_{3-3x}I_{3x} + CsPuI_{13} + Cs_3Pu_2I_9$ = L |
| 0.689 | 0.117 | 713 | $\beta$-$Cs_3PuCl_6 + Cs_3PuI_6 + Cs_2PuCl_7$ = L |

Table 8.3: Calculated quaternary invariant equilibria in the CsCl−CsI−$PuCl_3$−$PuI_3$ system.

## 8.4. SUMMARY

A thermodynamic model of the octonary molten salt system (Na,Mg,Pu,Cs)(Cl,I) has been presented in this chapter. The binary subsystems of this higher-order system, as well as the pseudo-binary mixed-anion mixed-cation systems, have been optimized based on data from the literature, or experimental data obtained in this work.

First, the salt systems between CsCl and the base fuel NaCl−$MgCl_2$−$NdCl_3$ have been investigated. The system NaCl−CsCl is a simple binary eutectic system with no solid solubility. The binary system CsCl−$MgCl_2$ has been re-optimized based on the experimental data from Markov et al. [7]. This system is characterised by four intermediates: $CsMgCl_3$, $Cs_2MgCl_4$, $Cs_3MgCl_5$ and $CsMg_2Cl_7$. Contrary to previous assessments, the work of Markov et al. is taken as an optimization basis, as this is the only source of experimental data available to us. Finally, the CsCl−$NdCl_3$ system is characterised by

three intermediates: $Cs_3NdCl_6$, $Cs_2NdCl_5$ and $CsNd_2Cl_7$. The existence of the latter two intermediates is assumed based on the available DTA data, and crystallographic data on analogous compounds.

Secondly, the systems between CsI and the system $NaI-MgI_2-NdI_3$ have been investigated. The system NaI-CsI is a simple binary eutectic system and has been modelled as such. The system $CsI-MgI_2$ is characterised by three intermediates: $CsMgI_3$, $Cs_2MgI_4$ and $Cs_3MgI_5$. The thermodynamic model in this work has been optimized based on the experimental data from Seifert et al. [10] in addition to our own DSC data. The system $CsI-NdI_3$ has been optimized based on the experimental data by Kutscher et al. [27], and is characterised by three intermediates: $Cs_3NdI_6$, $Cs_3Nd_2I_9$ and $CsNd_4I_{13}$. The existence of these intermediates is based on the available DTA data, as well as crystallographic data for analogous compounds in the case of $Cs_3NdI_6$ and $Cs_3Nd_2I_9$.

Furthermore, the reciprocal systems $NaI-NaCl-CsI-CsCl$, $CsCl-CsI-MgCl_2-MgI_2$ and $CsCl-CsI-NdCl_3-NdI_3$ have been modelled based on the pseudo-binary reciprocal diagonals. In the system $NaCl-NaI-CsCl-CsI$, no higher order parameters had to be added to accurately model the liquidus behaviour reported by Ilyasov et al. [21]. A good agreement between the thermodynamic model and the pseudo-binary systems $NaCl-CsI$ and $CsCl-NaI$ has been obtained based on the binary interaction parameters alone. Additionally, the calculated quaternary eutectic equilibria are in good agreement with the measurements of Ilysasov et al. The assessment of the reciprocal system $CsCl-CsI-MgCl_2-MgI_2$ has been performed by fitting the model to the experimental data from Dixon et al. [36] for the $CsI-MgCl_2$ system, and the data obtained in this work for the $CsCl-MgI_2$ system. The thermodynamic model has been optimized to fit the experimental data, through which a good agreement between the two has been achieved. Finally, the investigation of the $CsCl-CsI-NdCl_3-NdI_3$ system has been performed in this work through the experimental investigation of the systems $CsI-NdCl_3$ and $CsCl-NdI_3$. These experimental data have been used to optimize the thermodynamic model, and the obtained agreement between the two is good.

Finally, the obtained experimental data from the literature, and those obtained in this work, for the Nd-systems, have been used for the optimization of the Pu-systems. The exception to this is the thermodynamic model of the $CsCl-PuCl_3$ system, the optimization of which was based on the experimental data by Benz et al. [4]. The thermodynamic models of the Pu-systems reproduce very closely the experimental data from the Nd-systems.

With the addition of both iodine (chapter 8, this chapter) and cesium (this chapter) as fission products to the base fuel salt $NaCl-MgCl_2-PuCl_3$, the effect of CsI formation in a molten salt reactor can be investigated. To this end, the full octonary system $NaCl-NaI-MgCl_2-MgI_2-PuCl_3-PuI_3-CsCl-CsI$ has been modelled. With this full thermodynamic model, application calculations to investigate the potential volatility of Cs, I, or CsI can be realised. The results of these calculations are shown in Chapter 9.

# BIBLIOGRAPHY


(1) Beneš, O.; Capelli, E.; Morelová, N.; Colle, J.-Y.; Tosolin, A.; Wiss, T.; Cremer, B.; Konings, R. *Physical Chemistry Chemical Physics* **2021**, *23*, 9512–9523.

(2) Capelli, E.; Beneš, O.; Konings, R. *Journal of Nuclear Materials* **2018**, *501*, 238–252.

(3) Capelli, E.; Beneš, O.; Beilmann, M.; Konings, R. J. M. *The Journal of Chemical Thermodynamics* **2013**, *58*, 110–116.

(4) Benz, R.; Douglass, R. *The Journal of Physical Chemistry* **1961**, *65*, 1461–1463.

(5) Murgulescu, I.; Sternberg, S. *Discussions of the Faraday Society* **1961**, *32*, 107–114.

(6) Hersh, L. S.; Kleppa, O. *The Journal of Chemical Physics* **1965**, *42*, 1309–1322.

(7) Markov, B.; Panchenko, I. *Zhurnal Obscheii Khimii* **1955**, *25*, 2038–2043.

(8) Al-Aql, A.; Ali, E.; Dughaish, Z.; Al-Shibani, K.; Al-Juffali, A. *Arab gulf journal of scientific research* **1998**, *16*, 319–330.

(9) Gibbons, C. S.; Reinsborough, V. C.; Whitla, W. A. *Canadian Journal of Chemistry* **1975**, *53*, 114–118.

(10) Seifert, H.; Fink, H. *Revue de Chimie Minerale* **1975**, *12*, 466–475.

(11) Seifert, H.; Thiel, G. *Zeitschrift fur Allgemeine und Anorganische Chemie* **1977**, *436*, 237–243.

(12) Yin, H.; Song, J.; Liu, W.; Hu, B. *Calphad* **2022**, *79*, 102476.

(13) Chartrand, P.; Pelton, A. D. *Canadian Metallurgical Quarterly* **2001**, *40*, 13–32.

(14) Kleppa, O.; McCarty, F. *The Journal of Physical Chemistry* **1966**, *70*, 1249–1255.

(15) Seifert, H.; Fink, H.; Uebach, J. *Journal of Thermal Analysis and Calorimetry* **1988**, *33*, 625–632.

(16) Seifert, H. *Journal of Thermal Analysis and Calorimetry* **2002**, *67*, 789–826.

(17) Reuter, G.; Sebastian, J.; Roffe, M.; Seifert, H.-J. *Thermochimica Acta* **1997**, *296*, 47–52.

(18) Meyer, G.; Ax, P.; Cromm, A.; Linzmeier, H. *Journal of the Less Common Metals* **1984**, *98*, 323–337.

(19) Gaune-Escard, M.; Bogacz, A.; Rycerz, L.; Szczepaniak, W. *Thermochimica Acta* **1994**, *236*, 67–80.

(20) Davis, H. T.; Rice, S. A. *The Journal of Chemical Physics* **1964**, *41*, 14–24.

(21) Ilyasov, I. I.; Bergman, A. G. *Russian Journal of Inorganic Chemistry* **1964**, *9*, 768–771.

(22) Scuro, N.; Fitzpatrick, B.; Geiger, E.; Poschmann, M.; Dumaire, T.; Beneš, O.; Piro, M. *The Journal of Chemical Thermodynamics* **2024**, *193*, 107272.

(23) Seifert, H. et al. *Revue de Chimie Minerale* **1980**, 147–157.

(24) McPherson, G. L.; McPherson, A. M.; Atwood, J. L. *Journal of Physics and Chemistry of Solids* **1980**, *41*, 495–499.

(25) Østvold, T., *A thermodynamic study of some fused salt mixtures containing alkali and alkaline earth chlorides, bromides and iodides*; Institute of Physical Chemistry, University of Trondheim, NTH: 1971; Vol. 91.

(26) Hong, K.; Kleppa, O. *The Journal of Physical Chemistry* **1978**, *82*, 1596–1603.

(27) Kutscher, J.; Schneider, A. *Zeitschrift für anorganische und allgemeine Chemie* **1971**, *386*, 38–46.

(28) Van Hattem, A.; Alders, D. C.; Konings, R. J. M.; Smith, A. L. *The Journal of Physical Chemistry C* **2023**, *127*, 17482–17496.

(29) Wang, S. H.; Luo, S.; Eick, H. A.; Krämer, K.; Meyer, G. *Journal of the Less Common Metals* **1989**, *155*, 45–48.

(30) Guthrie, D.; Meyer, G.; Corbett, J. *Inorganic Chemistry* **1981**, *20*, 1192–1196.

(31) Meyer, G.; Corbett, J. D. *Inorganic Chemistry* **1981**, *20*, 2627–2631.

(32) Gaune-Escard, M.; Rycerz, L.; Hoch, M. *Journal of Molecular Liquids* **1999**, *83*, 83–94.

(33) Weyand, J. The Pm3m-Fm3m Transformation and Phase Equilibrium in Solid Solutions of Calcium-Chloride with Potassium-Chloride, Rubidium-Chloride and Cesium-Bromide. Ph.D. dissertation, University of Missouri - Rolla, 1971.

(34) Melnichak, M.; Kleppa, O. *The Journal of Chemical Physics* **1972**, *57*, 5231–5241.

(35) Ilyasov, I.; Bostandzhiyan, A. *Soviet Research in Fused Salts, 1956, in English Translation* **1958**, 768–771.

(36) Dixon, C. M.; Manissery, A. P.; Palma, J. P. S.; Booth, R. E.; Schorne-Pinto, J.; Aziziha, M.; Mofrad, A. M.; Wermers, J.; Wilson, J. A.; Besmann, T. M. *Journal of Chemical Thermodynamics* **2025**, *20*, 2627–2631.

(37) Balamurugan, N.; Arulchakkaravarthi, A.; Selvakumar, S.; Lenin, M.; Kumar, R.; Muralithar, S.; Sivaji, K.; Ramasamy, P. *Journal of Crystal Growth* **2006**, *286*, 294–299.

(38) Seifert, H.; Sandrock, J.; Uebach, J. *Zeitschrift für anorganische und allgemeine Chemie* **1987**, *555*, 143–153.

(39) Reuter, G.; Frenzen, G. *Journal of Solid State Chemistry* **1995**, *116*, 329–334.

# 9

# SAFETY ASSESSMENT FOR THE MSR: APPLICATION CALCULATIONS

*The global aim of this work is the safety analysis of fission products in molten salt reactors, achieved through the creation of an accurate thermodynamic model to describe molten salt systems in combination with various fission products. Using the extensive thermorynamic database developed in this dissertation, the effect of fission products on the thermochemical properties of a molten salt fuel can now be scrutinized. With the thermodynamic models presented in the main body of this work, as well as in several chapters of the appendix, the higher order systems* $NaCl-MgCl_2-PuCl_3-SrCl_2-BaCl_2-CeCl_3-NdCl_3-UCl_3-ThCl_4-SmCl_3-YCl_3$ *and* $NaCl-NaI-MgCl_2-MgI_2-PuCl_3-PuI_3-CsCl-CsI$ *have been described, allowing us to assess effect of soluble fission products (Sr, Ba, Ce, Nd, Sm, Y) and potentially volatile fission products (Cs, I), respectively. This final chapter is the culmination of this work, where the application and potential of these thermodynamic models in reactor safety analysis are presented. Two major concerns for safe operation of an MSR are addressed: (1) precipitation of highly radioactive fissile material (U, Pu) that would lead to hotspots of activity and temperature in the reactor, and (2) preferential vaporization of volatile fission products from the fuel that could spread outside the reactor core in case of an accident scenario.*

*The risk of fissile element precipitation in molten salt mixtures is investigated through calculations with the fission products Ba, Sr, Ce, Nd, Y and Sm in four different molten salt fuels that are candidate fuels in US and European MSR designs:* $NaCl-PuCl_3$, $NaCl-MgCl_2-PuCl_3$, $NaCl-ThCl_4-PuCl_3$ *and* $NaCl-UCl_3$. *For this purpose, the solid-liquid equilibria of these systems are investigated upon the individual introduction of* $5_{mol}$% *of fission products, and the primary crystallization phases are identified. This allows for the identification of potentially problematic fission products. Subsequently, a more realistic scenario is simulated where the fissile material (i.e. U or Pu) is replaced by a mixture of fission products, with the relative fractions based on data reported in the literature [1]. Additionally, the*

*risk of preferential volatilization from the melt is assessed in the fuel salt $NaCl-MgCl_2-PuCl_3$ upon addition of the fission products Cs and I based on vapor pressure calculations.*

Throughout this work, the aim has been to assess the effect of fission products on molten salt thermochemistry, through the use of thermodynamic models for multi-element systems describing {fuel salt mixture + fission products}, thus mimicking irradiated nuclear fuel. The predictive capability of the database developed in this work is first assessed in Section 9.1 by benchmarking predictions on transition temperatures for multi-element systems against experimental data collected by DSC. Theapplication calculations were performed to assess two main concerns for the safety of the MSR, namely the risk of fission material precipitation and volatilization of fission products, respectively.

The salt-soluble fission products Sr, Ba, Ce, Nd, Sm and Y have been investigated in this work for the (partial) precipitation risks or melt solidification risk they pose. Full solidification of the melt is fairly unlikely to be a direct effect of fission product accumulation, as the first occurrence of solidification is usually an equilibrium where the melt transitions to a {liquid + solid} mixture (*i.e.* a liquidus equilibrium). For safety reasons it must be guaranteed that the fissile elements remain distributed homogeneously in the molten salt, and precipitation of solid phases, particularly containing fissile materials, must be excluded when burn up increases or in case of a temperature drop. This scenario is investigated in Section 9.2 for four different fuel systems that have been selected for current MSR designs [2, 3]: NaCl−$PuCl_3$, NaCl−$UCl_3$, NaCl−$MgCl_2$−$PuCl_3$ and NaCl−$ThCl_4$−$PuCl_3$. The calculations performed hereafter are predicated on the assumption that there is a sufficient amount of chlorine in the molten salt after fission of plutonium, for all fission products to remain chlorides. This assumption is supported by the Ellingham diagrams [4] for molten chlorides. Furthermore, metallic fission product precipitates (Mo, Ru, Rh, Nb, etc.) are not considered here as they do not interact with the molten chlorides.

Another scenario for which the thermodynamic database developed here is relevant, is the assessment of the relative retention of volatile fission products in the melt. This is a main concern for the fission products Cs and I, which have been shown to interact with each other and evaporate out of the melt in fluoride-based systems [5–7]. For this reason, the risk of CsI volatilization in molten chlorides is investigated in Section 9.3 for the fuel system NaCl−$MgCl_2$−$PuCl_3$. Finally, Section 9.4 will conclude the results of this chapter, as well as this dissertation.



## 9.1. THERMODYNAMIC MODEL VALIDATION

The thermodynamic models presented in this work were optimized for several binary, ternary and quaternary sub-systems, culminating in a comprehensive database with 16 end-members. Before application calculations can be performed, the accuracy of the database for calculations with multiple elements must be demonstrated. To validate the reliability of the higher-order extrapolations, several parallel experiments and calculations were performed, and compared. Three fuel compositions of interest were considered and investigated as presented in Table 9.1, to which a mix of representative fission products was added, thereby simulating irradiated fuel. Those compositions were prepared in the laboratory, where $NdCl_3$ was used as a simulant for $PuCl_3$, and subsequently

subjected to DSC analysis to derive the phase transitions of those complex mixtures..

| Fuel system | Label | x(NaCl) | x($MgCl_2$) | x($NdCl_3$) | x($CeCl_3$) | x($BaCl_2$) | x($SrCl_2$) | x(CsCl) | x(CsI) |
|---|---|---|---|---|---|---|---|---|---|
| NaCl−$MgCl_2$−$PuCl_3$ (0.5616-0.3516-0.0808) | Sample-A | 0.571 | 0.352 | 0.043 | 0.012 | 0.0069 | 0.0047 | 0.0051 | 0.0047 |
| NaCl−$PuCl_3$ (0.9:0.1) | Sample-B | 0.887 | 0 | 0.099 | 0.0045 | 0.0026 | 0.002 | 0.0045 | 0.0014 |
| NaCl−$PuCl_3$ (0.668:0.332) | Sample-C | 0.640 | 0 | 0.317 | 0.013 | 0.008 | 0.006 | 0.013 | 0.004 |

Table 9.1: Compositions investigated for the verification of the reliability of the thermodynamic database.

The compositions listed in Table 9.1 mimic an irradiated fuel in which $5_{mol}$% of Pu is replaced by a mixture of fission products. The relative yields used for these fission products are given in Table 9.2, taken from the work of Taube et al. [1], who perfomed neutronics calculations using fast neutrons in a $PuCl_3$-based molten chloride fuel. Because this dissertation has the aim of investigating the effect of the fission products Ba, Sr, Ce, Nd, Y, Sm, Cs and I on molten salt fuels, the approximation was made that all $5_{mol}$% of Pu fissions into these elements. Additionally, because of the similarities in their chemistry and to simplify the experimental and modelling investigations slightly, La as fission product was added to the yield of Ce, and Pr as fission product was added to the yield of Nd. For the experimental compositions listed in table 9.1, the fission products Sm and Y were not included for the purpose of simplification. Furthermore, since the reported fission yield of Cs (*i.e.* 13.34) is higher than that of I (*i.e.* 6.2), the assumption was made for the speciation of Cs and I that all iodine forms CsI, while the excess Cs forms CsCl.

| **Fission product** | **Absolute yield** (atoms per 100 Pu fissioned) | **Relative yield** (%) |
|---|---|---|
| Ba | 9.5 | 12.3 |
| Sr | 5.5 | 7.1 |
| Ce[a] | 19.8 | 25.6 |
| Nd[b] | 16.2 | 20.9 |
| Sm | 3.74 | 4.9 |
| Y | 3.03 | 3.9 |
| Cs | 13.34 | 17.3 |
| I | 6.2 | 8.0 |

Table 9.2: Fission product yields used in the calculations in this chapter, taken from the work of Taube et al. [1] who performed neutronics calculations for molten $PuCl_3$-fuel in a fast neutron spectrum.
[a] Also includes the yield of La as fission product
[b] Also includes the yield of Pr as fission product

The transition temperatures measured by DSC upon heating the samples listed in Table 9.1 are presented in Table 9.3. The measured values are compared to the values calculated with the thermodynamic database at the same compositions. For each system in Table 9.3, the largest heat flow peak is highlighted in bold as well as the transition with the highest calculated change in energy. The results of these validatory experiments show that the thermodynamic model provides an excellent prediction of the measured transitions, with 18 out of 21 of the predicted transitions falling within ±20 K of the measured values. Most transitions that are modelled, but not observed experimentally, can

be attributed to peak overlap, *e.g.* the predicted peak at T = 653 K for Sample A overlapping with the peak at T = 660 K. Furthermore, it is possible that these undetected transitions are too low in energy to be measured, considering the sensitivity of the DSC. Overall, a good agreement between the predicted values and the experimentally measured values is observed, which confirms that the thermodynamic database gives accurate predictions even for higher order systems.

| **Sample-A** | | **Sample-B** | | **Sample-C** | |
|---|---|---|---|---|---|
| T(K, measured)[a] | T(K, model) | T(K, measured)[a] | T(K, model) | T(K, measured)[a] | T(K, model) |
| 736 | 700 | **1012** | **1021** | 765 | 762 |
| **694** | **686** | **705** | **713** | - | 758 |
| 674 | 674 | 697 | 706 | - | 720 |
| 659 | 660 | 688 | 677 | **708** | **707** |
| - | 653 | 621 | 633 | 690 | 689 |
| 624 | 623 | 601 | 606 | 680 | 665 |
| 613 | - | - | 591 | 622 | 605 |
| 564 | - | 560 | 553 | - | 596 |
| | | | | 587 | 581 |
| | | | | 555 | 556 |

Table 9.3: DSC measurements of the investigated compositions listed in Table 9.1. Highlighted in bold are the transitions with the highest heat flow peak area (measured transitions) and the highest associated energy (modelled transitions).
[a] The error on the measured temperature is ± 10 K.

## 9.2. PRECIPITATION AND MELTING BEHAVIOUR

For the assessment of precipitation risk, six fuel compositions in four fuel systems have been investigated. The fuel compositions have been selected based on those investigated in current European projects such as the MIMOSA project [3] ($NaCl-MgCl_2-PuCl_3$, $NaCl-ThCl_4-PuCl_3$) and fuel systems selected by other start-up companies (*e.g.* eutectic compositions in the systems $NaCl-PuCl_3$, $NaCl-UCl_3$, $NaCl-MgCl_2-PuCl_3$ and $NaCl-ThCl_4-PuCl_3$). For the latter categories, the exact fuel compositions are not known, and instead the calculations will be based on binary or ternary eutectic compositions. The compositions of each investigated fuel are presented in Table 9.4.



| **x(NaCl)** | **x($MgCl_2$)** | **x($PuCl_3$)** | **x($ThCl_4$)** | **x($UCl_3$)** | $T_{melt}$ (K) | Source |
|---|---|---|---|---|---|---|
| 0.615 | | 0.385 | | | 725 | Eutectic |
| 0.5676 | 0.3516 | 0.0808 | | | 703 | MIMOSA project [3] |
| 0.582 | 0.233 | 0.173 | | | 697 | Ternary eutectic |
| 0.5 | | 0.2 | 0.3 | | 624 | Saddle point |
| 0.468 | | 0.159 | 0.373 | | 610 | Ternary eutectic |
| 0.644 | | | | 0.356 | 790 | Eutectic |

Table 9.4: Investigated fuel compositions for solidification calculations.

To visualise the effect of fission products on the melting and solidification behaviour of the fuel salts, the change in melting temperature as a function of fission product con-

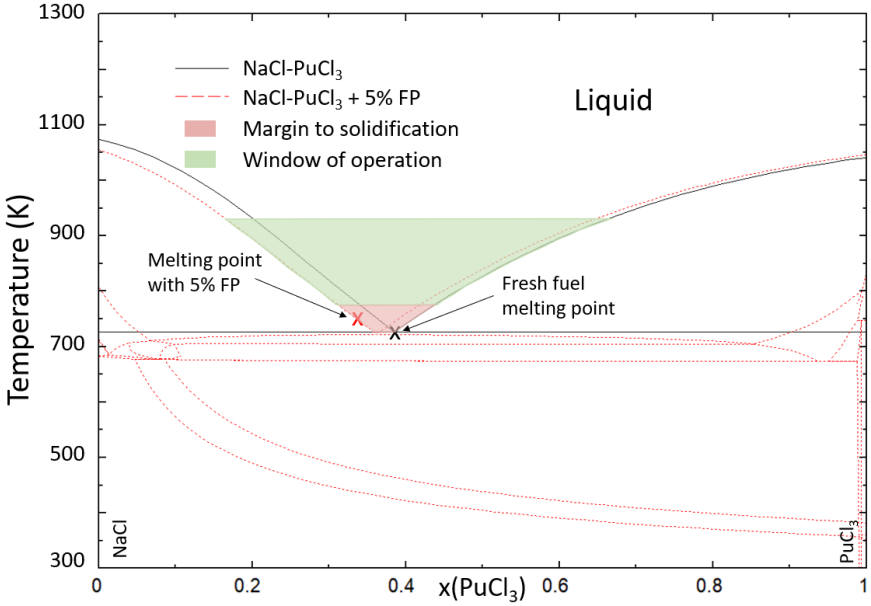


Figure 9.1: Phase diagram of the NaCl−$PuCl_3$ system (solid black line), compared to the same system mixed with $5_{mol}$% fission products Ba, Sr, Nd, Ce, Sm and Y using the ratios in Table 9.2 (dashed red line). Indicated on the phase diagram are the melting point of the fresh fuel (black x, {0.615 NaCl + 0.385 $PuCl_3$}) and the melting point of the fuel with $5_{mol}$% fission products (red x, {0.615 NaCl + 0.335 $PuCl_3$ + 0.008 $BaCl_2$ + 0.005 $SrCl_2$ + 0.017 $CeCl_3$ + 0.014 $NdCl_3$ + 0.003 $SmCl_3$ + 0.003 $YCl_3$}). Additionally, a possible operating window, and the margin to solidification, are indicated in green and red, respectively.

centration is investigated. A simple example of how a molten salt system changes upon the addition of fission products is given in Figure 9.1. This example serves to illustrate how the phase diagram of a molten salt system changes upon introduction of a mixture of fission products (Ba, Sr, Ce, Nd, Sm, Y, ratio presented in Table 9.2). Upon fission, the phase diagram of the fuel with fission products becomes highly complex, shown here by the appearance of many phase fields and the affected liquidus temperature. These phase fields are calculated to investigate whether, in case of precipitation, there is a risk of precipitation of the fissile element. Also shown on this phase diagram are two temperature ranges to consider: (1) up to 50 K above the melting point of the eutectic mixture (*i.e.* 775 K, red area in Figure 9.1), which represents the margin to solicification, and (2) an operating window up to 150 K the operating temperature for a design-based transient (*i.e.* 925 K, green area in Figure 9.1). In the example case, it is shown that the melting point upon introduction of fission products stays within the allowable temperature range.

The investigation of the solidification risk is first analysed for each investigated fission product individually. The concentrations used are exaggerated compared to a real scenario for the purpose of visualization of the individual effects. To do this, the change in melting temperature is calculated when the fissile element, in all calculations taken as Pu, is replaced by an equal amount of fission product. For the individual effect of the fission products on the melting behaviour of the fuel, calculations up to $5_{mol}$% of each

fission product are performed. The effects of fission products on the melting behaviour of the $NaCl-MgCl_2-PuCl_3$ fuel compositions are presented in Figures 9.2 and 9.3.

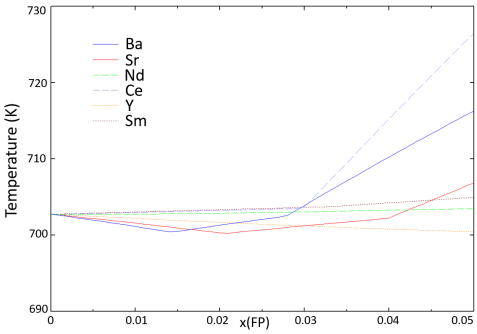


Figure 9.2: Calculated change in melting temperature of the {0.5676 NaCl + 0.3516 $MgCl_2$ + 0.0808 $PuCl_3$} fuel mixture (*i.e.* a composition chosen in the MIMOSA project [3]) when replacing up to $5_{mol}$% of Pu by fission products Sr, Ba, Ce, Nd, Sm and Y.

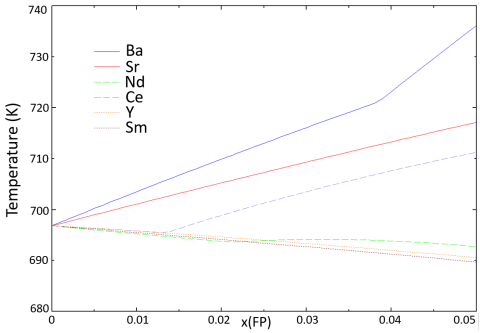


Figure 9.3: Calculated change in melting temperature of the {0.582 NaCl + 0.233 $MgCl_2$ + 0.173 $PuCl_3$} fuel mixture (*i.e.* a eutectic composition in the ternary system) when replacing up to $5_{mol}$% of Pu by fission products Sr, Ba, Ce, Nd, Sm and Y.

As shown in Figures 9.2 and 9.3, the fission products that cause the largest increase in melting temperature are Ba and Ce. For these fuel compositions, the maximum increase in melting temperature is between 20 and 30 K upon adding $5_{mol}$% of fission product. While a definite increase in melting temperature is visible for some fission products (Ba and Ce), the increase in the melting temperature of the fuel system is generally small enough that it lies within the safety margin of operation of a molten salt reactor. This safety margin depends on the exact conditions under which the reactor is operating, but a lower limit of 50 K is a reasonable assumption. An operating window of 150 K was chosen for the purpose of visualisation in Figure 9.1, but this is subject to change depending on the eventual needs during MSR operation. The primary crystallization phases, *i.e.* the first phases to precipitate, of the {0.582 NaCl + 0.233 $MgCl_2$ + 0.173 $PuCl_3$} fuel are intermediate compounds in the $NaCl-MgCl_2$ system up to $3.5_{mol}$% of fission product. This means that the precipitation of these compounds, while undesirable because of clogging risks, is no considerable threat to reactor operation. Between 3.5-$5_{mol}$%, the primary crystallization phases are the solid solutions $Na_{3x}M_{2-x}Cl_6$ (M = Ce, Nd), meaning there is no expected risk of local runaway reactions due to Pu precipitation. However, if follow-up studies show that the $Na_{3x}Pu_{2-x}Cl_6$ phase hypothesised in Chapter 3 exists, one could expect Pu precipitation in the $Na_{3x}M_{2-x}Cl_6$ phase. Therefore, we strongly recommend that this hypothesis be tested.

Figures 9.4 and 9.5 show the same calculation as described above, performed for the compositions in the $NaCl-ThCl_4-PuCl_3$ fuel system mentioned in Table 9.4. Contrary to the fuel compositions in the system $NaCl-MgCl_2-PuCl_3$, the addition of Ba does not affect the melting behaviour significantly. However, the effects of Ce and Nd are significantly greater than in the previously investigated fuel system. In particular, the addition of Ce and Nd cause an increase of the melting temperature of the fuel in Figure 9.4 of

approximately 50 K. This is a significant deviation from the margin of safe operation, and could pose a risk of precipitation. The primary crystallization phases for these fuel compositions are $Na_2ThCl_6$ and $Th_{1-x}Pu_xCl_{4-x}$. This means that when precipitation occurs in these systems, some of the fissile element Pu is removed from the molten salt and precipitates in the aforementioned phases. It must be noted, however, that the effects of Ce and Nd (and to a lesser extent Sm) as shown in Figure 9.4 and 9.5 are highly dependent on the ternary optimization of the system $NaCl-ThCl_4-RECl_3$ (RE = Ce, Nd, Sm). The ternary parameters included in these systems have been taken from the respective $PuCl_3$ system modelled by Dumaire et al. [8], but experimental investigation of these ternary systems is necessary to obtain a better model for the safety assessment of $NaCl-ThCl_4-PuCl_3$ fuels.

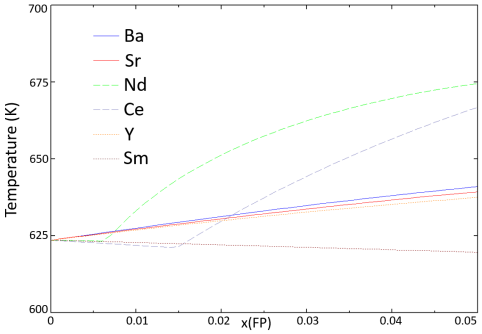


Figure 9.4: Calculated change in melting temperature of the {0.5 NaCl + 0.3 $ThCl_4$ + 0.2 $PuCl_3$} fuel mixture (*i.e.* a saddle point in the ternary system) when replacing up to $5_{mol}$% of Pu by fission products Sr, Ba, Ce, Nd, Sm and Y.

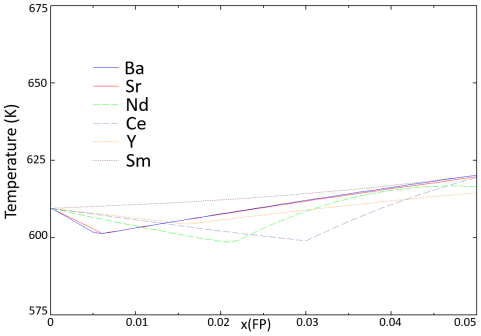


Figure 9.5: Calculated change in melting temperature of the {0.468 NaCl + 0.373 $ThCl_4$ + 0.159 $PuCl_3$} fuel mixture (*i.e.* a eutectic composition in the ternary system) when replacing up to $5_{mol}$% of Pu by fission products Sr, Ba, Ce, Nd, Sm and Y.



The effects of the individual fission products on the molten salt fuel $NaCl-UCl_3$ are shown in Figure 9.6. In this case, the addition of rare earth elements Ce, Nd, Sm and Y have little effect on the melting properties of this fuel system. The addition of Ba and Sr, however, does lead to an increase in fuel melting temperature of up to 50 K, which is significant compared to a possible margin to solidification of 50 K. However, during actual operation, there will not be a scenario where all fission products are either Ba or Sr, and these elements will always appear in a mixture with other FPs. Furthermore, the primary crystallization phase of this system upon addition of fission products is NaCl. Other than potential clogging, this presents no risk for maintaining reactor operation. The same is true for the $NaCl-PuCl_3$ fuel mixture (Figure 9.7), where the primary crystallization phase is also NaCl, and the increase in melting temperature of the fuel is approximately 60 K.

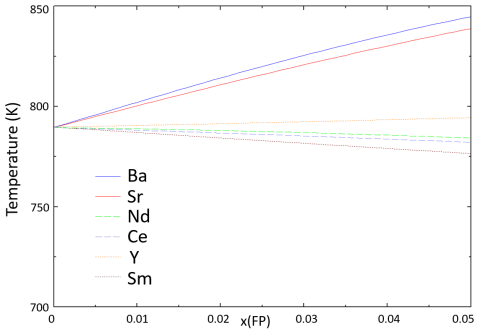


Figure 9.6: Calculated change in melting temperature of the {0.65 NaCl + 0.35 $UCl_3$} fuel mixture when replacing up to $5_{mol}$% of Pu by fission products Sr, Ba, Ce, Nd, Sm and Y.

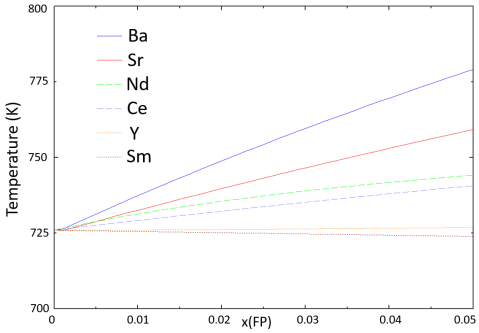


Figure 9.7: Calculated change in melting temperature of the {0.643 NaCl + 0.357 $PuCl_3$} fuel mixture when replacing up to $5_{mol}$% of Pu by fission products Sr, Ba, Ce, Nd, Sm and Y.

Thus far, the effects of individual fission products on the melting behaviour of the fuel have been presented. However, during actual reactor operation, there will always be a mixture of fission products interacting with the fuel. To investigate this, a mixture of fission products based on the fission yields of Pu, shown in Table 9.2 is considered. In these calculated ratios, the yields of La and Pr have been included in the yields of Ce and Nd respectively. This effectively means that up to $5_{mol}$% of $PuCl_3$ is replaced in the calculations by the mixture {$0.8_{mol}$% $BaCl_2$ + $0.5_{mol}$% $SrCl_2$ + $1.7_{mol}$% $CeCl_3$ + $1.4_{mol}$%$NdCl_3$ + $0.3_{mol}$%$SmCl_3$ + $0.3_{mol}$%$YCl_3$}. This assessment is performed for all fuel compositions listed in Table 9.4. Additionally, these calculations are based on a scenario where there is no fission product removal in the reactor.

As seen in Figure 9.8, the effects of adding a mixture of fission products to the molten salts are significantly lower than when the fission products were considered individually (Figures 9.2-9.6). The reason for this lies in the fact that the fission products that overall present the biggest effects on melting behaviour, Ba, Ce and Nd, are less abundant in these scenarios.

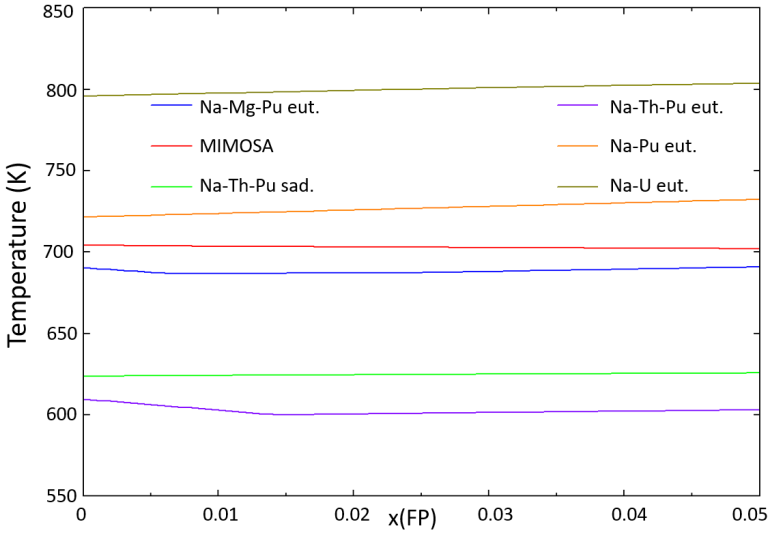


Figure 9.8: Calculated change in melting temperature of the fuel systems in Table 9.4 upon replacing up to $5_{mol}$% of Pu by fission products Sr, Ba, Ce, Nd, Sm and Y, with the ratio between these determined in Table 9.2.

As shown in Figure 9.8, the effect of fission products on the melting properties of molten salt fuels NaCl−$MgCl_2$−$PuCl_3$, NaCl−$UCl_3$ and NaCl−$PuCl_3$ is minor. In the NaCl−$MgCl_2$−$PuCl_3$ fuel systems, there is a decrease in melting temperature of approximately 5 K when adding fission products. For the NaCl−$UCl_3$ and NaCl−$PuCl_3$ fuel systems, the melting temperature increase is approximately 5-10 K. The effect of fission products on the melting behaviour of the NaCl−$ThCl_4$−$PuCl_3$ systems is largely negligible, with the investigated eutectic composition even showing a decrease of the melting point of 5-10 K. However, as mentioned previously, this is highly contingent upon the optimization of the ternary systems NaCl−$ThCl_4$−$RECl_3$ (RE = Ce, Nd, Sm), which has to be verified experimentally. Additionally, like in the assessments in Figure 9.4 and 9.5, the primary crystallization phases are $Na_2ThCl_6$ and $RE_xPu_{1-x}Cl_3$ (RE = Ce, Nd) solid solutions. The fact that the predicted primary crystallization phase in the NaCl−$ThCl_4$−$PuCl_3$ fuel could contain Pu should be investigated experimentally.

## 9.3. FISSION PRODUCT RETENTION

The potential risk of fission product volatilization from NaCl−$MgCl_2$−$PuCl_3$ fuels has been assessed in this work. The primary concern here is the low retention of fission products that are known to be volatile in solid oxide fuels and molten fluoride fuels such as Cs and I in the molten salt. Vapor pressure calculations in the system (Na,Mg,Pu,Cs)(Cl,I) have been performed over a range of temperatures to investigate if any species are likely to vaporise. The calculations of the partial pressures in the temperature range 500-2000 K for the fuel mixture {0.5676 NaCl + 0.3516 $MgCl_2$ + 0.0308 $PuCl_3$ + 0.034 Cs + 0.016 I}, *i.e.* the base fuel mixture with $5_{mol}$% {Cs + I}, is presented in Figure 9.9. The ratio between produced Cs and I is calculated from Table 9.2. For these calculations, the assumption is that all plutonium fissions to Cs and I. While this is not entirely accurate, it serves to show the behaviour of the fuel in an excess of CsI. A selection of activity calculations is shown in Figure 9.10 based on the species with the highest calculated activity in Figure 9.9.

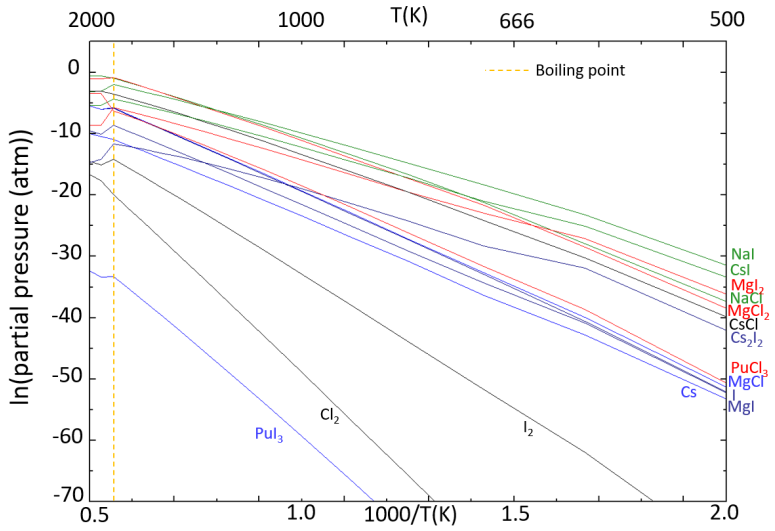


Figure 9.9: Calculated activities of the species in the (Na,Mg,Pu,Cs)(Cl,I) octonary system using the thermodynamic database presented in this work. The boiling point of the salt mixture is around 1800 K, which explains the change in slope at this temperature.

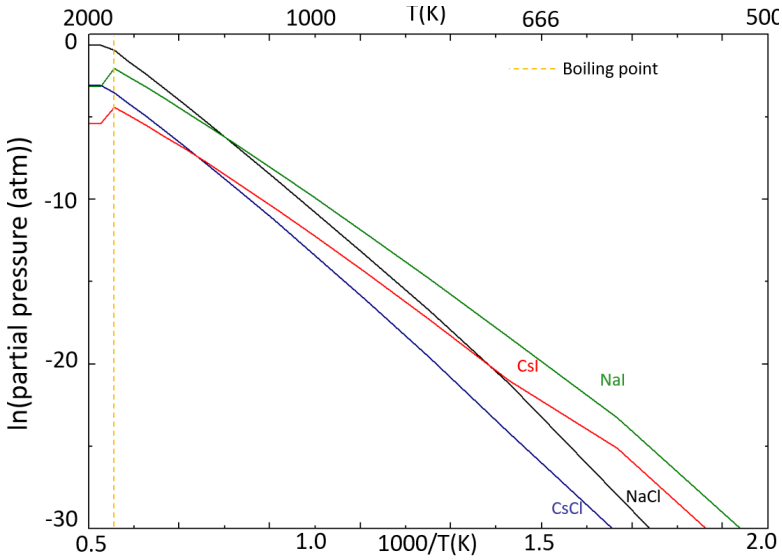


Figure 9.10: Calculated activities of the species NaCl, NaI, CsCl and CsI in the (Na,Mg,Pu,Cs)(Cl,I) octonary system using the thermodynamic database presented in this work. The boiling point of the salt mixture is around 1800 K, which explains the change in slope at this temperature.

Shown in Figure 9.10 is that the activity of CsI (g) in the molten salt is higher than that of NaCl (g) and CsCl (g), but lower than that of NaI (g). This means that the phase most likely to form a gaseous species in the molten fuel is NaI, rather than the expected CsI. Furthermore, the vapor pressure of NaI and CsI calculated in the molten salt fuel is compared to the vapor pressure of the pure species in Figures 9.11 and 9.12, respectively. These figures show that there is a consistent difference between the volatility of NaI and CsI in a molten salt mixture compared to the pure compounds, opposite to what Beneš et al. [5] found in the molten fluoride system LiF−$ThF_4$. Given the fact that the vapor pressures of NaI and CsI in molten salt mixtures is several orders of magnitude lower than those of the pure compounds in the operating temperature range (*i.e.* 775-925 K), it is unlikely that either species will evaporate in significant amounts out of the melt. Seeing as these two iodides are the most volatile species in the molten salt, shown in Figure 9.9, it is unlikely that under the conditions used for these application calculations volatility will pose any significant risk to reactor operation.

The calculations of the vapor pressure as shown in this section were additionally performed for the fuel compositions {0.582 NaCl + 0.233 $MgCl_2$ + 0.173 $PuCl_3$} and {0.643 NaCl + 0.357 $PuCl_3$}. The same results were obtained as for the calculations on the {0.5676 NaCl + 0.3516 $MgCl_2$ + 0.0808 $PuCl_3$} fuel composition, hence they are not shown here.

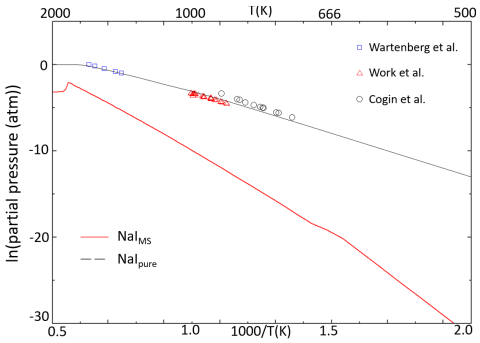


Figure 9.11: Comparison between NaI vapor pressure calculated in the molten salt fuel ($NaI_{MS}$, red line), calculated as a pure compound ($NaI_{pure}$, black line), and experimental data presented by Work et al. [9] (open red triangles), Wartenberg et al. [10] (open blue squares) and Cogin et al. [11] (open black circles).

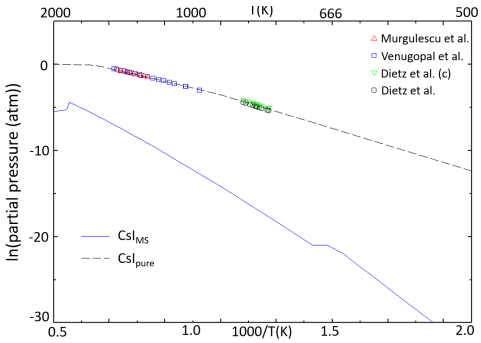


Figure 9.12: Comparison between CsI vapor pressure calculated in the molten salt fuel ($CsI_{MS}$, blue line), calculated as a pure compound ($CsI_{pure}$, black dashed line), and experimental data presented by Murgulescu et al. [12] (open red triangles), Venugopal et al. [13] (open blue squares), Deitz et al. [14] (open black circles), as well as the values of Deitz et al. corrected by Roki et al. [15] (open green triangles).

## 9.4. SUMMARY AND CONCLUDING REMARKS

This final chapter presents examples of the application of the comprehensive thermodynamic database created in this work. For the sake of consistency and comparability, calculations have been performed on different fuel systems using the same conditions: up to $5_{mol}$% of Pu is fissioned to produce fission products. Based on the different effects the fission products are predicted to have on the melt, they are classified as potentially causing a precipitation risk due to a change in melting point (Ba, Sr, Ce, Nd, Sm, Y) or a volatilization risk due to a lack of fission product retention (Cs, I).

The precipitation risks in the molten salt fuel $NaCl-MgCl_2-PuCl_3$ were investigated for two fuel compositions. In both cases, the major fission products contributing to an increased melting point were Ba and Ce. The calculations performed using fission yields reported in the literature showed that there is no appreciable increase in melting temperature as a consequence of fission product accumulation for either of the investigated salt compositions. The primary crystallization phases found with the calculations in these systems are intermediate compounds in the $NaCl-MgCl_2$ system, indicating no immediate risk of fissile element precipitation. However, if the solid solution $Na_{3x}Pu_{2-x}Cl_6$, as hypothesised in Chapter 3, is shown to exist in the $NaCl-PuCl_3$ system, this might lead to a different conclusion.

Another fuel that was investigated is the $NaCl-ThCl_4-PuCl_3$ fuel salt, and in this system two compositions were selected as potential fuel candidates for investigative purposes. For both fuel compositions, it was clear that the largest influence of fission products on the melting behaviour stems from Nd and Ce. When adding a mixture of fission products, no significant deviation from the melting point of the selected compositions was observed. It must be noted that especially the ternary behaviour in the

$NaCl-ThCl_4-RECl_3$ systems (RE = Ce, Nd, Sm) must be investigated experimentally to confirm the ternary phase equilibria, as this could have a significant effect on the precipitation behaviour of the fuel. Furthermore, the precipitating phases were found to be $RE_xPu_{1-x}Cl_3$ solid solutions, meaning that part of the fissile material would precipitate out of the melt. These findings could both prove relevant risks for reactor operation of a $NaCl-ThCl_4-PuCl_3$-based molten salt reactor, and should also be investigated experimentally. Additionally, the fuel compositions can be optimised with the thermodynamic database to minimize the risk of precipitation.

The final fuel mixtures that were studied for the purpose of precipitation risk assessment are the $NaCl-UCl_3$ and $NaCl-PuCl_3$ fuel systems. The calculations performed in this chapter showed that the fission products that have the largest contribution to the increase in melting point of these fuel are Sr and Ba. Contrary to the other fuel systems, the rare earth elements (Ce, Nd, Sm, Y) have little effect on the melting point of these molten salt fuels. When performing the calculations with the fission yields reported in the literature, no significant increase in melting temperature of the fuels was found. Furthermore, the primary crystallization phase in these systems was found to be NaCl, meaning that there is no predicted risk of fissile element precipitation.

Finally, for the system $NaCl-MgCl_2-PuCl_3$, volatilization calculations were performed to assess the potential risk of CsI vaporization from the molten salt. To this end, the vapor pressures were assessed through activity calculations of the molten salt fuels upon introduction of $5_{mol}$% of {Cs + I}. Contrary to the behaviour of CsI in fluoride-based molten salts, these fission products are stable in the liquid phase in molten chlorides. Only at temperatures above 1800 K, when the base fuel salt starts to itself evaporate, is CsI expected to go to the gaseous phase. These calculations indicate that there is no significant risk of CsI volatilization from the molten chlorides.

In summary, the calculations performed herein show that there is no appreciable effect of fission product accumulation on the thermodynamic properties of the molten salt fuel $NaCl-MgCl_2-PuCl_3$ during normal operating conditions. Furthermore, the $NaCl-ThCl_4-PuCl_3$, $NaCl-UCl_3$ and $NaCl-PuCl_3$ fuels show no significant risk of precipitation. Moreover, in the $NaCl-ThCl_4-PuCl_3$ system, additional experimental investigations are necessary to verify a) the behaviour of rare earth chlorides in the $NaCl-ThCl_4-RECl_3$ system and b) the primary crystallization phases upon fission product addition, identified here as $Na_2ThCl_6$ and $RE_xPu_{1-x}Cl_3$ (RE = Ce, Nd). Finally, in the systems $NaCl-PuCl_3$ and $NaCl-UCl_3$ no significant risk of precipitation has been identified based on the performed calculations. However, if the actinide phases $Na_{3x}An_{2-x}Cl_6$ (An = U, Pu) exist like they do in the lanthanide systems (*i.e.* $Na_{3x}Ln_{2-x}Cl_6$ (Ln = Ce, Nd), different results would be obtained as this introduces a new precipitation risk for U and Pu through the formation of a mutual solid solution. For this reason, it is important that the existence of these phases is investigated thoroughly.

# BIBLIOGRAPHY


(1) Taube, M. *Fast reactors using molten chloride salts as fuel*; tech. rep.; INFCE (Switzerland), 1978.

(2) Latkowski, J. In *Proceedings of the Merits and Viability of Different Nuclear Fuel Cycles and Technology Options and the Waste Aspects of Advanced Nuclear Reactors, Virtual Meeting*, 2021, pp 28–29.

(3) Smith, A.; Capelli, E.; Laureau, A.; Merle, E.; Ocadiz-Flores, J.; Beneš, O. *Technical note regarding the selection of salt composition in WP2 (Milestone MS2))*; tech. rep.; MIMOSA project, 2022.

(4) Besmann, T. M.; Schorne-Pinto, J.; Aziziha, M.; Mofrad, A. M.; Booth, R. E.; Yingling, J. A.; Paz Soldan Palma, J.; Dixon, C. M.; Wilson, J. A.; Hartanto, D. *Materials* **2024**, *17*, 495.

(5) Beneš, O.; Capelli, E.; Morelová, N.; Colle, J.-Y.; Tosolin, A.; Wiss, T.; Cremer, B.; Konings, R. *Physical Chemistry Chemical Physics* **2021**, *23*, 9512–9523.

(6) Capelli, E.; Beneš, O.; Konings, R. *Journal of Nuclear Materials* **2018**, *501*, 238–252.

(7) Dumaire, T. Advances in the chemistry of Molten Salt fuels with emphasis on Fission Products and Corrosion Products, Ph.D. Thesis, Delft University of Technology, 2024.

(8) Dumaire, T.; Ocádiz-Flores, J. A.; Konings, R. J. M.; Smith, A. L. *Calphad* **2022**, *79*, 102496.

(9) Work, D. E. *The Journal of Chemical Thermodynamics* **1981**, *13*, 491–501.

(10) Wartenberg, H.; Albrecht, P. *Zeitschrift für Elektrochemie* **1921**, *27*, 162–167.

(11) Cogin, G. E.; Kimball, G. E. *Journal of Chemical Physics* **1948**, *16*, 1035–1048.

(12) Murgulescu, I.; Sternberg, S. *Discussions of the Faraday Society* **1961**, *32*, 107–114.

(13) Venugopal, V.; Prasad, R.; Sood, D. *Journal of Nuclear Materials* **1985**, *130*, 115–121.

(14) Deitz, V. *The Journal of Chemical Physics* **1936**, *4*, 575–580.

(15) Roki, F.-Z.; Ohnet, M.-N.; Fillet, S.; Chatillon, C.; Nuta, I. *The Journal of Chemical Thermodynamics* **2014**, *70*, 46–72.

# SUMMARY & CONCLUSIONS

The advent of molten salts in the nuclear industry has technically been over half a century ago, *i.e.* in the 1950's at Oak Ridge National Laboratory with the Aircraft Reactor Experiment (ARE) and Molten Salt Reactor Experiment (MSRE), but that avenue of research was discontinued in favour of liquid metal cooled reactors. Recent developments in the nuclear energy industry, however, have caused enough renewed interest for a renaissance. Nuclear energy systems based on molten salt fuels exhibit innovative safety advantages related to the attractive thermochemical properties the molten salts exhibit (low melting point, heat transport properties, low vapor pressures, etc.). The Molten Salt (Fast) Reactor has a bright and promising future in the nuclear energy landscape, and the aim of this work is to address some of the remaining questions regarding the safety of MSRs during operation. Where the initial experiments with the Molten Salt Reactor (ARE, MSRE) used fluoride-based fuels, another type of fuel systems, chloride-based fuels, has gained much traction lately because of the different properties chloride salts offer compared to fluorides (*e.g.* higher actinide solubility, compatibility with current reprocessing technologies). A big question mark in the safety analysis of chloride-based Molten Salt Reactors is the behaviour and management of fission products in irradiated molten salt fuel, which is covered in the main body of this work.

Molten fuel salt systems are usually comprised of two or more end-members, *e.g.* NaCl, $MgCl_2$, and $PuCl_3$, and contain at least a fissile element (*e.g.* $PuCl_3$, $UCl_3$), as well as one or more salts that improve thermochemical properties such as melting behaviour or vapor pressure of the molten fuel salt (NaCl, $MgCl_2$). A comprehensive and thorough thermochemical understanding of fuel salts like this already necessitates a solid understanding of at least four systems (*i.e.* the binary systems NaCl−$MgCl_2$, NaCl−$PuCl_3$ and $MgCl_2$−$PuCl_3$, as well as the ternary system NaCl−$MgCl_2$−$PuCl_3$). The introduction of fission products in - already complicated - molten salt fuel systems brings about an even higher complexity by creating higher-order systems. To illustrate: if a molten salt fuel is comprised of three end-members, adding one fission product already requires thermodynamic modelling of an additional three binary, and three ternary systems. The fission products (FPs) that are formed during the nuclear chain reaction can be classified as salt-soluble FPs (*e.g.* Ba, Ce, Nd), (potentially) volatile FPs (*e.g.* Cs, I, Xe) and metallic precipitates (*e.g.* Pt, Rh, Ru). This work focuses on the interactions between salt-soluble FPs (Ba, Sr, Ce, Nd, Sm, Y), as well as volatile FPs (Cs, I), and molten salt fuels (*e.g.* NaCl−$MgCl_2$−$PuCl_3$, NaCl−$ThCl_4$−$PuCl_3$, NaCl−$UCl_3$) for the precipitation risks and risks of preferential vaporization they carry, respectively. These interactions are investigated with experimental techniques such as Differential Scanning Calorimetry (DSC), X-Ray Diffraction (XRD) and Neutron Diffraction (ND).

Describing irradiated fuel systems with thermodynamic models allows us to predict

their behaviour in a molten salt reactor during normal operation as well as accidental conditions. This thermodynamic description relies on the Gibbs free energy, a thermodynamic potential that indicates the stability of one phase over another at any given temperature and composition. The most stable combination of phases in any given system is the one with the lowest total Gibbs free energy. In this work, thermodynamic models of molten salt systems, made with the CALPHAD (CALculation of PHase Diagrams) method, allow us to reproduce the available experimental data (*e.g.* invariant equilibria, mixing enthalpies). Additionally, these models allow us to perform predictive calculations on multi-element systems in regions of temperature and composition which have not been measured experimentally. In the CALPHAD models constructed in this work, we use the Quasi-Chemical formalism in the Quadruplet Approximation, allowing for the modelling of the local structure in the molten salt. We fit these models to experimental data available in the literature (*e.g.* phase diagram and mixing enthalpy data) or measured data on invariant equilibria (using Differential Scanning Calorimetry, DSC) and crystal structures (using X-Ray Diffraction, XRD, or Neutron Diffraction, ND), to obtain the most accurate thermodynamic descriptions possible.

Much of this work pertains to the thermodynamic modelling of $PuCl_3$-based systems, and since $PuCl_3$ was not available for experiments, and its use should be as limited as possible due to the hazardous nature of the material, an alternate approach is necessary. The chosen approach involves the use of simulants: elements whose thermochemical behaviour closely resembles that of $PuCl_3$, without the safety hazard. In Chapter 3 of this work, a very reliable simulant for the melting behaviour of $PuCl_3$ is found in $NdCl_3$. Moreover, a good simulant for $UCl_3$, which shares a lot of the concerns of working with $PuCl_3$ but to a lesser degree, is found in $CeCl_3$. Additionally, the thermodynamic model of the base fuel $NaCl-MgCl_2-PuCl_3$ is presented based on experimental data from the literature, as well as a thorough crystallographic investigation of the simulant systems $NaCl-NdCl_3$ and $NaCl-CeCl_3$. The latter revealed a homogeneity range $Na_{3x}RE_{2-x}Cl_6$ (RE = Ce, Nd) that was incorporated in the thermodynamic model. This thermodynamic description of the base fuel, as well as the choice of $NdCl_3$ as an accurate simulant for $PuCl_3$, provide a good basis to start investigating the effect of fission products on the thermochemical behaviour of molten fuel salts.



The first fission products that are considered in this work are barium and strontium. The choice of the former as prime candidate for an investigation is evident: of all the fission product chlorides, $BaCl_2$ has the highest melting point, as well as a high fission yield. Strontium chloride is also relatively high-melting and abundant, and is an obvious choice considering the similarities between Ba and Sr, as both are alkaline-earth metals. An investigation of the simulant systems $BaCl_2-RECl_3$ and $SrCl_2-RECl_3$ (RE = Ce, Nd) is presented in Chapter 4, showing the gaps in knowledge in the literature by introducing previously unknown solid solutions ($Ba_{1-x}RE_xCl_{2+x}$ (cub) and $Ba_yRE_{1-y}Cl_{3-y}$ (hex) (RE = Ce, Nd), respectively), as well as identifying the previously unknown intermediate compound $Ba_3RE_2Cl_{12}$ (RE = Ce, Nd). In the $SrCl_2-RECl_3$ (RE = Ce, Nd) systems, solid solutions were also found ($Sr_{1-x}RE_xCl_{2+x}$ (cub) and $Sr_yRE_{1-y}Cl_{3-y}$ (hex) (RE = Ce, Nd), respectively), and the intermediate compounds $Sr_9RE_5Cl_{33}$ (RE = Ce, Nd) were identified.

In Chapter 5, the results obtained in the simulant system $BaCl_2$–$CeCl_3$ were used to define targeted experiments for the $BaCl_2$–$UCl_3$ system that could prove the similar chemistry between the two, and support the similar interpretation of the $BaCl_2$–$UCl_3$ and $BaCl_2$–$CeCl_3$ systems. These experiments indeed confirmed that the high-temperature solid solution $Ba_{1-x}U_xCl_{2+x}$ (cub) and the intermediate compound $Ba_3U_2Cl_{12}$ exist, allowing us to re-assess the thermochemistry of the $BaCl_2$–$UCl_3$ system and cementing the simulant approach as a valid strategy. Finally, to allow the assessment of fission products Ba and Sr in $ThCl_4$-based fuels as well, thermodynamic models of the $SrCl_2$–$ThCl_4$ and $BaCl_2$–$ThCl_4$ systems are presented in Chapter 5.

Another important fission product for the safety assessment of molten chloride reactors is iodine, because of the partial vaporization it could cause. To add this fission product to the thermodynamic database however, is not so trivial: iodine is an anionic fission product, as opposed to most of the other fission products, meaning that the system to be described becomes a mixed-cation mixed-anion system. To illustrate, adding a cationic fission product to the molten base fuel NaCl–$MgCl_2$–$PuCl_3$ requires, as mentioned before, the thermodynamic modelling of six (three binary, three ternary) additional systems. Adding an anion to the same fuel necessitates the modelling of 12 additional binary systems alone. For this reason, the investigation of iodine as a fission product is first investigated through its effect on the fuel carrier matrix NaCl–$MgCl_2$ (*i.e.* the system NaCl–NaI–$MgCl_2$–$MgI_2$) in Chapter 6. Presented in this chapter is the thermodynamic evaluation of the binary systems NaCl–NaI, NaI–$MgI_2$, $MgCl_2$–$MgI_2$, as well as the reciprocal systems NaCl–$MgI_2$ and NaI–$MgCl_2$. Extending this investigation to the higher-order molten salt system NaCl–$MgCl_2$–$PuCl_3$ (Chapter 7) requires the additional investigation of the systems NaI–$PuI_3$, $MgI_2$–$PuI_3$ and $PuCl_3$–$PuI_3$, as well as the reciprocal systems NaCl–$PuI_3$, NaI–$PuCl_3$, $MgCl_2$–$PuI_3$ and $MgI_2$–$PuCl_3$. A thermodynamic model for the system (Na,Mg,Pu)(Cl,I) is presented, which allows us to investigate the behaviour of iodine in the molten salt fuel NaCl–$MgCl_2$–$PuCl_3$. For the experimental investigation of these systems, carried out in this work, Nd is used as a simulant for Pu in all cases.

Another element that could add to the vaporization risk, especially in combination with iodine, is cesium. For this reason, Chapter 8 focuses on the addition of cesium to the thermodynamic model of the mixed system (Na,Mg,Pu)(Cl,I) constructed in the previous chapter. Adding Cs to this database requires the modelling of many different binary and pseudo-binary systems: the systems NaCl–CsCl, $MgCl_2$–CsCl, $PuCl_3$–CsCl, NaI–CsI, NaCl–CsI, NaI–CsCl, $PuI_3$–CsI and $MgCl_2$–CsI were assessed based on experimental data reported in the literature. The other systems, *i.e.* $MgI_2$–CsI, $MgI_2$–CsCl, $PuCl_3$–CsI and $PuI_3$–CsCl were assessed based on experimental data obtained in this work, allowing us to model the system (Na,Mg,Pu,Cs)(Cl,I) in order to assess the effect of CsI on the molten fuel salt NaCl–$MgCl_2$–$PuCl_3$.

To conclude, Chapter 9 gives an example of the application of a thermodynamic database like the one constructed in this work. First, the validation of the database is carried out by comparing invariant equilibria calculated using the developed thermody-

namic database to experimentally measured values under the same conditions, showing a good agreement between the two. For this, a multi-component salt was synthesised and investigated by DSC to simulate the behaviour of irradiated nuclear fuel. Subsequently, the risk of each of the investigated fission products, *i.e.* Sr, Ba, Ce, Nd, Sm and Y, on the melting behaviour of the fuel salts (*i.e.* NaCl−$MgCl_2$−$PuCl_3$, NaCl−$ThCl_4$−$PuCl_3$, NaCl−$PuCl_3$ and NaCl−$UCl_3$) is characterised with thermodynamic calculations. It is shown that while the effect of one single element could indeed increase the risk of precipitation in an irradiated fuel, adding a mixture of fission products based on their respective fission yields has no adverse effects on the melting behaviour due to the lower concentrations of each individual fission product. Additionally, the retention of volatile fission products Cs and I in the molten fuel salt NaCl−$MgCl_2$−$PuCl_3$ is investigated through vapor pressure calculations. It is shown that compared to molten fluoride salts, where CsI vaporization is known to be a potential issue, the retention in molten chlorides is significantly higher.

In conclusion, this work presents an extensive thermodynamic basis for safety calculations in a molten salt fuel under irradiation, but that does not mean all knowledge gaps have been addressed. For example, the existence of the homogeneity range $Na_{3x}Pu_{2-x}Cl_6$ in the NaCl−$PuCl_3$ system and potential mutual solubility with the $Na_{3x}RE_{2-x}Cl_6$ homogeneity range (RE = Ce, Nd) could pose an added risk of precipitation for any fuel where this intermediate is formed. Thus, its existence should be investigated experimentally. Furthermore, especially in the NaCl−$ThCl_4$−$PuCl_3$ fuel, the behaviour of fission products in ternary systems should be investigated further: the assumption made in this work is that lanthanide fission products (*i.e.* Ce, Nd, Sm) would behave similarly to Pu in a ternary mixture with NaCl and $ThCl_4$. However, if that assumption turns out to be incorrect, it could be critical to the precipitation behaviour of fissile elements in molten NaCl−$ThCl_4$−$PuCl_3$ fuels. The chosen compositions of the fuel can furthermore be optimized with the thermodynamic database, allowing us to select a composition that minimizes the risk of precipitation. Moreover, more experimental data in systems containing $SmCl_3$ and $YCl_3$, especially in combination with $ThCl_4$, are necessary to more reliably assess their effect on the thermochemical properties of molten salt fuels. Finally, vapor pressure measurements in the molten salt systems with Cs and I should be carried out to verify the calculated vaporization behaviour, as well as the preferential association of I with Na over Cs.

# SAMENVATTING & CONCLUSIES

De opkomst van gesmolten zouten in de kernenergiebranche is technisch gezien al meer dan een halve eeuw geleden, *i.e.* in de jaren 50 van de vorige eeuw bij Oak Ridge National Laboratory met hun Aircraft Reactor Experiment (ARE) en Molten Salt Reactor Experiment (MSRE), maar dit onderzoek werd stopgezet omdat de voorkeur werd gegeven aan reactoren gekoeld met vloeibare metalen. Recente ontwikkelingen op het gebied van kernenergie hebben echter gezorgd voor een ware nucleaire renaissance. Kernenergiesystemen op basis van gesmolten zouten bieden vernieuwende voordelen op het gebied van veiligheid, vanwege de aantrekkelijke eigenschappen van gesmolten zouten (laag smeltpunt, goede warmtetransport, lage dampdruk, etc.). De gesmoltenzoutreactor (MSR, naar het Engelse *Molten Salt Reactor*) heeft een veelbelovende toekomst in het kernenergielandschap, en het doel van dit werk is het adresseren van enkele openstaande vragen op het gebied van veiligheid van MSRs. De eerste gesmoltenzoutreactoren (ARE, MSRE) gebruikten fluoridezouten als brandstof, maar tegenwoordig is er steeds meet aandacht voor chloridezouten als mogelijke brandstof vanwege eigenschappen zoals hogere oplosbaarheid van actinides en verenigbaarheid met de huidige afvalverwerkingsprocessen. Een groot vraagteken in de veiligheidsanalyse van op chlorides gebaseerde gesmoltenzoutreactoren is het gedrag en de behandeling van splijtingsproducten in bestraalde (*i.e.* actieve) brandstof, dat in dit werk behandeld wordt.

Gesmoltenzoutbrandstoffen bestaan doorgaans uit twee of meer componenten, *e.g.* NaCl, $MgCl_2$ end $PuCl_3$, en bevatten minstens een splijtbare stof (*e.g.* $PuCl_3$, $UCl_3$) in combinatie met één of meer zouten die de thermochemische eigenschappen zoals smeltpunt en dampdruk van de brandstof verbeteren (*e.g.* NaCl, $MgCl_2$). Een uitgebreid en grondig begrip van de thermochemie van dit soort brandstoffen vergt het begrijpen van minimaal vier systemen (*i.e.* de binaire systemen NaCl−$MgCl_2$, NaCl−$PuCl_3$ en $MgCl_2$−$PuCl_3$, evenals het ternaire systeem NaCl−$MgCl_2$−$PuCl_3$). Het introduceren van splijtingsproducten in - reeds gecompliceerde - gesmolten zouten maakt deze systemen nog complexer door er hogere-ordesystemen van de maken. Ter illustratie: als een brandstof bestaat uit drie componenten en daar één splijtingsproduct aan wordt toegevoegd, vergt dat al het modelleren van drie binaire-, en drie ternaire systemen bovenop het model van de basisbrandstof. De splijtingsproducten (FPs, naar het Engelse *Fission Product*) die gevormd worden tijdens het splijtingsproces vallen in één van drie categorieën: oplosbare FPs (*e.g.* Ba, Ce, Nd), vluchtige FPs (*e.g.* Cs, I, Xe) en metallische FPs (*e.g.* Pt, Rh, Ru). In dit werk ligt de focus op de interacties tussen oplosbare splijtingsproducten (Ba, Sr, Ce, Nd, Sm, Y), en vluchtige splijtingsproducten (Cs, I), met gesmoltenzoutbrandstoffen (*e.g.* NaCl−$MgCl_2$−$PuCl_3$, NaCl−$ThCl_4$−$PuCl_3$, NaCl−$UCl_3$), en de mogelijke risico's met betrekking tot stolling van de splijtbare stof en verdamping van vluchtige elementen uit de brandstof. Deze interacties worden onderzocht met behulp van experimentele technieken als Dynamische Differentiecalorimetrie (DSC, naar

het Engelse *Differential Scanning Calorimetry*), röntgendiffractie (XRD, naar het Engelse *X-Ray Diffraction*) en neutronendiffractie (ND).

Door deze systemen van gesmolten zouten te beschrijven met thermodynamische modellen kunnen we het gedrag tijdens normaal bedrijf, evenals in ongevalsscenario's voorspellen. Deze thermodynamische modellen zijn gebaseerd op de Gibbsenergie, een thermochemische potentiaal die aangeeft welke fasen stabiel zijn bij een gegeven temperatuur en compositie. De meest stabiele combinatie van fasen is degene met de laagste totale Gibbsenergie. In dit werk stellen thermodynamische modellen van zoutsystemen, gemaakt met de CALPHAD methode (naar het Engelse *CALculation of PHAse Diagrams*), ons in staat om voorspellende berekeningen te doen in systemen met meerdere elementen bij temperaturen en composities waar geen experimentele data beschikbaar voor zijn. In onze CALPHAD modellen maken we gebruik van het quasi-chemische formalisme in de quadruplet-benadering, waardoor we ook de lokale structuur van de gesmolten zouten in het model kunnen meenemen. Deze modellen passen we aan experimentele data uit de betreffende literatuur (*e.g.* fasediagrammen en mengenthalpie en) of experimenteel gemeten data van thermodynamische evenwichten (met Dynamische Differentiecalorimetrie) en kristalstructuren (met röntgendiffractie, dan wel neutronendiffractie), om zo de meest accuraat mogelijke thermodynamische beschrijvingen te vinden.

In dit werk wordt er veel gedaan met het thermodynamisch modelleren van systemen met $PuCl_3$, en aangezien er geen $PuCl_3$ beschikbaar was voor de experimenten en het sowieso beter is zo min mogelijk ervan te gebruiken met het oog op de schadelijkheid van het materiaal, was een andere aanpak hier wenselijk. De gekozen methode is het gebruik van surrogaatelementen: elementen die thermochemisch gezien erg op $PuCl_3$ lijken, maar significant veiliger zijn om mee te werken. In Hoofdstuk 3 van dit werk vinden we een zeer betrouwbaar surrogaatelement voor $PuCl_3$, namelijk $NdCl_3$. Daarnaast zien we hoe $UCl_3$, een element waavoor dezelfde bezwaren - in mindere mate - over het werken ermee gelden als voor $PuCl_3$, het best geïmiteerd wordt door $CeCl_3$. Verder wordt een thermodynamisch model gepresenteerd van de gesmoltenzoutbrandstof $NaCl{-}MgCl_2{-}PuCl_3$ op basis van data uit de literatuur, en wordt er een kristallografisch onderzoek naar de surrogaatsystemen $NaCl{-}NdCl_3$ en $NaCl{-}CeCl_3$ getoond. Uit dat laatste bleek dat er een homogeniteitsregime $Na_{3x}RE_{2-x}Cl_6$ (RE = Ce, Nd) bestond, die vervolgens meegenomen is in het model. Dit thermodynamische model, samen met de keuze voor $NdCl_3$ als surrogaatelement, vormt een goede basis om te beginnen met het onderzoeken van de effecten van splijtingsproducten op de thermochemie van gesmoltenzoutbrandstoffen.



De eerste splijtingsproducten die behandeld worden zijn barium en strontium. Bariumchloride heeft het hoogste smeltpunt van de chloridevormende splijtingsproducten, en zou dus een significant effect op het smeltgedrag kunnen hebben. Voor strontiumchloride geldt dit tot op zekere hoogte ook, maar strontium als splijtingsproduct is ook interessant vanwege de gelijkenissen tussen Ba en Sr, daar beiden aardalkalimetalen zijn. Het onderzoek naar de thermochemische eigenschappen van de systemen

$BaCl_2$–$RECl_3$ en $SRCl_2$–$RECl_3$ (RE = Ce, Nd) wordt gepresenteerd in Hoofdstuk 4. Hier wordt duidelijk waar de huidige literatuur tekortschoot met de identificatie van de vaste oplossingen (respectievelijk $Ba_{1-x}RE_xCl_{2+x}$ (kubisch) en $Ba_yRE_{1-y}Cl_{3-y}$ (hexagonaal) (RE = Ce, Nd)) en de intermediare stof $Ba_3RE_2Cl_{12}$ (RE = Ce, Nd). In het $SrCl_2$–$RECl_3$ systeem (RE = Ce, Nd) zijn ook vaste oplossingen gevonden (respectievelijk $Sr_{1-x}RE_xCl_{2+x}$ (kub.) en $Sr_yRE_{1-y}Cl_{3-y}$ (hex.) (RE = Ce, Nd)) en een intermediaire stof $Sr_9RE_5Cl_{33}$ (RE = Ce, Nd).

In Hoofdstuk 5 worden de resultaten behaald in het $BaCl_2$–$CeCl_3$ systeem gebruikt om met een zeer gerichte aanpak het systeem $BaCl_2$–$UCl_3$ te onderzoeken, waarmee de thermochemische gelijkenissen tussen de twee systemen konden worden aangetoond. Deze experimenten bevestigden dat er inderdaad een vaste oplossing bestaat bij hoge temperatuur ($Ba_{1-x}U_xCl_{2+x}$ (kub.)) en een intermediaire verbinding ($Ba_3U_2Cl_{12}$), wat een gegronde reden gaf tot het heroptimaliseren van het $BaCl_2$–$UCl_3$ systeem. Ook laten we hiermee zien dat de aanpak met surrogaatchemie een valide methode is om actinidesystemen te onderzoeken met behulp van lanthanides. Tot slot, om ook veiligheidsberekeningen te kunnen doen voor thoriumhoudende brandstoffen worden de modellen van $SrCl_2$–$ThCl_4$ en $BaCl_2$–$ThCl_4$ gepresenteerd in dit hoofdstuk.

Een ander belangrijk splijtingsproduct voor de veiligheidsbeoordeling van chloridehoudende gesmoltenzoutreactoren is jodium, vanwege het inherente verdampingsrisico dat het met zich meebrengt. Dit splijtingsproduct toevoegen aan de thermochemische database is echter verre van triviaal: jodium is, in tegenstelling tot de meeste andere splijtingsproducten, een anion, wat betekent dat het toevoegen van jodium aan de database een systeem omvat met gemengde kationen én anionen. Ter illustratie, zoals reeds genoemd, moeten er voor het toevoegen van een kation zes systemen (drie binaire en drie ternaire systemen) gemodelleerd worden. Voor het toevoegen van een anion, zijn dat alleen al 12 binaire systemen. Hierom wordt het toevoegen van jodium aan de database eerst onderzocht vanuit het simpele systeem NaCl–$MgCl_2$ (*i.e.* het systeem NaCl–NaI–$MgCl_2$–$MgI_2$) in Hoofdstuk 6. In dit hoofdstuk komt het onderzoek naar de binaire systemen NaCl–NaI, NaI–$MgI_2$ en $MgCl_2$–$MgI_2$ aan bod, evenals de systemen NaCl–$MgI_2$ en NaI–$MgCl_2$. Verder onderzoek naar het toevoegen van jodium aan het thermodynamische model van de brandstof NaCl–$MgCl_2$–$PuCl_3$ wordt gepresenteerd in Hoofdstuk 7, met de toevoeging van de binaire systemen NaI–$PuI_3$, $MgI_2$–$PuI_3$ en $PuCl_3$–$PuI_3$, evenals de pseudo-binaire systemen NaCl–$PuI_3$, NaI–$PuCl_3$, $MgCl_2$–$PuI_3$ en $MgI_2$–$PuCl_3$. Een thermodynamisch model voor het volledige systeem (Na,Mg,Pu)(Cl,I) is hiermee bereikt, wat ons in staat stelt on het gedrag van jodium in de brandstof NaCl–$MgCl_2$–$PuCl_3$ te karakteriseren. Voor het experimentele werk in deze systemen met Pu werd Nd als surrogaatelement gebruikt.

Een ander element dat een vluchtigheidsrisico met zich meebrengt is cesium, in het bijzonder als er (in de aanwezigheid van jodium) cesiumjodide gevormd kan worden. In Hoofdstuk 8 wordt uiteengezet hoe de toevoeging van cesium aan het systeem (Na,Mg,Pu)(Cl,I) is bereikt. Dit vergt wederom het modelleren van veel verschillende binaire systemen: de systemen NaCl–CsCl, $MgCl_2$–CsCl, $PuCl_3$–CsCl, NaI–CsI, NaCl–CsI, $PuI_3$–CsI en $MgCl_2$–CsI, die geoptimaliseerd zijn op basis van data uit de literatuur, en

de systemen $MgI_2$−CsI, $MgI_2$−CsCl, $PuCl_3$−CsI en $PuI_3$−CsCl, die op basis van nieuwe experimentele data geoptimaliseerd zijn. Derhalve zijn we erin geslaagd om een thermodynamisch model te verkrijgen van het systeem (Na,Mg,Pu,Cs)(Cl,I), dat ons in staat stelt om het effect van CsI op de brandstof NaCl−$MgCl_2$−$PuCl_3$ te onderzoeken.

Als conclusie wordt in Hoofdstuk 9 laten zien hoe de ontwikkelde thermodynamische database toegepast kan worden. Als eerste wordt aangetoond dat de gemeten equilibria (met DSC) voor gemengde zout bestaande uit meerdere componenten overeenkomen met de evenwichten voorspeld door het thermodynamische model. Vervolgens wordt het effect van elk indivudele splijtingsproduct (Sr, Ba, Ce, Nd, Sm en Y) op verschillende brandstoffen (NaCl−$MgCl_2$−$PuCl_3$, NaCl−$ThCl_4$−$PuCl_3$, NaCl−$PuCl_3$ en NaCl−$UCl_3$) onderzocht door middel van thermodynamische berekeningen. Deze berekeningen tonen aan dat hoewel het effect van één element het stollingsrisico kan verhogen in een bestraalde brandstof, de aanwezigheid van een mengsel van splijtingsproduten geen nadelige effecten heeft op het smeltgedrag vanwege de lagere concentraties van elk splijtingsproduct. Daarnaast is de retentie van vluchtige splijtingsproducten (Cs, I) onderzocht met behulp van dampdrukberekeningen. Hiermee wordt aangetoond dat vergeleken met fluoridezouten, waar verdamping van CsI een bekend probleem is, de retentie van Cs en I (dan wel CsI) significant hoger is.

Samenvattend wordt er in dit werk een thermodynamische basis gepresenteerd voor het uitvoeren van veiligheidsberekeningen voor een bestraalde gesmoltenzoutbrandstof. Dit betekent echter niet dat alle vraagstukken hiermee opgelost zijn. Zo bestaat de mogelijkheid dat het homogeniteitsregime $Na_{3x}Pu_{2-x}Cl_6$ bestaat in het NaCl−$PuCl_3$ systeem, wat mogelijk wederzijdse vaste oplosbaarheid vertoont met de gevonden $Na_{3x}RE_{2-x}Cl_6$ (RE= Ce, Nd) intermediairen. Dit zou neerslag van de splijtbare stof (*i.e.* Pu) als gevolg kunnen hebben, en daarom is het van belang dat dit experimenteel onderzocht wordt. Daarnaast dient het gedrag van splijtingsproducten in ternaire systemen, in het bijzonder in het NaCl−$ThCl_4$−$PuCl_3$ systeem, verder onderzocht te worden: de aanname in dit werk is dat de lanthanoïden (*e.g.* Ce, Nd, Sm) hetzelfde gedrag vertonen als Pu in een ternair systeem met NaCl en $ThCl_4$. Als deze aanname echter onjuist blijkt, kan dit kritieke gevolgen hebben voor de neerslag van splijtstof in gesmolten NaCl−$ThCl_4$−$PuCl_3$ brandstoffen. Daarnaast kan het thermodynamische model gebruikt worden voor de selectie van de optimale beginsamenstelling van de brandstof om het risico op neerslag te minimaliseren. Verder zijn er meer experimentele data nodig in de systemen met $SmCl_3$ en $YCl_3$, in het bijzonder in combinatie met $ThCl_4$, om het risico op stollen nog betrouwbaarder te kunnen beschouwen. Tot slot is het noodzakelijk dat er dampdrukmetingen in systemen van gesmolten zouten met Cs en I gedaan worden om aan te tonen of het verdampgedrag accuraat voorspeld is, evenals het onderzoeken van de voorkeursassociatie van jodium met natrium, ten faveure van cesium.

# Dennis ALDERS

*What is a PhD thesis without an appendix? A highly efficient one. However, in many cases, not all data obtained during a PhD trajectory has a dedicated place in the final thesis. An appendix is then a great solution to present information that is necessary to achieve the final goal of a doctoral thesis, but does not necessarily have a place in the main body of text. This appendix does exactly that: present the information that is either underlying the various chapters, or adds to the various chapters in a way that wouldn't have fit in the chapter itself.*

# A

# THERMODYNAMIC MODELLING WITH $ThCl_4$

Phase diagram studies on $ThCl_4$ systems - those with $SrCl_2$ and $BaCl_2$ notwithstanding as they are already covered in Chapter 5 - that are necessary to perform application calculations on $ThCl_4$-based fuels are presented in this section. For the sake of clarity, the phase diagrams will mostly be presented in separate sections.

The mixing enthalpy of $ThCl_4$-based systems has not been measured experimentally or calculated reliably via MD simulations. The mixing enthalpies reported in this work are calculated from the thermodynamic models, and are given in a separate subsection.

## A.1. PHASE DIAGRAM STUDIES AND EQUILIBRIA

### A.1.1. NaCl–$ThCl_4$

The system NaCl–$ThCl_4$ has been investigated experimentally Oyamada et al. [1], Tanii et al. [2] and Vokhmyakov et al. [3], and has been assessed by Ocádiz Flores et al. [4]. The assessment of Ocádiz Flores et al. is retained in this work, and the calculated phase diagram is shown in Figure A.1. The congruently melting intermediate compound $Na_2ThCl_6$ was identified by Tanii et al. and Oyamada et al. based on the measured invariant equilibria, but no crystal structure has been reported in the literature to date. Vdovenko et al. reported an intermediate with a different stoichiometry instead, *i.e.* $NaThCl_5$, but based on the shape of the liquidus line it seems unlikely that this compound exists instead of $Na_2ThCl_6$.

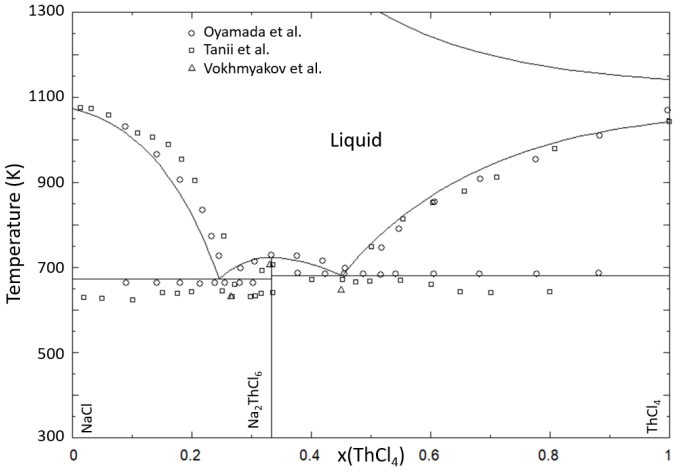


Figure A.1: Phase diagram of the NaCl−$ThCl_4$ system, calculated with the thermodynamic model presented by Ocádiz Flores et al. [4]. Experimental data from Oyamada et al. (open black circles), Tanii et al. (open black squares) and Vokhmyakov et al. (open black triangles).

### A.1.2. $MgCl_2$−$ThCl_4$

The system $MgCl_2$−$ThCl_4$ has been investigated experimentally by Korshunov et al. [5] and Gorbunov et al. [6]. Both authors found the system to be a simple binary eutectic with no apparent solid solubility. The calculated phase diagram of this system is shown in Figure A.2.

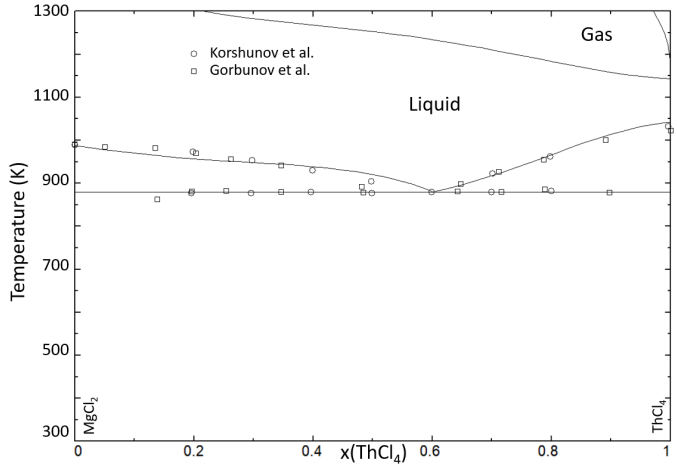


Figure A.2: Phase diagram of the $MgCl_2$−$ThCl_4$ system, calculated with the thermodynamic model presented in this work. Experimental data from Korshunov et al. [7] (open black circles) and Gorbunov et al. [6] (open black squares).

### A.1.3. $PuCl_3$–$ThCl_4$

Experimental investigations of the $PuCl_3$–$ThCl_4$ system have been reported by Vorobei et al. [8]. In their assessment of the system, Vorobei et al. found a solid solution in the $ThCl_4$-rich part of the phase diagram, mostly stable at elevated temperature, in $Th_{1-x}Pu_xCl_{4-x}$. For the thermodynamic model of the $PuCl_3$–$ThCl_4$ system, the model presented by Dumaire et al. [9], who retain the interpretation of Vorobei et al., was used. The calculated phase diagram is presented in Figure A.3.

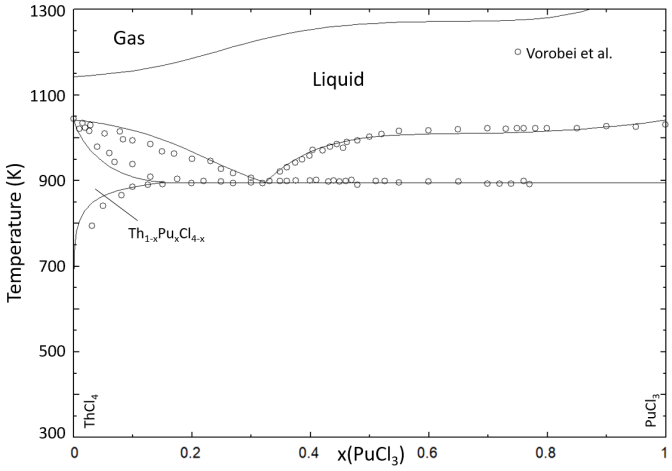


Figure A.3: Phase diagram of the $ThCl_4$—$PuCl_3$ system, calculated with the thermodynamic model presented by Dumaire et al. [9]. Experimental data from Vorobei et al. [8] (open black circles).

### A.1.4. $RECl_3$–$ThCl_4$ (RE = Ce, Nd)

The system $CeCl_3$–$ThCl_4$ has been investigated by Korshunov et al. [7], who identified it as simple binary eutectic system. No experimental data have been reported on the system $NdCl_3$–$ThCl_4$, but experimental data are known for the system $PuCl_3$–$ThCl_4$. As shown abundantly in this dissertation, $NdCl_3$ can be used as a simulant for $PuCl_3$. Through the transitive nature of simulant chemistry, the inverse must also be true, and we can use $PuCl_3$ as simulant for $NdCl_3$. For this reason, the same parameters that Dumaire et al. [9] reported in their assessment of the $PuCl_3$–$ThCl_4$ binary are used here to model the $NdCl_3$–$ThCl_4$ binary. The phase diagrams of the systems $RECl_3$–$ThCl_4$ (RE = Ce, Nd) are presented in Figures A.4 and A.5, respectively.

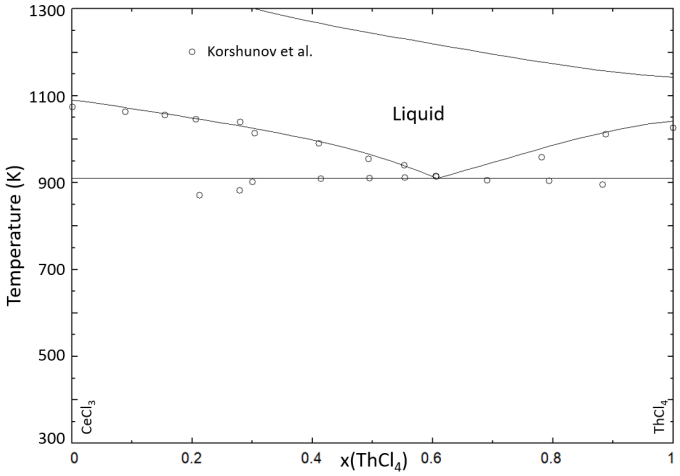


Figure A.4: Phase diagram of the $CeCl_3$—$ThCl_4$ system, calculated with the thermodynamic model presented in this work. Experimental data from Korshunov et al. [7] (open black circles).

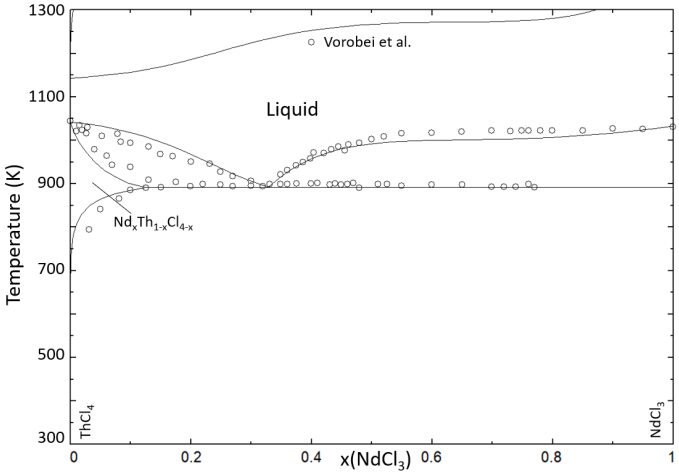


Figure A.5: Phase diagram of the $NdCl_3$—$ThCl_4$ system, calculated with the thermodynamic model presented in this work. $PuCl_3$—$ThCl_4$ experimental data from Vorobei et al. [8] (open black circles).

### A.1.5. MIXING ENTHALPIES

No experimental mixing enthalpy data have been reported in the literature on any of the $ThCl_4$ systems covered in this Appendix. The calculated mixing enthalpies presented in Figure A.6 are therefore not optimized, and are only shown for comparative purposes as discussed below.

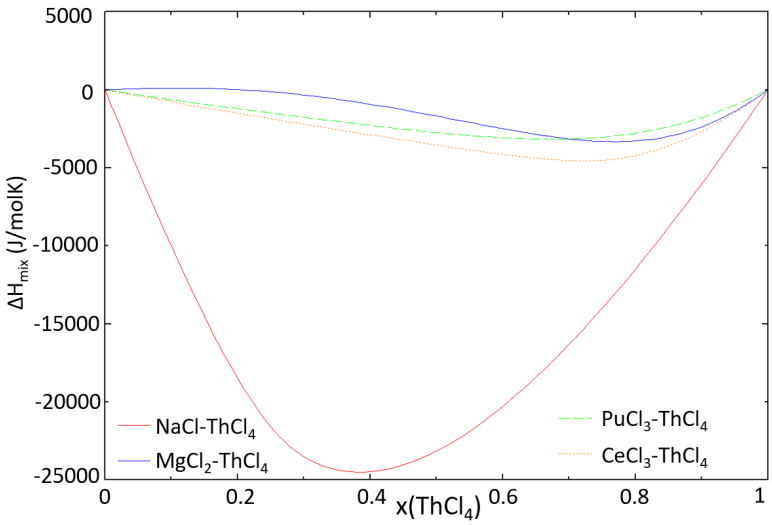


Figure A.6: Mixing enthalpy of the systems $MgCl_2-ThCl_4$ (solid blue line), $CeCl_3-ThCl_4$ (dotted orange line), $PuCl_3-ThCl_4$ (dashed green line) and $NaCl-ThCl_4$ (solid red line). The latter is compared to computational ab-initio molecular dynamics (AIMD) data from Wang et al. [10]. The calculated mixing enthalpy of the $NdCl_3-ThCl_4$ system is identical to that of $PuCl_3-ThCl_4$.

Shown in the figure above is that the mixing enthalpies of the systems $MCl_3-ThCl_4$ (M = Ce, Pu, Nd) are in good agreement with each other, with the latter two being identical. They are also in good agreement with the mixing enthalpy of the $UCl_3-ThCl_4$ system presented in Chapter 5. The mixing enthalpy of the $MgCl_2-ThCl_4$ system shows a slight positive deviation at low concentrations of $ThCl_4$. This is not uncommon for alkaline earth chloride systems [11, 12]. The thermodynamic models presented in this Appendix should be updated when experimental mixing enthalpy data for any of these systems become available.

### A.1.6. TERNARY SYSTEMS

Excess Gibbs energy parameters in the ternary system $NaCl-ThCl_4-PuCl_3$ have been presented by Dumaire et al. [9]. Their excess Gibbs energy functions were retained in this work and show a good agreement with the experimental data by Desyatnik et al. [13]. Three ternary invariant equilibria reported by Dumaire et al., and as measured by Desyatnik et al. are presented in Table A.1.

| x(NaCl) | x($ThCl_4$) | x($PuCl_3$) | T (K) | Source |
|---|---|---|---|---|
| **Eutectic 1** | | | | |
| 0.470 | 0.354 | 0.176 | 597 | Dumaire et al. [9] |
| 0.465 | 0.350 | 0.185 | 598 | Desyatnik et al. [13] |
| **Eutectic 2** | | | | |
| 0.574 | 0.223 | 0.203 | 598 | Dumaire et al. [9] |
| 0.585 | 0.230 | 0.185 | 603 | Desyatnik et al. [13] |
| $Na_2ThCl_6-PuCl_3$ eutectic | | | | |
| 0.521 | 0.261 | 0.218 | | Dumaire et al. [9] |
| 0.520 | 0.260 | 0.220 | | Desyatnik et al. [13] |

Table A.1: Calculated ternary invariant equilibria in the $NaCl-ThCl_4-PuCl_3$ system by Dumaire et al. [9], compared to experimental data from Desyatnik et al. [13].

A significant deviation from ideality is seen in the thermodynamic model of the ternary system $NaCl-ThCl_4-PuCl_3$ (see the excesss Gibbs energy parameters in Chapter 2, taken from Dumaire et al. [9]). The addition of these parameters to the thermodynamic model has significant effects on the application calculations performed in Chapter 9. Due to the fact that, based on experimental data, the $NaCl-ThCl_4-PuCl_3$ system required re-optimiztion in the ternary field, the same can be expected of similar systems. In this work, the ternary systems $NaCl-ThCl_4-RECl_3$ (RE = Ce, Nd, Sm) have been optimized using the ternary excess parameters of the $NaCl-ThCl_4-PuCl_3$ system. The liquidus projections of the ternary systems $NaCl-ThCl_4-MCl_3$ (M = Pu, Nd, Ce, Sm) are presented in Figures A.7-A.10, and the invariant equilibria are given in Table A.2. While there are clear similarities between the $NaCl-ThCl_4-MCl_3$ (M = Ce, Nd, Sm, Pu) systems, experimental verification of the ternary fields in the rare earth chloride systems is necessary, as the ternary optimization of these systems greatly affects the results of the application calculations in Chapter 9. One of the biggest discrepancies in the calculated invariant equilibria in Table A.2 arises from the intermediate compound $Na_{3x}RE_{2-x}Cl_6$, which has been proven to exist in the $NaCl-NdCl_3$ and $NaCl-CeCl_3$ systems, but require follow-up studies the $NaCl-PuCl_3$ and $NaCl-SmCl_3$ systems.

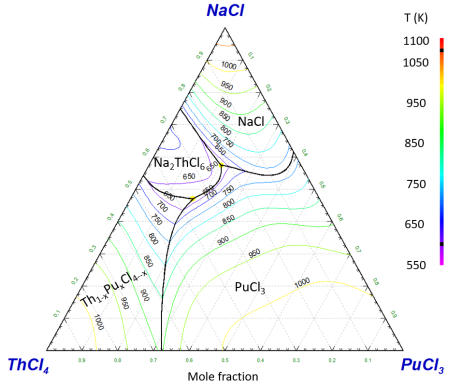


Figure A.7: Projected liquidus surface of the $NaCl-ThCl_4-PuCl_3$ system, calculated with the thermodynamic model presented by Dumaire et al. [9]. Phases listed on the ternary diagram are the primary crystallization phases at that composition. The calculated ternary equilibria are presented in Table A.2.

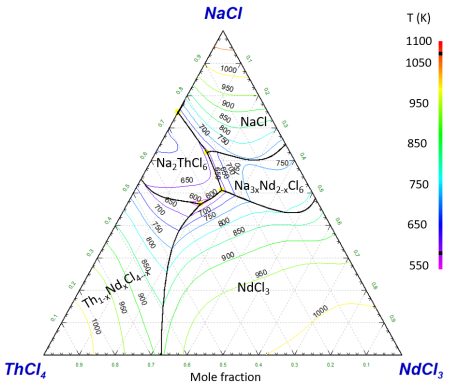


Figure A.8: Projected liquidus surface of the $NaCl-ThCl_4-NdCl_3$ system, calculated with the thermodynamic model presented in this work. Phases listed on the ternary diagram are the primary crystallization phases at that composition. The calculated ternary equilibria are presented in Table A.2.

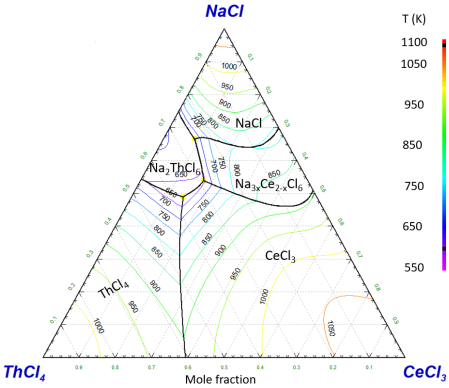


Figure A.9: Projected liquidus surface of the $NaCl-ThCl_4-CeCl_3$ system, calculated with the thermodynamic model presented in this work. Phases listed on the ternary diagram are the primary crystallization phases at that composition. The calculated ternary equilibria are presented in Table A.2.

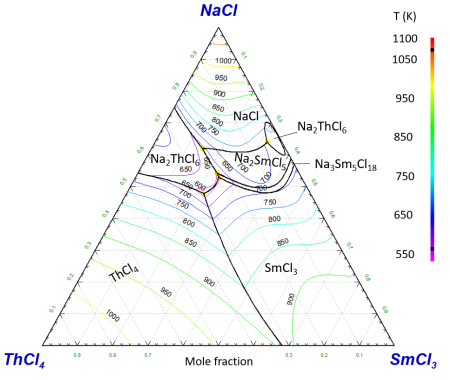


Figure A.10: Projected liquidus surface of the $NaCl-ThCl_4-SmCl_3$ system, calculated with the thermodynamic model presented in this work. Phases listed on the ternary diagram are the primary crystallization phases at that composition. The calculated ternary equilibria are presented in Table A.2.

A

| x(NaCl) | x($ThCl_4$) | x($MCl_3$) | T (K) | Invariant equilibrium |
|---|---|---|---|---|
| **NaCl−$ThCl_4$−$PuCl_3$ - Dumaire et al. [9]** | | | | |
| 0.574 | 0.223 | 0.203 | 598 | NaCl + $Na_2ThCl_6$ + $PuCl_3$ |
| 0.470 | 0.354 | 0.176 | 598 | $Na_2ThCl_6$ + $PuCl_3$ + $Th_{1-x}Pu_xCl_{4-x}$ |
| **NaCl−$ThCl_4$−$NdCl_3$ - This work** | | | | |
| 0.625 | 0.231 | 0.144 | 631 | NaCl + $Na_2ThCl_6$ + $Na_{3x}Nd_{2-x}Cl_6$ |
| 0.509 | 0.248 | 0.242 | 610 | $NdCl_3$ + $Na_2ThCl_6$ + $Na_{3x}Nd_{2-x}Cl_6$ |
| 0.466 | 0.329 | 0.206 | 586 | $Na_2ThCl_6$ + $NdCl_3$ + $Th_{1-x}Nd_xCl_{4-x}$ |
| **NaCl−$ThCl_4$−$CeCl_3$ - This work** | | | | |
| 0.664 | 0.248 | 0.087 | 647 | NaCl + $Na_2ThCl_6$ + $Na_{3x}Nd_{2-x}Cl_6$ |
| 0.538 | 0.287 | 0.175 | 637 | $CeCl_3$ + $Na_2ThCl_6$ + $Na_{3x}Ce_{2-x}Cl_6$ |
| 0.489 | 0.368 | 0.143 | 599 | $Na_2ThCl_6$ + $CeCl_3$ + $ThCl_4$ |
| **NaCl−$ThCl_4$−$SmCl_3$ - This work** | | | | |
| 0.639 | 0.042 | 0.320 | 695 | $MgCl_2$ + $SmCl_3$ + $Na_3Sm_5Cl_{18}$ |
| 0.619 | 0.235 | 0.146 | 624 | $MgCl_2$ + $SmCl_3$ + $Na_3Sm_5Cl_{18}$ |
| 0.543 | 0.232 | 0.226 | 593 | $MgCl_2$ + $SmCl_3$ + $Na_3Sm_5Cl_{18}$ |
| 0.529 | 0.234 | 0.237 | 590 | $MgCl_2$ + $Na_3Sm_5Cl_{18}$ + $Na_2Mg_3Cl_8$ |
| 0.478 | 0.302 | 0.220 | 578 | NaCl + $Na_6MgCl_8$ + $Na_3Sm_5Cl_{18}$ |

Table A.2: Calculated ternary invariant equilibria in the NaCl−$ThCl_4$−$MCl_3$ systems (M = Pu, Nd, Ce, Sm).

# B

# Y AND Sm AS FISSION PRODUCTS

From a fission yield perspective, the fission products covered in this dissertation (*i.e.* Sr, Ba, Ce, Nd, I and Cs) are highly relevant. Other fission products such as samarium and yttrium, however, are produced in a nuclear reactor in comparable amounts. These elements have not been covered in this thesis so far, but they have been included in the application calculations. The reason for this is that these systems have been modelled exclusively based on data from the literature, and no additional experimental data have been added. Nonetheless, they are important for the application calculations, so this section will show the thermodynamic models underlying the behaviour of Y and Sm in molten chloride salts.

## B.1. EQUILIBRIA WITH $SmCl_3$

### B.1.1. PHASE DIAGRAM STUDIES

To start with $SmCl_3$, it is important that the interactions of samarium with the base fuel of NaCl−$MgCl_2$−$PuCl_3$ are modelled accurately. To this end, the binary systems NaCl−$SmCl_3$, $MgCl_2$−$SmCl_3$ and $PuCl_3$−$SmCl_3$ have been modelled based on data from the literature.

The system NaCl−$SmCl_3$ has been investigated experimentally by Seifert et al. [1]. In their assessment of this system, Seifert et al. identified two intermediates in $Na_2SmCl_5$ and $Na_3Sm_5Cl_{18}$. These intermediates have had their crystal structures characterised by Wickleder et al. [2] and Lissner et al. [3], respectively. The intermediate $Na_3Sm_5Cl_{18}$ is an analog to the intermediates $Na_3Ce_5Cl_{18}$ and $Na_3Nd_5Cl_{18}$, which form a homogeneity range in the form of $Na_{3x}RE_{2-x}Cl_6$ (RE = Ce, Nd) as shown in Chapter 3. Considering the unexplained equilibria that Seifert et al. measured above x($SmCl_3$) = 0.55, between 700-750 K, it is likely that in this system there is also solubility of the end-members in the intermediate $Na_3Sm_5Cl_{18}$. However, due to the fact that this hasn't been shown experimentally yet, this solubility was not incorporated in the thermodynamic model. The phase diagram of this system is shown in Figure B.1.

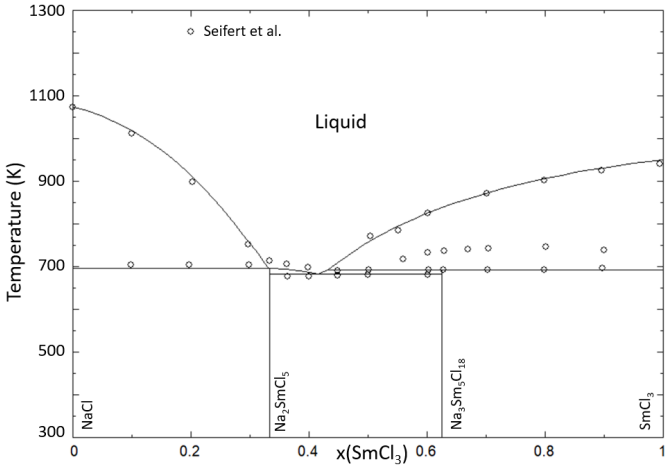


Figure B.1: Phase diagram of the NaCl−$SmCl_3$ system, calculated with the thermodynamic model presented in this work. Experimental data from Seifert et al. [1] (open black circles).

The system $MgCl_2$−$SmCl_3$ has been investigated by Vogel et al. [4] using DTA. In their assessment of the system, Vogel et al. concluded that it is a simple binary eutectic system, and this is how it has been incorporated in the thermodynamic model. The phase diagram of this system is shown in Figure B.2.

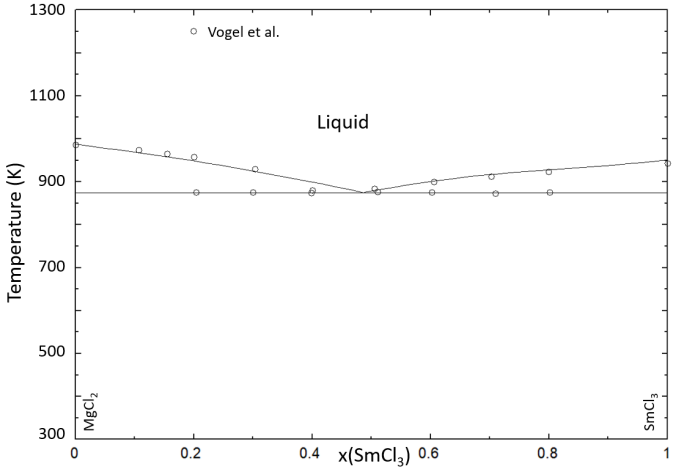


Figure B.2: Phase diagram of the $MgCl_2$−$SmCl_3$ system, calculated with the thermodynamic model presented in this work. Experimental data from Vogel et al. [4] (open black circles).

There is no available experimental data on the $SmCl_3$−$PuCl_3$ system, but data in the simulant system with $NdCl_3$ has been reported in the literature by Niselson et al. [5]. Based on their experimental investigation of the $SmCl_3$−$NdCl_3$ system, a thermodynamic model of the $SmCl_3$−$PuCl_3$ system was constructed, as shown in Figure B.3.

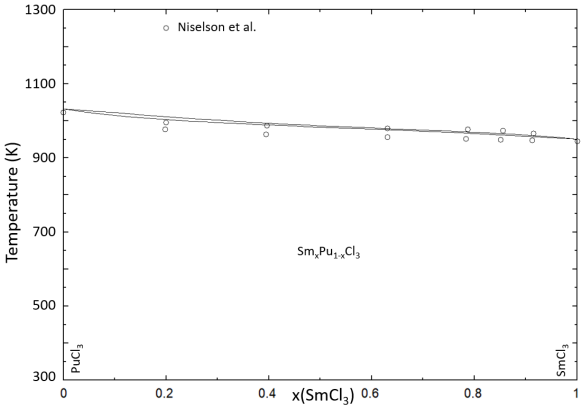


Figure B.3: Phase diagram of the $PuCl_3-SmCl_3$ system, calculated with the thermodynamic model presented in this work, compared to experimental data of the $NdCl_3-SmCl_3$ system from Niselson et al. [5] (open black circles) .

In addition to the interactions of $SmCl_3$ with the base fuel, the interactions with other fuel components must be modelled. First off are the interactions between $SmCl_3$ and other fissile elements, in order to investigate the effect on fuels containing $UCl_3$ and $ThCl_4$. However, neither the $SmCl_3-UCl_3$, nor $SmCl_3-ThCl_4$ phase diagrams have been reported in the literature. For this reason, simulant systems were used to model the interactions between these salts.
The thermodynamic model of the $SmCl_3-UCl_3$ system has been based on the experimental data on the $SmCl_3-LaCl_3$ system as reported by Niselson et al. [5]. The calculated phase diagram of this system is reported in Figure B.4.

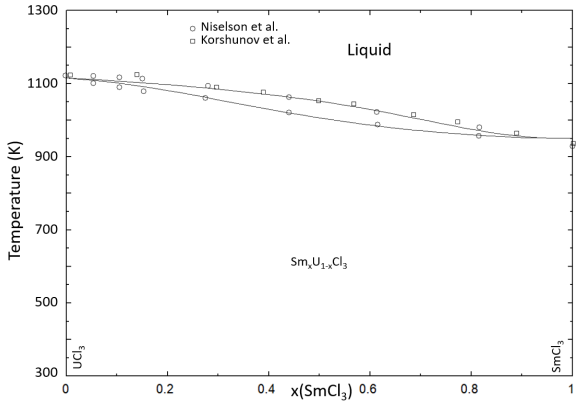


Figure B.4: Phase diagram of the $SmCl_3-UCl_3$ system calculated with the thermodynamic model presented in this work, compared to the experimental data on the $SmCl_3-LaCl_3$ system reported by Niselson et al. [5].

For the $SmCl_3-ThCl_4$ system, finding a suitable simulant is more complicated. Fig-

ures B.5a and B.5b are variations on the liquidus comparison in Chapter 3, focused on $SmCl_3$ and $YCl_3$. These figures show that for these rare earth chlorides, $HoCl_3$ would be the most suitable simulant. However, considering the only experimental data that is available is that of the systems $ThCl_4$−$PuCl_3$, $ThCl_4$−$UCl_3$ and $ThCl_4$−$CeCl_3$, the choice of simulant is a limited one. Of these three systems, the melting behaviour of the $PuCl_3$ system is closest to that of the $SmCl_3$ and $YCl_3$ systems, as shown in Figures B.6a and B.6b. For this reason, the phase diagrams of the $SmCl_3$−$ThCl_4$ and $YCl_3$−$ThCl_4$ systems were modelled based on the composition and temperature of the eutectic in the $PuCl_3$−$ThCl_4$ system. The calculated phase diagram of the $SmCl_3$−$ThCl_4$ system is presented in Figure B.7.

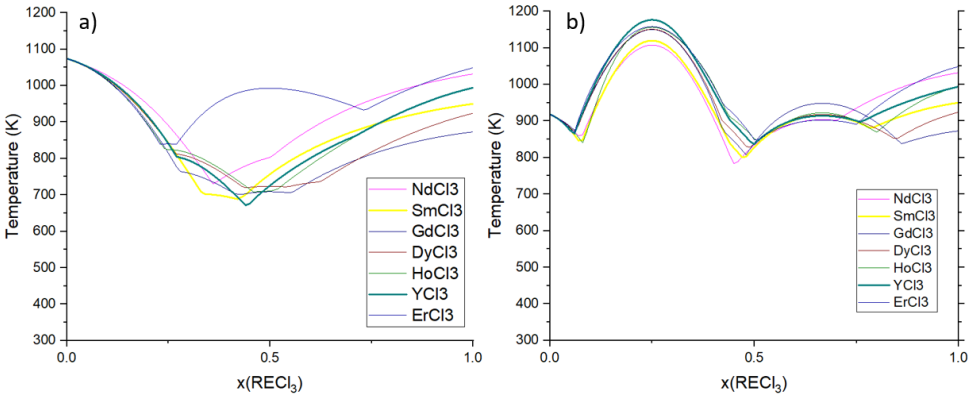


Figure B.5: Comparison of the liquidus data on the NaCl−$RECl_3$ (a) and CsCl−$RECl_3$ (b) (RE = Nd, Sm, Y, Ho, Er, Dy, Gd) systems. Data previously shown in Chapter 4.

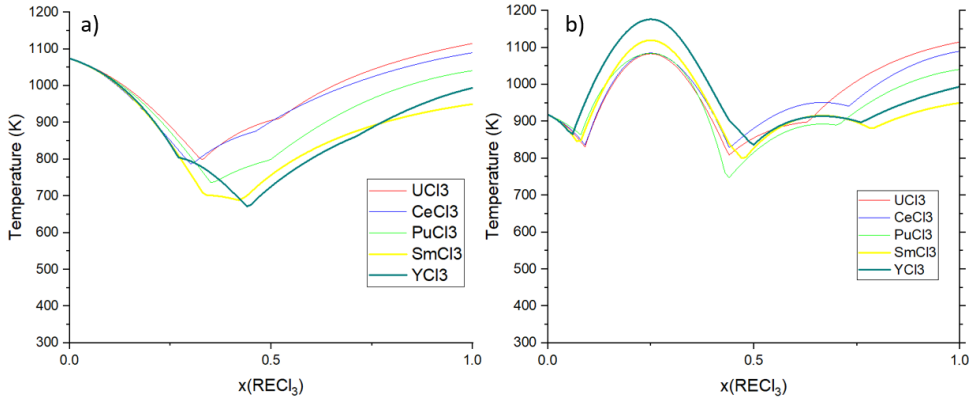


Figure B.6: Comparison of the liquidus data on the NaCl−$RECl_3$ (a) and CsCl−$RECl_3$ (b) (RE = Sm, Y, Ce, U, Pu) systems. Data previously shown in Chapter 4.

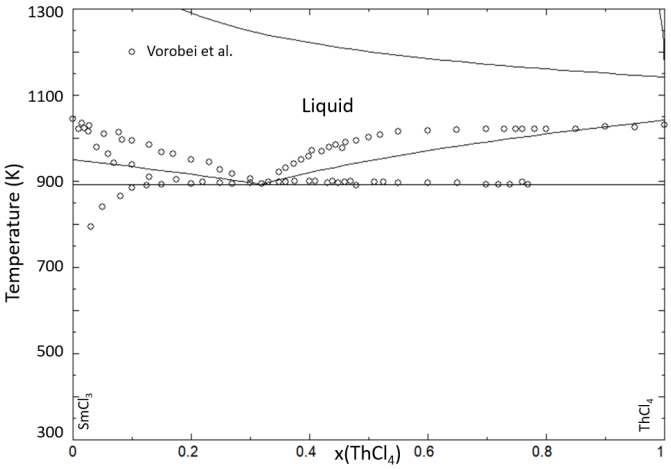


Figure B.7: Phase diagram of the $SmCl_3$−$ThCl_4$ system calculated with the thermodynamic model presented in this work, compared to the experimental data on the $PuCl_3$−$ThCl_4$ system reported by Vorobei et al. [6].

Finally, the interactions between $SmCl_3$ and other fission products must be modelled to include them in the application calculations. For this, the systems $SrCl_2$−$SmCl_3$, $BaCl_2$−$SmCl_3$, $NdCl_3$−$SmCl_3$ and $CeCl_3$−$SmCl_3$ have been modelled. The experimental data has been reported in the literature for the $SrCl_2$−$SmCl_3$ system by Blachnik et al. [7] and Morozov et al. [8]. Both authors report a single intermediate at high $SrCl_2$ content, but give different stoichiometries ($Sr_2SmCl_7$ and $Sr_3SmCl_9$, respectively). Lochner et al. [9] identified this intermediate as $Sr_9Sm_5Cl_{33}$ instead, analogous to the intermediates $Sr_9Nd_5Cl_{33}$ and $Sr_9Ce_5Cl_{33}$ we found in the $SrCl_2$−$NdCl_3$ and $SrCl_2$−$CeCl_3$ systems, respectively. This intermediate fits the experimental data on the invariant equilibria as well as the other stoichiometries. Since the intermediate $Sr_9Sm_5Cl_{33}$ has been synthesised and characterised by XRD by Lochner et al., this is our intermediate of choice in this system. The phase diagram of the $SrCl_2$−$SmCl_3$ system is presented in Figure B.8.

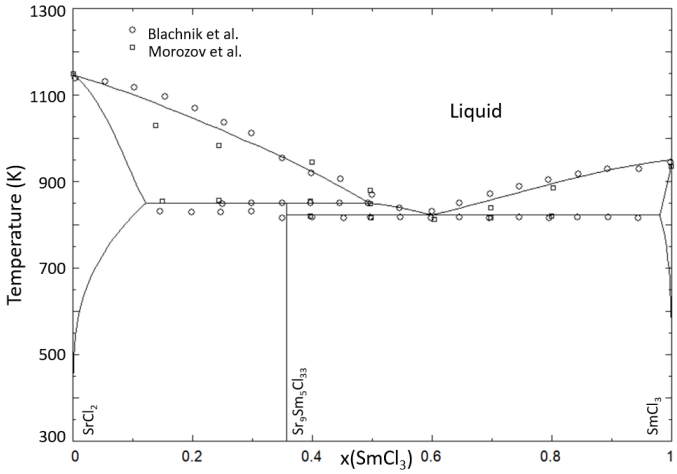


Figure B.8: Phase diagram of the $SrCl_2-SmCl_3$ system calculated with the thermodynamic model in this work. Experimental data from Blachnik et al. [7] (open black circles) and Morozov et al. [8]. The intermediate composition $Sr_9Sm_5Cl_{33}$ was reported by Lochner et al. [9].

On the $BaCl_2-SmCl_3$ system, Blachnik et al. [7] reported experimental data on the invariant equilibria. Furthermore, the authors performed an XRD study of the system, and found several intermediates ($Ba_3SmCl_9$, $Ba_2SmCl_7$ and $BaSmCl_5$), in addition to a high-temperature solid solution in $\beta$-$BaCl_2$, like in the $BaCl_2-RECl_3$ (RE = Ce, Nd) systems investigated in this work. It is possible that, like in the analogous systems with $NdCl_3$ and $CeCl_3$, one of the intermediates in this system is actually $Ba_3Sm_2Cl_{12}$, but without additional experimental data on the crystallography of this system we cannot be sure of this. For this reason, the interpretation of the data from Blachnik et al. [7] is retained, and their suggested intermediates were incorporated in the thermodynamic model. The calculated phase diagram of this system is presented in Figure B.9.

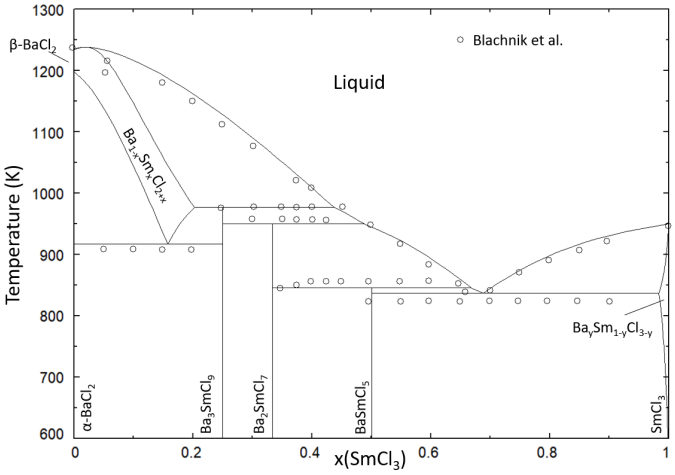


Figure B.9: Phase diagram of the $BaCl_2-SmCl_3$ system calculated with the thermodynamic model in this work. Experimental data from Blachnik et al. [7] (open black circles).

The system $NdCl_3-SmCl_3$ has been investigated experimentally by Niselson et al. [5], who observed complete solid solubility between the end members. On the salt system $CeCl_3-SmCl_3$ no experimental investigations have been reported in the literature. For this reason, the system $LaCl_3-SmCl_3$ as reported by Niselson et al. [5] and Korshunov et al. [10] was used as a simulant system. The phase diagrams of the systems $NdCl_3-SmCl_3$ and $CeCl_3-SmCl_3$ are reported in Figures B.10 and B.11, respectively.

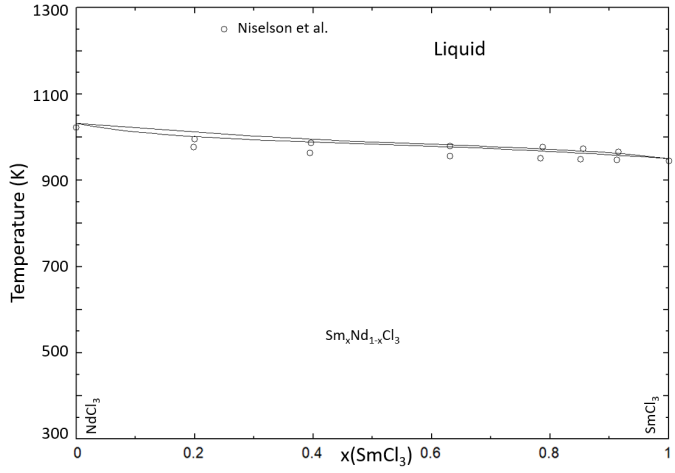


Figure B.10: Phase diagram of the $NdCl_3-SmCl_3$ system calculated with the thermodynamic model in this work. Experimental data from Niselson et al. [7] (open black circles).

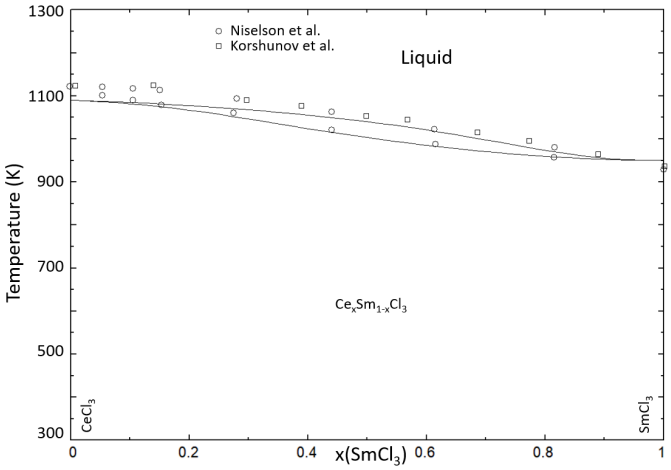


Figure B.11: Phase diagram of the $CeCl_3-SmCl_3$ system calculated with the thermodynamic model in this work. Experimental data on the $LaCl_3-SmCl_3$ from Niselson et al. [7] (open black circles) and Korshunov et al. [10] (open black squares) used as a simulant system.

### B.1.2. MIXING ENTHALPY

The mixing enthalpy of the systems containing $SmCl_3$ modelled in this work is presented in Figure B.12. The data used to fit the mixing enthalpy of the $NaCl-SmCl_3$ system was measured by Dienstbach et al. [11] at 1153 K, and the modelled curve was calculated at the same temperature. Furthermore, Davis' method was used to estimate the mixing enthalpies of the $AECl_2-SmCl_3$ (AE = Mg, Sr, Ba) systems. No data are available for the systems $MCl_3-SmCl_3$ (M = Ce, Nd, Pu, U). Furthermore, the mixing enthalpy of the $SmCl_3-ThCl_4$ system is not shown, as no excess Gibbs energy parameters were necessary to obtain good agreement with the predicted eutectic equilibrium (recall that no $SmCl_3-ThCl_4$ data were available, thus the $PuCl_3-ThCl_4$ system was used as reference point).

A good fit between the experimental or estimated data and the thermodynamic model was obtained through optimization. The mixing enthalpy of the $MCl_3-SmCl_3$ (M = Pu, U, Ce) systems show similar behaviour, *i.e.* all showing a small negative deviation from ideality. The $NdCl_3-SmCl_3$ system, however, is slightly different, showing a positive deviation from ideality. This can be explained by the excess Gibbs energy parameters used to model the solid solution in this system, where positive $L^{11}_{AB}$ terms were needed, meaning that in the liquid model a positive term is also necessary.

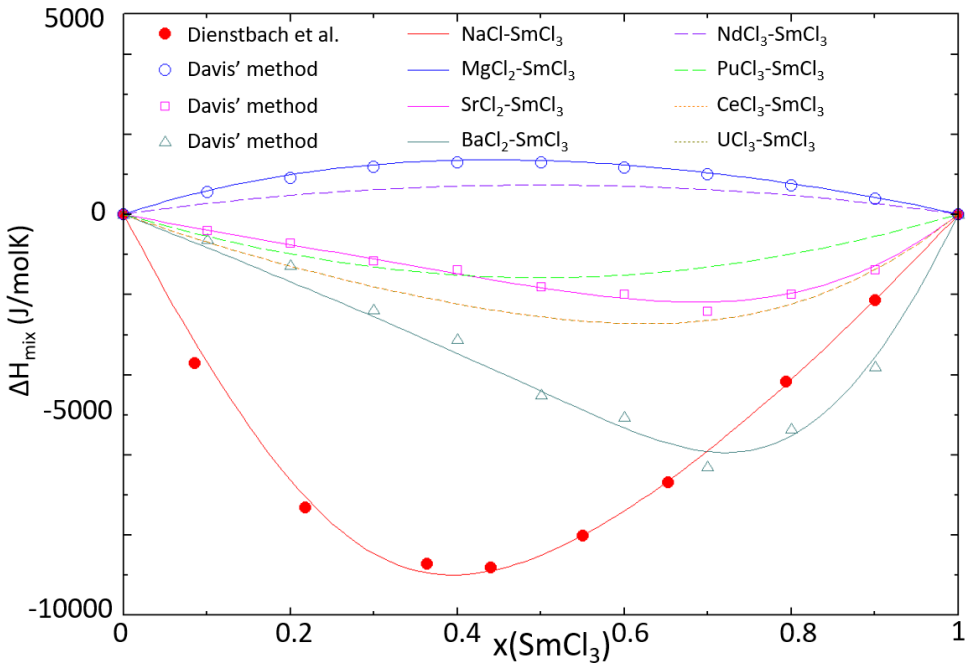


Figure B.12: Mixing enthalpy of the systems NaCl−$SmCl_3$ (solid red line), $MgCl_2$−$SmCl_3$ (solid blue line), $SrCl_2$−$SmCl_3$ (solid pink line), $BaCl_2$−$SmCl_3$ (solid teal line), $NdCl_3$−$SmCl_3$ (dashed purple line), $PuCl_3$−$SmCl_3$ (dashed green line), $CeCl_3$−$SmCl_3$ (dotted orange line) and $UCl_3$−$SmCl_3$ (dotted gold line). The experimental data in the NaCl−$SmCl_3$ system by Dienstbach et al. [11] (closed red circles) and estimated data using Davis' method for the systems $MgCl_2$−$SmCl_3$ (open blue circles), $SrCl_2$−$SmCl_3$ (open pink squares) and $BaCl_2$−$SmCl_3$ (open teal triangles) are shown on top of the calculated values.

## B.2. EQUILIBRIA WITH $YCl_3$

### B.2.1. PHASE DIAGRAM STUDIES

The same considerations that were given to the $SmCl_3$ systems in Section B.1 must be given to $YCl_3$ in order to add it to the thermodynamic model of the fuel system with fission products. To start, the interactions of $YCl_3$ with the base fuel were modelled. The systems NaCl−$YCl_3$, $MgCl_2$−$YCl_3$ and $PuCl_3$−$YCl_3$ have been investigated in the literature by Mochinaga et al. [12] (NaCl−$YCl_3$) and Morozov et al. ($MgCl_2$−$YCl_3$ [13], $NdCl_3$−$YCl_3$ [14]). The system NaCl−$YCl_3$ as interpreted by Mochinaga et al. contains three intermediates in $Na_3YCl_6$, $NaYCl_4$ and $NaY_9Cl_{28}$. Of these intermediates, the first two have been characterised by XRD by Wickleder et al. [15] and Liao et al. [16], respectively. The latter, while no crystal structure is reported in the literature, fits the experimentally determined invariant equilibria very well, and was therefore retained from the assessment of Mochinaga et al. [12]. The calculated phase diagram of the NaCl−$YCl_3$ system is presented in Figure B.13.

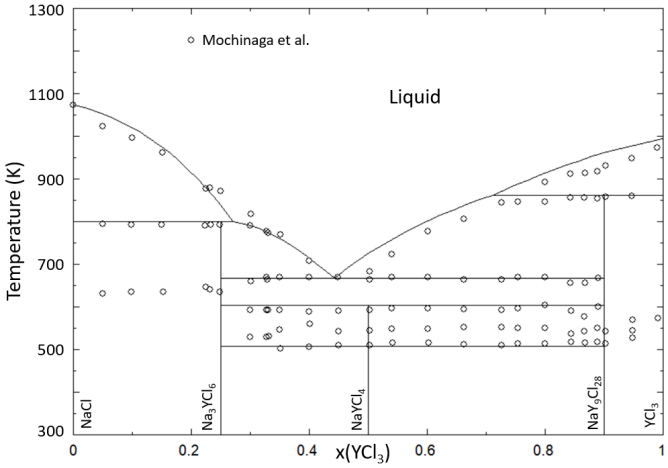


Figure B.13: Phase diagram of the $NaCl-YCl_3$ system calculated with the thermodynamic model in this work. Experimental data from Mochinaga et al. [12] (open black circles).

The $MgCl_2-YCl_3$ and $PuCl_3-YCl_3$ systems as investigated by Morozov et al. [13, 14] are presented in Figures B.14 and B.15, respectively. In their assessment of the $MgCl_2-YCl_3$ system, Morozov et al. suggested the existence of an intermediate $Mg_3Y_2Cl_{12}$ to account for unexplained sub-solidus equilibria they observed upon cooling. In their assessment of the $NdCl_3-YCl_3$ system, they observed partial mutual solubility of the end-members, but still a system of the eutectic type. Both assessments of Morozov et al. were retained when constructing the thermodynamic models.

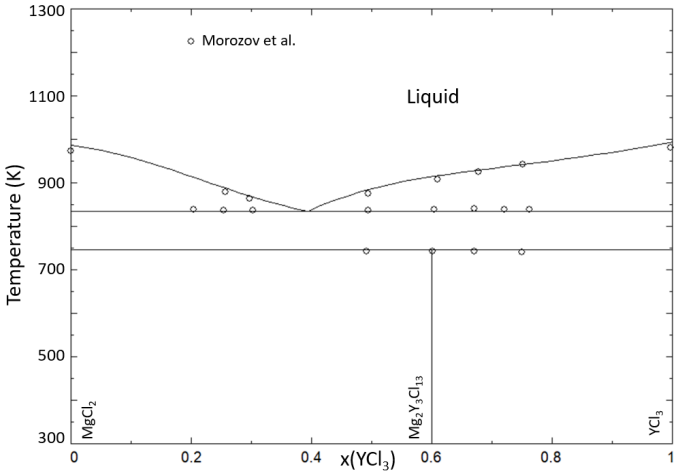


Figure B.14: Phase diagram of the $MgCl_2-YCl_3$ system calculated with the thermodynamic model in this work. Experimental data from Morozov et al. [13] (open black circles).

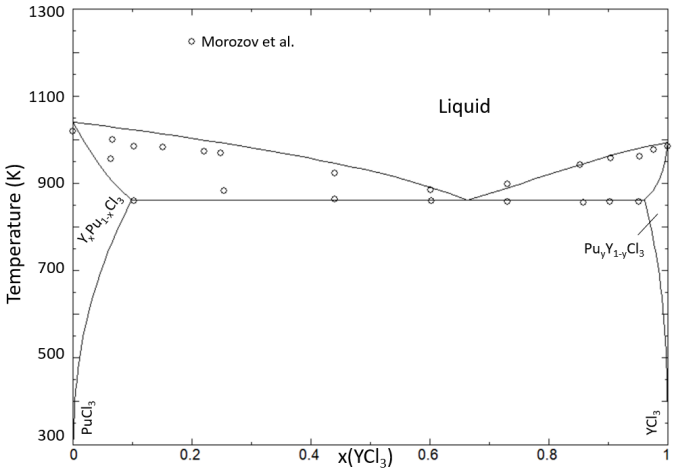


Figure B.15: Phase diagram of the $PuCl_3-YCl_3$ system calculated with the thermodynamic model in this work. Experimental data on the $NdCl_3-YCl_3$ system from Morozov et al. [14] (open black circles).

Aside from the interactions of $YCl_3$ with the molten salt fuel $NaCl-MgCl_2-PuCl_3$, the interactions with $UCl_3$ and $ThCl_4$ must be modelled so that other fuel assemblies may be investigated as well. As explained in Section B.1, due to the lack of data on the $YCl_3-ThCl_4$ system or similar systems, the eutectic composition and temperature of the $PuCl_3-ThCl_4$ system are used as a simulant for modeling the interactions between $YCl_3$ and $ThCl_4$. Like with the $SmCl_3$ system, the system $YCl_3-LaCl_3$ serves as a simulant system in the absence of experimental data on either the $YCl_3-UCl_3$ or $YCl_3-CeCl_3$ systems. The calculated phase diagrams of $YCl_3-ThCl_4$ and $YCl_3-UCl_3$ are presented in Figures B.16 and B.17.

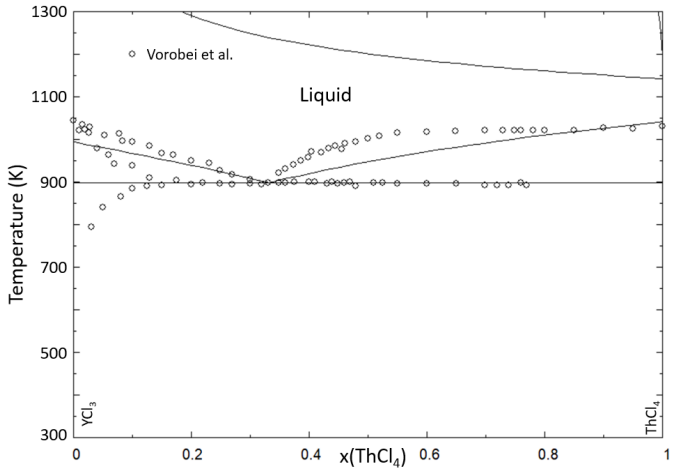


Figure B.16: Phase diagram of the $YCl_3-ThCl_4$ system calculated with the thermodynamic model in this work. Experimental data on the $PuCl_3-ThCl_4$ system from Vorobei et al. [6] (open black circles).

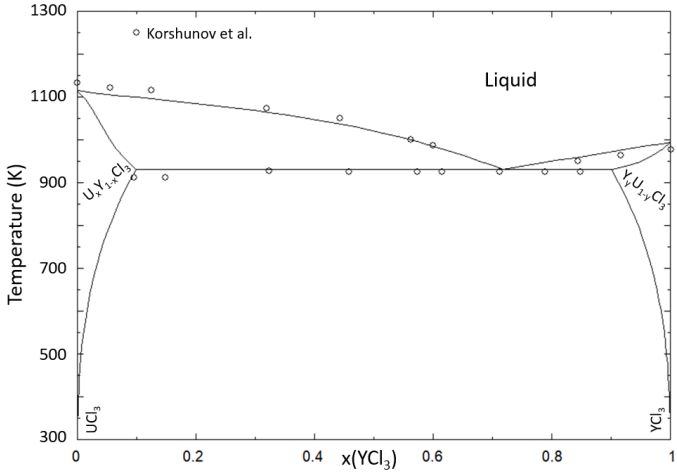


Figure B.17: Phase diagram of the $YCl_3-UCl_3$ system calculated with the thermodynamic model in this work. Experimental data on the $YCl_3-LaCl_3$ system from Korshunov et al. [10] (open black circles).

Finally, to be able to include $YCl_3$ in the application calculations, the interactions between $YCl_3$ and other fission products must be modelled. For this, the binary systems $SrCl_2-YCl_3$, $BaCl_2-YCl_3$, $CeCl_3-YCl_3$, $NdCl_3-YCl_3$ and $SmCl_3-YCl_3$ systems have been modelled.

No experimental investigation of invariant equilibria in the $SrCl_2-YCl_3$ system has been reported in the literature. For this reason, the experimental data for the $SrCl_2-SmCl_3$ system was used as simulant system, as Figure B.5 shows a reasonable similarity between the two systems. However, in the absence of further experimental data, the original assessment of Blachnik et al. [7] of this system (*i.e.* with intermediate $Sr_2SmCl_7$) is retained for the modelling of the $SrCl_2-YCl_3$ system. The phase diagram of this system is presented in Figure B.18.

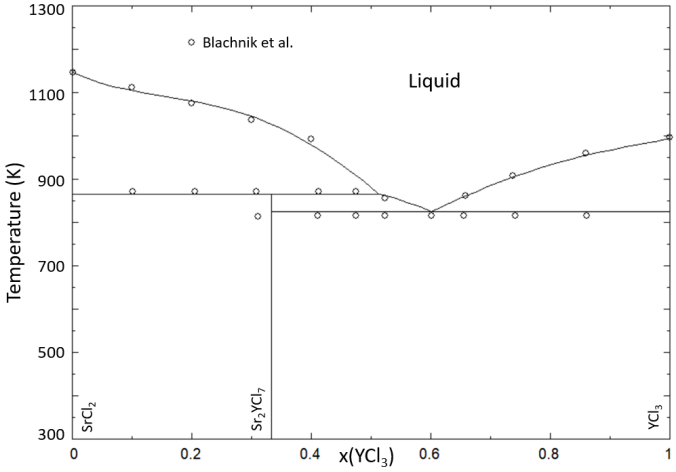


Figure B.18: Phase diagram of the $SrCl_2-YCl_3$ system calculated with the thermodynamic model in this work. Experimental data on the $SrCl_2-SmCl_3$ system from Blachnik et al. [7] (open black circles). The existence of intermediate $Sr_2YCl_7$ is based on the assessment of Blachnik et al., who identified the intermediate $Sr_2SmCl_7$ in their work.

The system $BaCl_2-YCl_3$ has been investigated experimentally by Morozov et al. [8]. Morozov et al. identified the intermediate $Ba_3YCl_9$ in their assessment of the system based on their DTA data, however they report no crystallographic investigation. Wickleder et al. [17] report an intermediate in this system with composition $Ba_2YCl_7$ instead, which also fits the experimental data on the invariant equilibria presented by Morozov et al. [8]. Seeing as Wickleder et al. present a crystallographic basis for their suggested intermediate, their assessment is retained in the phase diagram in Figure B.19.

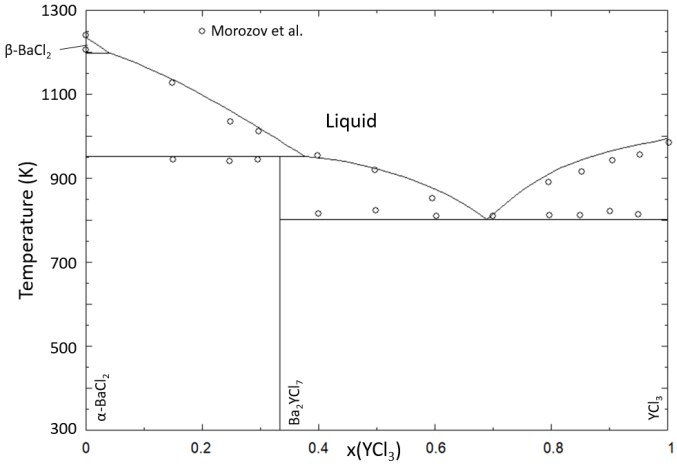


Figure B.19: Phase diagram of the $BaCl_2-YCl_3$ system calculated with the thermodynamic model in this work. Experimental data from Morozov et al. [8] (open black circles). The existence of intermediate $Ba_2YCl_7$ is taken from Wickleder et al. [17].

The interactions of $YCl_3$ with other rare-earth element trichlorides has been modelled based on data from the literature. The systems $NdCl_3$−$YCl_3$ and $SmCl_3$−$YCl_3$ have been reported by [14] and [10] respectively. No experimental data on the system $CeCl_3$−$YCl_3$ has been reported, so the system $LaCl_3$−$YCl_3$ is used as a simulant for this system. The phase diagrams of the systems $NdCl_3$−$YCl_3$, $CeCl_3$−$YCl_3$ and $YCl_3$−$SmCl_3$ are shown in Figures B.20-B.22.

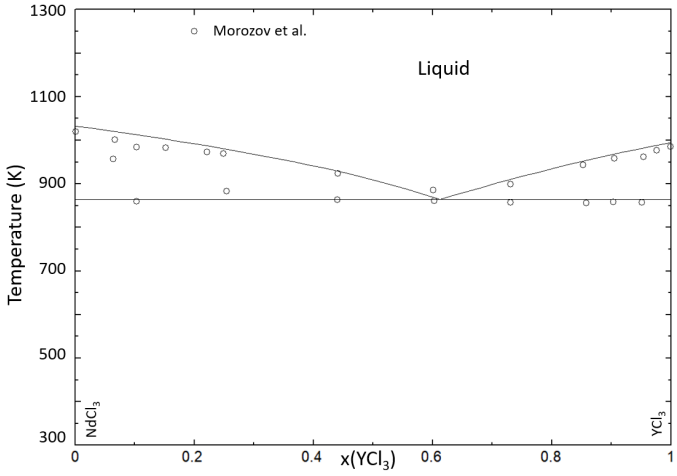


Figure B.20: Phase diagram of the $NdCl_3$−$YCl_3$ system calculated with the thermodynamic model in this work. Experimental data from Morozov et al. [14] (open black circles).

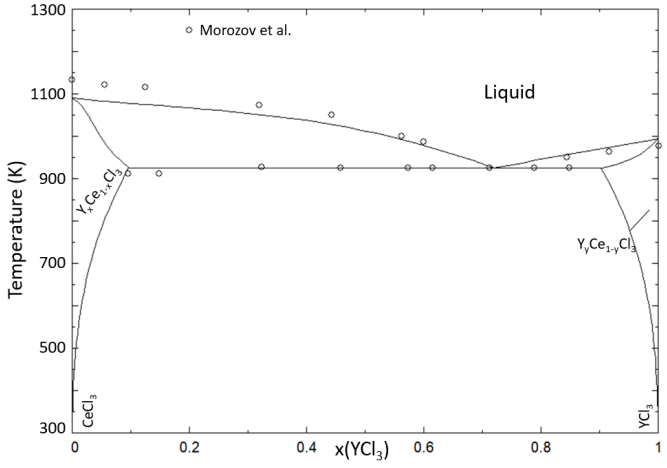


Figure B.21: Phase diagram of the $CeCl_3$−$YCl_3$ system calculated with the thermodynamic model in this work. Experimental data on the $LaCl_3$−$YCl_3$ system from Korshunov et al. [10] (open black circles).

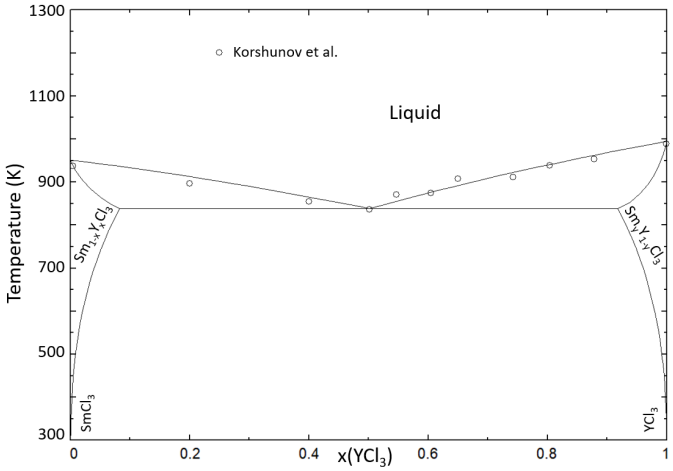


Figure B.22: Phase diagram of the $YCl_3-SmCl_3$ system calculated with the thermodynamic model in this work. Experimental data from Korshunov et al. [10] (open black circles).

### B.2.2. MIXING ENTHALPY

The mixing enthalpy of the systems containing $YCl_3$ modelled in this work is presented in Figure B.12. The data used to fit the mixing enthalpy of the $NaCl-YCl_3$ system was measured by Papatheodorou et al. [18] at 1143 K, and the modelled curve was calculated at the same temperature. Furthermore, Davis' method was used to estimate the mixing enthalpies of the $AECl_2-YCl_3$ (AE = Mg, Sr, Ba) systems. No data are available for the systems $MCl_3-YCl_3$ (M = Ce, Nd, Sm, Pu, U). Furthermore, the mixing enthalpy of the $YCl_3-ThCl_4$ system is not shown, as no excess Gibbs energy parameters were necessary to obtain good agreement with the predicted eutectic equilibrium, like in the $SmCl_3-ThCl_4$ system.

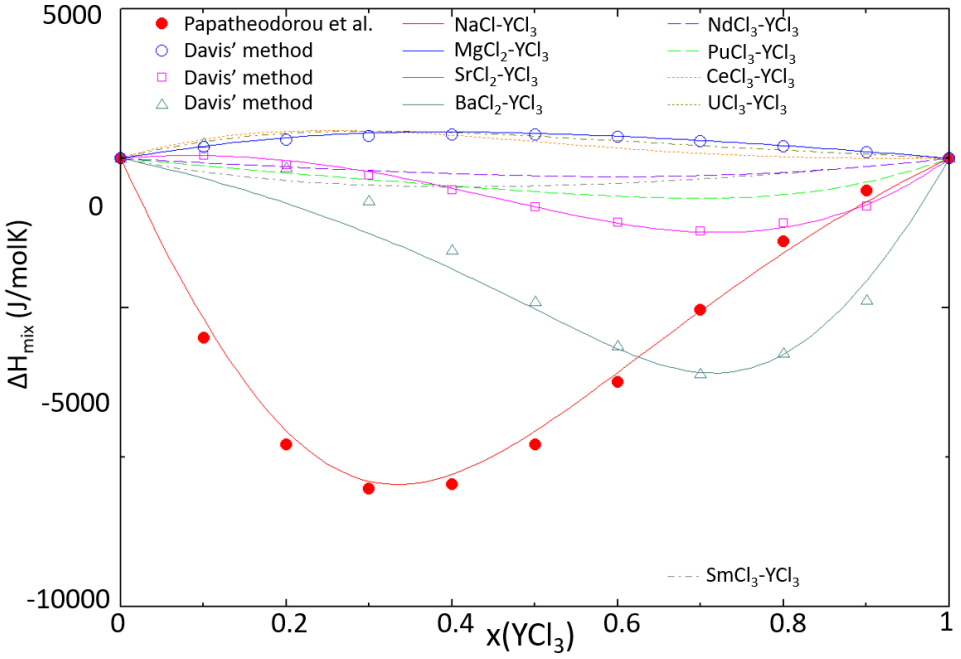


Figure B.23: Mixing enthalpy of the systems NaCl−$YCl_3$ (solid red line), $MgCl_2$−$YCl_3$ (solid blue line), $SrCl_2$−$YCl_3$ (solid pink line), $BaCl_2$−$YCl_3$ (solid teal line), $NdCl_3$−$YCl_3$ (dashed purple line), $PuCl_3$−$YCl_3$ (dashed green line), $CeCl_3$−$YCl_3$ (dotted orange line), $UCl_3$−$YCl_3$ (dotted gold line) and $SmCl_3$−$YCl_3$ (dotted grey line). The experimental data in the NaCl−$SmCl_3$ system by Papatheodorou et al. [18] (closed red circles) and estimated data using Davis' method for the systems $MgCl_2$−$YCl_3$ (open blue circles), $SrCl_2$−$YCl_3$ (open pink squares) and $BaCl_2$−$YCl_3$ (open teal triangles) is shown on top of the calculated values.

# C

# XRD REFINEMENTS

In this chapter, the XRD refinements that have been performed to support various molten salt systems are presented.

## C.1. CHAPTER 7

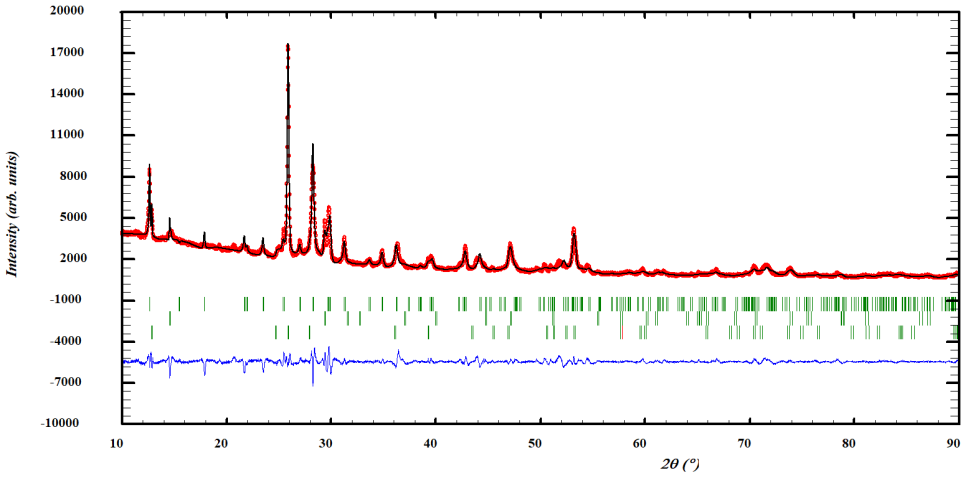


Figure C.1: Profile refinement of the synthesised sample as x($NdCl_3$) = 0.2 in the $MgI_2$—$NdCl_3$ system. The phases present in the sample are $NdCl_{3-3x}I_{3x}$, $MgCl_{2y}I_{2-2y}$ and $MgCl_{2-2x}I_{2x}$. The observed intensity (red circles) is shown alongside the calculated intensity (black line), and the difference between the two is shown (blue line). The angles at which reflections occur, i.e. the bragg positions, are shown as well (green, vertical lines).

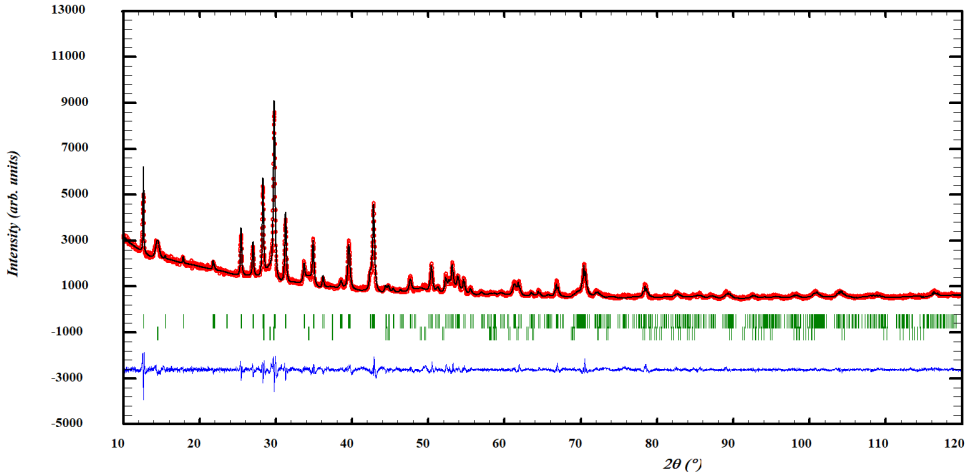


Figure C.3: Profile refinement of the synthesised sample as x($NdI_3$) = 0.40 in the $MgCl_2$—$NdI_3$ system. The phases identified in the sample are $NdCl_{3y}I_{3-3y}$ and $MgCl_{2-2x}I_{2x}$. The observed intensity (red circles) is shown alongside the calculated intensity (black line), and the difference between the two is shown (blue line). The angles at which reflections occur, i.e. the bragg positions, are shown as well (green, vertical lines).

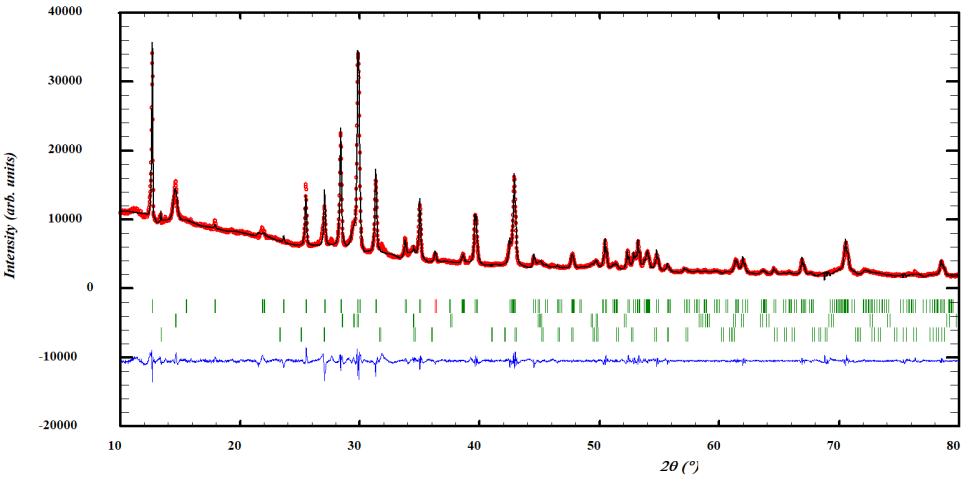


Figure C.2: Profile refinement of the synthesised sample as x($NdCl_3$) = 0.42 in the $MgI_2$—$NdCl_3$ system. The phases present in the sample are $NdCl_{3-3x}I_{3x}$, $NdCl_{3y}I_{3-3y}$ and $MgCl_{2y}I_{2-2y}$. The observed intensity (red circles) is shown alongside the calculated intensity (black line), and the difference between the two is shown (blue line). The angles at which reflections occur, i.e. the bragg positions, are shown as well (green, vertical lines).

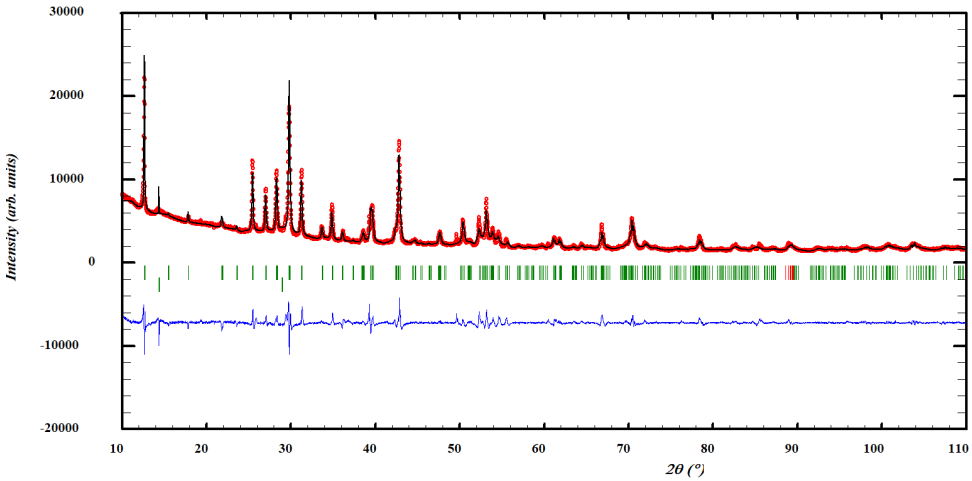


Figure C.4: Profile refinement of the synthesised sample as x($NdI_3$) = 0.40 in the $MgCl_2$−$NdI_3$ system. The phases identified in the sample are $NdCl_{3y}I_{3-3y}$ and $MgCl_{2-2x}I_{2x}$. The observed intensity (red circles) is shown alongside the calculated intensity (black line), and the difference between the two is shown (blue line). The angles at which reflections occur, i.e. the bragg positions, are shown as well (green, vertical lines).

# D

# PHASE EQUILIBRIA MEASUREMENTS

## D.1. CHAPTER 4

Table D.1: Equilibrium data in the $BaCl_2-CeCl_3$ system as measured by DSC

| $x_{CeCl_3}$ [a] | T (K) [b] | Equilibrium | Equilibrium reaction |
|---|---|---|---|
| 0 | 1197 | $\alpha$-$\beta$ transition | $\alpha$-$BaCl_2$ = $\beta$-$BaCl_2$ |
| | 1235 | Congruent melting | $\beta$-$BaCl_2$ = L |
| 0.024 | 1164 | Unknown | - |
| | 1196 | Solidus | $\alpha$-$BaCl_2$+ $Ba_{1-x}Ce_xCl_{2+x}$ = $Ba_{1-x}Ce_xCl_{2+x}$ |
| | 1237 | Liquidus | $Ba_{1-x}Ce_xCl_{2+x}$ = L |
| 0.037 | 1176 | Solidus | $\alpha$-$BaCl_2$ + $Ba_{1-x}Ce_xCl_{2+x}$ = $Ba_{1-x}Ce_xCl_{2+x}$ |
| | 1235 | Liquidus | $Ba_{1-x}Ce_xCl_{2+x}$ + L' = L |
| 0.060 | 952 | Eutectoid | $\alpha$-$BaCl_2$ + $Ba_3Ce_2Cl_{12}$ = $Ba_{1-x}Ce_xCl_{2+x}$ |
| | 1147 | Solidus | $\alpha$-$BaCl_2$ + $Ba_{1-x}Ce_xCl_{2+x}$ = $Ba_{1-x}Ce_xCl_{2+x}$ |
| | 1239 | Liquidus | $Ba_{1-x}Ce_xCl_{2+x}$ + L' = L |
| 0.075 | 943 | Eutectoid | $\alpha$-$BaCl_2$ + $Ba_3Ce_2Cl_{12}$ = $Ba_{1-x}Ce_xCl_{2+x}$ |
| | 1235 | Liquidus | $Ba_{1-x}Ce_xCl_{2+x}$ + L' = L |
| 0.098 | 944 | Eutectoid | $\alpha$-$BaCl_2$ + $Ba_3Ce_2Cl_{12}$ = $Ba_{1-x}Ce_xCl_{2+x}$ |
| | 1236 | Liquidus | $Ba_{1-x}Ce_xCl_{2+x}$ + L' = L |
| 0.126 | 943 | Eutectoid | $\alpha$-$BaCl_2$ + $Ba_3Ce_2Cl_{12}$ = $Ba_{1-x}Ce_xCl_{2+x}$ |
| | 1235 | Liquidus | $Ba_{1-x}Ce_xCl_{2+x}$ + L' = L |
| 0.170 | 944 | Eutectoid | $\alpha$-$BaCl_2$ + $Ba_3Ce_2Cl_{12}$ = $Ba_{1-x}Ce_xCl_{2+x}$ |
| | 966 | Unknown | - |
| | 1233 | Liquidus | $Ba_{1-x}Ce_xCl_{2+x}$ + L' = L |
| 0.175 | 943 | Eutectoid | $\alpha$-$BaCl_2$ + $Ba_3Ce_2Cl_{12}$ = $Ba_{1-x}Ce_xCl_{2+x}$ |
| | 1197 | Unknown | - |
| | 1225 | Liquidus | $Ba_{1-x}Ce_xCl_{2+x}$ + L' = L |
| 0.199 | 1217 | Liquidus | $Ba_{1-x}Ce_xCl_{2+x}$ + L' = L |
| 0.200 | 945 | Eutectoid | $\alpha$-$BaCl_2$ + $Ba_3Ce_2Cl_{12}$ = $Ba_{1-x}Ce_xCl_{2+x}$ |
| | 1064 | Unknown | - |
| | 1233 | Liquidus | $Ba_{1-x}Ce_xCl_{2+x}$ + L' = L |

Continued on next page

**Table D.1 – continued from previous page**

| $x_{CeCl_3}$ [a] | T (K) [b] | Equilibrium | Equilibrium reaction |
|---|---|---|---|
| 0.249 | 944 | Eutectoid | $\alpha$-$BaCl_2 + Ba_3Ce_2Cl_{12} = Ba_{1-x}Ce_xCl_{2+x}$ |
| | 1082 | Solidus | $Ba_{1-x}Ce_xCl_{2+x} = Ba_{1-x}Ce_xCl_{2+x} + L'$ |
| | 1227 | Liquidus | $Ba_{1-x}Ce_xCl_{2+x} + L' = L$ |
| 0.278 | 1057 | Peritectic | $Ba_3Ce_2Cl_{12} = Ba_{1-x}Ce_xCl_{2+x} + L'$ |
| | 1174 | Liquidus | $Ba_{1-x}Ce_xCl_{2+x} + L' = L$ |
| 0.3 | 1066 | Peritectic | $Ba_3Ce_2Cl_{12} = Ba_{1-x}Ce_xCl_{2+x} + L'$ |
| | 1163 | Liquidus | $Ba_{1-x}Ce_xCl_{2+x} + L' = L$ |
| 0.336 | 1069 | Peritectic | $Ba_3Ce_2Cl_{12} = Ba_{1-x}Ce_xCl_{2+x} + L'$ |
| | 1139 | Liquidus | $Ba_{1-x}Ce_xCl_{2+x} + L' = L$ |
| 0.347 | 1053 | Unknown | - |
| | 1072 | Peritectic | $Ba_3Ce_2Cl_{12} = Ba_{1-x}Ce_xCl_{2+x} + L'$ |
| | 1113 | Liquidus | $Ba_{1-x}Ce_xCl_{2+x} + L' = L$ |
| 0.39 | 1052 | Unknown | |
| | 1077 | Peritectic | $Ba_3Ce_2Cl_{12} = Ba_{1-x}Ce_xCl_{2+x} + L'$ |
| 0.4 | 960 | Eutectic | $Ca_{1-y}Ba_yCl_{3-y} + Ba_3Ce_2Cl_{12} = L$ |
| | 1062 | Peritectic | $Ba_3Ce_2Cl_{12} = Ba_{1-x}Ce_xCl_{2+x} + L'$ |
| | 1080 | Liquidus | $Ba_{1-x}Ce_xCl_{2+x} + L' = L$ |
| 0.444 | 942 | Eutectic | $Ca_{1-y}Ba_yCl_{3-y} + Ba_3Ce_2Cl_{12} = L$ |
| | 1043 | Unknown | - |
| | 1067 | Liquidus | $Ba_3Ce_2Cl_{12} + L' = L$ |
| 0.5 | 962 | Unknown | - |
| | 965 | Eutectic | $Ca_{1-y}Ba_yCl_{3-y} + Ba_3Ce_2Cl_{12} = L$ |
| | 1058 | Liquidus | $Ba_3Ce_2Cl_{12} + L' = L$ |
| 0.573 | 969 | Eutectic | $Ca_{1-y}Ba_yCl_{3-y} + Ba_3Ce_2Cl_{12} = L$ |
| | 1025 | Liquidus | $Ba_3Ce_2Cl_{12} + L' = L$ |
| 0.616 | 975 | Eutectic | $Ca_{1-y}Ba_yCl_{3-y} + Ba_3Ce_2Cl_{12} = L$ |
| | 986 | Liquidus | $Ba_3Ce_2Cl_{12} + L' = L$ |
| 0.655 | 979 | Liquidus | $Ba_3Ce_2Cl_{12} + L' = L$ |
| 0.699 | 971 | Eutectic | $Ca_{1-y}Ba_yCl_{3-y} + Ba_3Ce_2Cl_{12} = L$ |
| | 1003 | Liquidus | $Ca_{1-y}Ba_yCl_{3-y} + L' = L$ |
| 0.779 | 967 | Eutectic | $Ca_{1-y}Ba_yCl_{3-y} + Ba_3Ce_2Cl_{12} = L$ |
| | 1032 | Liquidus | $Ca_{1-y}Ba_yCl_{3-y} + L' = L$ |
| 0.905 | 968 | Eutectic | $Ca_{1-y}Ba_yCl_{3-y} + Ba_3Ce_2Cl_{12} = L$ |
| | 1073 | Liquidus | $Ca_{1-y}Ba_yCl_{3-y} + L' = L$ |
| 0.95 | 959 | Solidus | $Ba_3Ce_2Cl_{12} + Ca_{1-y}Ba_yCl_{3-y} = Ca_{1-y}Ba_yCl_{3-y}$ |
| | 1084 | Liquidus | $Ca_{1-y}Ba_yCl_{3-y} + L' = L$ |
| 0.973 | 946 | Solidus | $Ba_3Ce_2Cl_{12} + Ca_{1-y}Ba_yCl_{3-y} = Ca_{1-y}Ba_yCl_{3-y}$ |
| | 1089 | Liquidus | $Ca_{1-y}Ba_yCl_{3-y} + L' = L$ |
| 1 | 1087 | Congruent melting | $CeCl_3 = L$ |

[a] The uncertainties on compositions $x_{CeCl3}$ are ±0.005.

[b] The uncertainties on temperatures are ±5 K for pure end-members and ±10 K for mixtures.

| $x_{NdCl_3}$ [a] | T (K) [b] | Equilibrium | Equilibrium reaction |
|---|---|---|---|
| 0 | 1235 | Congruent Melting | $\beta$-$BaCl_2$ = L |
| | 1198 | $\alpha$-$\beta$ transition | $\alpha$-$BaCl_2$ = $\beta$-$BaCl_2$ |
| 0.06 | 1234 | Liquidus | $Ba_{1-x}Nd_xCl_{2+x}$ + L′ = L |
| | 1134 | Solidus | $\alpha$-$BaCl_2$ + $Ba_{1-x}Nd_xCl_{2+x}$ = $Ba_{1-x}Nd_xCl_{2+x}$ |
| | 941 | Eutectoid | $\alpha$-$BaCl_2$ + $Ba_3Nd_2Cl_{12}$ = $Ba_{1-x}Nd_xCl_{2+x}$ |
| 0.148 | 1202 | Liquidus | $Ba_{1-x}Nd_xCl_{2+x}$ + L′ = L |
| | 939 | Eutectoid | $\alpha$-$BaCl_2$ + $Ba_3Nd_2Cl_{12}$ = $Ba_{1-x}Nd_xCl_{2+x}$ |
| 0.207 | 1172 | Liquidus | $Ba_{1-x}Nd_xCl_{2+x}$ + L′ = L |
| | 1020 | Peritectic | $Ba_3Nd_2Cl_{12}$ = $Ba_{1-x}Nd_xCl_{2+x}$ + L′ |
| | 939 | Eutectoid | $\alpha$-$BaCl_2$ + $Ba_3Nd_2Cl_{12}$ = $Ba_{1-x}Nd_xCl_{2+x}$ |
| 0.249 | 1153 | Liquidus | $Ba_{1-x}Nd_xCl_{2+x}$ + L′ = L |
| | 1023 | Peritectic | $Ba_3Nd_2Cl_{12}$ = $Ba_{1-x}Nd_xCl_{2+x}$ + L′ |
| | 939 | Eutectoid | $\alpha$-$BaCl_2$ + $Ba_3Nd_2Cl_{12}$ = $Ba_{1-x}Nd_xCl_{2+x}$ |
| 0.265 | 1132 | Liquidus | $Ba_{1-x}Nd_xCl_{2+x}$ + L′ = L |
| | 1024 | Peritectic | $Ba_3Nd_2Cl_{12}$ = $Ba_{1-x}Nd_xCl_{2+x}$ + L′ |
| | 938 | Eutectoid | $\alpha$-$BaCl_2$ + $Ba_3Nd_2Cl_{12}$ = $Ba_{1-x}Nd_xCl_{2+x}$ |
| 0.305 | 1113 | Liquidus | $Ba_{1-x}Nd_xCl_{2+x}$ + L′ = L |
| | 1031 | Peritectic | $Ba_3Nd_2Cl_{12}$ = $Ba_{1-x}Nd_xCl_{2+x}$ + L′ |
| 0.370 | 1045 | Liquidus | $Ba_{1-x}Nd_xCl_{2+x}$ + L′ = L |
| | 1018 | Peritectic | $Ba_3Nd_2Cl_{12}$ = $Ba_{1-x}Nd_xCl_{2+x}$ + L′ |
| 0.380 | 1043 | Liquidus | $Ba_{1-x}Nd_xCl_{2+x}$ + L′ = L |
| | 1017 | Peritectic | $Ba_3Nd_2Cl_{12}$ = $Ba_{1-x}Nd_xCl_{2+x}$ + L′ |
| 0.391 | 1039 | Liquidus | $Ba_{1-x}Nd_xCl_{2+x}$ + L′ = L |
| | 1019 | Peritectic | $Ba_3Nd_2Cl_{12}$ = $Ba_{1-x}Nd_xCl_{2+x}$ + L′ |
| | 893 | Eutectic | $Ba_3Nd_2Cl_{12}$ + $Nd_{1-y}Ba_yCl_{3-y}$ = L |
| 0.405 | 1035 | Liquidus | $Ba_{1-x}Nd_xCl_{2+x}$ + L′ = L |
| | 1015 | Peritectic | $Ba_3Nd_2Cl_{12}$ = $Ba_{1-x}Nd_xCl_{2+x}$ + L′ |
| | 894 | Eutectic | $Ba_3Nd_2Cl_{12}$ + $Nd_{1-y}Ba_yCl_{3-y}$ = L |
| 0.41 | 1018 | Peritectic | $Ba_3Nd_2Cl_{12}$ = $Ba_{1-x}Nd_xCl_{2+x}$ + L′ |
| | 908 | Eutectic | $Ba_3Nd_2Cl_{12}$ + $Nd_{1-y}Ba_yCl_{3-y}$ = L |
| 0.431 | 896 | Eutectic | $Ba_3Nd_2Cl_{12}$ + $Nd_{1-y}Ba_yCl_{3-y}$ = L |
| 0.498 | 1010 | Liquidus | $Ba_3Nd_2Cl_{12}$ + L′ = L |
| | 910 | Eutectic | $Ba_3Nd_2Cl_{12}$ + $Nd_{1-y}Ba_yCl_{3-y}$ = L |
| 0.55 | 989 | Liquidus | $Ba_3Nd_2Cl_{12}$ + L′ = L |
| | 912 | Eutectic | $Ba_3Nd_2Cl_{12}$ + $Nd_{1-y}Ba_yCl_{3-y}$ = L |
| 0.600 | 924 | Liquidus | $Nd_{1-y}Ba_yCl_{3-y}$ + L′ = L |
| | 899 | Eutectic | $Ba_3Nd_2Cl_{12}$ + $Nd_{1-y}Ba_yCl_{3-y}$ = L |
| 0.674 | 912 | Eutectic | $Ba_3Nd_2Cl_{12}$ + $Nd_{1-y}Ba_yCl_{3-y}$ = L |
| 0.753 | 962 | Liquidus | $Nd_{1-y}Ba_yCl_{3-y}$ + L′ = L |
| | 902 | Eutectic | $Ba_3Nd_2Cl_{12}$ + $Nd_{1-y}Ba_yCl_{3-y}$ = L |
| 0.850 | 1000 | Liquidus | $Nd_{1-y}Ba_yCl_{3-y}$ + L′ = L |
| | 915 | Eutectic | $Ba_3Nd_2Cl_{12}$ + $Nd_{1-y}Ba_yCl_{3-y}$ = L |
| | 899 | Unknown | - |
| 0.948 | 1026 | Liquidus | $Nd_{1-y}Ba_yCl_{3-y}$ + L′ = L |
| | 904 | Eutectic | $Nd_{1-y}Ba_yCl_{3-y}$ = L |
| | 897 | Solidus | $Ba_3Nd_2Cl_{12}$ + $Nd_{1-y}Ba_yCl_{3-y}$ = $Nd_{1-y}Ba_yCl_{3-y}$ |
| 0.969 | 1030 | Liquidus | $Nd_{1-y}Ba_yCl_{3-y}$ + L′ = L |
| | 970 | Solidus | $Nd_{1-y}Ba_yCl_{3-y}$ = $Nd_{1-y}Ba_yCl_{3-y}$ + L′ |
| | 894 | Solidus | $Ba_3Nd_2Cl_{12}$ + $Nd_{1-y}Ba_yCl_{3-y}$ = $Nd_{1-y}Ba_yCl_{3-y}$ |

Table D.2: Equilibrium data in the $BaCl_2$−$NdCl_3$ system as measured by DSC.
[a] The uncertainties on compositions $x_{NdCl3}$ are ±0.005.
[b] The uncertainties on temperatures are ±5 K for pure end-members and ±10 K for mixtures.

| $x(NdCl_3)$[a] | T (K)[b] | Equilibrium | Equilibrium reaction |
|---|---|---|---|
| 0 | 1147 | Congruent Melting | $SrCl_2 = L$ |
| 0.100 | 1123 | Liquidus | $Sr_{1-x}Nd_xCl_{2+x} + L' = L$ |
| 0.150 | 1104 | Liquidus | $Sr_{1-x}Nd_xCl_{2+x} + L' = L$ |
| 0.203 | 1075 | Liquidus | $Sr_{1-x}Nd_xCl_{2+x} + L' = L$ |
| 0.229 | 1064 | Liquidus | $Sr_{1-x}Nd_xCl_{2+x} + L' = L$ |
| | 897 | Peritectic | $Sr_9Nd_5Cl_{33} = Sr_{1-x}Nd_xCl_{2+x} + L'$ |
| 0.251 | 1045 | Liquidus | $Sr_{1-x}Nd_xCl_{2+x} + L' = L$ |
| | 883 | Peritectic | $Sr_9Nd_5Cl_{33} = Sr_{1-x}Nd_xCl_{2+x} + L'$ |
| 0.269 | 1037 | Liquidus | $Sr_{1-x}Nd_xCl_{2+x} + L' = L$ |
| | 894 | Peritectic | $Sr_9Nd_5Cl_{33} = Sr_{1-x}Nd_xCl_{2+x} + L'$ |
| 0.359 | 981 | Liquidus | $Sr_{1-x}Nd_xCl_{2+x} + L' = L$ |
| | 894 | Peritectic | $Sr_9Nd_5Cl_{33} = Sr_{1-x}Nd_xCl_{2+x} + L'$ |
| | 872 | Eutectic | $Sr_9Nd_5Cl_{33} + Nd_{1-y}Sr_yCl_{3-y} = L$ |
| 0.449 | 910 | Liquidus | $Sr_{1-x}Nd_xCl_{2+x} + L' = L$ |
| | 883 | Peritectic | $Sr_9Nd_5Cl_{33} = Sr_{1-x}Nd_xCl_{2+x} + L'$ |
| | 874 | Eutectic | $Sr_9Nd_5Cl_{33} + Nd_{1-y}Sr_yCl_{3-y} = L$ |
| 0.530 | 885 | Eutectic | $Sr_9Nd_5Cl_{33} + Nd_{1-y}Sr_yCl_{3-y} = L$ |
| 0.570 | 873 | Eutectic | $Sr_9Nd_5Cl_{33} + Nd_{1-y}Sr_yCl_{3-y} = L$ |
| 0.599 | 919 | Liquidus | $Nd_{1-y}Sr_yCl_{3-y} + L' = L$ |
| | 874 | Eutectic | $Sr_9Nd_5Cl_{33} + Nd_{1-y}Sr_yCl_{3-y} = L$ |
| 0.699 | 955 | Liquidus | $Nd_{1-y}Sr_yCl_{3-y} + L' = L$ |
| | 875 | Eutectic | $Sr_9Nd_5Cl_{33} + Nd_{1-y}Sr_yCl_{3-y} = L$ |
| 0.899 | 1009 | Liquidus | $Nd_{1-y}Sr_yCl_{3-y} + L' = L$ |
| | 874 | Eutectic | $Sr_9Nd_5Cl_{33} + Nd_{1-y}Sr_yCl_{3-y} = L$ |
| 0.948 | 1019 | Liquidus | $Nd_{1-y}Sr_yCl_{3-y} + L' = L$ |
| | 868 | Eutectic | $Sr_9Nd_5Cl_{33} + Nd_{1-y}Sr_yCl_{3-y} = L$ |
| 1 | 1031 | Congruent Melting | $NdCl_3 = L$ |

Table D.3: Equilibrium data in the $SrCl_2-NdCl_3$ system as measured by DSC.
[a] The uncertainties on compositions $x_{NdCl3}$ are ±0.005.
[b] The uncertainties on temperatures are ±5 K for pure end-members and ±10 K for mixtures.

| $x(CeCl_3)$ [a] | T (K) [b] | Equilibrium | Equilibrium reaction |
|---|---|---|---|
| 0 | 1143.93 | Congruent melting | $SrCl_2 = L$ |
| 0.05 | 1149 | Liquidus | $Sr_{1-x}Ce_xCl_{2+x} = L$ |
| 0.099 | 1159 | Liquidus | $Sr_{1-x}Ce_xCl_{2+x} = L$ |
| 0.15 | 1133 | Liquidus | $Sr_{1-x}Ce_xCl_{2+x} = L$ |
| 0.199 | 1144 | Liquidus | $Sr_{1-x}Ce_xCl_{2+x} = L$ |
| | 912 | Peritectic | $Sr_9Ce_5Cl_{33} = Sr_{1-x}Ce_xCl_{2+x} + Ce_{1-y}Sr_yCl_{3-y}$ |
| 0.236 | 915 | Peritectic | $Sr_9Ce_5Cl_{33} = Sr_{1-x}Ce_xCl_{2+x} + Ce_{1-y}Sr_yCl_{3-y}$ |
| 0.3 | 1090 | Liquidus | $Sr_{1-x}Ce_xCl_{2+x} = L$ |
| 0.357 | 924 | Eutectic | $Sr_{1-x}Ce_xCl_{2+x} + Ce_{1-y}Sr_yCl_{3-y} = L$ |
| | 908 | Peritectic | $Sr_9Ce_5Cl_{33} = Sr_{1-x}Ce_xCl_{2+x} + Ce_{1-y}Sr_yCl_{3-y}$ |
| 0.395 | 1044 | Liquidus | $Sr_{1-x}Ce_xCl_{2+x} = L$ |
| | 1022 | Unknown | - |
| | 919 | Peritectic | $Sr_9Ce_5Cl_{33} = Sr_{1-x}Ce_xCl_{2+x} + Ce_{1-y}Sr_yCl_{3-y}$ |
| 0.4 | 1001 | Liquidus | $Sr_{1-x}Ce_xCl_{2+x} = L$ |
| | 936 | Eutectic | $Sr_{1-x}Ce_xCl_{2+x} + Ce_{1-y}Sr_yCl_{3-y} = L$ |
| | 919 | Unknown | - |
| | 911 | Peritectic | $Sr_9Ce_5Cl_{33} = Sr_{1-x}Ce_xCl_{2+x} + Ce_{1-y}Sr_yCl_{3-y}$ |
| 0.446 | 912 | Peritectic | $Sr_9Ce_5Cl_{33} = Sr_{1-x}Ce_xCl_{2+x} + Ce_{1-y}Sr_yCl_{3-y}$ |
| 0.5 | 925 | Eutectic | $Sr_{1-x}Ce_xCl_{2+x} + Ce_{1-y}Sr_yCl_{3-y} = L$ |
| | 909 | Peritectic | $Sr_9Ce_5Cl_{33} = Sr_{1-x}Ce_xCl_{2+x} + Ce_{1-y}Sr_yCl_{3-y}$ |
| 0.55 | 973 | Liquidus | $Ce_{1-y}Sr_yCl_{3-y} = L$ |
| | 932 | Eutectic | $Sr_{1-x}Ce_xCl_{2+x} + Ce_{1-y}Sr_yCl_{3-y} = L$ |
| | 910 | Peritectic | $Sr_9Ce_5Cl_{33} = Sr_{1-x}Ce_xCl_{2+x} + Ce_{1-y}Sr_yCl_{3-y}$ |
| 0.6 | 986 | Liquidus | $Ce_{1-y}Sr_yCl_{3-y} = L$ |
| | 936 | Eutectic | $Sr_{1-x}Ce_xCl_{2+x} + Ce_{1-y}Sr_yCl_{3-y} = L$ |
| | 910 | Peritectic | $Sr_9Ce_5Cl_{33} = Sr_{1-x}Ce_xCl_{2+x} + Ce_{1-y}Sr_yCl_{3-y}$ |
| 0.625 | 997 | Liquidus | $Ce_{1-y}Sr_yCl_{3-y} = L$ |
| | 937 | Eutectic | $Sr_{1-x}Ce_xCl_{2+x} + Ce_{1-y}Sr_yCl_{3-y} = L$ |
| | 911 | Peritectic | $Sr_9Ce_5Cl_{33} = Sr_{1-x}Ce_xCl_{2+x} + Ce_{1-y}Sr_yCl_{3-y}$ |
| 0.7 | 1018 | Liquidus | $Ce_{1-y}Sr_yCl_{3-y} = L$ |
| | 928 | Eutectic | $Sr_{1-x}Ce_xCl_{2+x} + Ce_{1-y}Sr_yCl_{3-y} = L$ |
| | 924 | Unknown | - |
| | 905 | Peritectic | $Sr_9Ce_5Cl_{33} = Sr_{1-x}Ce_xCl_{2+x} + Ce_{1-y}Sr_yCl_{3-y}$ |
| 0.725 | 1033 | Liquidus | $Ce_{1-y}Sr_yCl_{3-y} = L$ |
| | 938 | Eutectic | $Sr_{1-x}Ce_xCl_{2+x} + Ce_{1-y}Sr_yCl_{3-y} = L$ |
| | 911 | Peritectic | $Sr_9Ce_5Cl_{33} = Sr_{1-x}Ce_xCl_{2+x} + Ce_{1-y}Sr_yCl_{3-y}$ |
| 0.75 | 1062 | Liquidus | $Ce_{1-y}Sr_yCl_{3-y} = L$ |
| | 916 | Eutectic | $Sr_{1-x}Ce_xCl_{2+x} + Ce_{1-y}Sr_yCl_{3-y} = L$ |
| | 909 | Peritectic | $Sr_9Ce_5Cl_{33} = Sr_{1-x}Ce_xCl_{2+x} + Ce_{1-y}Sr_yCl_{3-y}$ |
| | 900 | Unknown | - |
| 0.8 | 1050 | Liquidus | $Ce_{1-y}Sr_yCl_{3-y} = L$ |
| | 923 | Eutectic | $Sr_{1-x}Ce_xCl_{2+x} + Ce_{1-y}Sr_yCl_{3-y} = L$ |
| | 910 | Peritectic | $Sr_9Ce_5Cl_{33} = Sr_{1-x}Ce_xCl_{2+x} + Ce_{1-y}Sr_yCl_{3-y}$ |
| 0.9 | 1076 | Liquidus | $Ce_{1-y}Sr_yCl_{3-y} = L$ |
| | 925 | Eutectic | $Sr_{1-x}Ce_xCl_{2+x} + Ce_{1-y}Sr_yCl_{3-y} = L$ |
| | 909 | Peritectic | $Sr_9Ce_5Cl_{33} = Sr_{1-x}Ce_xCl_{2+x} + Ce_{1-y}Sr_yCl_{3-y}$ |

Table D.4: Equilibrium data in the $SrCl_2-CeCl_3$ system as measured by DSC.
[a] The uncertainties on compositions $x_{CeCl3}$ are ±0.005.
[b] The uncertainties on temperatures are ±5 K for pure end-members and ±10 K for mixtures.

## D.2. CHAPTER 6

| $x_{MgI_2}$ [a] | T (K) [b] | Equilibrium | Equilibrium reaction |
|---|---|---|---|
| 0 | 934 | Congruent Melting | $NaI = L$ |
| 0.099 | 901 | Liquidus | $Na_{1-x}Mg_xI_{1+x} + L' = L$ |
| 0.099 | 669 | Eutectic | $Na_{1-x}Mg_xI_{1+x} + Na_yMg_{1-y}I_{2-y} = L$ |
| 0.197 | 854 | Liquidus | $Na_{1-x}Mg_xI_{1+x} + L' = L$ |
| 0.197 | 671 | Eutectic | $Na_{1-x}Mg_xI_{1+x} + Na_yMg_{1-y}I_{2-y} = L$ |
| 0.303 | 671 | Eutectic | $Na_{1-x}Mg_xI_{1+x} + Na_yMg_{1-y}I_{2-y} = L$ |
| 0.420 | 672 | Eutectic | $Na_{1-x}Mg_xI_{1+x} + Na_yMg_{1-y}I_{2-y} = L$ |
| 0.693 | 671 | Eutectic | $Na_{1-x}Mg_xI_{1+x} + Na_yMg_{1-y}I_{2-y} = L$ |
| 0.693 | 830 | Liquidus | $Na_yMg_{1-y}I_{2-y} + L' = L$ |
| 0.800 | 657 | Eutectic | $Na_{1-x}Mg_xI_{1+x} + Na_yMg_{1-y}I_{2-y} = L$ |
| 0.800 | 847 | Liquidus | $Na_yMg_{1-y}I_{2-y} + L' = L$ |
| 1 | 911 | Congruent Melting | $MgI_2 = L$ |

Table D.5: Equilibrium data in the NaI−$MgI_2$ system as measured by DSC.
[a] The uncertainties on compositions $x_{MgI2}$ are ±0.005.
[b] The uncertainties on temperatures are ±5 K for pure end-members and ±10 K for mixtures.

| $x_{MgI_2}$ [a] | T (K) [b] | Equilibrium | Equilibrium reaction |
|---|---|---|---|
| 0 | 988 | Congruent Melting | $MgCl_2 = L$ |
| 0.1 | 958 | Liquidus | $MgCl_{2-2x}I_{2x} + L' = L$ |
| 0.1 | 782 | Eutectic | $MgCl_{2-2x}I_{2x} + MgI_{2-2y}Cl_{2y} = L$ |
| 0.176 | 930 | Liquidus | $MgCl_{2-2x}I_{2x} + L' = L$ |
| 0.176 | 780 | Eutectic | $MgCl_{2-2x}I_{2x} + MgI_{2-2y}Cl_{2y} = L$ |
| 0.249 | 901 | Liquidus | $MgCl_{2-2x}I_{2x} + L' = L$ |
| 0.249 | 778 | Eutectic | $MgCl_{2-2x}I_{2x} + MgI_{2-2y}Cl_{2y} = L$ |
| 0.295 | 891 | Liquidus | $MgCl_{2-2x}I_{2x} + L' = L$ |
| 0.295 | 782 | Eutectic | $MgCl_{2-2x}I_{2x} + MgI_{2-2y}Cl_{2y} = L$ |
| 0.396 | 784 | Liquidus | $MgCl_{2-2x}I_{2x} + L' = L$ |
| 0.396 | 818 | Eutectic | $MgCl_{2-2x}I_{2x} + MgI_{2-2y}Cl_{2y} = L$ |
| 0.503 | 814 | Liquidus | $MgI_{2-2y}Cl_{2y} + L' = L$ |
| 0.503 | 787 | Eutectic | $MgCl_{2-2x}I_{2x} + MgI_{2-2y}Cl_{2y} = L$ |
| 0.598 | 784 | Liquidus | $MgI_{2-2y}Cl_{2y} + L' = L$ |
| 0.771 | 861 | Eutectic | $MgCl_{2-2x}I_{2x} + MgI_{2-2y}Cl_{2y} = L$ |
| 0.771 | 778 | Liquidus | $MgI_{2-2y}Cl_{2y} + L' = L$ |
| 0.832 | 871 | Eutectic | $MgCl_{2-2x}I_{2x} + MgI_{2-2y}Cl_{2y} = L$ |
| 0.832 | 775 | Liquidus | $MgI_{2-2y}Cl_{2y} + L' = L$ |
| 0.893 | 885 | Liquidus | $MgI_{2-2y}Cl_{2y} + L' = L$ |
| 0.949 | 903 | Liquidus | $MgI_{2-2y}Cl_{2y} + L' = L$ |
| 1 | 911 | Congruent Melting | $MgI_2 = L$ |

Table D.6: Equilibrium data in the $MgCl_2$−$MgI_2$ system as measured by DSC.
[a] The uncertainties on compositions $x_{MgI2}$ are ±0.005.
[b] The uncertainties on temperatures are ±5 K for pure end-members and ±10 K for mixtures.

| $x_{MgI_2}$ [a] | T (K) [b] | Equilibrium | Equilibrium reaction |
|---|---|---|---|
| 0 | 1074 | Congruent melting | $NaCl = L$ |
| 0.098 | 987 | Liquidus | $NaCl + L' = L$ |
| 0.098 | 911 | unknown | - |
| 0.09 | 747 | unknown | - |
| 0.098 | 705 | Peritectic | $Na_6MgCl_8 = NaCl + L'$ |
| 0.098 | 668 | unknown | - |
| 0.3 | 755 | Liquidus | $Na_{1-x}Mg_xCl_{1+x} + L' = L$ |
| 0.3 | 676 | Eutectic | $Na_2Mg_3Cl_8 + MgCl_{2-2x}I_{2x} = L'$ |
| 0.475 | 696 | Liquidus | $MgI_{2-2y}Cl_{2y} + L' = L$ |
| 0.475 | 632 | Eutectic | $MgCl_2 + Na_{1-x}Mg_xI_{1+x} = L'$ |
| 0.68 | 783 | Liquidus | $MgI_{2-2y}Cl_{2y} + L' = L$ |
| 0.68 | 630 | Eutectic | $MgCl_2 + Na_{1-x}Mg_xI_{1+x} = L'$ |
| 0.731 | 810 | Liquidus | $MgI_{2-2y}Cl_{2y} + L' = L$ |
| 0.731 | 630 | Eutectic | $MgCl_2 + Na_{1-x}Mg_xI_{1+x} = L'$ |
| 0.93 | 891 | Liquidus | $MgI_{2-2y}Cl_{2y} + L' = L$ |
| 0.93 | 606 | unknown | - |
| 1 | 911 | Congruent melting | $MgI_2 = L$ |

Table D.7: Equilibrium data in the NaCl−$MgI_2$ system as measured by DSC.
[a] The uncertainties on compositions $x_{MgI2}$ are ±0.005.
[b] The uncertainties on temperatures are ±5 K for pure end-members and ±10 K for mixtures.

| $x_{MgCl_2}$ [a] | T (K) [b] | Equilibrium | Equilibrium reaction |
|---|---|---|---|
| 0 | 934 | Congruent melting | $NaI = L$ |
| 0.2 | 849 | Liquidus | $Na_{1-x}Mg_xCl_{1+x} + L'' = L$ |
| 0.2 | 696 | Eutectic | $MgI_{2-2y}Cl_{2y} + Na_{1-x}Mg_xI_{1+x} = L''$ |
| 0.2 | 636 | unknown | - |
| 0.2 | 619 | unknown | - |
| 0.299 | 765 | Liquidus | $Na_{1-x}Mg_xCl_{1+x} + L'' = L$ |
| 0.299 | 691 | Eutectic | $MgI_{2-2y}Cl_{2y} + Na_{1-x}Mg_xI_{1+x} = L''$ |
| 0.5 | 743 | Liquidus | $MgI_{2-2y}Cl_{2y} + L'' = L$ |
| 0.5 | 686 | Eutectic | $MgI_{2-2y}Cl_{2y} + Na_{1-x}Mg_xI_{1+x} = L''$ |
| 0.5 | 678 | Peritectic | $Na_2Mg_3Cl_8 = L'$ |
| 0.749 | 895 | Liquidus | $MgI_{2-2y}Cl_{2y} + L'' = L$ |
| 0.749 | 690 | Eutectic | $MgI_{2-2y}Cl_{2y} + Na_{1-x}Mg_xI_{1+x} = L''$ |
| 0.749 | 677 | Peritectic | $Na_2Mg_3Cl_8 = L'$ |
| 1 | 988 | Congruent melting | $MgCl_2 = L$ |

Table D.8: Equilibrium data in the NaI−$MgCl_2$ system as measured by DSC.
[a] The uncertainties on compositions $x_{MgCl2}$ are ±0.005.
[b] The uncertainties on temperatures are ±5 K for pure end-members and ±10 K for mixtures.

## D.3. CHAPTER 7

| $x_{MgI_2}$ [a] | T (K) [b] | Equilibrium | Equilibrium reaction |
|---|---|---|---|
| 0 | 906 | Congruent Melting | $MgI_2 = L$ |
| 0.05 | 896 | Liquidus | $MgI_2 + L' = L$ |
| 0.099 | 893 | Liquidus | $MgI_2 + L' = L$ |
| 0.21 | 851 | Eutectic | $MgI_2 + \alpha\text{-}NdI_3 = L$ |
| | 883 | Liquidus | $MgI_2 + L' = L$ |
| 0.3 | 853 | Eutectic | $MgI_2 + \alpha\text{-}NdI_3 = L$ |
| | 878 | Liquidus | $MgI_2 + L' = L$ |
| 0.43 | 852 | Eutectic | $MgI_2 + \alpha\text{-}NdI_3 = L$ |
| 0.69 | 851 | Eutectic | $MgI_2 + \alpha\text{-}NdI_3 = L$ |
| | 984 | Liquidus | $\alpha\text{-}NdI_3 + L' = L$ |
| 1 | 859 | Polymorphism | $\alpha\text{-}NdI_3 = \beta\text{-}NdI_3$ |
| | 1057 | Congruent Melting | $\beta\text{-}NdI_3 = L$ |

Table D.9: Equilibrium data in the $MgI_2-NdI_3$ system as measured by DSC.
[a] The uncertainties on compositions $x_{MgI2}$ are ±0.005.
[b] The uncertainties on temperatures are ±5 K for pure end-members and ±10 K for mixtures.

| $x_{MgI_2}$ [a] | T (K) [b] | Equilibrium | Equilibrium reaction |
|---|---|---|---|
| 0 | 1031 | Congruent Melting | $NdCl_3 = L$ |
| 0.205 | 795 | Eutectic | $NdCl_3 + NdCl_{3x}I_{3-3x} = L$ |
| | 941 | Liquidus | $NdCl_3 + L' = L$ |
| 0.536 | 799 | Eutectic | $NdCl_3 + NdCl_{3x}I_{3-3x} = L$ |
| 0.702 | 800 | Eutectic | $NdCl_3 + NdCl_{3x}I_{3-3x} = L$ |
| | 918 | Liquidus | $NdCl_{3x}I_{3-3x} + L' = L$ |
| 0.897 | 799 | Eutectic | $NdCl_3 + NdCl_{3x}I_{3-3x} = L$ |
| | 821 | Liquidus | $NdCl_{3x}I_{3-3x} + L' = L$ |
| 1 | 859 | Polymorphism | $\alpha\text{-}NdI_3 = \beta\text{-}NdI_3$ |
| | 1057 | Congruent Melting | $\beta\text{-}NdI_3 = L$ |

Table D.10: Equilibrium data in the $NdCl_3-NdI_3$ system as measured by DSC.
[a] The uncertainties on compositions $x_{MgI2}$ are ±0.005.
[b] The uncertainties on temperatures are ±5 K for pure end-members and ±10 K for mixtures.

# About the Author

## Dennis Alders

Delft, Tuesday September $27^{th}$, 1994 - Dennis Charley Alders is born at the Oude Delft, in Delft, the Netherlands, firstborn of Marijke and Rob Alders. After living here for two years, he moved to the quaint town of Bergschenhoek, where he attended elementary school (RKBS Puis X, Bergschenhoek) and high school (Wolfert Lyceum, Bergschenhoek), both within a radius of one kilometer of his residence. After his graduation, he still didn't venture very far, and went on to study Molecular Science and Technology - a joint degree between Delft University of Technology (his father's *alma mater*) and Leiden University (his mother's *alma mater*). He completed his Bachelor thesis in the Applied Radiation and Isotopes group at the Reactor Institute Delft, marking his first real contact with the nuclear sciences. After recognising that his strengths lied more in differential equations and thermodynamics, rather than organic chemistry, he continued his studies at the TU Delft with a Master Chemical Engineering. During a design project he met Anna and Jaén, who introduced him to the wondrous world of Molten Salt Reactors - a topic that would keep him busy during his Master thesis and subsequent PhD project. Nowadays he's still not done with the thermodynamics of the complex liquids, and is pursuing a project as postdoctoral researcher in the field.

# List of Publications

1. A. van Hattem, **D.C. Alders**, R.J.M. Konings, A.L. Smith, *Ternary System CsI−−$PbI_2$−−$BiI_3$ and Thermodynamic Stability of Cesium Metal Halide Perovskites*, Journal of Physical Chemistry C **127**, 35 (2023).

2. **D.C. Alders**, J. Vlieland, M. Thijs, R.J.M. Konings, A.L. Smith, *Experimental investigation and thermodynamic assessment of the $BaCl_2$−$CeCl_3$ system*, Journal of Molecular Liquids **396** (2024).

3. **D.C. Alders**, D.J. Cette, R.J.M. Konings, A.L. Smith, *Experimental investigation and thermodynamic assessment of the $AECl_2$−$NdCl_3$ (AE = Sr, Ba) systems*, Physical Chemistry, Chemical Physics **26** (2024).

4. **D.C. Alders**, B.A.S. Rooijakkers, R.J.M. Konings, A.L. Smith, *Experimental Investigation and Thermodynamic Modeling Assessment of the NaCl−−NaI−−$MgCl_2$−−$MgI_2$ Quaternary System*, Journal of Physical Chemistry C **129**, 5 (2025).

5. **D.C. Alders**, A. Sacristán-Civera, M.J. Wolff, E. Capelli, C. Hennig, E. Lawrence-Bright, R.J.M. Konings, A.L. Smith, *Simulant chemistry for uranium and plutonium molten fuel salts: crystallographic investigation and thermodynamic modelling assessment of the NaCl−$RECl_3$ and NaCl−$MgCl_2$−$RECl_3$ (RE = Ce, Nd) systems*,

6. **D.C. Alders**, D. Panneerselvam, E. Capelli, K. Krämer, R.J.M. Konings, A.L. Smith, *Thermodynamic studies of cesium and iodine in molten salt systems: CALPHAD modelling of the (Na,Cs,Mg,Nd,Pu)(Cl,I) system*, Journal of Physical Chemistry B (2026) *in publication.*

7. **D.C. Alders**, M.J.A. IJszenga, N.T.H. ter Veer, E. Capelli, R.J.M. Konings, A.L. Smith, *Fission products Sr and Ba in actinide (U, Th) chloride systems: thermodynamic modelling, experimental investigation and application calculations*, Nuclear Materials and Energy (2026) *in publication.*

# ACKNOWLEDGEMENTS

The journey to completing this PhD dissertation was not a lonely one by any means. There are many, many people who contributed in one way or another to this epic, and I would like to use this section to express my gratitude to them all.

First off, I cannot thank my promotors Anna Smith and Rudy Konings enough. They have been there for me every step of the way, not even letting maternity leave or retirement stop them. I am most grateful for all the discussions, the (sometimes *very* necessary) feedback on my writing, their confidence in my ability to figure things out, and all other things they helped me with. Anna, Rudy, you are both amazing people, and I hope all your past and future PhD candidates will recognise that. Additionally, I owe a huge debt to Elisa Capelli for the support and guidance she provided during my PhD trajectory. Thank you for making sense of my ideas, from the first phase diagram to the last.

Next, I would like to thank John Vlieland, Sebastian Couweleers, Dick de Haas and Trudy Beentjes for all their support over the years. Any time Anna or I had a wild idea to test in the lab, John, Sebas and Dick were happy to help, and occasionally shoot down ideas. Their support, both in the lab and at the coffee table, has been invaluable, and I cannot thank them enough. Trudy, on the other hand, is a different kind of miracle worker. Any time I needed to get something signed, mailed, booked, organised or arranged, she was there. I am fully convinced that she may have actual superpowers, and I am very grateful for all her support. For all the other help I got in the labs and in the building, my gratitude goes out to Robert Dankelman, Hanan Al-Kutubi, Michel Thijs, Michel van Steenvoorden, Astrid van der Meer and Hugo van der Kort for their aid in various ways.

Then, my colleagues. I could, and would, write a paragraph for each and every one of you, but I do not want this chapter to go into the double digits, so I will try to keep it brief. Daphné Cette, Bas Rooijakkers, Max IJszenga, Mädchen Wolff and Dhivya Panneerselvam: it was a pleasure to supervise you during your theses, and I am very pleased to report that each of your names will soon be on a publication. I also want to thank Kamran and Loic for teaching me valuable lessons about student supervision.

To the greatest office-roomies known to man, Andries van Hattem, Nicolo Magro, Anish Kodyingal, Laurent de Geus, Ruben Dewes, and even Aron Selmeci and Meghann Fucina - however brief their stay may have been - I want to express my utmost gratitude. I can honestly say that my PhD life became that much more interesting because you were a part of it. Thank you for all the laughs, discussions, collaborations and distractions over the years. And even though technically he's not in our office (he certainly spends enough time there), that includes Nick ter Veer. Thanks for all the memes we didn't know we needed, great spots to take a nap, and the necessary cooking skills to make actinide halides.

The other PhD candidates, PostDocs, students and staff in the RPNM and MPT groups, Jaen, Thomas, Marc, Anand, Jasper, Ana, Jelte, Alessandro, Mykolai, Pia, Tibi, Celebrity, Bouke,

Daphné, Nikita, Jocelyn, Eva, Ronan, Martin, Danny, Jan-Leen, a whole army of students (who somehow tend to come back for a PhD position), and please tell me I'm not forgetting anyone here - thank you for everything. The coffee breaks, lunch breaks, ping pong breaks, volleyball breaks, puzzle breaks, limitless supply of cake, the evenings in 't Koepeltje, and of course the interesting discussions - scientific or not - made the days that much more enjoyable.

Furthermore, I want to thank my colleagues on the PhD council. Not just the old guard, with Marc, Andries, Rogier, Mark, Max, Jasper, David, Svenja, Xavier and Pedro, but also the heroes who picked up the mantle, with Nikita, Anish, Nicolo, Jeffrey and Gauri. Taking part in the council was one of the best decisions I was forced to make during my PhD. The invention of PIzza Talks was nothing short of brilliant, and I have taken great pleasure in organising all sorts of events with our little council and meeting great people like you.

Even though I already wrote finally, that's not quite the case. Because even outside of the work environment, there have been plenty of people who helped me greatly along this journey. Kyra and Riley, for example, who taught me the insanely valuable skill of being able to work in a very noisy and hectic environment with virtually limitless disctractions. My brother, Tim, and father, Rob, with whom I've discussed so many salts, ideas and struggles that it amazes me that they continued to listen. I'd also like to thank them for proofreading parts of this manuscript - it surprises me how many mistakes I had left in it. My fiancée, Sjanne, who's supported me through this crazy ride, helped me style this book and even agreed to marry me despite all the talk about salts: I am so very grateful that we met, and that I get to experience your support, love and perpetual craziness on a daily basis. And finally, my mother: I did it, mom. I hope you were watching.

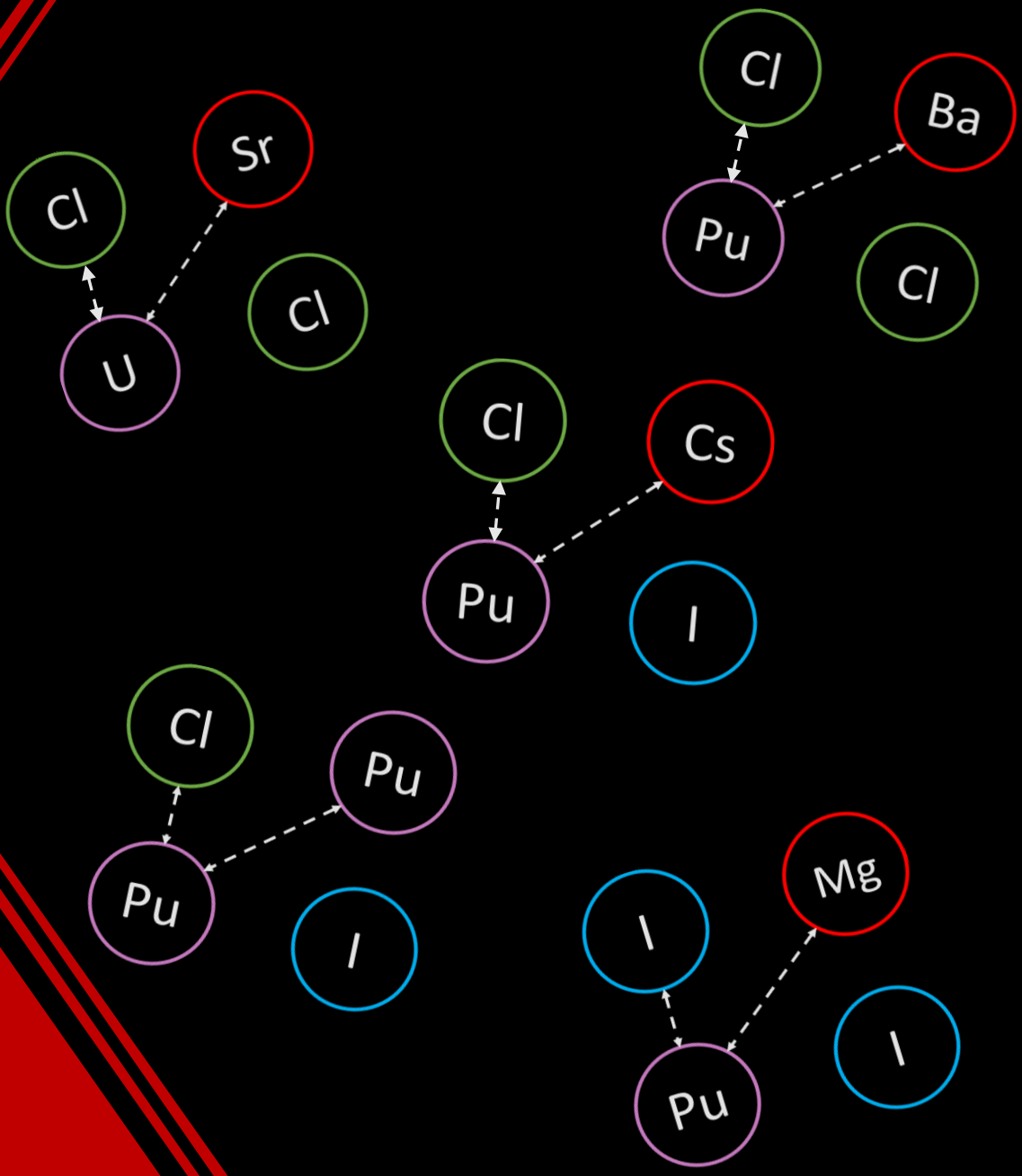
Cl
Sr
Cl
U
Cl
Cl
Ba
Pu
Cl
Cl
Cs
Pu
I
Cl
Pu
Pu
I
I
Mg
Pu
I